Fusion Power Demonstrations I and II

Technical Editor: J. N. Doggett

January 1985
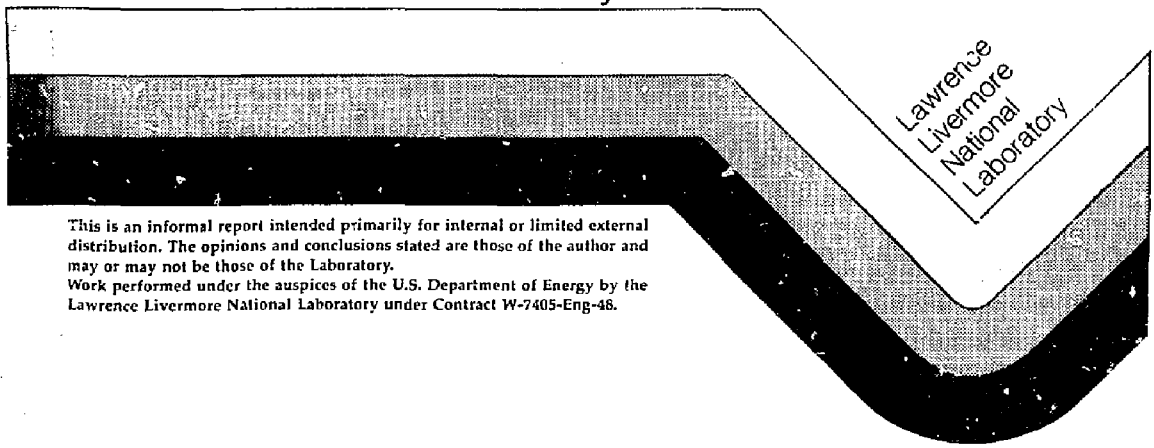
Lawrence
Livermore
National
Laboratory

CONTRIBUTING AUTHORS

Lawrence Livermore National Laboratory

L. J. Perkins, R. H. Bulmer, B. G. Logan, J. D. Lee,
J. N. Doggett, W. L. Barr, S. R. Devoto, W. S. Neef
D. W. Dorn, R. C. Maninger

Negion

J. H. Fink

TRW

R. B. Campbell, M. E. Fenstermacher

Grumman Aerospace Corporation

I. Clarkson, T. Luzzi

INEL/EG&G

P. Hsu

General Dynamics/Convair Division

J. Parmer

Oak Ridge National Laboratory/Fusion Engineering Design Center

W. D. Nelson, S. S. Kalsi, V. C. Srivistava, S. A. Freije
G. E. Gorker, J. R. Haines, W. R. Hamilton, J. Kirchner,
T. L. Mann, D. H. Metzler, J. A. O'Toole, R. L. Reid,
P. T. Spampinato, F. W. Wiffin

Bechtel

S. Ghose

Argonne National Laboratory

P. A. Finn, M. Y. Gohar

MASTER

i/ii

CONTENTS

iii

SCOPE

In this report we present a summary of the first phase of the Fusion Power Demonstration (FPD) design study. During this first phase, we investigated two configurations, performed detailed studies of major components, and identified and examined critical issues. In addition to these design specific studies, we also assembled a mirror-systems computer code to help optimize future device designs.

The two configurations that we have studied are based on the MARS magnet configuration and are labeled FPD-I and FPD-II. The FPD-I configuration employs the same magnet set used in the FY83 FPD study, whereas the FPD-II magnets are a new, much smaller set chosen to help reduce the capital cost of the system.

As part of the FPD study, we also identified and explored issues critical to the construction of an Engineering Test Reactor (ETR). These issues involve subsystems or components, which because of their cost or state of technology can have a significant impact on our ability to meet FPD's mission requirements on the assumed schedule. General Dynamics and Grumman Aerospace studied two of these systems, the high-field choke coil and the halo pump/direct converter, in great detail and their findings are presented in this report.

Because this is an interim report presenting the results of this work to date, the document has not been extensively edited to eliminate minor inconsistencies and omissions. An additional report will be produced in the early part of 1985 at the completion of the FPD-III phase of this study.

Section 1
INTRODUCTION

1.0 INTRODUCTION

The Fusion Power Demonstration (FPD) is an Engineering Test Reactor (ETR) class device. The FPD design includes all systems required in a Demonstration Power Reactor except for a turbine plant. We based the first two iterations of the FPD design on the physics concepts developed in the MARS study that was completed in September, 1983.[1]

The plasma engineering configuration of FPD follows the principles employed in MARS[1] and comprises a low-field (2.5-T) solenoidal-central-cell region, the high-field (24-T) central-cell choke coils, and an end-cell magnet system composed of a double quadrupole anchor/plug yin-yang pair. Central-cell passing particles that trap in the long end-cell transition regions are radially "drift pumped" to the plasma halo and represent a major power loss from the system. To reduce costs, the ignition conditions for FPD-I and FPD-II were obtained at the minimum central-cell length where fusion alpha particle heating balances the drift pump and other system losses.

The engineering design philosophy for FPD-I and FPD-II reflects the configuration developed in the 1983 Mirror Fusion Test Facility-Upgrade (MFTF-Upgrade) study that minimizes size and emphasizes ease of maintenance.

The FPD-I configuration has a central cell length of 74 m and produces 360 MW of fusion power (see Fig. 4-1 in Sec. 4). With a recirculation power of approximately 170 MW, this option, with minor revision, could reach engineering breakeven. The most visible difference, between the MARS and FPD-I concepts, is the application of sheet coils to the central cell in FPD-I, which reduces field ripple and improves performance. A test cell is included in the FPD-I concept; and in this case the test cell will develop a wall loading of 2 MW/m^2 of uncollided 14-MeV neutrons.

The FPD-II configuration has a central cell length of 96 m and produces 480 MW of fusion power (see Fig. 5-1 in Sec. 5). At this power level, this device could produce about 200 MW of net electrical power when using a reasonably efficient turbine plant. A test cell is included in the FPD-II concept, which produces an uncollided 14-MeV neutron flux of 4 MW/m^2. A revision of the geometry and a better understanding of the physics account for the differences in performance between this device and FPD-I.

The FPD-I and FPD-II studies are each based on somewhat different physics; and the costs for each were generated with different algorithms. The physics changes are an outcome of our continuing work in modeling mirror systems. The costing revisions are based on the methods used in costing Tokamak Fusion Core Experiment (TFCX) during this same period of time. When adjustments are made for the above differences, the results show that we have made progress in reducing the size and mass of the mirror system by using an aggressive approach in designing subsystems, particularly the magnet systems. Capital costs will follow this trend, but at some point the capital cost saving will be overwhelmed by increased operating costs.

REFERENCE

1. B. G. Logan, <u>MARS Mirror Advanced Reactor Study</u>, Lawrence Livermore
    National Laboratory, Livermore, CA, UCRL-53480 (1984).

Section 2
THE ENGINEERING TEST REACTOR MISSION

2.0 THE ENGINEERING TEST REACTOR MISSION

INTRODUCTION

The FPD mission statement that follows consists of the tandem mirror relevant portions of the draft generic Engineering Test Reactor (ETR) mission statement generated by Grumman Aerospace Corporation as part of their responsibilities as the Technical Support Services contractor to the Department of Energy (DOE) Office of Fusion Energy.

MISSION

The ETR mission is (1) to test critical reactor components in an environment that can be extrapolated to a commercial fusion power reactor, and (2) to demonstrate the safe and reliable operation of a fusion reactor that is representative of a commercial fusion power reactor.

The ETR is an element of the overall national program of development for Magnetic Fusion Energy as summarized in the Comprehensive Program Management Plan (CPMP) of the U.S. Department of Energy, June 1983. The design of the ETR will be based on the confinement concept selected during the Product Definition Phase (tokamak and tandem mirror concepts are the current leading candidates) and on the initial plasma optimization efforts of the Product Development Phase. The ETR will concentrate on the demonstration of technologies in support of and leading to a Fusion Demonstration Powerplant (DEMO). The DEMO will address the economics of producing electrical power from fusion energy. Goals and objectives of both the ETR and DEMO are expanded in the following paragraphs.

This mission statement is written to provide guidance for current Reactor Design Studies in preparation for future ETR definition/design activities. The ETR goals and objectives are based on the assumption that the ETR will be the next major machine to be built. If additional reactors such as Tokamak Fusion Core Experiment (TFCX), Burning Core Experiment (BCX), or upgrades to Mirror Fusion Test Facility (MFTF-B) are incorporated into the CPMP, several of the ETR objectives may be reassigned to these machines and others may be redefined accordingly.

GENERIC ETR OBJECTIVES

The following objectives are applicable to both tokamak and tandem mirror concepts.

- Demonstrate startup, fractional power, and shutdown operations in a reactor relevant regime.
- Demonstrate full fuel-cycle operation including fuel injection, tritium recovery from a breeder blanket, tritium handling throughout the system, and the potential for self-sufficiency of fuel. (The demonstration of self-sufficiency of fuel is an objective of the DEMO mission.)
- Demonstrate neutron thermalization and thermal energy transfer to a blanket coolant at high enough temperatures to be of engineering significance. (The demonstration of electricity production may be included, but is not a primary objective of the ETR mission.)
- Demonstrate the remote handling operations required to attain the desired maintainability for a commercial power reactor. (The demonstration of commercially acceptable availability is an objective of the DEMO mission.)
- Demonstrate shielding effectiveness to prove that the radiation environment of a commercial reactor can be reduced to levels that are acceptable for the operation of radiation sensitive components and to permit the use of projected maintenance scenarios to meet maintainability goals.
- Demonstrate acceptable behavior of critical components when exposed to radiation intensities and dosages that might be expected during a commercial reactor's lifeline. (Although the ETR components will generally not experience such intensities and dosages, low-effectiveness shielding may be used in areas of the device to allow exposure of selected components to integrated dosages representative of a commercial reactor radiation environment.)
- Provide sufficient testing capability to permit comparative demonstrations of competing alternative configurations for subsystems or components, when such evaluation cannot be effectively performed in a complementary program.

TANDEM MIRROR ETR OBJECTIVES

- Demonstrate ignited operation with M as defined below applying
  to the central cell only:

$$M = \text{ignition margin} = \frac{\text{alpha heating power}}{\text{total plasma power losses}} \quad .$$

- Demonstrate negative-ion-based neutral-beam heating systems.
- Demonstrate impurity removal and vacuum pumping by plasma
  halos (dense boundary layers).

Section 3
PLASMA ENGINEERING

3.0 PLASMA ENGINEERING

The plasma engineering effort for FPD-I and FPD-II was conducted to meet
the following three main design goals

1. The central cell should be ignited, i.e., the power deposited by the
    fusion alpha particles in the central-cell plasma volume should
    balance the total power loss (energetic particles and radiation) from
    this volume.
2. The central-cell length should be the minimum required to achieve
    ignition.
3. The device should be capable of making net electrical power, i.e.,
    the engineering Q (gross electric power divided by recirculating
    electric power) should be greater or equal to unity.

Both FPD-I and FPD-II employ end cell magnets based on the Mirror
Advanced Reactor Study (MARS) configuration,[1] namely a double quadrupole set
with separate anchor and plug regions. The FPD-I magnet set is identical to
that used in the FY83 FPD study,[2] and represents an initial attempt to
design a self-consistent tandem-mirror Engineering Test Reactor (ETR). The
FPD-II magnet set is a result of system optimization studies performed during
FY84 and represents the most compact end-cell magnet set for a minimum cost
ignition machine based on the MARS configuration. Figure 3-1a,b compares the
magnetic configurations of FPD-I and FPD-II, whereas Table 3-1 compares the
corresponding baseline plasma parameters.

The major advances in FPD plasma engineering in FY84 to date are
summarized in Table 3-2. The principal task of the FPD plasma engineering
effort this year has been the optimization of the system design through
extensive parametric analysis consistent with the above design goals. To
achieve system optimization, we have searched for minimum length ignition
cases by characterizing the close coupling between the major plasma parameters
and the magnetic configuration. In particular, as described in more detail
below, we were able to demonstrate the strong dependence of the central-cell

3-1

(a)

FPD I

FPD II

(b)
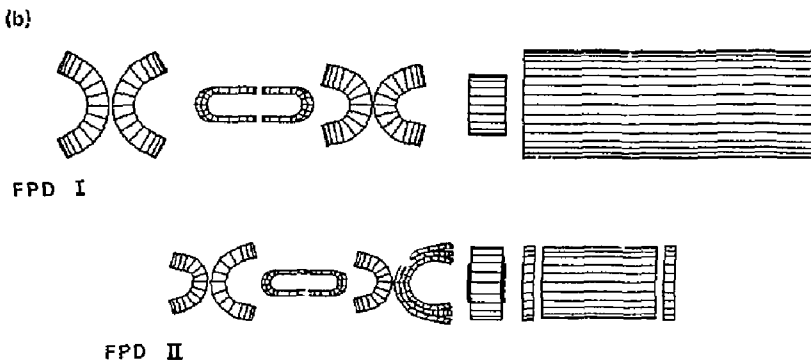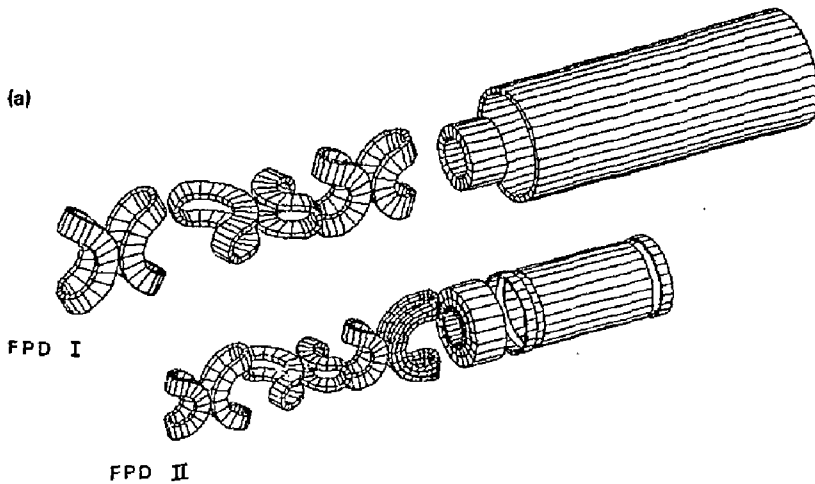
FPD I

FPD II

Figure 3-1. Two views (a and b) comparing the magnetic configurations for
FPD-I and FPD-II. For FPD-I, a short section of a representative, continuous
solenoid is shown for the central cell magnets. For FPD-II, one of the
central cell sheet solenoids with accompanying trim coils is shown.

Table 3-1. Principal plasma parameters for FPD-I and FPD-II.

Parameter	FPD-I	FPD-II
General		
Fusion power (MW)	828	479
Q	28.4	36.7
Neutron wall loading (MW/m^2)	1.44	1.00
Cold fueling current (kA)	0.660	0.249
End cell magnet configuration	MARS-mode	MARS-mode
End cell trapping length[a] (m)	∿17.2	∿13.6
Central Cell		
L_c (m)	90	90
r_c (m)	0.60	0.458
First wall radius (m)	0.81	0.674
B_c (T)	2.5	2.5
$<\beta_c>$	0.6	0.6
T_i (keV)	36.7	40
T_e (keV)	25.7	27.7
n_c (cm^{-3})	1.69×10^{14}	1.65×10^{14}
Choke Region		
r_{plasma} (m)	0.154	0.118
r_{coil} (m)	0.177	0.14
B (T)	24	24
Anchor		
$<\beta_{anchor}>$	0.50	0.14
ICRH power[b] (MW)	10.4	0.26

Table 3-1. (continued.)

Parameter	FPD-I	FPD-II
Plug		
$<\beta_{pl,3}>$[a]	0.367	0.30
ECRH power,[b] A (MW)	1.15	0.345
ECRH power,[b] B (MW)	16.7	11.09
Sloshing ion beam power[b] (MW)	0.89	1.37
Drift Pump Parameters		
Transition Coil:		
Central frequency (MHz)	0.064	0.107
Frequency spread	0.4	0.37
Antenna flux required (Wb)	0.072	0.0054
Plug Coil:		
Central frequency (MHz)	1.1	0.83, 1.33[c]
Frequency spread	0.66	0.10, 0.10[c]
Antenna flux required (Wb)	0.0065	0.0035

[a]Distance between 24-T peak and plug electrostatic potential peak.

[b]Trapped power, both ends.

[c]Separate frequencies for cold ions and sloshing ions.

Table 3-2. Major advances in FPD plasma engineering in FY84.

General

- Parameterized physics and magnetics scaling of ignition conditions in optimized (i.e., minimum length) ETR configurations.
- Characterized the dependence of the minimum central-cell length for ignition on the end-cell magnet configuration and central-cell alpha physics.
- Improved modeling of ion trapping rates in the end cell including multispecies (D,T, alpha) dependence.
- Revised TMRBAR power balance code extensively to improve running time, flexibility, and "user-friendliness". Code is now able to solve for minimum length for ignition, with or without fixed fusion power.

Alpha and Halo Physics

- Characterized central-cell alpha-particle confinement due to nonadiabaticity.
- Modeled alpha-particle energy loss to the halo for cases where the alpha larmor diameter is an appreciable fraction of the central-cell plasma radius.
- Improved modeling of halo physics including power flow, fueling, shielding requirements, and end-dump heat loads.

Magnetics

- Replaced discrete (MARS-type) central cell magnets with lower-cost, lower-ripple, sheet solenoids.
- Optimized central-cell trim solenoids to yield minimum rms field curvature and maximum beta.
- Investigated central-cell ripple reduction using field-shaping iron inserts.
- Increased central-cell volume-averaged betas from 49% to 60%.
- Shortened end-cell transition lengths by developing a new transition coil design.
- Reconfigured the TMG magnetics design code to allow for different magnetic mirror ratios in the plug and anchor regions.
- Implemented a new version of the TEBASCO magnetohydrodynamic (MHD) stability code permitting lower anchor and plug betas for a given central cell beta.

ignition length on both the end-cell magnetic configuration and central-cell alpha-particle energy deposition. As a major consequence of these studies, we determined that an optimized mirror ETR based on the MARS magnet configuration requires a minimum central cell length for ignition of about 90 m. At this length, the physics Q (plasma power gain, i.e., plasma fusion power divided by absorbed plasma heating power) is ~37; whereas Q_{eng} (engineering power gain, i.e., gross electric power divided by recirculating electric power) is ~2. In fact, because of this long-minimum ignition length, the optimized machine will always exhibit an engineering power gain greater than unity.

Although the magnet set for FPD-I is identical to that employed in last year's study,[2] the updated physics parameters in Table 3-1 show some marked differences. These differences are due to two main changes: (1) Improved central-cell magnet design has resulted in smaller and lower magnetic-ripple solenoids (see Fig. 3-1), which permit higher beta operation of the central cell plasma (60% vol averaged--compared with 49% in last year's study). (2) Refined Fokker-Planck calculations of end-cell particle-trapping rates, including multispecies effects for D, T and alpha particles; these calculations have unfortunately resulted in longer ignition-length requirements for the central cell of FPD-II (90 m compared with 67.5 m in FPD I). Although requiring a longer ignition length, FPD-II does exhibit a higher neutron wall loading than the FY83 baseline (1.44 MW/m^2 compared with 0.85 MW/m^2). The large overall size of FPD-I and the resulting high capital cost led us, in FPD-II, to seek a more optimized ignition test machine through the performance of parametric analyses.

For a given central-cell magnetic-field, the central-cell ignition length in FPD-II is minimized for a certain central-cell plasma radius r_c. Values of r_c larger than the optimum require larger (and more expensive) end cell magnets, which lead to larger end-cell ion-trapping currents and, therefore, longer central cell lengths L_c. Values of r_c smaller than the optimum also result in longer values of L_c due to the reduced efficiency of fusion alpha-particle-energy deposition in the central cell plasma volume.

We investigated L_c vs r_c scaling for FPD-II by generating four distinct magnetic configurations, A through D, differing in the characteristic volume of the end-cell magnet system. Figure 3-2 compares the end cell magnet configurations for three of these sets, namely A, B and D. Table 3-3 summarizes the results of this parametric trade study for all four magnetic configurations.

Figure 3-2. Comparison of the end cell magnet dimensions for magnet sets A, B, and D employed in the comparative trade study.

ignition length on both the end-cell magnetic configuration and central-cell alpha-particle energy deposition. As a major consequence of these studies, we determined that an optimized mirror ETR based on the MARS magnet configuration requires a minimum central cell length for ignition of about 90 m. At this length, the physics Q (plasma power gain, i.e., plasma fusion power divided by absorbed plasma heating power) is $\sim$37; whereas Q_{eng} (engineering power gain, i.e., gross electric power divided by recirculating electric power) is $\sim$2. In fact, because of this long-minimum ignition length, the optimized machine will always exhibit an engineering power gain greater than unity.

Although the magnet set for FPD-I is identical to that employed in last year's study,[2] the updated physics parameters in Table 3-1 show some marked differences. These differences are due to two main changes: (1) Improved central-cell magnet design has resulted in smaller and lower magnetic-ripple solenoids (see Fig. 3-1), which permit higher beta operation of the central cell plasma (60% vol averaged--compared with 49% in last year's study). (2) Refined Fokker-Planck calculations of end-cell particle-trapping rates, including multispecies effects for D, T and alpha particles; these calculations have unfortunately resulted in longer ignition-length requirements for the central cell of FPD-II (90 m compared with 67.5 m in FPD I). Although requiring a longer ignition length, FPD-II does exhibit a higher neutron wall loading than the FY83 baseline (1.44 MW/m^2 compared with 0.85 MW/m^2). The large overall size of FPD-I and the resulting high capital cost led us, in FPD-II, to seek a more optimized ignition test machine through the performance of parametric analyses.

For a given central-cell magnetic-field, the central-cell ignition length in FPD-II is minimized for a certain central-cell plasma radius r_c. Values of r_c larger than the optimum require larger (and more expensive) end cell magnets, which lead to larger end-cell ion-trapping currents and, therefore, longer central cell lengths L_c. Values of r_c smaller than the optimum also result in longer values of L_c due to the reduced efficiency of fusion alpha-particle-energy deposition in the central cell plasma volume.

We investigated L_c vs r_c scaling for FPD-II by generating four distinct magnetic configurations, A through D, differing in the characteristic volume of the end-cell magnet system. Figure 3-2 compares the end cell magnet configurations for three of these sets, namely A, B and D. Table 3-3 summarizes the results of this parametric trade study for all four magnetic configurations.

Figure 3-2. Comparison of the end cell magnet dimensions for magnet sets A, B, and D employed in the comparative trade study.

Table 3-3. Selected features of parametric trade studies for FPD-II.[a]

Magnet set	Central-cell plasma radius, r_c (m)	End-cell trapping length (m)	Choke coil radius (m)	Fusion power (MW)	Neutron wall loading (MW/m^2)	Q	Q_{eng}	Minimum central-cell ignition length, L_c (m)
A	35.7	12.7	0.114	440	0.78	46.6	~2.1	125
B	45.8	13.8	0.140	492	1.08	29.6	~1.9	86
C	50.7	16.0	0.153	591	1.24	25.4	~1.9	84
D	64.5	18.6	0.188	943	1.66	31.0	~2.7	84

[a]Parametric trades for optimum central-cell field formed a separate, parallel study and resulted in B_c = 2.5 T.

For a constant central cell field B_c (a value of 2.5 T was employed here, which is a result of a separate, parallel optimization study), a larger end-cell magnet volume implies a larger attainable central-cell plasma radius r_c because we must conserve magnetic flux mapping

$$\phi = \pi r_c^2 B_c \ (1 - <\beta_c>)^{1/2} = A(z) \ B(z) \ (1 - <\beta_z>)^{1/2} \ ,$$

through the system. As shown in Table 3-3, the smallest magnet set (set A) can support a maximum central-cell plasma radius of 35.7 cm; the largest (set D) can support a radius of 64.5 cm. Note that as r_c is increased from 35.7 cm to 64.5 cm (i.e., magnet sets A through D), the minimum central cell length for ignition L_c decreases from 125 m to 84 m. A further increase in end-cell magnet size above that of set D in Table 3-3 would result in a value of L_c larger than 84 m.

The apparent minimum in the ignition length for magnet sets can be explained as follows: larger end-cell magnet sets result in longer end-cell trapping lengths (i.e., the distance between the choke-coil mirror peak and

the end-cell potential peak). This, in turn, results in corresponding y
larger end-cell trapping rates. Because central cell ignition requires that
alpha heating essentially supports the radial losses incurred by trapping in,
and pumping out of the end cell region, central cell lengths determined only
by end-cell trapping would minimize for very small central cell radii.
Unfortunately, our relatively low B_c of 2.5 T and high $<\beta_c>$ of 60% imply large
alpha particle Larmor orbits. Hence, a decreasing central cell radius results
in a greater fraction of the fusion alpha energy escaping the plasma and being
deposited in the halo. Figure 3-3 illustrates this effect where the fraction
of the central-cell alpha power deposited in the halo outside the plasma is
plotted as a function of a parameter p, which incorporates the dependence of
r_c, B_c, and $<\beta_c>$ as shown. It is interesting to note that with the optimum
values of B_c and r_c at 2.5 T and 0.45 m, respectively, our ETR attains its
"optimized" ignition length by discarding ∿20% of its central-cell alpha
heating power to the halo! Hence, our minimum length is a compromise between
end-cell lengths/volumes and central-cell alpha-energy deposition.

Note that magnet set D yields an ignition length that is only 2 m less
than that of set B, although the former exhibits both larger plasma-heating
power requirements (Q times the fusion power) and larger end cell magnets, and
consequently, larger capital cost. In this respect, a design of FPD-II based
on magnet set B with r_c = 45.8 cm, represents the most desirable option.
The final parameters for FPD-II given previously in Table 3-1 show slightly
different values from those for set B in Table 3-3 because of further slight
refinements in both the magnetic configuration and the physics models. The
final baseline exhibits a respectable wall loading of 1 MW/m^2 at a fusion
power of 479 MW and a minimum ignition length of 90 m. Because of this long
ignition length, the physics Q (fusion power divided by absorbed heating
power) is high at 36.7 and yields a system engineering power gain (gross
electric output power divided by recirculating electric power) of ∿2.

Tables 3-1 and 3-3 both indicate that an ignition machine with end plugs
based on the MARS configuration will be a rather long and relatively expensive
device. In the current phase of the FPD project (i.e., FPD-III), these
factors have led us to consider a much more compact and cheaper ignition
machine based on an octopole end-cell magnetic configuration. Further details
on this are given in MFE/RTCD/84-2740a:0127a in the Appendix.
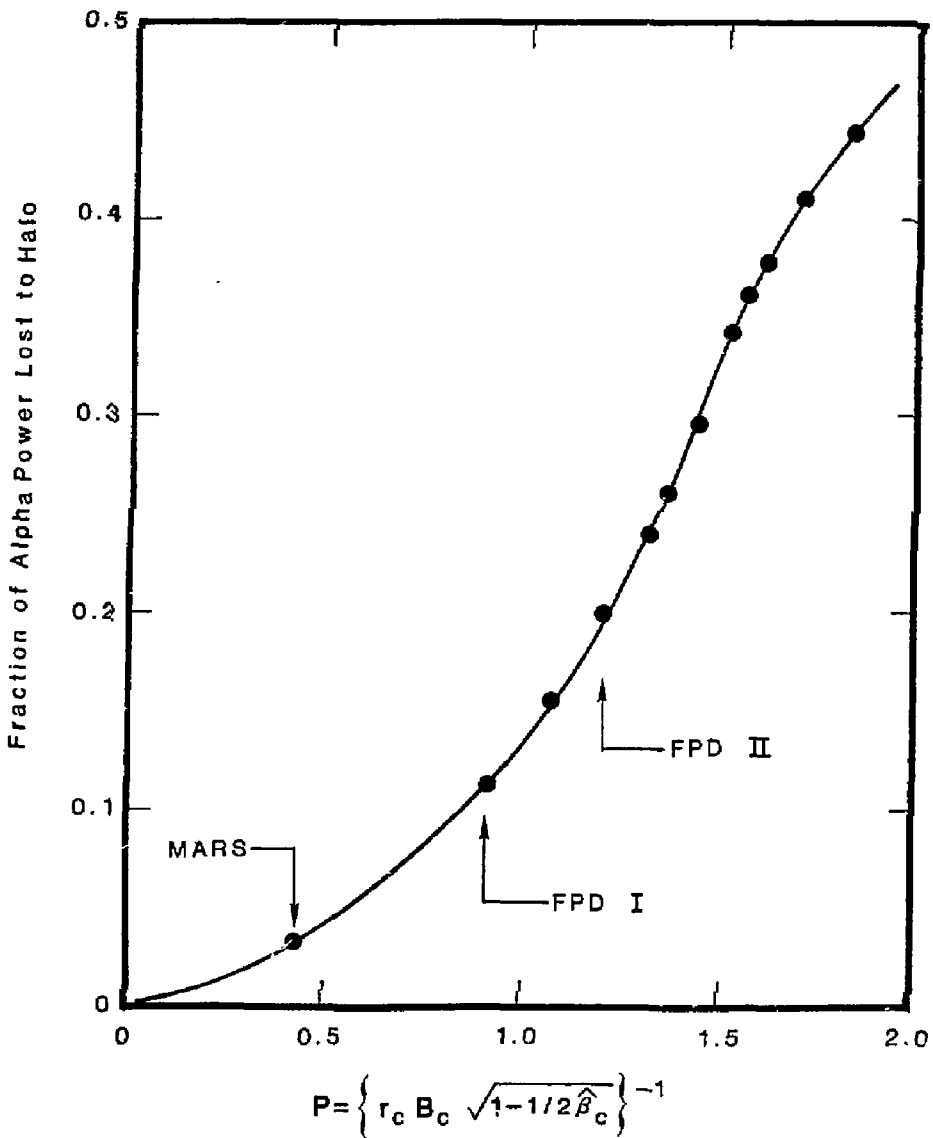
Figure 3-3. Fraction of the central cell fusion alpha power deposited in the halo, expressed in terms of a system parameter P. P is a function of the central cell plasma radius (r_c), the central cell B-field ($\hat{B}_c$), and the central cell peak beta (β_c).

TEST CELL CONFIGURATIONS

This section will focus on an option for FPD-II in which the first half of its full power operating lifetime would be dedicated to high-Q ignition operation and the second half would concentrate on integrated component testing of reactor-like blanket modules at high neutron wall loading. To accomplish the latter goal, one or more of the central cell magnet/blanket modules would be replaced by an axisymmetric, high-field test-cell insert driven by mixed DT neutral beam injection. In this configuration, called FPD-II+T, high wall loading in the test cell would be obtained by reducing the ion confinement of the device through modification of the axial potential profile and by injecting sufficient current into the test cell to establish a density that is more than a factor of 2 greater than that in the central cell of FPD-II.

We performed scoping studies of FPD-II+T configurations using an expanded version of the TMRBAR tandem mirror physics code,[3] subject to the following general constraints. First, the requirements on the end cell systems (drift pumping, ECRH, ICRH, sloshing-ion neutral beams, and related systems) have been held to near the FPD-II values or below to avoid costly changes to the end cells. Second, optimized self-consistent operating parameters have been sought that produce the highest test-cell wall loading for the lowest injection neutral beam power.

Two test-cell configurations have been examined--one accommodating two blanket test modules and the other accommodating four. The short test cell would replace a single 8.7-m-long FPD-II central cell magnet/blanket module. The long test cell would replace three central cell modules, and would require additional central-cell-like modules of appropriate length to fill in on either side of the test cell.

Examples of the parametrics that have been performed for both configurations are given in Figs. 3-4 and 3-5. From these studies a partially optimized parameter list for the short test cell has been obtained (see Table 3-4) in which the test-cell wall loading is $\Gamma_{tc} = 3.0$ MW/m^2 with neutral beam power $P_{nb,tc} = 26$ MW at the MHD beta limits set by stability considerations. For the longer test cell, the comparable case at $\Gamma_{tc} = 3.0$ MW/m^2 requires less neutral

Example Trade-off for FPD-II+T Short Test Cell Configuration
(Central Cell Beta = .20)
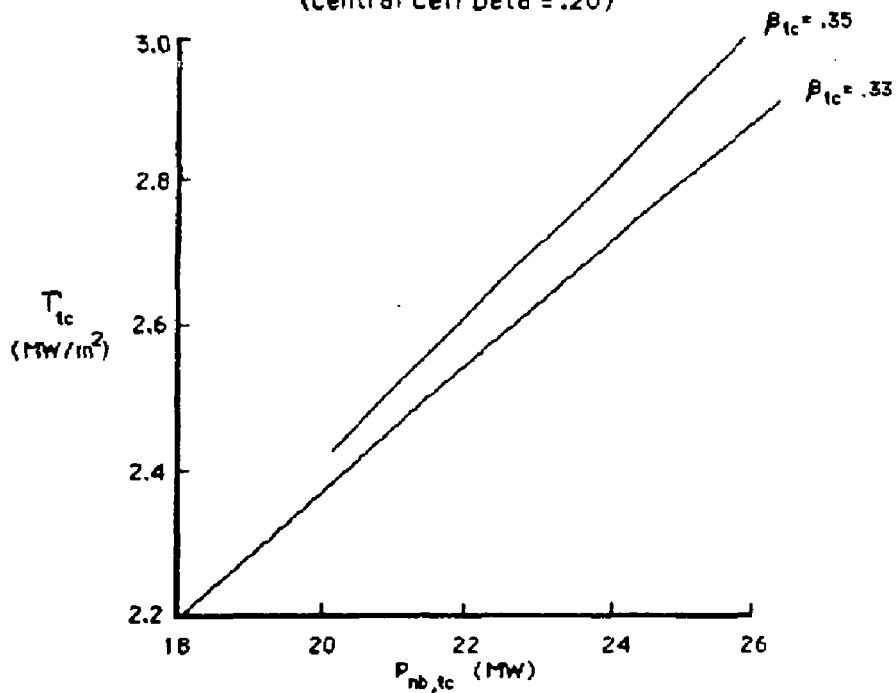
Figure 3-4. Neutron wall loading as a function of neutral beam power for the short test-cell configuration (central cell beta = 0.20).

Example Trade-off for FPD-II+T Long Test Cell Configuration
(Central Cell Beta = .36)
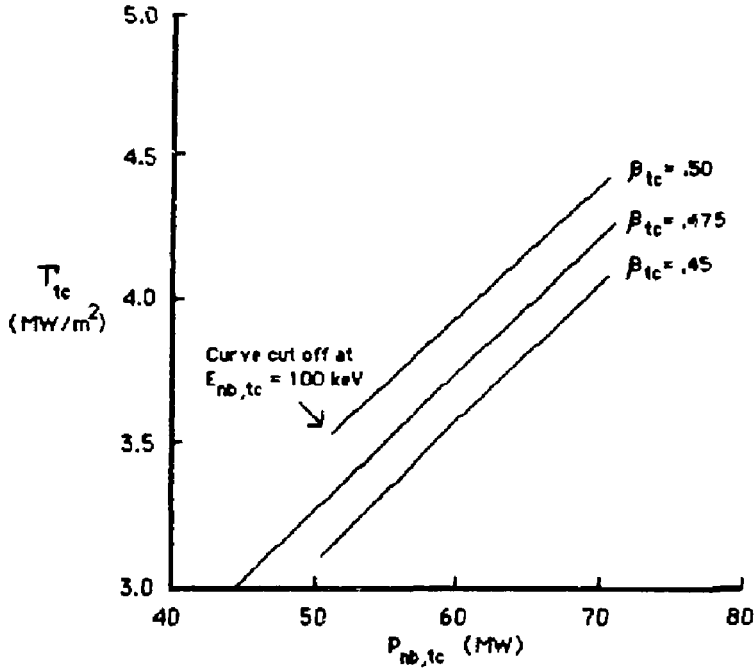
Figure 3-5. Neutron wall loading as a function of neutral beam power for the long test-cell configuration (central cell beta = 0.36).

Table 3-4. Optimized FPD-II+T operation parameters.

Parameter	Test-cell size	
	Short	Long
Test-cell wall loading, T_{tc} (MW/m^2)	3.0	3.0
Central cell ion density, $n_{i,c}$ (cm^{-3})	1.1×10^{14}	1.2×10^{14}
Central cell ion temperature, $T_{i,c}$ (keV)	16.0	24.9
Test-cell ion energy, E_{hot} (keV)	46.7	63.7
Central cell peak beta, β_c	0.20	0.36
Test-cell peak beta, β_{tc}	0.35	0.475
ECRH power at a, $P_{ecrh,a}$ (MW)	0.17[a]	0.11[a]
ECRH power at b, $P_{ecrh,b}$ (MW)	10.4[a]	11.0[a]
Anchor ICRH power, P_{icrh} (MW)	3.63[a]	0.76[a]
Neutral beam power at a', $P_{nb,a'}$ (MW)	0.15[a]	0.15[a]
Neutral beam energy at a', $E_{nb,a'}$ (keV)	250	280
Test-cell neutral beam power, $P_{nb,tc}$ (MW)	25.7[b]	44.4[b]
Test-cell neutral beam energy, $E_{nb,tc}$ (keV)	69.3	100.4
Test-cell neutral beam current, $I_{nb,tc}$ (A)	371[b]	443[b]
Central cell fueling current, $I_{fuel,c}$ (A)	5.0	0.0
Transition trapping current, I_{trap}' (A)	199	92
Direct-converter inner collector heat flux, $P_{dc,ic}$ (MW/m^2)	2.1	4.4

[a]Absorbed.

[b]Delivered.

beam power per unit test-cell effective length because of the higher beta values achievable at the longer length. Finally, although the value of 3 MW/m^2 may be near the maximum achievable wall loading in the short test cell (without significantly exceeding the capabilities of the FPD-II end cell systems), operation of the long test cell on the stability boundary, subject to the same constraints, can produce a wall loading in excess of 5 MW/m^2.

This study has not considered further optimization that might be achieved by modifying the shape of the magnetic field profile in the test-cell region. Careful design of the field shape could lead to higher beta limits from MHD stability calculations (if the bad curvature drive could be reduced) and better confinement (if the effective mirror ratio could be increased). Both of these effects improve test-cell performance.

REFERENCES

1. B. G. Logan, et al, <u>Mirror Advanced Reactor Study (MARS): Final Design
    Report</u>, Lawrence Livermore National Laboratory, Livermore, CA, UCRL-53480
    (1984).
2. C. D. Henning, et al, <u>Fusion Power Demonstration: Baseline Report</u>,
    Lawrence Livermore National Laboratory, Livermore, CA, UCID-19975 (1984).
3. R. B. Campbell, <u>TMRBAR - A Code to Calculate Plasma Parameters for Tandem
    Mirror Reactors Operating in the MARS Mode</u>, Lawrence Livermore National
    Laboratory, Livermore, CA, UCID-19875 (1983).

Section 4
FPD-I

THE FPD-I CONFIGURATION OVERVIEW

The first option of the Fusion Power Demonstration (FPD) that we studied
is FPD-I (Fig. 4-1). This configuration has a central cell length of 74 m,
measured from the center of one choke coil to the other, and produces 360 MW
of fusion power. With a recirculating power of approximately 175 MW and a
power generation capability of 170 MW, this option can be expected, with minor
revision, to reach its goal of breakeven. With the addition of a test cell,
which can be configured in a manner similar to the Mirror Fusion Test
Facility α+T (MFTF-α+T)[1] concept, FPD-I will be able to provide a
neutron wall loading of 2.0 MW/m^2 to a surface approximately 3 m^2. An
evaluation of the configuration shows that a 50% availability goal can be met,
thus allowing an accumulation of 10 full power years over an operating
lifetime of 20 years.

The central cell is configured in a modular fashion using 10-m-long
central cell modules (Fig. 4-1). Each module is made up of a pair of liquid
lead, lithium-cooled blanket modules that can be inserted from opposite ends;
thus each blanket module will be 5 m long (Fig. 4-2). We chose this length to
limit the magnetohydrodynamic (MHD) effects on the blanket, while at the same
time meeting restrictions on the geometry and total module weight.

We selected a geometry where the central cell is divided into six 10-m
modules and two 5-m modules. The 5-m modules are paired with the choke coils
(Fig. 4-3) so that the high axial force acting on the portion of the central
cell solenoid coil closest to the choke coil can be carried by permanent
structure. Study of the axial magnetic loading on the solenoid shows that the
forces resulting from the choke coil are contained mostly within the first 5 m
of the solenoid. We also selected the 10-m length so that a complete module
will weigh less than 5000 tons, which we judge a reasonable upper limit for
handling and positioning by an overhead bridge crane.

The remainder of the module is composed of a surrounding nuclear shield
supported in a circumscribing vacuum vessel by a truss so that the shield can
be extracted from the end of the 10-m-long cylindrical vessel. Between the
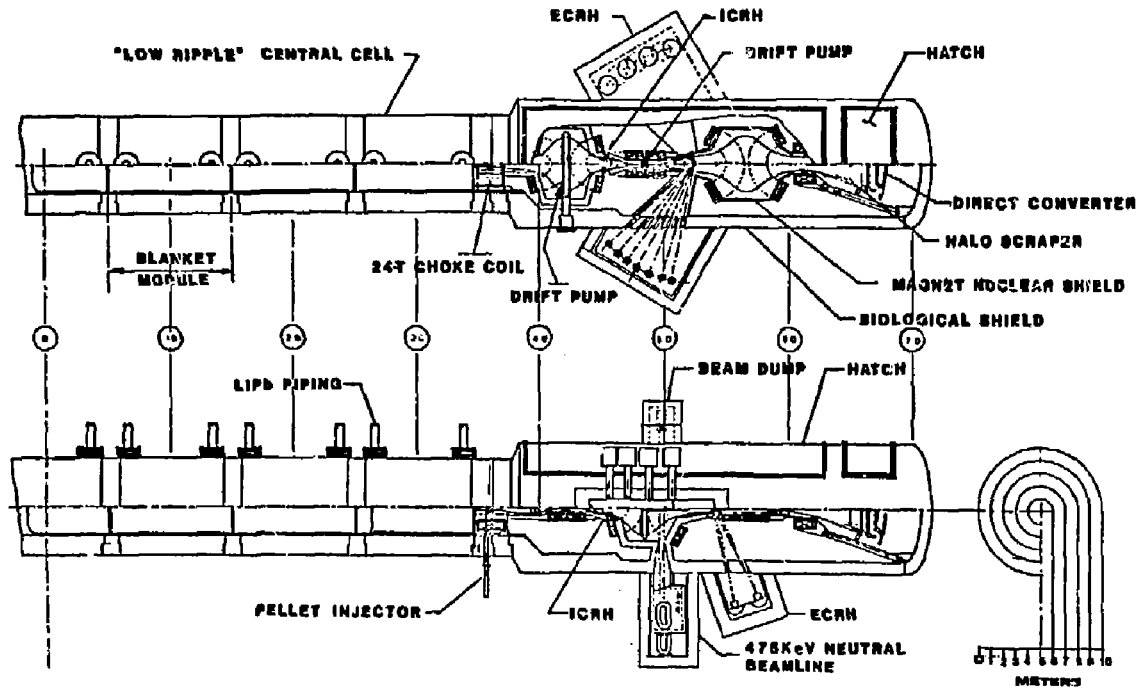
Figure 4-1. The first configuration for FPD (2/9/84).

BULKHEAD

BLANKET

REFLECTOR/
SHIELD

SUPPORT
LEG

SOLENOID COIL

OUTER
SHELL

INNER SHELL
(VACUUM BOUNDARY)

LONGITUDINAL
STIFFENER
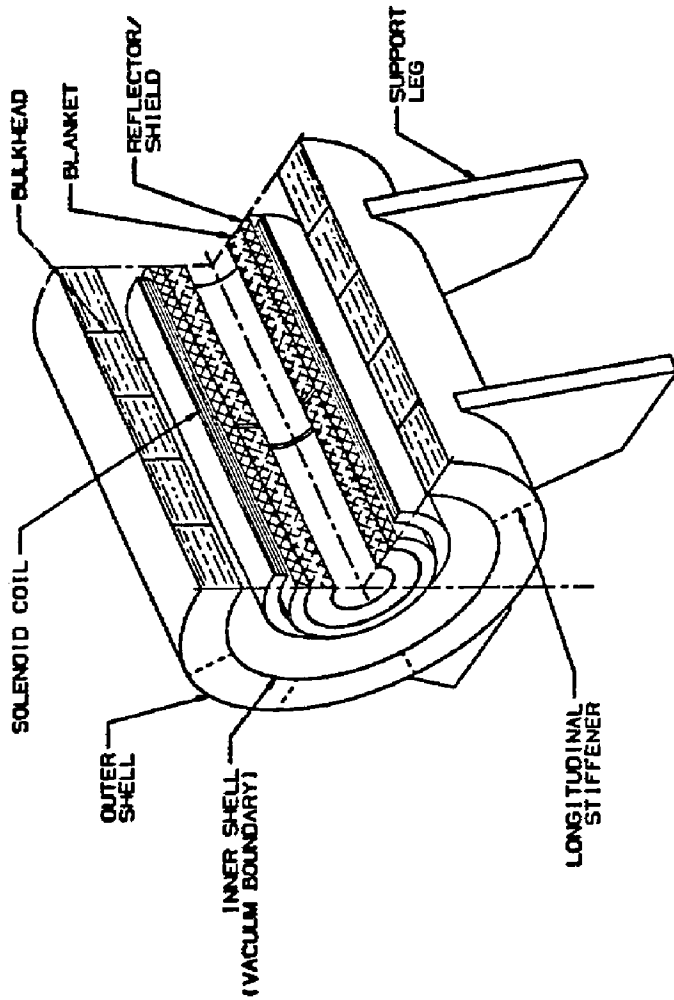
Figure 4-2. Typical central-cell-segment configuration.

4-3

BEAM DUMP
475KeV NEUTRAL BEAM LINE
LOCATION

MAGNET NUCLEAR SHIELD

DIRECT CONVERTER
HALO SCRAPER

GYROTRON

DRIFT PUMP
PELLET INJECTOR

AA

BB

HATCH OPENING
BIOLOGICAL SHIELD

ECRH

ICRH

BLANKET MODULE

CHOKE COIL
"LOW RIPPLE" CENTRAL CELL

METERS
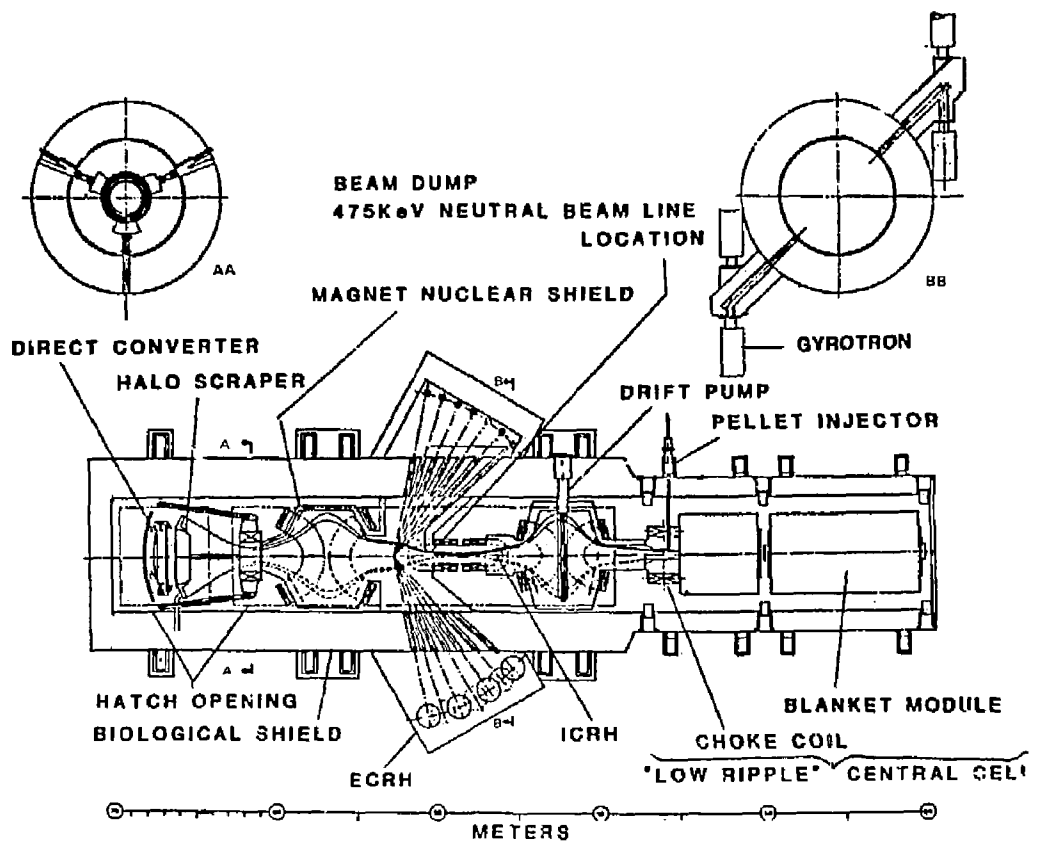
Figure 4-3. The configuration of FPD (2/22/84).

vessel and the nuclear shield lies a 9.25-m-long superconducting solenoid coil, which provides the 2.5 T central field. The solenoid coils are also supported for removal with the nuclear shield. Thermal isolation is provided by a system of struts to the main supporting truss frame. This configuration, which uses a long, thin solenoid, was developed to satisfy the need for minimum magnetic field ripple, a condition necessary to achieve high central cell beta. The vessel is of a double-walled construction that is filled with water. The water acting with a layer of B_4C and lead serves as a biological nuclear shield to reduce the radiation level to acceptable levels. A dose rate of 0.5 mrem/hour, twenty-four hours after shutdown, was established as a goal based on the as low as reasonably achievable (ALARA) guideline.

The choke coils create peak field on axis of 24 T. Each is constructed using a normal conducting insert coil together with a superconducting background coil. The choke coils are mated to their companion solenoid coils in a modular fashion. The module could be moved to provide access for replacement of the insert coil, which is not envisioned to be a lifetime component. The pancakes of the coils are slightly separated to make provision for the radial injection of fueling pellets from a rail gun (Fig. 4-3).

Each of the end cells are configured to permit easy assembly of the machine and to permit relatively easy replacement of all of the internal components, including the large C coils that are considered to be lifetime components. The concept employed is based on the design developed for the MFTF-α+T study.[1] The double-walled end-cell vessel contains a large hatch (Fig. 4-1), which is also of a double-walled construction. The double wall is used to contain the water that forms a part of the biological nuclear shield. It also provides an excellent structural support to the vacuum loading. The six C-shaped and one recircularizing solenoid superconducting coils are placed on cold tables, which are supported by a set of truss struts tied to the lower trough structure of the vessel. The coils are tied together by a set of axial struts that carry the axial magnetic loading to the end of the vessel. This approach has the advantage that, should it prove necessary to replace a coil, the replacement can be accomplished with minimal impact on the other coils and components that are operating satisfactorily.

Nuclear shielding is provided within the end cell coils to reduce the refrigeration load. This shielding reduces the fluence to the magnets, allowing them to become lifetime components.

The end cell heating subsystems consist of ion-cyclotron resonant heating (ICRH), electron-cyclotron resonant heating (ECRH), drift pumping, and negative-ion-based beam systems (Figs. 4-1 and 4-3).

The ICRH is applied to the transition region using a set of four loop antennae, which we selected because the coil winding configuration does not provide sufficient space for a rigid waveguide.

The ECRH is applied at two positions along the axis of the machine in each of the two end cells. The point "a" ECRH system requires one gyrotron to provide the basic power needed; a second one is placed to serve as an on-line spare. Access for these two systems, which employ a quasi-optical transport and launching system, is relatively straightforward. The point "b" ECRH subsystem is somewhat more difficult, primarily, because it requires 12 active and 2 spare gyrotrons. The quasi-optical transport and launching system was selected to make it possible to apply the required power through the relatively small space available. The launchers are arrayed axially so that the beams may pass through the major radius of the anchor one coil. The gyrotrons are mounted on a wing-like vacuum box with gate valves so that the gyrotrons can be replaced without bringing the whole vacuum system up to air.

Drift pumping coils are provided in pairs at two locations. These coils are arranged in a module together with a nuclear shield plug so that they may be withdrawn radially for replacement. This concept was conceived during the MARS effort and further developed for the MFTF-α+T study.[1]

Lastly, the 475-keV negative-ion-based neutral beamline subsystem is positioned to produce the required sloshing ion distribution in the anchor region. The integration of this system proved the most difficult of all tasks. The target point is located with respect to the C coils such that axial fanning of the beams from each of the three required sources is not possible. It is necessary that the three beams, two active and one on-line spare, be arranged in a circumferential fan as shown in Fig. 4-3. This arrangement, which allows marginal nuclear shielding in the throat of the adjacent C coils, has two major disadvantages. One disadvantage is the

possibility that a detailed evaluation would show that the nuclear shielding within the throat of the C coils must be increased in thickness, resulting in an increase in the coil size and therefore in the size of all of the coils. A second disadvantage is that access to two of the beam sources is more difficult.

The halo scraper and direct converter are considered lifetime components. These components can be removed, should this prove necessary, by lifting them vertically through their dedicated hatch (Fig. 4-1) in the vessel. This vertical lifting arrangement minimizes the length of the vault while being compatible with the vertical access philosophy of the rest of the components.

End cell configuration is, with the exception of the quasi-optical ECRH and circumferentially arrayed sloshing beamline, based on the earlier MFTF-α+T study.[1]

The configuration study for FPD-I broke new ground with the first look at the semi-continuous central cell solenoid design. We developed an attractive, modular approach (from both a commercial-reactor and an experimental-machine point of view). Further discussion of this concept is contained later in this report.

<center>FPD CHOKE COIL</center>

There are two choke coils in the FPD machine. Their present locations (C83 version) are at $z = \pm 48.00$ m, just outside of each end of the central cell. The choke coils are solenoids that produce a central axial field of 24 T (this includes the background field of about 1.0 T) produced by adjacent coils. These coils are physically constrained to consist of a clear inner bore of 0.3 m and a winding width of no more than 2.0 m. At this time any additional constraints due to coil supports, service line access, or adjacent coil structure are not defined.

The choke coil is a hybrid design in that it utilizes a resistive insert coil and a superconducting backing coil. This design is necessary because today's superconductor technology does not permit design of an all-superconducting coil in which the superconductor has to operate at fields larger than 16 T.

<center>4-7</center>

The FPD resistive insert design was derived from the Mirror Advanced Reactor Study (MARS)[2] choke coil design. This approach utilizes a spirally-machined disc of high-strength AMZIRC copper to create the coil.

A resistive insert producing 8 T on axis is our baseline. This coil has 26 pancakes, each 2.2 cm wide with 0.1-cm insulation between them. Two pancakes form a basic unit of the coil; they are joined by rivets and dowels at the center. Each pancake has three conductors, and each is machined to carry a soldered-in-place stainless steel coolant tube (stainless tubing is used to allow high coolant velocities). The tubing spirals down one pancake, crosses over to the other one at the hub, and then spirals out.

The coolant water is routed individually to each conductor of each first pancake and is then taken away individually from each conductor of the second pancake. This is repeated for all 13 double pancakes. The feasibility of manifolding the coolant lines will be investigated. Three current lead pairs are required. All three conductors are electrically common at the hub. The outer arms of the coil are joined by shear pins so that the tangential load of one conductor arm is reacted by that of its counterpart in the second pancake.

The outer radius of the resistive coil (not counting cooling lines, etc.) is 0.5 m and its width is 0.6 m. The current in each conductor is 33600 A, and the power consumed is 21.6 MW. We envision a resistive coil supported by struts from the superconducting backing coil.

Insulating the resistive coil is a problem because of neutron radiation. Organic insulators breakdown under radiation and suitable ceramic insulators are extremely brittle and expensive. The use of anodized metallic strips for electrical insulation is currently under investigation and early test results are encouraging.

Machining of the pancakes is a feasible operation. This feasibility is demonstrated by experience with two test pancakes. The electrical discharge machining (EDM) process was used to cut the spirals and an end mill was used to cut the coolant tube groove. The AMZIRC copper for the test coil was rolled and heat treated to an average yield stress of 57,000 psi. There was no evidence of distortion after machining.

The geometry of the resistive insert, including provision for the coolant tubes and any necessary radiation shielding, will define the inner radius of

the encircling superconducting coil. For an 8-T resistive insert, the inner radius of the superconducting coil is approximately 0.85 m. A peak field of approximately 16 T+ can be expected at the inner radius of the superconducting backing coil.

Preliminary calculations indicate that this coil should be cooled with He II and that the superconductor should be $Nb_3Sn:Ti$. The conductor should be steel reinforced to withstand the high hoop stresses developed, but its current density will be limited by cryostability considerations. The conductor would be graded as the field drops off with radius so that the superconductor could be changed to Nb_3Sn and then to NbTi.

For economical reasons, we expect that the superconducting coil will be a single unit rather than having two coils with separate cases. Figure 4-4 shows the 0.42 m^3 resistive insert coil and the 16.7 m^3 superconducting backing coil.

<center>CENTRAL CELL</center>

CENTRAL CELL MAGNET SYSTEM

The central cell magnet system consists of seven full-size modules. Each module has correction coils to reduce the ripple in the plasma region to an acceptable level.

System Function Summary

The central cell magnets confine the plasma over its entire length. The length of the central cell is determined by plasma requirements, such as sufficient particle-confinement time to ensure ignition.

Requirement Summary

The length of the central cell is 70 m. The field required on the plasma axis is 2.5 T, and the magnetic field ripple must be less than 1%. The central cell magnet system must be built from practical length modules. Axial
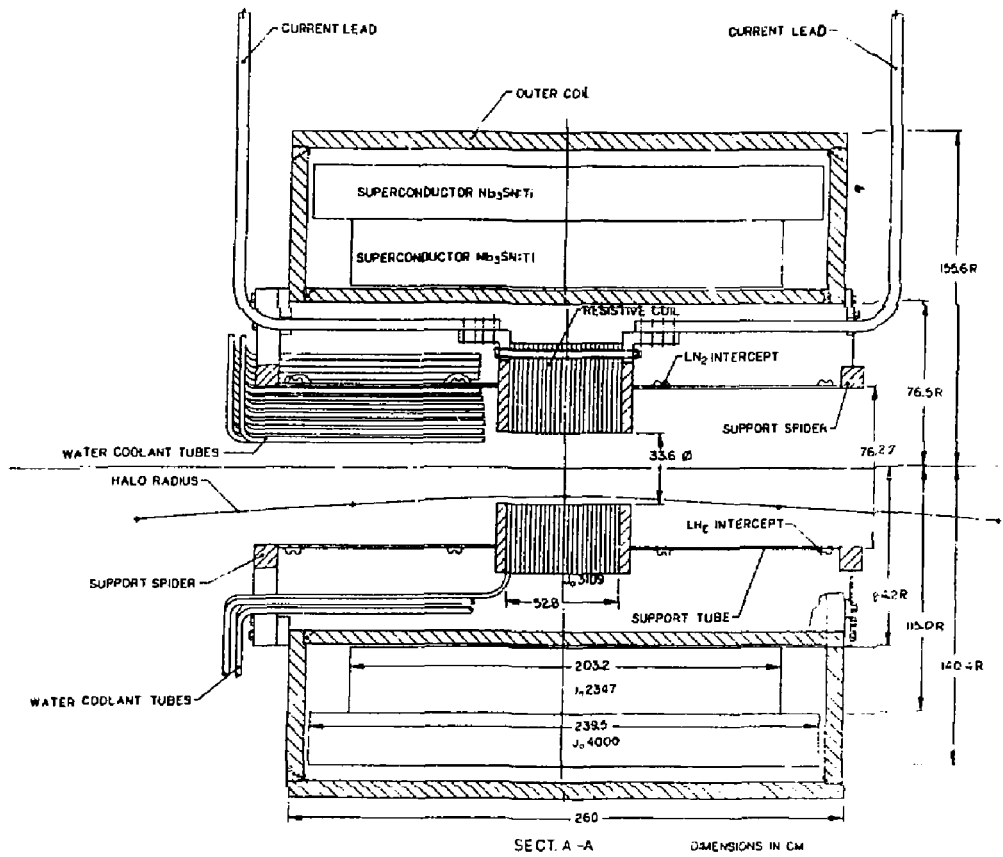
Figure 4-4. The FPD choke coil.

space must be provided between the adjacent modules to accommodate coolant
feed for the nuclear shielding and blanket systems located within the solenoid
module. The magnet structure must be adequate to withstand mechanical loads
such as magnetic loads, dead weight, 1-g seismic load (externally and
vertically), and operating pressure differentials.

The FPD is required to operate for 10 years. During this period, the
magnets will be energized and de-energized 12,000 times and warmed up 120
times. The magnet structure must be designed to withstand these events.

Magnet Layout

The central cell magnet wire bundle is shown in Fig. 4-5 along with the
key design parameters. Layout of a solenoid module is also shown. The
solenoid module is designed to achieve the desired current density of
6000 A/cm^2 at 3 T. The winding design is based on a Nb_3Sn cable-in-conduit
conductor and is cooled with forced-flow helium at 5.7 K. The solenoid winding
is a single layer of the force-cooled conductor. An additional layer (40-cm
axial length) is introduced at each end of the solenoid module to correct for
ripple. The conductor conduit thickness is 6.6 cm, which is four times
thicker than the Westinghouse LCP conductor conduit. The thicker conduit is
needed to carry the hoop load. It is impractical to fabricate 6.6-cm-wall
conduit, but it may be possible to build up the desired wall thickness from 3
to 4 concentric layers. Alternatively, it may be possible to utilize the
W-LCP conductor in an "as is" form. In this case, the conductor is cowound
with a stainless steel strip for carrying the hoop load. The average heat
load in each conductor is 0.12 mW/cm^3. This heat load can be removed by
5 g/s of helium flowing through a 10-turn cooling loop. The coil can be
safely discharged with 800 V (peak) without exceeding the hot spot temperature
of 280 K.

An alternative design was developed using NbTi conductor in the Mirror
Fusion Test Facility-B (MFTF-B) central cell coils. This conductor is cooled
with pool-boiling helium. The winding current density achieved with this
approach is 3000 A/cm^2 and the winding pack has 11 layers. Stress analysis
was performed with STANSOL computer code. It is difficult to control stresses
in the conductor unless a stainless steel strip is cowound with the conductor.

4-11
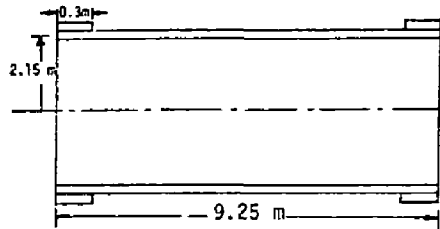
Central cell magnet dimension

Mean magnet radius (m)	2.15
Axial length (m)	70

Module dimensions

Module length (m)	9.25
Radial build (m)	0.06
Axial length of end-compensation zones (m)	0.3
Ampere-turns/module (MA-turns)	18.5
Current density, goal (A/cm^2)	6000
Field on axis (T)	2.5
Field at winding peak (T)	3.5
Nuclear heating peak (mW/cm^3)	1
Operating current (kA)	60
Energy stored in each module (MJ)	300
Weight x 10^5 (kg)	40

Figure 4-5. Central cell magnet parameters.

Conclusions

We concluded from feasibility studies of two alternative coil designs that a successful coil design can be developed with pool-boiling or forced-flow helium cooling approaches.

SHIELDING AND VACUUM CONTAINMENT

The overall proportions of the cylindrical central cell are shown in Fig. 4-6. The total length is approximately 74 m, and the outside diameter is 9.4 m. The shielding and vacuum containment consist of two basic components: *the coil shield to protect the coil from nuclear heating and the biological* shield for human protection, which is integral with the vacuum vessel.

The central cell is divided into eight modules. The six A modules are 10 mm in length. The two B modules, one at each extreme end of the central cell, are slightly over 5 mm in length. A typical radial composition of a module is shown in Fig. 4-2. Starting at the outside and moving inward, the first cylindrical layer is the integral vacuum vessel and biological shield. Next is the solenoid magnet, then the magnet shield, and finally the blanket/reflector region.

Vacuum Vessel/Biological Shield

The integral vacuum vessel/biological shield consists of two concentric stainless steel, cylindrical shells. The outer diameter is 9.4 m and the inner shell diameter is 7.0 m. The double-walled structure is stiffened with four bulkheads and eight longitudinal webs. The region between the shells is filled with water. The inner shell actually serves as the vacuum boundary.

To complete the shield, a 5-cm layer of B_4C with an additional 5 cm of lead, is attached to the outside of the outer vessel wall. The B_4C is packaged in stainless steel containers, and the shield performance is based on the composition of the filled container (40% stainless steel and 60% B_4C at 70% density).
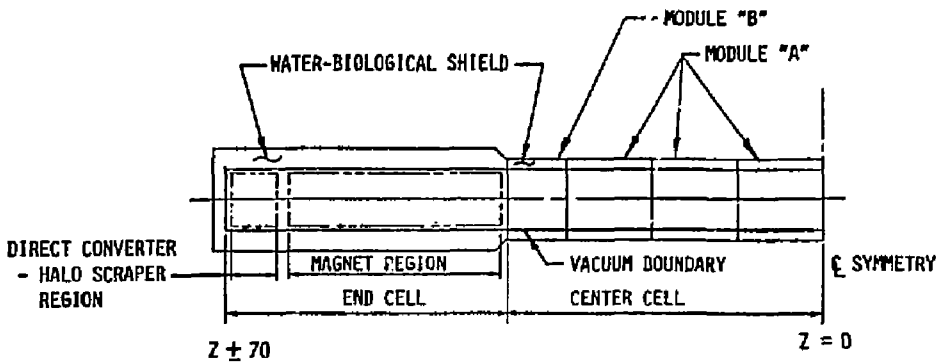
Figure 4-6. The FPD-I vacuum vessel and shield regions.

Figure 4-7 illustrates the manner in which the biological shield/vacuum vessel is integrated with some of the other module components. Because the blanket is divided into two parts, a $Li_{17}Pb_{83}$ (LiPb) inlet and outlet manifold are located near each end of the module. The LiPb enters the module at the top and flows out the bottom. Because the point at which the LiPb enters the blanket is at the extreme end, a potential neutron streaming path exists at the end of each module. This path is blocked in the assembly of the modules by removable water-shield plugs and an inner, steel/water shield plug, covering 180° of the gap between modules.

Magnet Shield

The solenoidal sheath magnet is protected from nuclear heating by an inner cylindrical steel/water shield (see Fig. 4-7). This shield is 75-cm thick and consists of 80% stainless steel and 20% water. In addition, a 5-m-thick layer of B_4C is placed at the other periphery of the steel/water shield.

The magnet shield serves also as a structural member to which the blanket segments are attached and is the support for the magnet itself. The support struts are illustrated in Fig. 4-8.

SUPPORT STRUCTURE

Each central cell module is supported by a set of four legs (Fig. 4-2) attached to the outer shell of the vacuum vessel/biological shield. The legs, which are in line with bulkheads that connect the inner and outer shells, (Fig. 4-2) transmit all loads to reinforced concrete piers (Fig. 4-9).

END CELL MAGNETS

The end cell magnet system consists of two transition (T), two plug (P), and two anchor (A) type C coils. A recircularizing coil is also needed as shown in the FPD-II configuration (Fig. 5-22 in Sec. 5). All C coils in the end cell region are similar in size and ampere-turn requirements. A summary of various coil dimensions and their ampere-turns is given in Table 4-1.
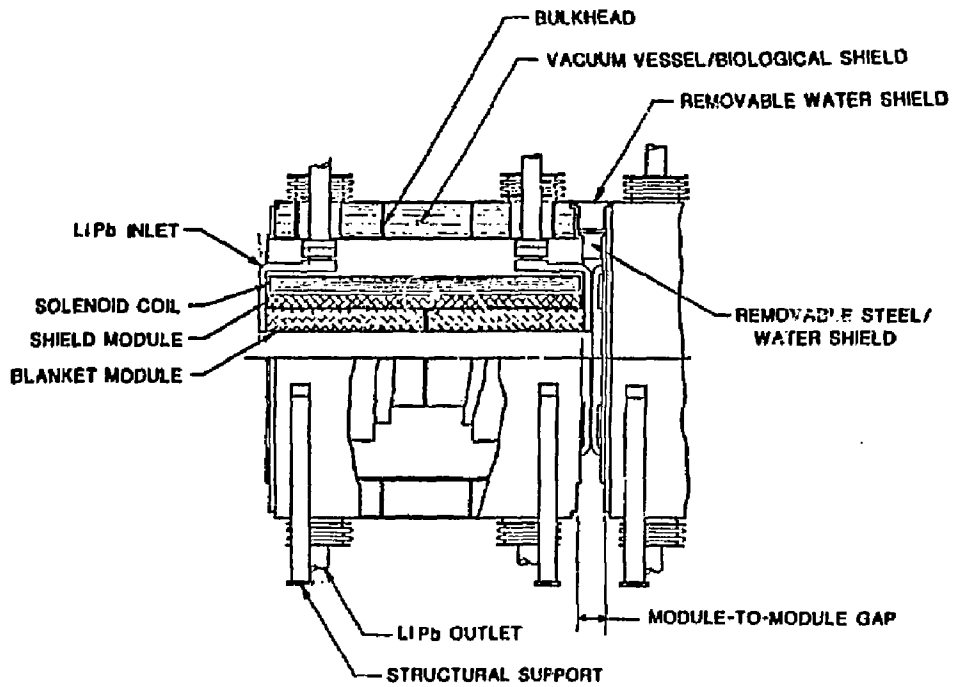
Figure 4-7. The FPD-I central cell module.

SOLENOID COIL

BULKHEAD

BLANKET

OUTER SHELL

REFLECTOR/ SHIELD

INNER SHELL (VACUUM BOUNDARY)

SUPPORT LEG

LONGITUDINAL STIFFENER
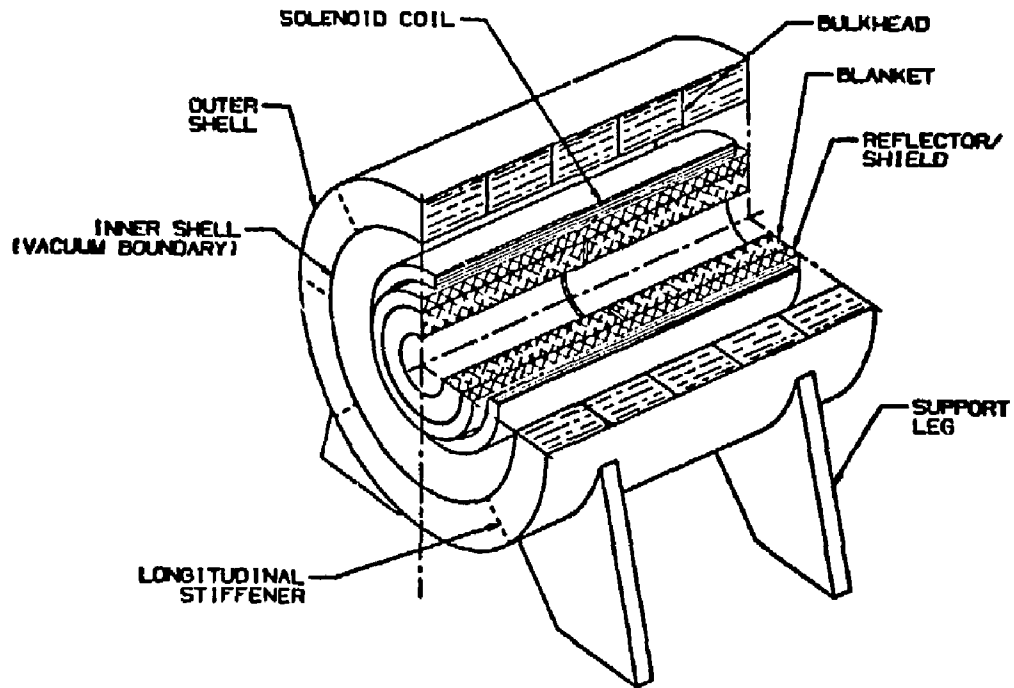
Figure 4-8. Typical FPD-I central cell module.

LI Pb INLET PIPE ⎯

LIPb INLET SUPPORT

VACUUM BOUNDARY ⎯

BLANKET MODULE

POWER CONNECTION ⎯

SHIELD

SOLENOID COIL

SUPPORT LEGS ⎯

SUPPORT STRUCTURE
4 REQ'D
TYPICAL BOTH ENDS

SHIELD COOLANT INLET ⎯

LIPb OUTLET PIPE
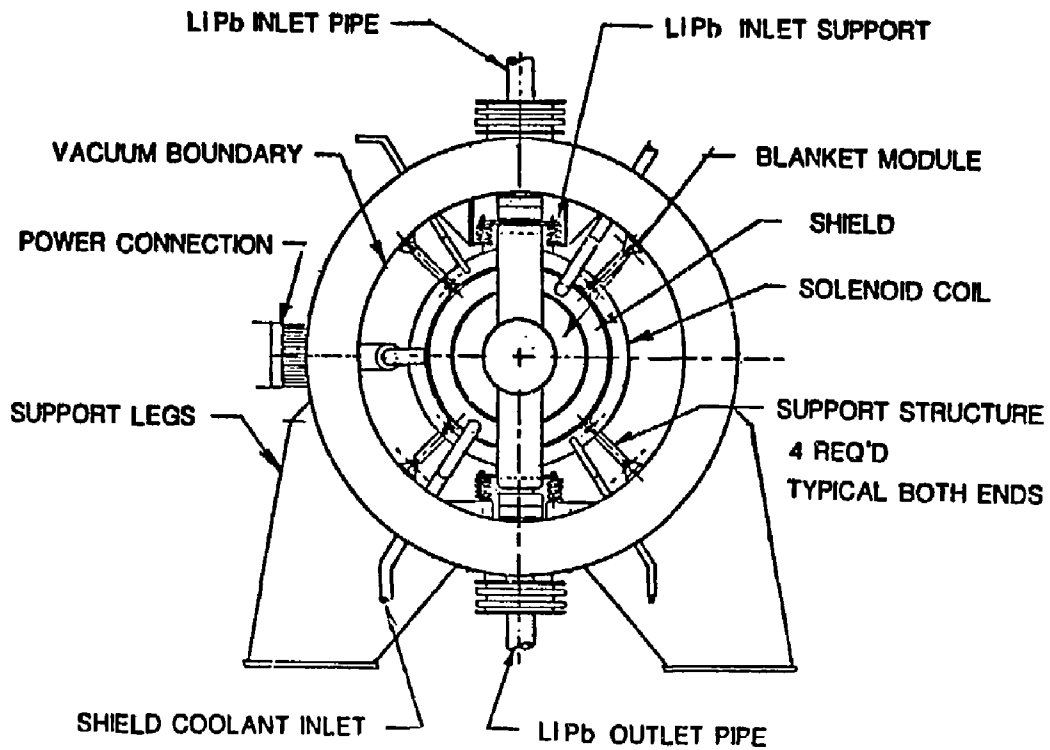
Figure 4-9.   End view of the FPD-1 central cell module.

Table 4-1. Main parameters of end-cell coils for FPD.

Coils/parameters	T1	A2/A1	P2/P1	T2
Axial location (m)	40.0	46.2/44.3	53.6/51.4	59.5
Major/minor radii (m)	1.5/0.8	1.5/0.8	2.25/0.8	2.25/0.8
Sweep angle (deg)	75	75	61.5/75	61.5
Winding dimensions S1/S2 (m)	1.2/0.3	1.2/0.3	1.2/0.3	1.2/0.3
Coil current (MAT)	11.37	11.37	13.78	13.78
Winding current density (A/cm^2)	3158	3158	3828	3828
Peak field on the axis (T)	6.0	6.3	7.5	7.5
Peak field at the coils (T)	8.2	8.2	9.7	9.5

In general, the generic end-cell C coil and recirculating coil requirements for FPD-I and FPD-II are similar. The coils employ the same type of conductor winding and structural supports. Even the fabrication/manufacturing problems are similar.

The FPD-II end-cell magnet set with slightly higher fields and current densities, but smaller winding pack, represents an evolution of the FPD-I design. C-coil design concepts are discussed below.

System Function Summary

The magnet system is sized and arranged to provide the on-axis magnetic field required for plasma performance. In addition, the end cells plug the machine and provide MHD stability.

Requirement Summary

On-Axis Field. The axial field profile in the end-cell region is shown in Fig. 4-10. The maximum center-line field in the end cell is 7.50 T at ±56 m. The minimum center-line field in the end cell is approximately 1.9 T at ±52.5 m.
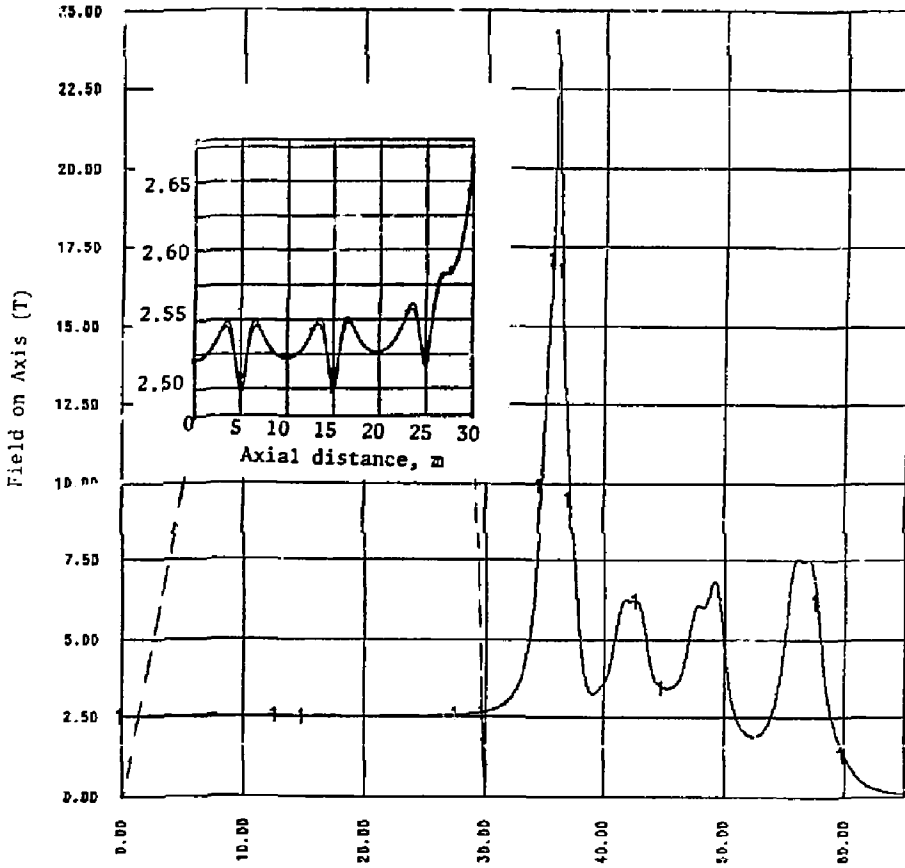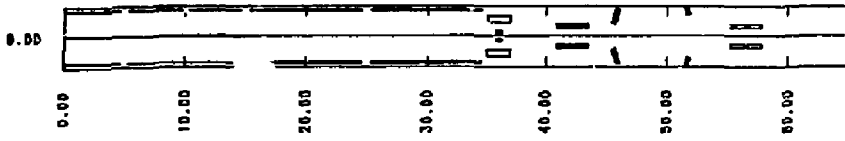
Figure 4-10. Field profile along z-axis.

Magnet Configuration and Design

The configuration for the FPD-I end cell is shown in Fig. 4-11. Locations, dimensions, currents, current densities, and fields associated with this configuration are shown in Table 4-1. This conceptual coil set meets the requirements summarized above. Specifics of conductor, structure, winding approach, and fabrication as noted above are basically the same for FPD-I and FPD-II C coils. These items are discussed in Sec. 5.

PLASMA HEATING SYSTEMS

The FPD I design is of the MARS tandem mirror configuration; consequently, the required end cell heating systems are similar to those for the MARS reactor,[2] and the subsequent MFTF-α+T device.[1] The ICRH is used to maintain high beta in the anchor cell, ensuring overall device stability. In the plug, a high energy negative-ion-based neutral beam (NINB) creates the sloshing ion distribution that provides microstability and contributes to the existence of the central-cell ion-confining potential peak. Also in the plug are two electron cyclotron resonant heating (ECRH) systems: one produces the thermal barrier that isolates central cell electrons from those in the potential peak region and the other system enhances the magnitude of the potential peak. Table 4-2 summarizes the heating systems' requirements. The sloshing beam trapping fraction is calculated in the tandem mirror reactor physics code (TMRBAR), whereas the remaining trapping fractions are educated guesses.

ECRH Systems

Two ECRH systems operate in the plug region. The thermal barrier system at point b is the highest power heating system and has the largest impact on the overall plug configuration. At 19 MW, an ECRH system based on current >200-kW gyrotrons and low efficiency transmission systems would be awkward and expensive. Hence as in MARS,[2] but on a more conservative note, 1 MW gyrotrons in the 30- to 60-GHz frequency range are assumed to be available in the FPD time frame. Because no beam recovery is expected in the conventional

4-21

CC1 to CC11

CCC1

T1   A1

A2   P1

P2   T2

(11.43)
11.5 cm Nom.

(8.89)
9 cm Min.*

(15.77)
14 cm Nom.
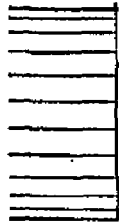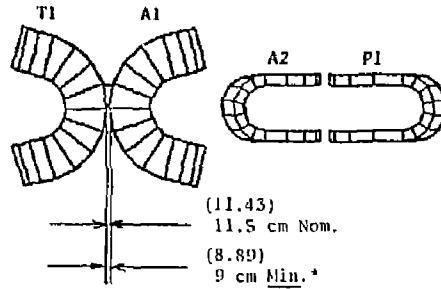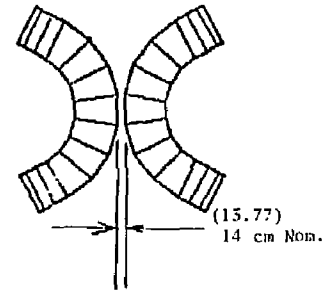
1. Case thicknesses based on plate bending only (no buckling deflection or stress concentrations included)

2. Assumes cases touch or are connected

CC1 to CC11

CCC1

T1   A1

A2   P1

P2   T2

(11.43)
11.5 cm Nom.
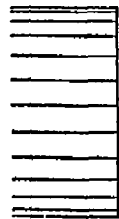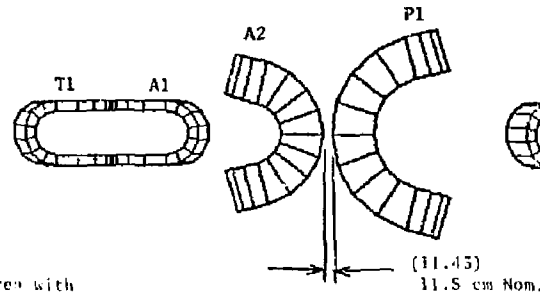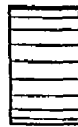
3. *Min. = Locally thin area with additional stiffening between coils

Figure 4-11.   The FPD-I end-cell configuration.

Table 4-2. The FPD-I heating system requirements.

	Anchor ICRH	Sloshing NINB	Potential peak ECRH	Thermal barrier ECRH
Heating point	--	a'	a	b
Location, z (m)	±43.65 & ±46.90	±50.0	±53.9	±52.55
Absorbed power (MW)	2.0	0.44	0.83	16.2
Trapping fraction	0.60	0.27	0.85	0.85
Delivered power (MW)	3.5	1.64	1.0	19.0
Vacuum frequency (Hz)	71.0×10^6	--	72.8×10^9	56.0×10^9
Heating frequency (Hz)	54.0×10^6	--	56.0×10^9	35.0×10^9
Delivered current (A)	--	3.5	--	--
Beam energy (keV)	--	475	--	--
Injection angle ($\perp$ to z-axis)	--	$30°$	--	--

closed-cavity gyrotron, we assume gyrotron efficiencies between 45 and 50%. To scope the transmission system and its efficiency, we also assume a TE_{02} output mode. These assumptions are justified based on current developmental program results and trends. The thermal barrier system, therefore, utilizes 1-MW tubes, whereas the potential peak system needs only 678-kW sources.

Technically, 1-MW power levels are achievable in 2-1/2-in. waveguides, but only at high pressures of sulfur hexafluoride. Windows then become an issue, especially in a fusion neutron environment. To eliminate windows and increase efficiencies, a vacuum quasi-optical transmission system has been utilized. Table 4-3 summarizes the ECRH systems configuration and key parameters.

At 35 GHz, the divergence angle of a quasi-optical beam is significant; to limit the beam size through the magnet region and at the plasma, an offset dual mode horn with parabolic reflector is used (see Fig. 4-12). The apex of

Table 4-3. The ECRH system summary.

● ECRH configuration

One ECRH transport system at each end for the point "a" ECRH system; two beam launchers per system (one operating/one redundant)

Two ECRH transport systems at each end for the point "b" ECRH system; seven beam launchers to system (6 operating/1 redundant)

● The ac/dc conversion is accomplished by two 30-MW ac/dc converter/transformers with one at each end of the device

Efficiency: 98%

● The 1-MW gyrotrons have a regulated (modulator/regulator tube) cathode voltage of 80 kV

Efficiency of modulator/regulator: 96%

Gyrotron rf-to-beam conversion efficiency: 45%

● The gyrotron-launcher interface is an evacuated circular waveguide section with mode converters to properly prepare the wave mode for the launcher

Efficiency: 76.8%

● Offset dual mode conical horn/parabolic reflector beam launcher

Efficiency: 96% (includes beam scrapeoff loss)

● Total system parameters

Efficiency: 32.5%

LHe requirements (for gyrotrons): 26 ℓ/hr

LN_2 requirements (for gyrotrons): 13 ℓ/hr

Cooling water requirements: 12,500 gpm

PARABOLOIDAL REFLECTOR
$X^2 + Y^2 = 4f(Z + f)$

CONICAL HORN
$y^2 + (Z - Z_0)^2 = k_0^2 X^2$

$k_0 = \tan a$

CONVERGING BEAM
(ZERO DIVERGENCE)
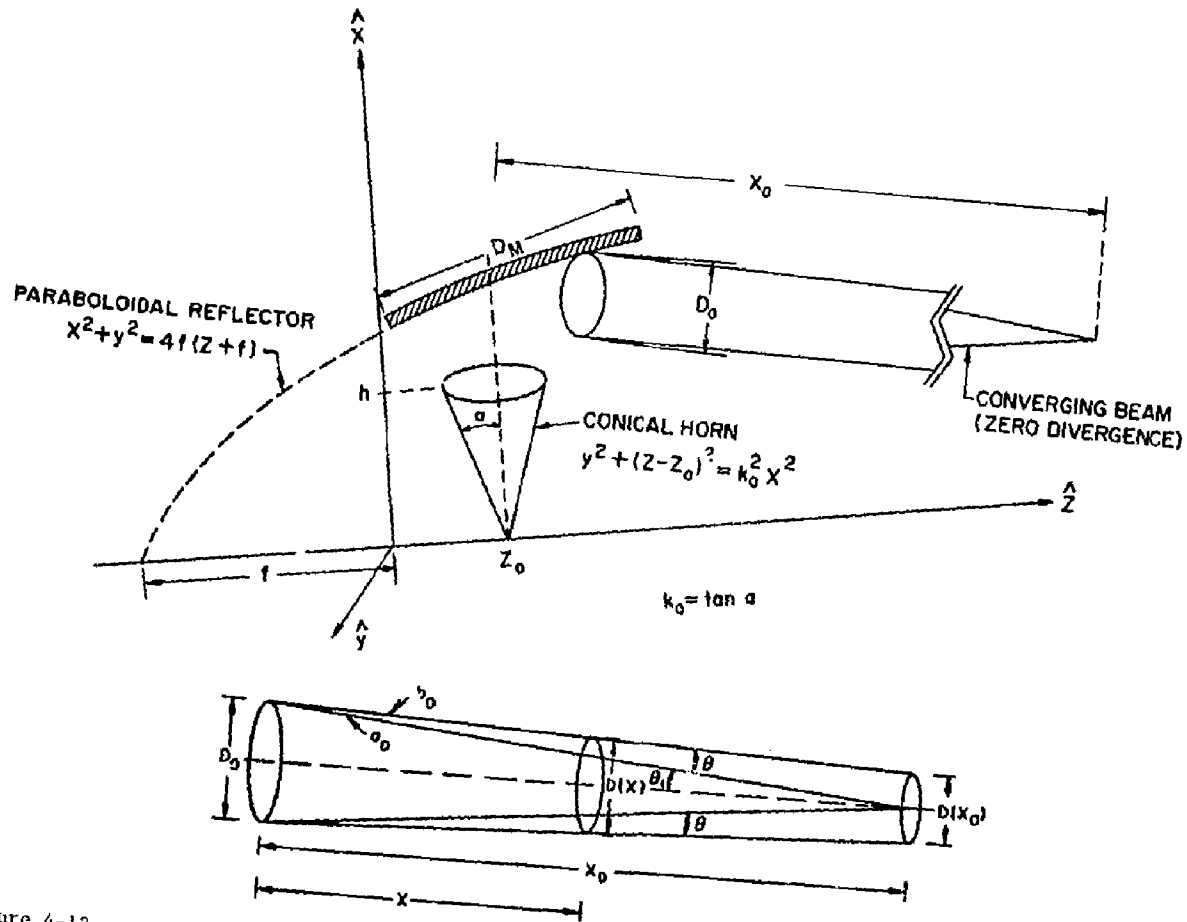
Figure 4-12. The ECRH beam launcher geometry.

the horn does not lie at the focal point of the reflector; the beam is thus focused. The launcher parameters for both ECRH systems are listed in Table 4-4 and a block diagram of the waveguide section, an interface between the gyrotron and launcher, is shown in Fig. 4-13.

The integration of the ECRH systems into the plug is depicted in Fig. 4-14 and the overall power flow is shown in Fig. 4-15.

Table 4-4. The ECRH launcher characteristics.

| | At "a" | | At "b" |
	Offset conical	Horn parabolic	Reflector
Conical angle, α (deg)		17	
Cone height, h (cm)	54.7		68.2
Paraboloid focal length, f (cm)	35.5		43.73
Mirror diameter, D_m (cm)	70.0		85.0
Initial beam diameter, D_0 (cm)	49.3		62.4
Distance from beam focal point, X_0 (cm)		9.5	
Distance to magnets, X (m)		∿7.5	
Maximum beam diameter in magnet region, D(X) (cm)	24.0		27.0
Beam diameter at plasma (cm)	14		17
Number of ECRH launchers/end	1		2
Number of beam launchers/ECRH launcher	2		7
Launcher transmission efficiency (includes 2% scrapeoff loss) (%)	96		96

INTERFACE

GYROTRON	ARC DETECTOR	MODE FILTER	D C BREAK	HIGH POWER SWITCH	DIRECTIONAL COUPLER	$TE_{02} \rightarrow TE_{01}$ MODE CONVERTOR	$TE_{01} \rightarrow TE_{11} + TM_{11}$ MODE CONVERTOR	CONICAL HORN
	(0.01)	(0.05)	(0.005)	(0.06)	(0.02)	(0.04)	(0.04)	(0.02)

WATER LOAD
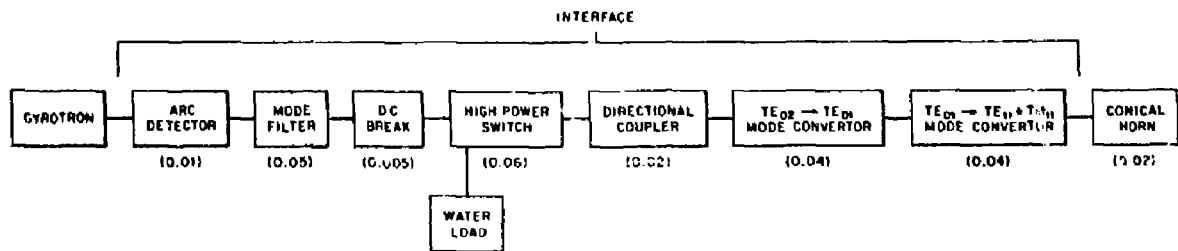
Figure 4-13. The ECRH gyrotron quasi-optical launcher interface. The values in parenthesis denote fractional power loss.
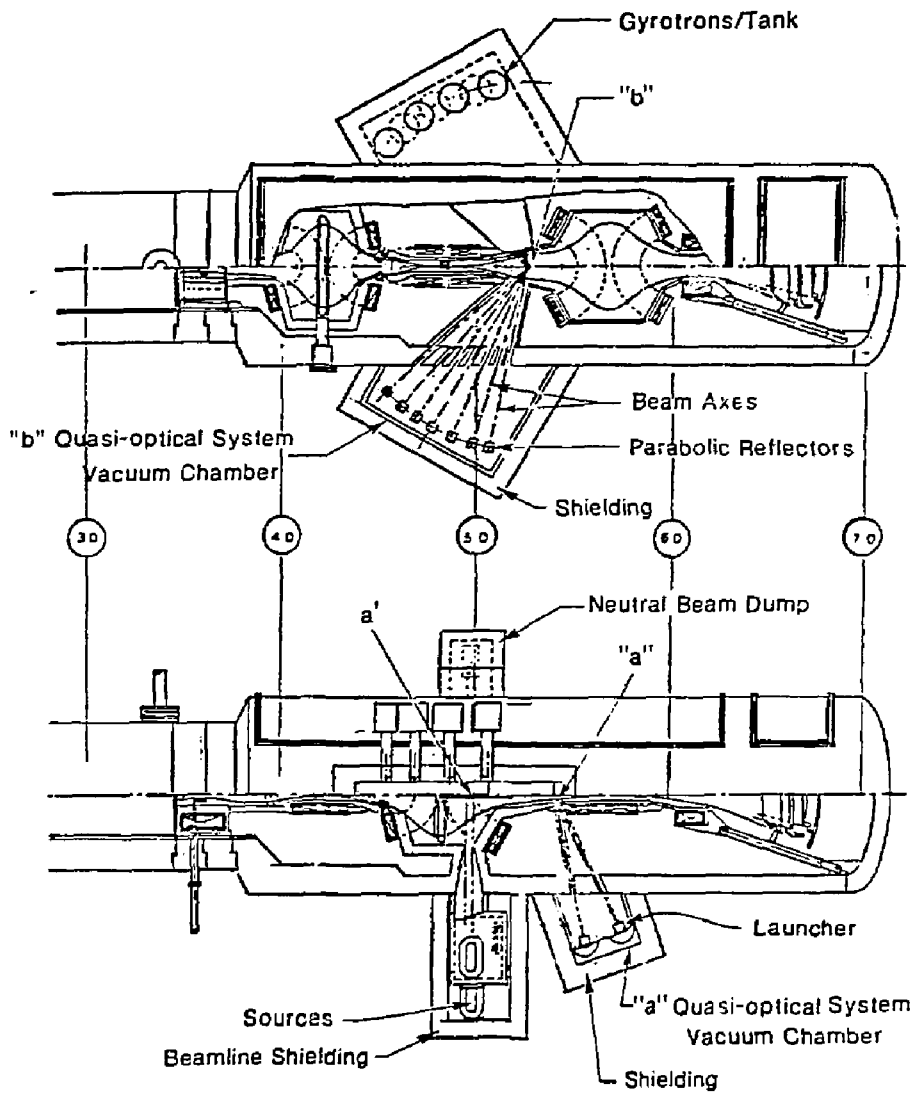
Figure 4-14. The ECRH transport system configurations in the plug region.
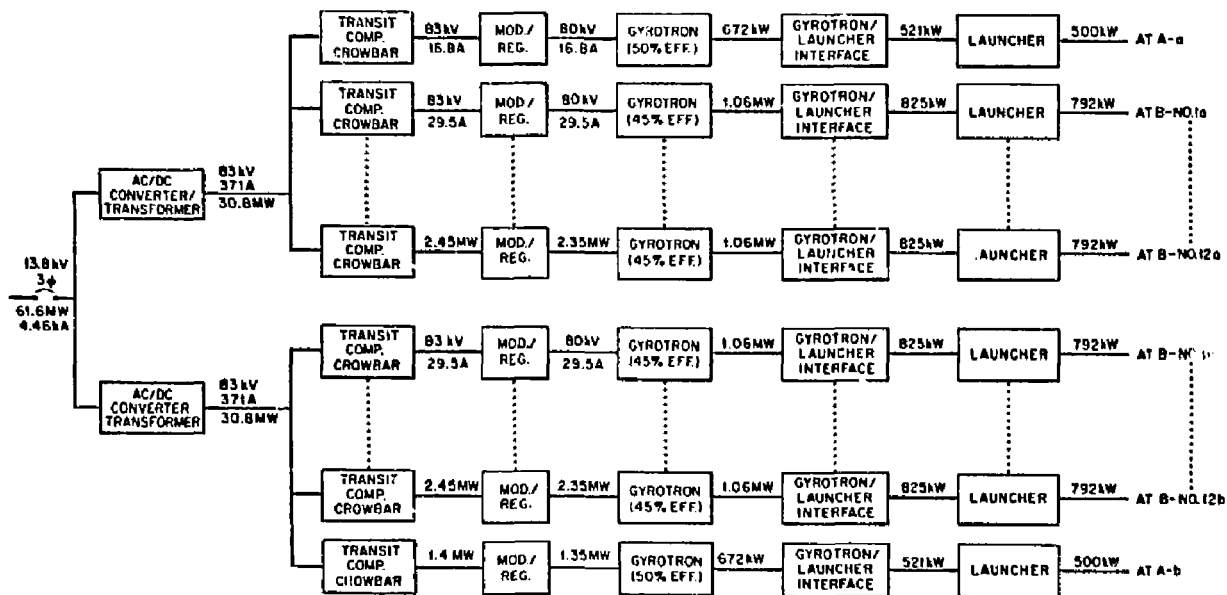
Figure 4-15. The FPD-I ECRH system power flow.

Anchor ICRH System

The anchor ICRH system must deliver 1.75 MW to each end cell at 54 MHz.
With the exception of waveguide vs loop antenna selection for the launcher,
the FPD I anchor ICRH system is considered conventional for plasma heating
applications. At 54 MHz, the width of a ridged-waveguide that is expected to
couple well to the plasma is slightly greater than 1.6 m; the plasma boundary
changes drastically in the anchor yin-yang magnet pair over this length. To
align the waveguide mouth parallel to the plasma surface within the geometry
constraints of the region, one of a number of waveguide distortions are
required (e.g., bends or oblique cuts of the face of the guide). Heating at
higher harmonics decreases the waveguide size, but fourth or fifth harmonics
are required before the contortions can be eliminated or become tolerable. At
the high ion temperature, this scenario may be plausible, but much analysis
will be required before a decision of this sort can be made. We have thus
opted for a loop antenna.

The description and expected performance of the system are summarized in
Fig. 4-16 and the following:

- Configuration:
  Four launchers per anchor (2 operating/2 redundant)
- Launcher: Center-fed loop antenna with Faraday shield
  Antenna power: 875 kW
  Efficiency: 95%
- Transmission System:
  Mainly 6-1/8-in. 50 Ω coax, taper down to 3-in.
  before entering minor radius gap
  3-stub turning system
  Efficiency: 84.7%
  Coolant loops:
  No. 1: Launcher and back to stub tuner
  20 gpm while operating
  7 gpm while not operating
  No. 2: Remainder--8.5 gpm

ABSORBED POWER: 2 MW

TRAPPING FRACTION: 0.6

DELIVERED POWER: 3.5 MW

$B_{R,VAC}$: .4.65 T

B_R: 3.56 T

HEATING FREQUENCY: 54 MHz

LAUNCHER: LOOP ANTENNAS
2/2 PER END

TRANSMISSION LINE: 6 1/8" – 50 Ω COAX
ONE LINE/LAUNCHER

TRANSMITTER: MULTI-STAGE CHAINS

EFFICIENCY: 53.5%
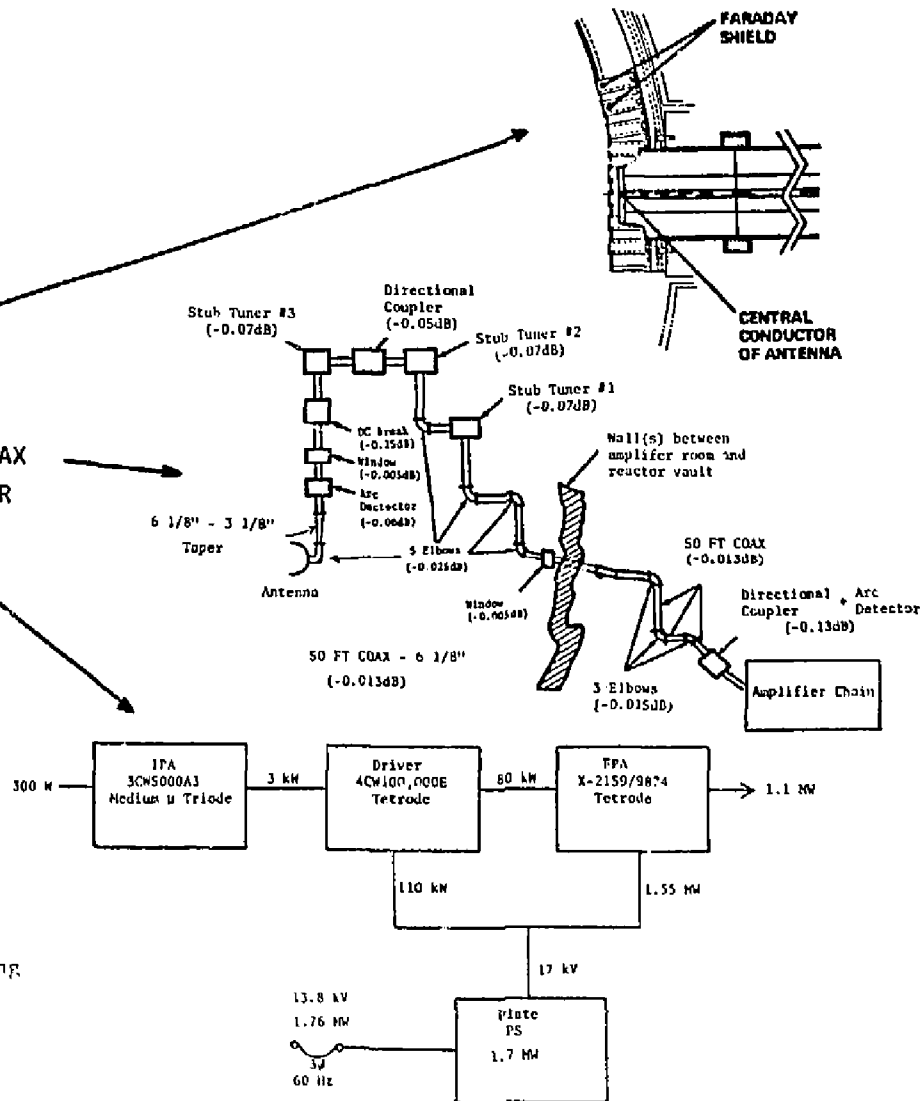
Figure 4-16. Ion-cyclotron resonant heating
(ICRH) system summary description.

- Transmitter: multistage
  Power supply
  Efficiency: 61.9%
  Coolant loop: 225 gpm
- Performance:
  Total line power: 7.04 MW
  Total system efficiency: 49.7%
  Total water coolant requirements: ∼1000 gpm.

Note that the power handling capability of the antenna corresponds to current experimental levels and is below that which could be expected in the FPD time frame. This result was not a result of conservatism, but arose because the 1.75-MW line requires a more complex and less efficient amplifier chain and consequently was a more costly system than one with two 875-kW lines.

Sloshing Negative-Ion Neutral-Beam (NINB) System

Each plug has one beamline that delivers 1.75 A at 475 keV of deuterium. The technology assessment and development required for this system have been well documented elsewhere and will not be repeated here.[2,3] The basic system consists of a self-extraction source with an 80-kV pre-accelerator, a transverse field focusing (TFF) transport and high voltage accelerator system, a gas neutralizer, and an ion-bending magnet and dumps, all contained in a vacuum vessel surrounded by magnetic shielding. The sources are similar to the current Lawrence Berkeley Laboratory (LBL) sources except for an rf plasma generator (vs filaments) and forced cesium diffusion from the back of the convertor plate (rather than a CS jet) to enable steady-state operation. The current level per meter is below both present source capability and future expected levels. The TFF concept is currently under development at LBL with a proof-of-principle experiment expected later this year. Since FPD is more near term than a MARS scale device,[2] a more conservative; i.e., lower power, laser system was assumed available than for MARS, resulting in roughly the same 60% neutralization efficiency as for a gas neutralizer. Because of the low delivered current (power) requirement, similar neutralization efficiencies,

and because the laser costs are greater than those associated with the increased gas load of a gas neutralizer, the gas neutralizer was chosen.

Figure 4-17 shows the beamline in context to the end plug configuration, whereas Table 4-5 and Figs. 4-18 and 4-19 describe the system to the next level of detail. Figure 4-20 is a power flow diagram for a beamline. The beamline power and current efficiencies are 43% and 41.9%, respectively; the fact that most of the current is lost at low energy is partially offset by the lower power supply efficiencies at the higher voltages.

DRIFT PUMPING

Requirements

There are two points in the end cell where drift pumping is required: the transition and plug cells. Drift pumping is accomplished by perturbing the geodesic curvature of the end cell's magnetic field. This enhances the radial drift. Table 4-6 shows the detailed requirements of this perturbation field for the transition and plug cell. The frequency is the center of the frequency spectrum, whereas Δf is the spectral width either in percent of center frequency or in kHz. The modulation does not have to be discrete tones (12 or 110), but tones are probably the easiest to implement because of the broad spectrum required. Finally, there is the specification of the perturbation flux in webers. If a coil configuration is assumed, in this case a MARS-like coil, then the circulating power required to create this flux can be calculated. Because the coil operates in close proximity to the shield surfaces, eddy currents are expected. These were calculated on the MFTF-α+T project[1] and are determined here by scaling.

Configuration

Arrangements of power amplifier chains with each chain passing one or more frequencies, are planned. These channels feed a pair of drift pump coils (one on each side of the plasma), which are connected in series. The output
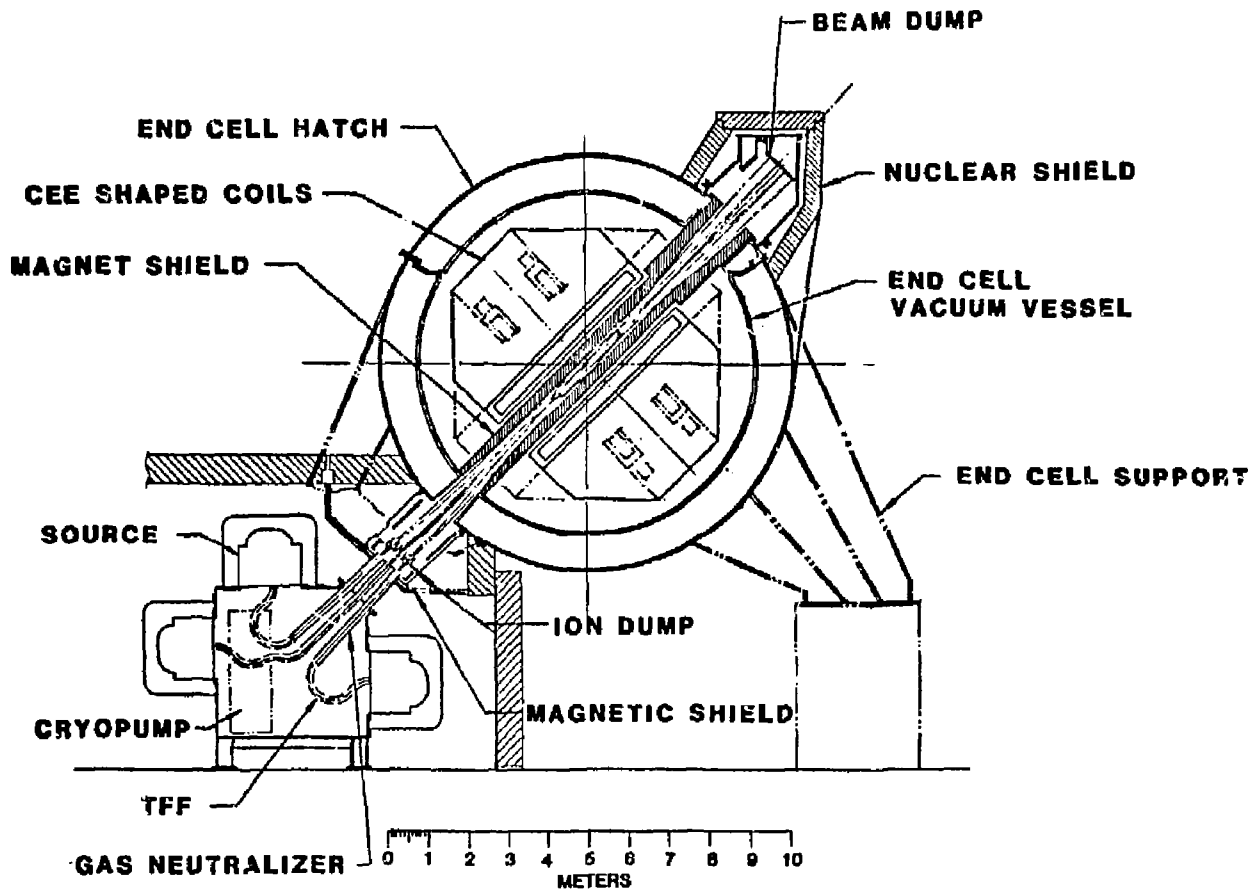
Figure 4-17. The 475-keV NINB configuration (sloshing beam).

Table 4-5. The NINB system summary description.

o Configuration:

   One beamline per plug;

   Three sources per beamline (2 operating/1 redundant).

o 2.1-A LBL-type self-extraction source at -475 kV, 2 x 50 cm^2 ribbon beam:

   RF plasma generator in magnetic multipole bucket containment;

   Forced cesium diffusion through converter plate;

   Small transverse magnetic fields to divert electrons;

   Standard 80-kV single-slot preaccelerator;

   Gas efficiency: 12% → gas flow: 3.1 T ℓ/s.

o The TFF transport and high voltage accelerator:

   80-kV TFF transport section (LEBT) at -395 kV with multistage
   differential pumping + 7.5 m^2 cryopumps;

   Four stage TFF high voltage accelerator (-305 kV, -220 kV, -135 kV,
   -50 keV);

   High energy beam transport section (HEBT);

   TFF focusing voltages range from ±25 kV to ±50 kV;

   Divergence: 0.45° x 1°;

   Pressure 1 x 10^{-5} Torr.

o Gas neutralizer:

   Optimum gas thickness: 6.5 x 10^{15} cm^{-2};

   Average gas pressure <p> = 7.5 x 10^{-4} Torr;

   Approximate dimensions: H x W x L = 15 cm x 55 cm x 130 cm;

   Gas load: 5.72 T ℓ/s.

o Ion magnet/dump region:

   Pressure 1 x 10^{-5} Torr;

   3.6 m^2 cryopumps.
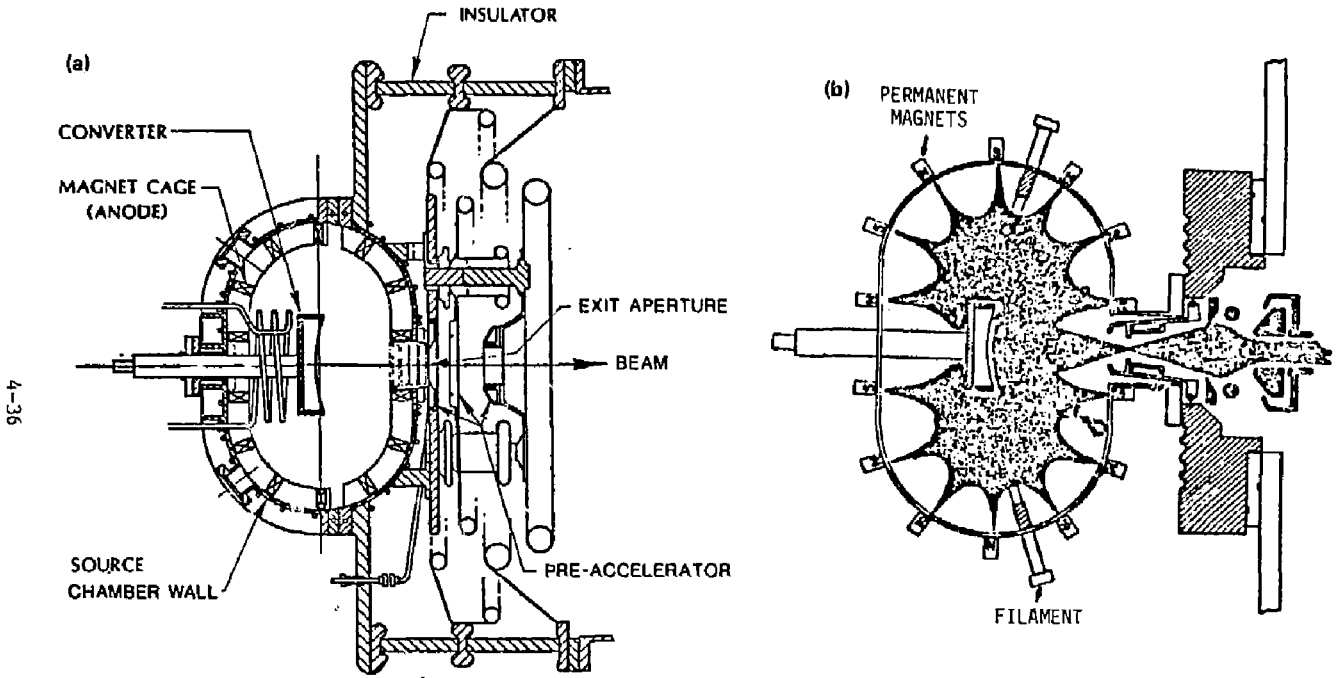
Figure 4-18. Negative ion source: (a) Self-extraction source with an rf plasma generator; (b) LBL Monte Carlo simulation of present filament driven source.
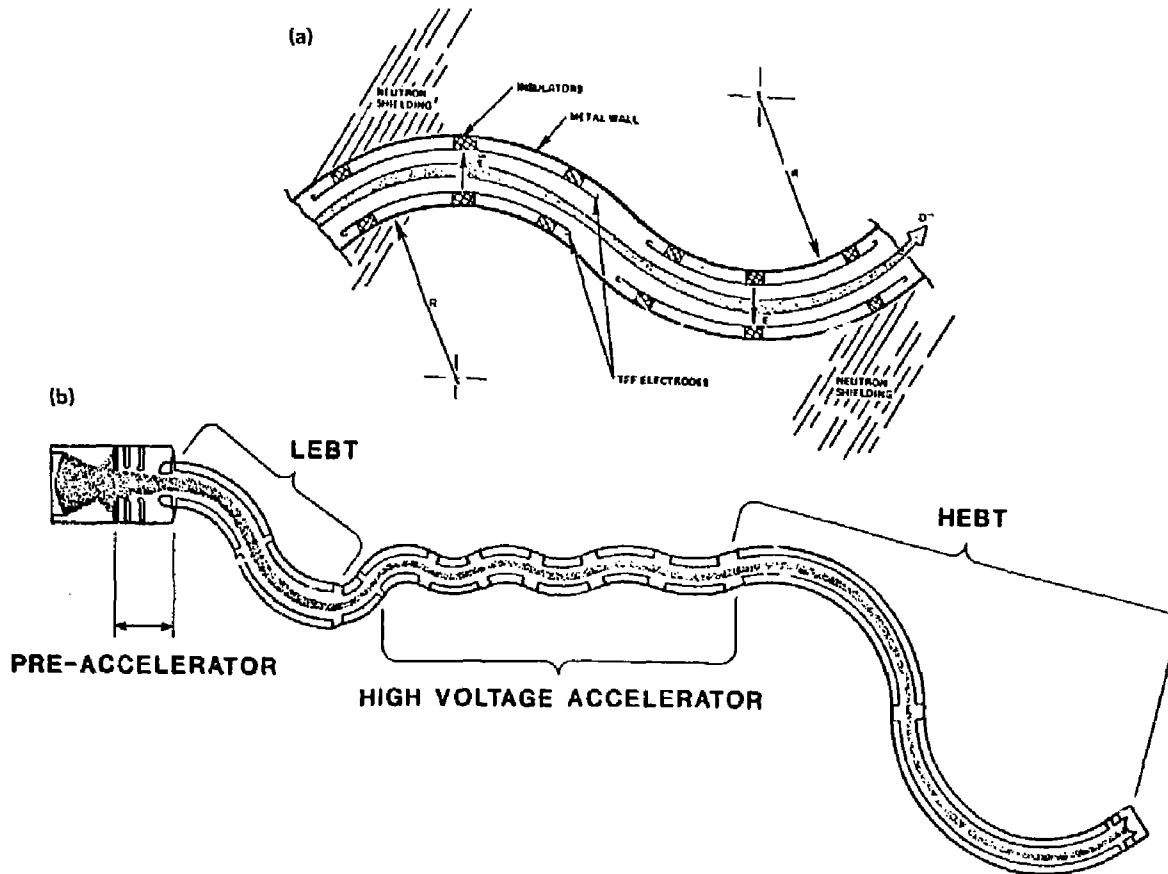
Figure 4-19. The TFF accelerator and transport system: (a) LBL Monte Carlo simulation of source and transport system; (b) section of TFF system.
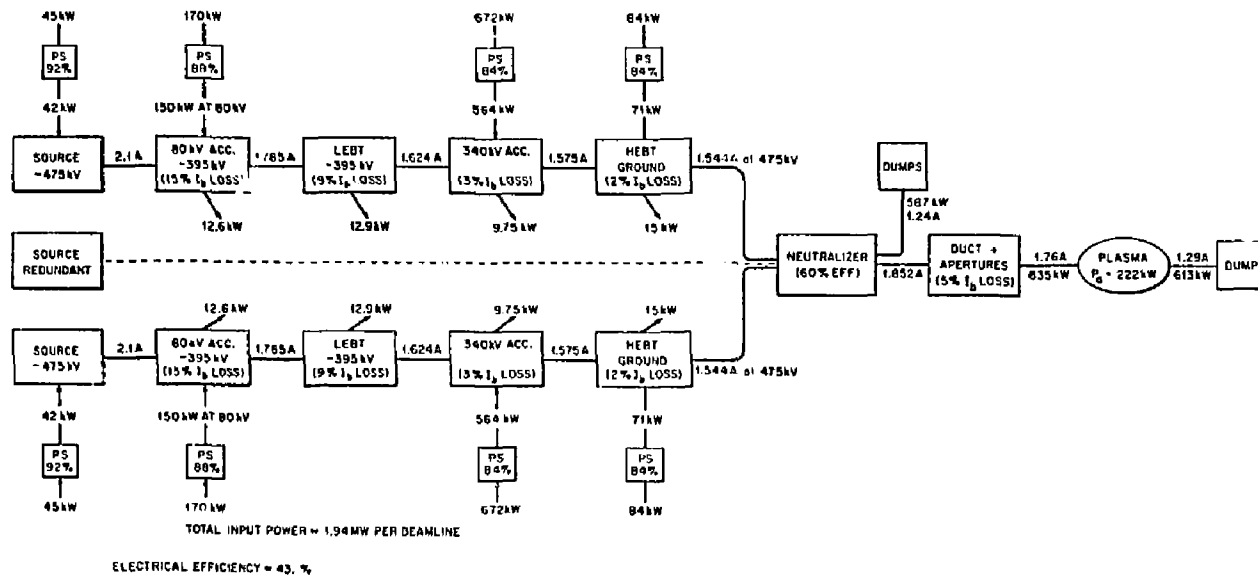
Figure 4-20. Beamline current and power flow.

Table 4-6. Drift pumping requirements.[a]

Transition	Parameter	Plug
64	Frequency (kHz)	1100
40	$\Delta f/f$ bandwidth (%)	66
25.6	Δf bandwidth (kHz)	726
12	Number of frequencies	110
0.072	Perturbation flux (W)	0.0065

[a] Assumptions:

    o MARS-like coil

       - Hairpin shape

       - Scaled in size

    o MFTF-α+T eddy current (scaled).

of each channel is matched to the coil pair through a narrow-band resonating circuit, which includes the drift pump coil. This configuration was first developed on the MFTF-α+T study.[1] Figures 4-21 and 4-22 portray this configuration. For the transition, there are only 12 channels required; each carrying a single tone. The plug cell is satisfied by a similar arrangement; however, 110 channels are required. This large number of channels is not desirable and can be reduced if each channel's bandwidth handles two or more tones. This point is addressed in the following section. The power of each channel is the total power multiplied by the ratio of tones per channel to total number of tones.

Performance

This performance analysis follows the one developed for the MFTF-α+T.[1] The total coil current I is given by solving

$$B = \frac{\phi}{A} = \frac{IL}{NA} \quad ,$$
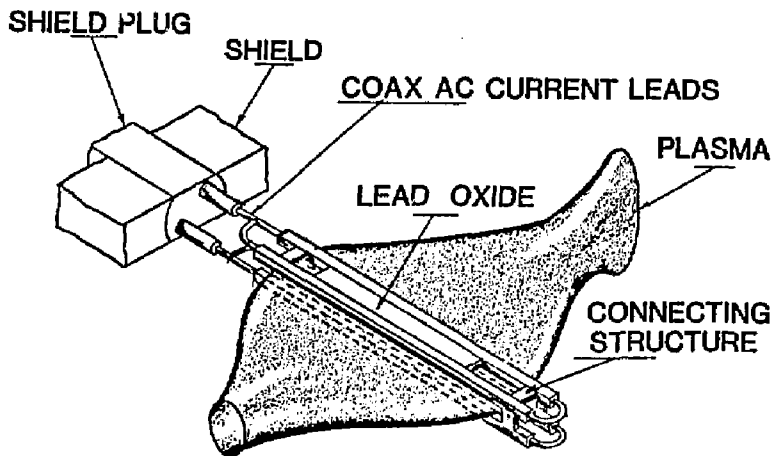
Figure 4-21. Drift-pump antenna arrangement.
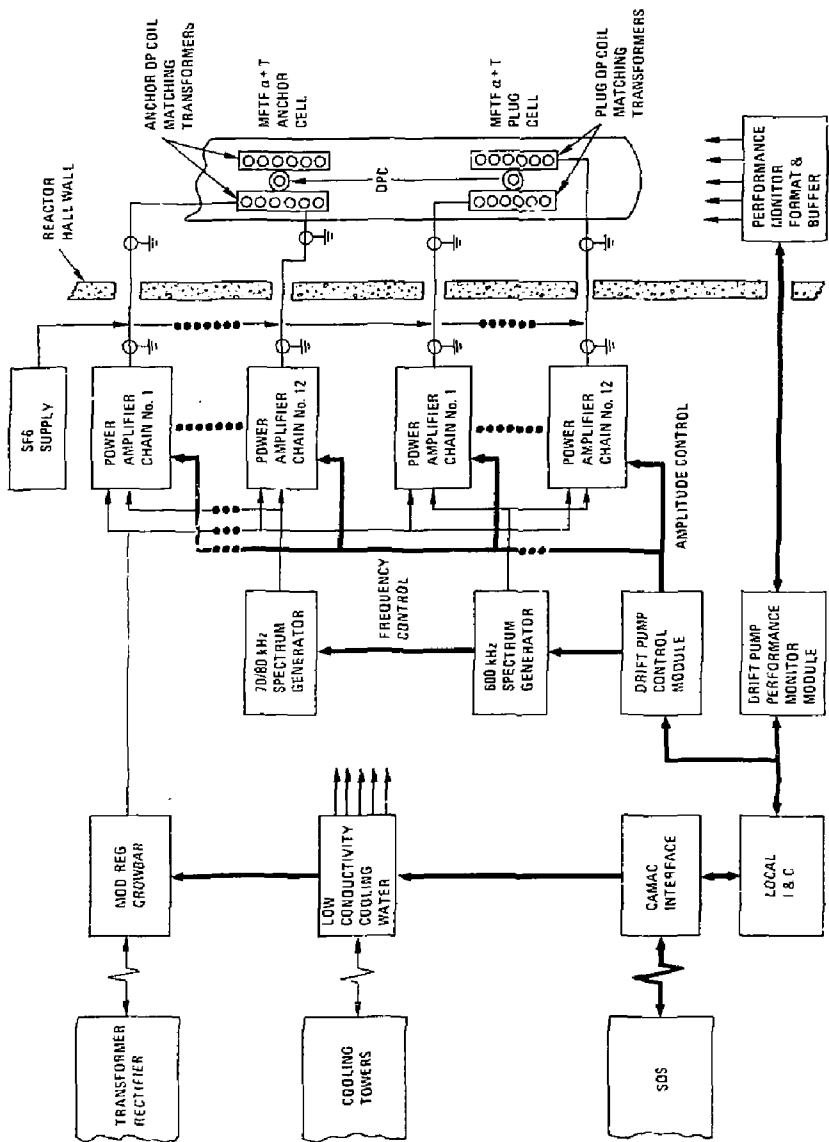
Figure 4-22. Drift pumping.

where the parameters have their usual meanings. Hence

$$I = \frac{\phi N}{L}$$

$$= 18 \text{ kA transition}$$

$$= 1.625 \text{ kA plug.}$$

Table 4-7 summarizes scaled down MARS drift-pump coil parameters at the FPD-I
frequencies. From this point, the delineation of performance will cover the
transition cell first followed by the plug cell.

The total real power supplied to each coil is

$$P = I^2 R_L = I^2 (R_{EC} + R_C) = 2.53 \text{ MW} \quad ,$$

where R_{EC} and R_C are the equivalent resistances for the eddy current loss
and the coil. The power and current supplied by each channel are

$$P = 211 \text{ kW,}$$

and

$$I = 5.2 \text{ kA.}$$

Figure 4-23 shows a sketch of these channels. Following the analysis from
MFTF-α+T, the component values are as follows:

$$C1 = 5.98 \times 10^{-1},$$
$$L1 = 2.77,$$
$$C2 = 3.05 \times 10^{-4},$$
$$L2 = 21,100,$$
$$C3 = 2.07 \times 10^{-2},$$
$$L3 = 362.8,$$
$$C4 = 5.2 \times 10^{-3},$$
$$L4 = 1741.2,$$

where capacitance is in microfarad and inductance is in microhenries. One
tube capable of ~ 0.75 MW is the EIMAC 2170.

Table 4-7. Performance.

Transition	Parameter	Plug
	Coil:	
4	Inductance (μH)	4
6.4	Resistance (mΩ)	26.5
246	Q	981
1.4	Load (mΩ)	5.9
202	Q loaded	801
454	Eddy loss (kW)	15.6
2073	Coil loss (kW)	70.0
18	Current (kA)	1.625
	Transmitter:	
714	Power/channel (kW)	2.6
377	Δf/channel (Hz)	2989
12	#/drift pump coil pair	110
1156	Prime power per channel (kW)	4.3
13,870	Prime power per drift-pump coil pair (kW)	466

4CX 3000 A $C_4 = 3156$ $C_3 = 742$ $C_2 = 44$ $C_1 = 5863$

FROM OTHER
MATCHING
NETWORKS

$50\ \Omega$
COAX ~ 100'

DP
COIL

$L_3 = 96$

$L_4 = 22$

$L_2 = 1608$

$L_1 = 4.2$

$R_1 = 0.03$

$L_C = 4$

$R_L = 0.173$

$L_C = 4$

$R_L = 0.173$

NOTE: INDUCTANCES IN μH
CAPACITANCES IN pF
RESISTANCES IN Ω
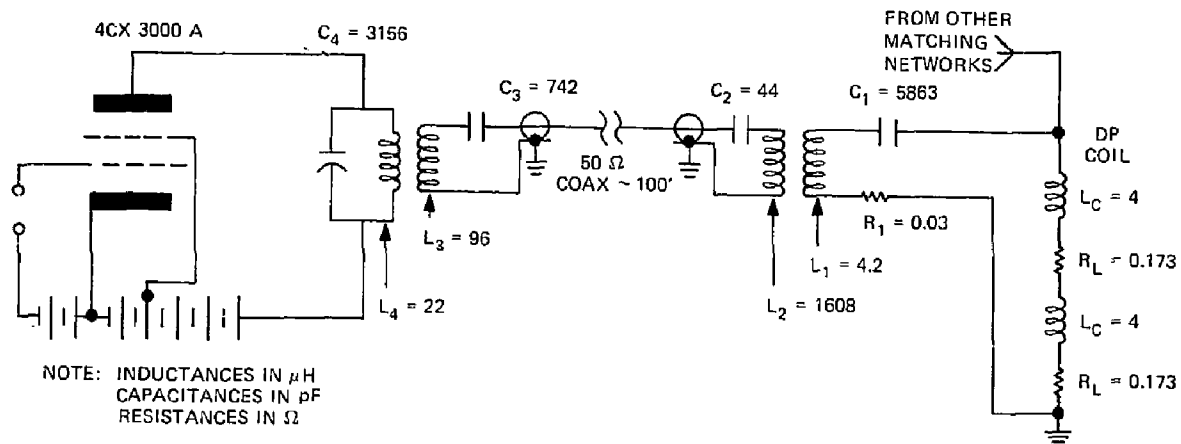
Figure 4-23. Transmitter channel diagram.

The plug cell requirements are very difficult to meet because of the large bandwidth along with the high Q of the drift pumping coil. Assuming only the load of eddy currents in the shield on the coil, results in a Q of about 800. In actuality, this Q is somewhat smaller because of connection resistance and plasma loading. If the required bandwidth of 66% is divided into 110 channels, each channel would have 0.6% bandwidth resulting in a Q of about 160. With these 110 channels, there would be continuous coverage across the 726 kHz band. Any modulation technique (noise, cw sweep, or discrete tones) could be used. However, the power dissipated rises by 800/160 or a factor of 5. The extra power dissipated would be 340 kW. This is an undesirable solution because 110 channels, operating with less than 10% efficiency, are required. For operations with only discrete tone modulation, the Q and efficiency could be higher and only limited by the plasma loading and circuit connections. Table 4-7 summarizes a design of this type in which the Q is about 370. Referring to Fig. 4-22, the values for these channels are as follows: $C1 = 1.97 \times 10^{-3}$, $L1 = 4$, $C2 = 8.4 \times 10^{-6}$, $L2 = 2820$, $C3 = 2.15 \times 10^{-3}$, $L3 = 16.3$, $C4 = 1.83 \times 10^{-4}$ and $L4 = 129.4$ (C in microfarads, L in microhenries). A tube in the 4CX3000A class would suffice.

Future Work

In FPD-II, the plug-cell drift-pump spectrum is defined in more detail. There are two distinct bands: one for the cold ions and another for the sloshing ions. This relieved the design complexity somewhat, but 45 channels are still required to interface with each drift-pump coil pair. A similar investigation of FPD-I should be carried out. The eddy current loading model requires more work as does the technique for flux routing around the drift-pump coil. Finally, some kind of recovery system in the matching network needs to be developed, which will allow wideband (low Q) operation with good efficiency (see MFTF-α+T report[1]).

Since the FPD-I effort was completed, new Fokker-Planck calculations for FPD-II have shown a decrease in the electron energy coupling from the plugs to the central cell. In retrospect, for FPD-I to remain ignited, 35 MW of power would have to be absorbed by the plasma; in this case, ICRH was chosen. The partitioning of absorbed power among the ions, electrons, and alphas does not matter, hence the trapping fraction is assumed to be quite high ~85 to 90%.

The central cell vacuum field is 2.5 T corresponding to 38 MHz for the second harmonic of deuterium, but the equilibrium beta is quite high with a peak value of 90%. To simplify the ICRH design and analysis, we have assumed that as beta increases, the frequency is held constant and the heating region is allowed to move up the slope of the choke field. At full plasma parameters, 38 MHz will heat the surface associated with a $\sim$3.5-T vacuum field at the ends of the central cell.

The system comprises twelve Faraday shielded center-feed loop antennas divided between the two ends of the central cell; each antenna is supplied by a high power transmission system with a three-stub matching network and a multistage amplifier chain. Each antenna covers nearly one-half the plasma circumference and is less than a quarter of a wavelength in length; a power density limitation of 1 kW/cm^2 defines an antenna width of $\sim$20 cm. The antenna, feedthrough, and Faraday shield are assumed to consume $\sim$8% of the power; the transmission system is similar to that described for the anchor ICRH system and is approximately 85% efficient. The transmitter is multistage with a very high power hybrid combiner and two high power hybrid combiners funneling 1.17 MW from four X-2159/9874 tetrodes into the 9-3/16-in. coaxial transmission system. The transmitter efficiency is $\sim$59%. Two converter/ transformers supply the dc power; each is rated at 45 MW at 25 kV. The line requirement for the system is 88 MW, and the ICRH system efficiency is 45.4%.

HALO SCRAPER/DIRECT CONVERTER

The following discussion is a brief summary of the design, supporting analyses, and calculations performed for the direct converter for FPD-I. The basis for the direct converter design and remote maintenance considerations for FPD-I is the A-18 magnet set. We assume that the distribution of power in the direct converter is similar to that in MARS.[2]

The electron collectors and the halo scrapers provide a collection system for the charged particles that exit the central cell. The escaping particles contain a significant amount of power (20% of the fusion power plus the injected power), which results in very high thermal power densities on the surface on which they are collected.

Design Assumptions

We made some assumptions in this study to arrive at a design for costing purposes, they are:

- Use circular plasma cross sectional shape at the direct converter plates.
- Use shape simplification to ease manufacturing--make all cooled elements flat.
- Limit the size of the direct converter so that it can be contained in a 7.0-m diameter vacuum vessel.
- Use 53.5 MW of charged particular energy per end distributed in the same proportion as with MARS[2] (see Table 4-8).

Table 4-8. Power distribution (MW per end).

		MARS	FPD-I
Outer halo		10.0	2.0
Inner halo		50.0	9.0
Outer end			
Thermal		11.0	2.0
Electrical		12.5	2.5
Inner end			
Thermal		69.5	13.0
Electrical		133.5	25.0
	Total	286.5	53.5

Design Options

There are several design options available depending on the goals chosen for a direct converter on FPD:

- o Use a high temperature coolant to permit recovery of the thermal energy at 300°C. This option requires high technology fabrication techniques for refactory metal (TZM) collectors.
- o Use low temperature collection of the thermal energy with no energy recovery. This option permits simple fabrication of copper collectors and low pressure water coolant.
- o Use low temperature collection of the thermal energy with a high temperature module to demonstrate feasibility.
- o Discard electrical energy.
- o Use electrical energy at collector potential.
- o Invert collected electrical energy and feed grid.

Design Description

We considered designs for both the high-temperature recovered-heat and the low-temperature discarded-heat options; and performed a costing exercise for both. The mechanical designs for both options are very similar (see Fig. 4-24) with the major difference being the collector and halo materials. A preliminary assessment of the vacuum pumping requirements was made. This assessment resulted in an estimated open duct pumping speed of 4.0×10^5 liter/s that could be achieved by using 80 TMPs at 5000 liter/s capacity or 5.6 m^2 or cryo panels backed by a roots blower.

Costs

Table 4-9 summarizes the costs of the two options considered for FPD-1 with a comparison to MARS.

HALO PUMP DUCT

COOLANT WATER PIPES

VENTED PLATE
(HALO)

HALO SCRAPER

INNER COLLECTOR

OUTER COLLECTOR

VACUUM PUMPING DUCT

CIRCULARIZER SOLENOID

DOUBLE WALLED VACUUM VESSEL
SPACE USED FOR SHIELD WATER

0   1   2   3
SCALE - METERS
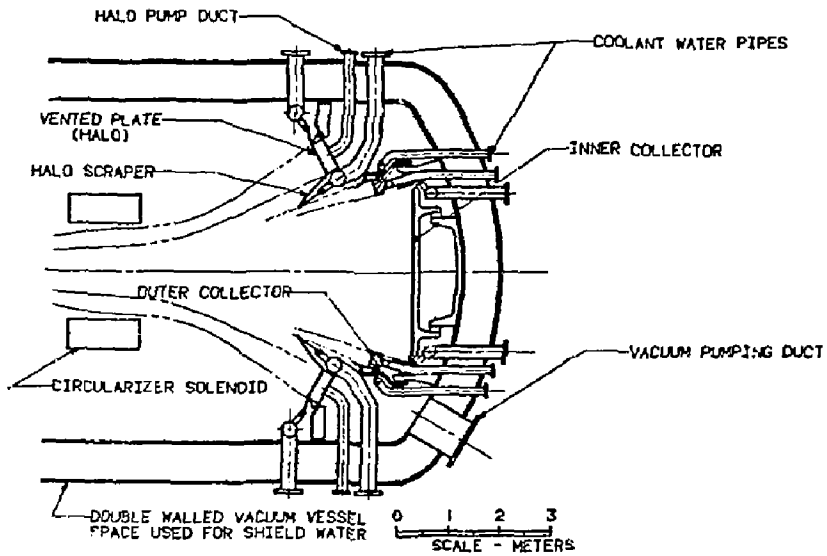
Figure 4-24. The FPD-1 direct converter.

Table 4-9. Costs in 1984 dollars including materials, fabrication, and installation.

| | MARS FPD-I | FPD-I | |
	TZM (m)	TZM (m)	Copper (m)
Piping and supports	1.63	0.94	0.28
Halo	4.13	1.71	0.34
Collector	4.00	0.77	0.15
Totals	9.76	3.42	0.77

FUELING INJECTION SYSTEMS

The FPD machine has two independent gas-puffing injection systems for initial loading and startup. Either gas-injection system can perform these operations with one system maintained while the other is in operation. The gas-injection systems can supply either hydrogen or deuterium gas, but not tritium. Therefore, the gas injection system developed for other machines can be procured without having to upgrade to meet tritium safety requirements. The maximum gas injection rate is 300 g/h. Both pulsed and analog modes of operating are available.

Two independent fuel pellet injectors are provided, with one at each end of FPD. Either injector can provide all the deep-fueling needs of the machine. The pellet injectors can inject 2.75 mm pellets with velocities up to 12,000 m/s, corresponding to a pellet penetration of about 50% of the radius near the throat of the choke coil. Table 4-10 contains the characteristic design data for two-stage pellet injectors consisting of a pneumatic-gun first-stage preinjector and an electromagnetic-rail-gun second-stage accelerator.

The fuel pellet can be controlled within a range from 0 to 10 per second to cover the large uncertainty in the plasma confinement time and effective s of the pellet fueling. The fuel pellet formers can make DT pellets with atomic mix ratios between 0.5 and 1.5. The pellets can

Table 4-10. Fuel pellet injector data.

No. of pellet injectors	2
Pneumatic gun data:	
Pellet diameter and length (mm)	2.75
Pellet rate (s^{-1})	0.10
Pellet velocity (m/s)	500
Pellet composition:	
Deuterium	>95%
Tritium	>95%
Atomic mix ratio	0.5 to 1.5
Propellent gas	D2
Supply pressure (PSIA)	150
Barrel length (m)	0.8
Electromagnetic rail-gun accelerator data:	
Pellet entry velocity (m/s)	500
Maximum pellet exit velocity (m/s)	12,000
Maximum theoretical rail-gun current (kA)	10.5
Rail-gun barrel length (m)	16.6
Rail-gun energy supply (kJ)	15.0
Fueling supply rate data:	
DT fuel injection rate (g/h)	32
Tritium fueling supply rate (g/h)	39
Deuterium fueling supply rate (g/h)	26
Other fuel system operating data:	
Vacuum pumping requirement (LPM)	2000
Liquid nitrogen supply rate (g/h)	225
Liquid helium supply rate (g/h)	125
Electric power consumption (kW)	100

be injected in the reduced section of the central cell plasma near the inboard side of the water-cooled choke coils. Isolation valves will be provided at the rail gun exit to permit operation with one injector out of service. Replacement of the pellet launcher and rail gun accelerator will be possible without entering the vault.

Although rail guns were developed to inject non-metallic pellets up to 11 km/s, no one has ever built one to accelerate frozen fuel pellets. Considerable development work is needed to determine the feasibility of using an electromagnetic rail gun for injecting high velocity fuel pellets.

END CELL

SHIELDING AND VACUUM CONTAINMENT

Shielding analyses for FPD-I have identified a need for two types of shield for the end cell. These two, shown in Fig. 4-5, are (1) magnet and (2) biological shields. The magnet shield is located between the plasma and the coils in the end cell. The biological shield is an integral part of the vacuum vessel.

Magnet Shields

The magnet shields tailored in shape and location to the individual coils in the end cell are shown in Fig. 4-24: therefore, they vary throughout the length of the end cell. The choke coil requires thicker shielding than the recircularizing coil. All of the C coils have 35-cm-thick shields. This shield consists of 30-cm steel shielding and 5 cm of boron shielding. The steel shield composition is 80% steel and 20% H_2O; the boron shielding composition is 40% steel and 60% B_4C. (B_4C has a density factor of 0.7.)

Vacuum Vessel/Biological Shield

The function of the biological shield is integrated with the function of vacuum containment in a double-walled vessel. The wall spacing of 2.4 m is set by the biological shutdown dose rate. In addition, a 5-cm-thick boron shield and a 5-cm-thick lead shield are attached to the outside of the

integral vessel. These three shield layers limit the shutdown dose rate to 0.5 mrem/hour, 24 hours after shutdown.

The end cell has the following physical dimensions:

- Length = approximately 33 m.
- Inside diameter = 7.0 m.
- Outside diameter = 11.8 m.

The end cell vacuum vessel consists of an inner and outer shell separated by six bulkheads, as shown in Fig. 4-25. Figure 4-26 shows the magnet cold structure integrated into the cylindrical vacuum vessel. The removable top hatch is framed by a beam structure. Both the hatch and the vacuum vessel have longitudinal stiffeners on 45° spacing. Each end cell has two hatches. The large hatch is for coil removal, and the smaller one is for the direct converter/halo scraper removal. The hatches are sealed with a single-convolution welded bellows.

SUPPORT STRUCTURE

The end cell is supported by three sets of legs, as shown i Fig. 4-25. These are situated on top of reinforced concrete piers. The suport legs sit on a roller tyre support, which allows axial movement (z-directi) for thermal expansion. All lateral or vertical movement is constrained. Each set of legs is in line with a vacuum-vessel bulkhead.

NEUTRONICS ANALYSIS

Neutronics analyses for the FPD-I design were performed for the central cell, choke area, and the end cell. The central cell analysis includes a blanket optimization to reduce the capital cost, a shield design the protection of the central cell coils, and a biological shield design for the reactor room access one day after shutdown. The choke area analysis was carried out to define nuclear responses in the copper insert coil and the superconductor portion of the coil. Rigorous analysis was performed for the end cell because the capital cost of the end cell amounts to ~60% of the total capital cost. An elaborate three-dimensional (3-D) radiation transport analysis for the complete reactor system, including the breeding blanket, the
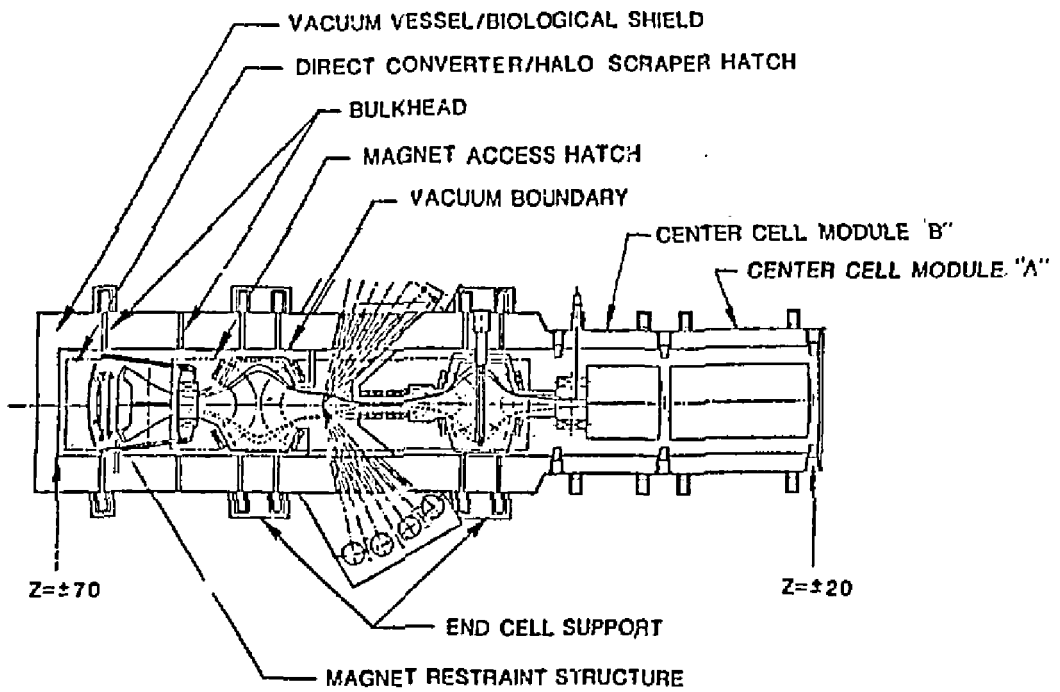
Figure 4-25. The FPD-I end-cell plan view.

VACUUM SEAL

LONGITUDINAL STIFFENERS

SUPPORT FOR
MAGNET COLD STRUCTURE

11.8m

3.5m

2.4m
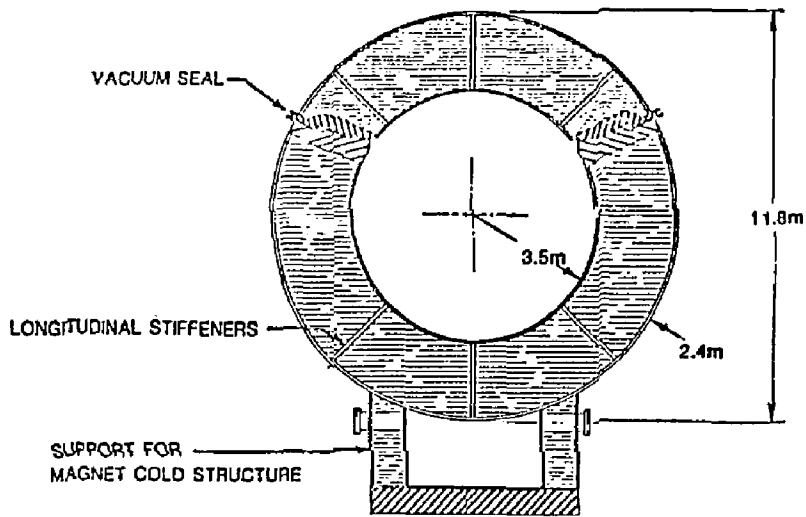
Figure 4-26. Section through the FPD-I end-cell vacuum vessel.

bulk shield, the central cell coils, the choke coils, the C coils, and the biological shield, was carried out. The general purpose Monte Carlo computer code, MCNP, was used for the calculations with a continuous energy representation for the nuclear cross sections based on ENDF/B-V nuclear data files. The energy spectrum and spatial distribution of the neutron source from the DT plasma in the central cell and the end cell were modeled explicitly in the calculations. The geometry of the C coils was modeled explicitly without approximation in the calculation model. Results from the 3D analysis include the net tritium breeding ratio, energy deposition in each component of the reactor, radiation damage parameters in each coil, neutron leakage from the central cell to the end cell, and the detailed shield design for the end cell.

RADIATION PROTECTION CRITERIA FOR THE COILS

In general, the effect of radiation on coil components tends to lower their performances. For superconductor materials, neutron irradiation reduces the critical density (J_c) and the critical temperature (T_c). For NbTi superconductors, J_c is decreased by $\sim 10\%$ at 4×10^{18} n/cm^2 (E > 0.1 MeV) fluence, whereas T_c is unchanged.[4,5] Irradiation experiments at RTNS-II[6] on NbTi superconductors show consistent results with previous work. On the other hand, J_c of Nb$_3$Sn generally increases, reaching a maximum and then decreases as the neutron fluence increases.[7] Irradiation experiments at 61 K (Refs. 4,5) with a maximum neutron fluence of 4×10^{18} n/cm^2 show that the maximum value and the increased rate of J_c increases with the magnetic field. At a magnetic field of 5 T, the 61 K irradiation resulted in a 16% increase in J_c after 2×10^8 n/cm^2 without reaching a peak. Irradiation experiments at higher temperatures (~ 350 K) show the same behavior for J_c. However, the J_c peak was lower than the corresponding value at lower temperature for the same magnetic field. For example, the 350 K irradiation gave an 8% increase corresponding to the 16% mentioned before at 6 K. Other irradiation experiments at 400 K and a 10 T field[8] resulted in a 90% increase for J_c at 4.4×10^{18} n/cm^2 and dropped to the original value of J_c at 10^{19} n/cm^2. Based on these experimental results,[4,7,8] the comparison between the room temperature and the 6 K irradiation results, and the maximum field of 11 T, a neutron fluence above 10^{19} n/cm^2 can be achieved in Nb$_3$Sn without a decrease in the critical current density.

The stabilizer material carries the current in the event that the superconductor temporarily becomes resistive. The coil is designed to remove the generated heat (I^2R) so that the normal region does not propagate. The resistance (R) of the stabilizer is the most important consideration for this process. Copper and aluminum are the two choices for the stabilizer material. However, copper is the prepared material because it has the lowest resistivity in the fusion environment.[9,10] The total resistivity of the copper stabilizer can be described as the sum of three components: the initial resistivity ρ_o, the magneto-resistivity ρ_u, and the irradiation induced resistivity ρ_{irr}. Magneto-resistance is a function of ρ_o, ρ_{irr}, and the magnetic field which complicates the evaluation of ρ. Few experimental studies[6,9-13] have been done on the change of copper resistivity as a function of field, neutron fluence, and number of cycles of alternate neutron irradiation (4 K) and annealing (300 K). The change in the copper resistivity can be accommodated by using more copper stabilizers, which increase the thickness of the coils, can be partially annealed out by warming the coils, or can be avoided by improving the shielding performance (increase shielding thickness or use better materials). The FPD design limits the irradiation-induced resistivity to $\sim 5 \times 10^{-8}$ cm in the copper stabilizer at the end of life to avoid any impact on the coil design.

The most sensitive component in the coils is the insulator material because the irreversible irradiation damage limits the operating life of the coils. The properties of interest for the coil designs are the electrical resistivity, dielectric strength, mechanical strength, and thermal insulation. Experimental results form neutron irradiation at 5 K suggests that polyimides can withstand a radiation of 10^{10} rads and retain high resistivity and mechnical strength. Glass-cloth reinforced epoxy type G10-CR or G11-CR shows a serious degradation at 2×10^9 rads. The FPD design assumes a 10^{10} rads maximum tolerable dose in the insulator material at the end of life.

The nuclear energy deposited in the coils impacts the refrigeration power required since about 500 W of electrical power is consumed to remove one watt from the coil at 4 K. This low removal efficiency calls for minimizing the nuclear energy deposited in the coils. Thus, limiting the maximum nuclear heating to a few mW/cm^3 is required to avoid a large cryogenic system.

CENTRAL CELL ANALYSIS

The central cell analysis covers the following three sections: (1) the tritium breeding blanket, (2) the shielding design to protect the central cell coils, and (3) the biological shields. In the design process for these three sections, the emphasis was on reducing the capital cost and the total weight of the central cell. The blanket is designed to convert the kinetic energy of the DT neutrons to recoverable heat and produce adequate tritium breeding to supply the tritium fuel requirement during the whole reactor lifetime; the blanket is designed as well to generate a surplus of tritium to compensate for operating with nonbreeding blanket sections or to start another reactor within a reasonable period of time. Economic and shielding considerations require the blanket design to maximize the recoverable heat produced, which is defined as the energy deposited in the first wall, breeding zone, and reflector per fusion neutron. A neutronics analysis was performed to study the performance of the self-cooled natural lithium-lead [$Li_{17}Pb_{83}$ (LiPb)] blanket concept. The impact of the breeding zone thickness, reflector material selection, reflector composition, and reflector zone thickness are analyzed to determine the main blanket parameters. In the analyses, five key parameters are considered to define the blanket for FPD. These parameters are the capital cost, the total weight, the tritium breeding ratio, the energy deposition in the blanket per fusion neutron, and the energy loss to the shielding system. For the LiPb blanket concept, the tritium inventory is less than 1.0 kg, which requires 1.01 net tritium breeding ratio to achieve about one year doubling time. However, the neutronics analysis was performed with a wide range for each key parameter. As an example of the results, Fig. 4-27 shows the tritium breeding ratio as a function of the breeding zone thickness (10 to 50 cm), for different reflector zone thicknesses (20, 30, and 40 cm). Table 4-11 gives the central cell parameters that resulted from the analysis for the FPD design.
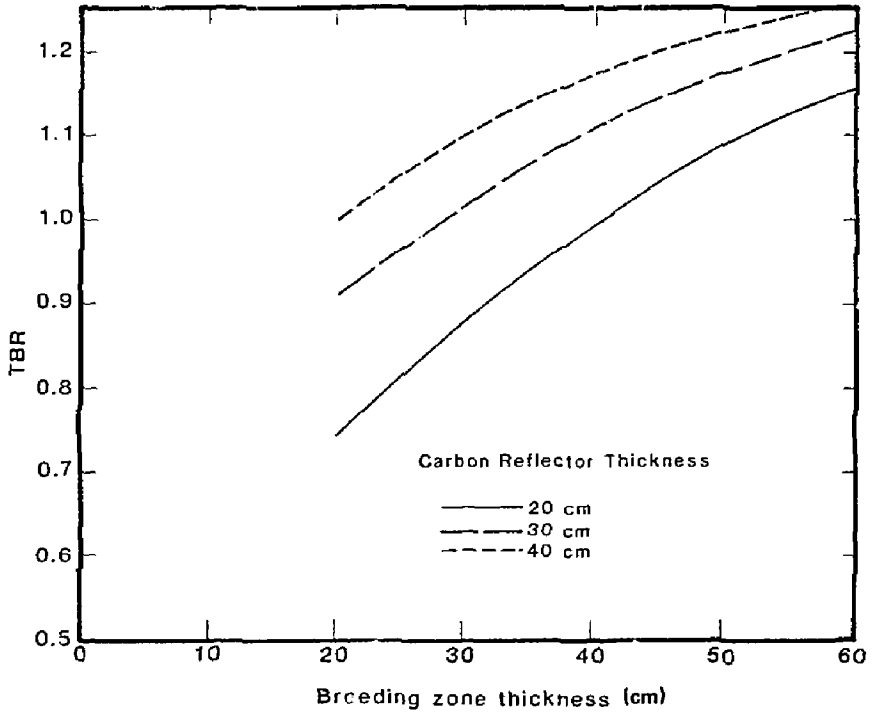
Figure 4-27. Tritium breeding as a function of the natural LiPb breeding zone thickness for different carbon reflector zone thicknesses.

Table 4-11. The FPD-I central cell and choke coil parameters.

Central Cell Blanket Parameters

Materials:

    Natural LiPb breeder

    Carbon reflector

    Ferritic steel structural

Dimensions and composition in the neutronics model:

First wall thickness (50% ferritic, 50% LiPb) (cm)	1
Breeder zone thickness (7.5% ferritic, 92.5% LiPb) (cm)	29
Reflector zone thickness (10% ferritic, 10% LiPb, 80% C) (cm)	49
Breeding blanket length (m^2)	70
Neutron wall loading (MS/m^2)	1.95

Performance parameters:

Tritium breeding ratio	1.11
Lithium-6 enrichment	Natural
Blanket energy multiplication factor	1.30
Total energy multiplication factor	1.37
Energy fraction deposited in the shield	4.83×10^{-2}

Central Cell Shield

Materials:

    Steel balls, water, B_4C (powder), lead

Dimension and composition under the coils:

Steel shield (60% Fe1422 steel alloy, 40% H_2O)	45 cm
Boron shield (42% B_4C, 20% Fe1422 steel alloy, 20% H_2O)	5 cm

Table 4-11. (Continued.)

Nuclear responses in the central cell coils:

Maximum nuclear heating in the coil case (mW/cm^3)	0.10
Maximum nuclear heating in the winding material (mW/cm^3)	0.03
Maximum dose in the thermal insulator ($rads/MW \cdot y/m^2$)	7.79×10^7
Maximum dose in the electrical insulator (rads, $MW \cdot y/m^2$)	2.70×10^7
Maximum dpa in the copper stabilizer ($dpa/MW \cdot y/m^2$)	2.11×10^{-6}
Fast neutron fluence in the winding material ($neutrons \cdot cm^2/MW \cdot y/m^2$)	8.85×10^{10}

FPD-I Choke Coil

Copper insert:

Neutron wall loading (MW/m^2)	0.6
Maximum nuclear heating in the coil case (W/cm^3)	7.0
Maximum nuclear heating in the copper coil (W/cm^3)	5.3
Maximum nuclear heating in the ceramic insulator ($rads/MW \cdot y/m^2$)	6.1×10^{12}
Maximum atomic displacement in the copper ($dpa/MW \cdot y/m^2$)	6.8

Superconductor:

Neutron wall loading (MW/m^2)	0.80
Maximum shielding thickness (cm)	70.0
Maximum nuclear heating in the coil case (mW/cm^3)	0.52
Maximum nuclear heating in the winding materials (mW/cm^3)	0.22
Maximum dose in the insulator ($rads/MW \cdot y/m^2$)	7.00×10^8
Maximum dose in the electrical insulator (rads, $MW \cdot y/m^2$)	2.92×10^8
Fast neutron fluence in the winding material ($E > 0.1$ MeV), ($n/cm^2/MW \cdot y/m^2$)	1.81×10^{17}
Maximum atomic displacement in the copper stabilizer ($dpa/MW \cdot y/m^2$)	1.23×10^{-4}

The shielding thickness for the central cell is defined to achiev‧
0.1 mW/cm^3 maximum nuclear heating in the coil case. At this nuclear
heating rate, th. capital cost for the central cell is at minimum based on the
MFTF-α+T design analysis.[1] The design criterion based on the nuclear
heating and the tive years operating time (100% availability) produce low
nuclear responses in the superconductor coils as shown in Table 4-11. The
design criteria for superconductor coil protection against radiation is about
two orders of magnitude higher than the values in Table 4-11.

CHOKE COIL ANALYSIS

The choke coil analysis was performed to define the nuclear responses in
both sections of the choke coil: the normal copper insert and the
superconductor section. The maximum neutron wall loading for each section is
shown in Table 4-12. Based on the nuclear responses given in Table 4-11, the
copper insert can operate for 1.7 years (100% availability) to reach 10^{13} rads
in the ceramic insulator which corresponds to 3 vol% swelling in the MgAl$_2$O$_4$.
The superconductor section has an adequate margin to operate for five years
(100% availability) without reaching any radiation design limit.

END CELL

An accurate 3D analysis was performed for the whole reactor to provide
the following information: (1) the neutron wall loading in the end cell,
(2) the energy deposition in each component, (3) the net tritium breeding
ratio, (4) the neutron leakage from the central cell to the end cell, and
(5) the hot spot points in the C coils. The 3D geometrical model for the
calculations is shown in Fig. 4-28. The key results from this analysis are
summarized in this section. The neutron wall loading in the end cell has a
0.15 mW/m^2 peak value at z = 46.1 m. The neutron wall loading distribution
shows that the C coils' shield thickness can be tapered to less than the 35 cm
starting from z = 54 m. Table 4-12 gives the energy deposition in each
component per fusion neutron and the statistical error within one standard
deviation. The energy deposition in the C coils and the end cell biological
shield is 90.4 and 35.6 kW, respectively. The shield thickness for the C coils

Table 4-12. Nuclear heating and power distribution.

	Neutron	Gamma	Total
	(MeV/DTn)		
Blanket			
First wall	0.3288 ± 0.51%	0.5991 ± 1.09%	0.9279
Breeding zone	4.8433 ± 0.63%	5.8394 ± 0.60%	10.6827
Reflector	2.9348 ± 0.69%	2.4177 ± 0.94	5.3525
Total	8.1069	8.8562	16.9631
Central cell coil shield			
Steel shield	1.4112-2 ± 3.86%	1.0859 ± 11.52%	1.1000
B_4C shield	6.2042-6 ± 10.58%	8.6578-6 ± 11.52%	1.4862-5
Total	1.4118-2	1.0859	1.1000
Central cell coil			
Coil case	2.2878-7 ± 17.12%	7.0058-6 ± 14.94%	7.2346-6
Coil winding	7.1454-7 ± 14.67%	1.0479-5 ± 23.06%	1.1194-5
Total	9.4332-7	1.7485-5	1.8428-5
Central cell biological shields			
B_4C shield	8.6626-8 ± 13.7%	5.4116-8 ± 15.0%	1.4074-7
Pb shield	62.417-9 ± 23.9%	4.5354-8 ± 18.1%	4.5978-8
Total	8.7250-8	9.9470-8	1.8672-7
Choke coil shield			
Steel shield	7.3229-2 ± 2.26%	4.5173-1 ± 2.29%	5.2496-1
B_4C shield	1.2498-7 ± 29.3%	1.3163-7 ± 34.6%	2.5661-7
Pb shield	2.4027-9 ± 80.1%	6.3297-8 ± 29.6%	6.5700-8
Total	7.3229-2	4.5173-8	5.2496-1
Copper choke coil			
Coil case	1.1434-3 ± 6.28%	4.5239-3 ± 6.13%	5.6673-3
Coil winding	2.0223-3 ± 5.05%	2.0665-3 ± 9.06%	4.0888-3
Total	3.1657-3	6.5904	9.7561-3

Table 4-12. (Continued.)

	(MeV/DTn)		
	Neutron	Gamma	Total
Superconductor choke coil			
Coil case	2.2060-6 $\pm$ 30.1%	8.7658-5 $\pm$ 27.8%	8.9864-5
Coil winding	1.5796-6 $\pm$ 26.1%	2.7122-5 $\pm$ 20.0%	2.8702-5
Total	3.7856-6	1.1478-4	1.1857-4
C coils shield			
Steel shield	3.9440-2 $\pm$ 2.26%	1.6293-1 $\pm$ 2.58%	2.0237-1
B_4C shield	1.7490-3 $\pm$ 4.36%	1.6874-3 $\pm$ 11.2%	3.436-3
Total	4.1189-2	1.6462-1	2.0580-1
C coils			
Coil cases	2.3006-5 $\pm$ 7.87%	4.9066-4 $\pm$ 3.92%	5.1366-4
Coil winding	1.7444-4 $\pm$ 5.78%	1.6501-3 $\pm$ 4.91%	1.8245-3
Total	1.9745-4	2.1408-3	2.3382-3
End cell biological shield			
Water shield	9.1126-4 $\pm$ 7.33%	1.1430-5 $\pm$ 33.5%	9.2269-4
B_4C shield	2.4537-10 $\pm$ 38.6%	1.1064-6 $\pm$ 78.4%	1.0166-6
Pb shield	3.1575-12 $\pm$ 58.5%	4.0372-7 $\pm$ 55.6%	4.0372-7
Total	9.1126-4	1.2850-5	9.2411-4

Power Parameters

Total DT neutron power (MW)	542.55
DT neutron power in the end cell (MW)	5.54
Neutron wall loading at first wall (MW/m^2)	1.95
Neutron leakage from central cell (n/DTn)	6.50×10^{-4}

4-64

Table 4-12. (Continued.)

| | Power Distribution | |
	MeV/DTn	MW
Blanket	16.96	654.86
Central cell coil shield	1.10	42.47
Central cell coil	1.84-5	7.10-4
Central cell biological shield	1.87-7	7.22-6
Choke coil shield	5-25-1	20.27
Copper choke coil	9.76-3	3.76-1
Superconductor choke coil	1.18-4	4.56-3
C coils shield	2.06-1	7.95
C coils	2.34-3	9.04-2
End cell biological shield	9.24-4	3.56-2
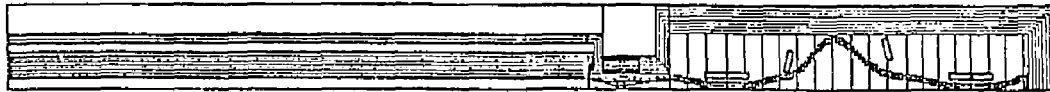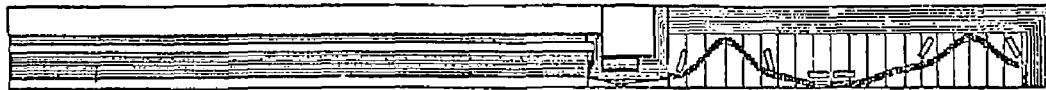
X - Z PLANE

X = Y - Z PLANE

Y - Z PLANE

Figure 4-28. Three-dimensional model.

in the 3D analysis is 35 cm. Figure 4-29 gives the energy deposition in the C coils as a function of the shield thickness for tungsten and steel type shield based on a one-dimensional cylindrical model.

This one-dimensional model assumes that the radiation leakage is completely deposited in the C coils. For the 35 cm of steel shields, the one-dimensional model estimates 133 kW deposited in the C coils compared with the 90.4-kW estimate from the 3D analysis. These results give a coverage ratio of 90.4/133 = 0.68. Using this coverage ratio, Table 4-13 gives the energy deposited in the C coils as a function of the shield thickness for both types of shield. For the FPD-I design, it is possible to use 45 cm of shield instead of 35 cm except where a few spots reduce the energy deposition in the C coils to about 26.4 kW. The point with minimum space for shielding has a 7.7 mW/cm^3 maximum nuclear heating rate in the coil case (a 2-cm coil case thickness was used in the 3D analysis), which is an allowable level for the C coil design.

MATERIALS

The projected operating lifetime of FPD is 2.5 effective full power years, with a first wall neutron loading near 1 MW/m^2. This exposure of 2.5 MW/y/m^2 or less raises questions about the potential life-limiting effects of radiation on component material. Although no complete analysis of component lifetime has been conducted, a few of the issues of potential concern are outlined here.

Because FPD must breed tritium, and a MARS-like blanket[2] has been assumed, the operating conditions for the first wall and blanket structural material are reactor relevant. The use of the LiPb breeding blanket will require temperatures in the range of 300 to 400°C, even though the thermal energy will only be rejected to a heat dump system. The neutron flux at the first wall will result in approximately 25 dpa at end of life and the generation of 250 to 400 at.ppm He in steels.
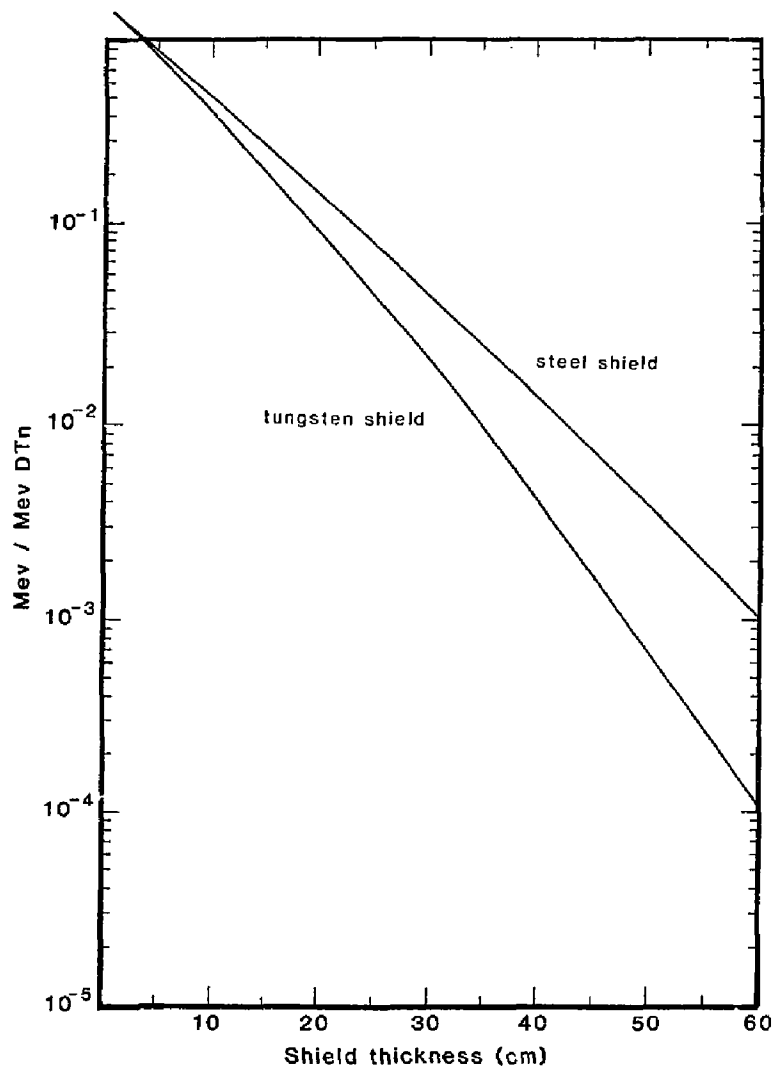
Figure 4-29. Energy deposited in the C coils as a function of the shield thickness.

Table 4-13. Energy deposited in the C coils as a
function of shield thickness for steel and tungsten
type shields.

Shield thickness (cm)	Power deposited in the C coils (kW)	
	Steel shield	Tungsten shield
35	90.4	33.9
40	49.0	14.3
45	26.4	6.0
50	14.3	2.6
55	7.6	1.0

The structural material specified for the MARS blanket is the
ferritic/martensitic steel HT-9. The compatibility, strength, ductility and
fabricability of this alloy should be adequate for the FPD application. For
the lifetime of 2.5 MW-y/m^2, the alloy is not expected to swell, and tensile
properties and irradiation creep rate will not limit the reactor performance.
A shift in the ductile-to-brittle transition temperature (DBTT) will result
from the irradiation of a ferritic/martensitic steel. Data on HT-9 show that
the DBTT could be shifted above 100°C by FPD conditions. The available
experimental results suggest that the 9 Cr-1 Mo steel under study for fusion
reactor application would be a better choice than HT-9 due to the lower
post-irradiation DBTT. Continuing efforts of the materials program can be
expected to qualify one of the steels, or a modified steel in the Cr-Mo
family, for service at FPD conditions. Progress of these efforts should be
monitored, so that the best candidate steel is selected for FPD.

An austenitic stainless steel such as type 316 or an advanced develop-
mental grade is also viable for the MARS-like first wall and blanket of FPD.
The data base for irradiation effects on austenitic steel is much larger than
on ferritic/martensitic steels, and the DBTT embrittlement does not occur in
these steels. The austenitic steels would also offer some simplification in
fabrication, but somewhat poorer thermal properties, relative to HT-9. The

compatibility limits of the austenitic stainless steels with liquid LiPb are inferior to the ferritic/martensitic steels, but would be adequate for a reduced temperature, MARS-like blanket.

The U.S. Fusion Reactor Materials Program has work in progress to develop low activation steels. The goal is to produce both austenitic and ferritic/martensitic grades with new compositions that wi l allow simplified disposal of spent reactor components under the Class C category of 10CFR61. There are two families of steels under study: austenitic steels with Mn replacing Ni and with low levels of Mo, N, Nb and Cu, and ferritic/martensitic steels with W and/or V replacing Mo and with low levels of Ni, N, Nb, and Cu. Because this program was not initiated until late 1983, it is not expected to deliver qualified steels in time for the FPD project. The use of these developmental steels without an adequate data base would not seem to be a justifiable risk.

Another class of critical components in FPD is the magnet materials. For the central cell superconducting magnets, the organic insulation is the critical component, and the shield must be designed to provide adequate protection of this insulation. The radiation limits on the insulation is poorly established, and is probably below 10^9 rad for epoxy-glass insulation and below 10^{10} rad for polyimide-glass insulation. Ongoing research will refine these limits in the next few years, and allow greater confidence in designing a shield to give adequate protection. The insert normal magnet in the choke coil is exposed to the unshielded neutron flux and will be a life-limiting reactor component that must be designed for simple replacement. Analysis of the lifetime of this magnet is provided in the MARS study.[2] Areas of uncertainty in these estimates lie in the effects of radiation on the ceramic insulator and on the copper alloy conductor. Active research on both materials will allow refined lifetime fluence estimates and may provide superior candidate materials in time for the FPD project.

Ceramic reactor components in addition to the choke coil insulation are susceptible to radiation damage. These materials may be used in the auxiliary heating systems, beamlines, direct converters, and other subsystems. The potential effects on these components have yet to be examined in detail.

Several other classes of materials will need to be investigated: candidate selection must be verified and service performance predicted. These materials may include the following: shield materials to provide superior performance to the steel-water shields (perhaps TiH), better thermal barriers in load support columns (perhaps using composite-metal combinations), tritium barrier materials, and a whole host of other component systems, each with its own specific set of material property requirements.

ELECTRICAL SYSTEMS

The electrical systems include the electric plant equipment of the ac power system, the power conversion for the confinement magnets, and the power conversion for the microwave and NBI systems. These electric systems also include the instrumentation and control systems.

AC POWER SYSTEM

The ac power system includes all the switch gear, transformers, and distribution feeders of FPD. In addition to the distribution of power to the electrical loads identified in Table 4-14, the ac power system includes the bussing and fault protection for the turbine generator and direct converters, and the inverters for the direct conversion system. Referring to Table 4-14, the total recycle power needed by FPD-I is 280 MW. The total electrical power output is 40 MW from direct converters and 135 MW from the turbine generator. Engineering Q_e, defined as power generated divided by power consumed by the plant, is 1.0.

Figure 4-30 is a one-line diagram of the FPD-I power distribution system. Mnemonics used in the diagram are identified in Table 4-15. Medium voltage power is provided at both 13.8 kV and 2.4 kV level. The direct converter and turbine generator provide power to the 13.8 kV bus through 1200 A and 3000 A circuit breakers, respectively. There is no net power delivered to the 230 kV utility line; neither is there any separate facility power substation. The two main transformers supply all the FPD-I power from one utility line.

4-71

Table 4-14. Estimate of FPD-I electrical power generation and loads.

Power generation or load description	Electrical power (MW)	
	Input	Output
Central cell neutral beam injectors	0	
Central cell ICRH power	95	
Plug cell neutral beam injectors	5	
Anchor cell ICRH	7	
Anchor and plug cell drift pumps	28	
Plug cell ECRH	60	
Resistive coil power	40	
Cryogenic system power	25	
Cooling system and vacuum system power	12	
Superconducting coil power systems	1	
Fuel processing and tritium cleanup	7	
Direct converters		40
Turbine-generator		135
Total (with axicell)	280	175
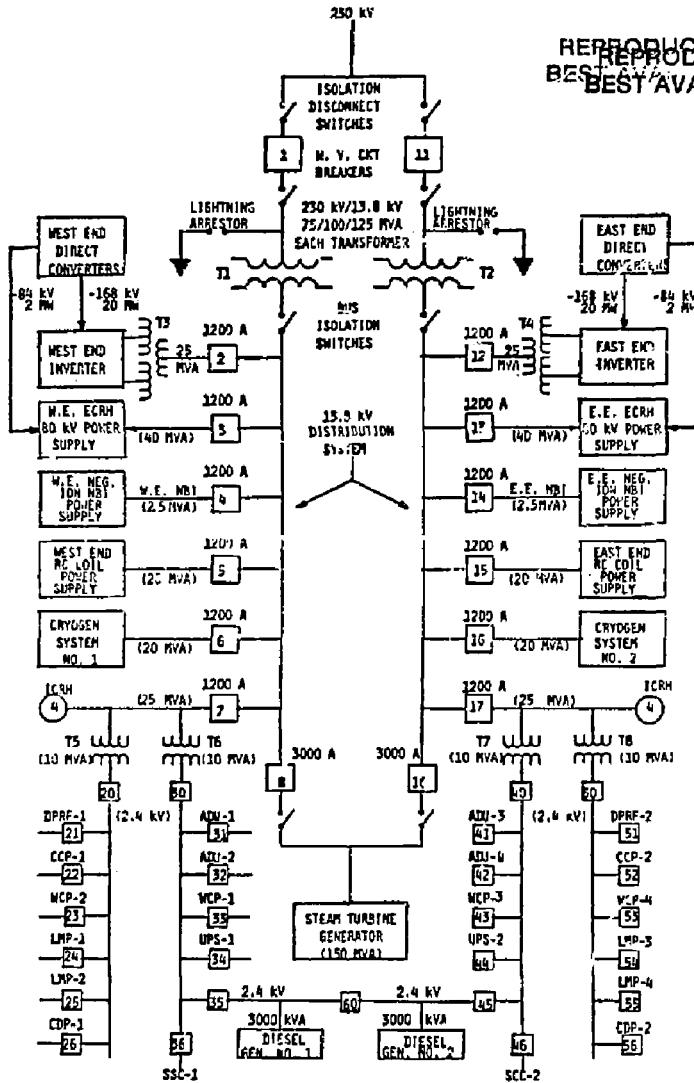
Figure 4-30. One-line diagram of the power distribution system for FED-I.

Table 4-15. Mnemonic definitions.

Mnemonic	Description
DPRF	Drift pump rf power
ADU	Atmospheric detritiation unit power
WCP	Water cooling pump power
LMP	Liquid metal pump power
UPS	Uninterruptible power supply
CFP	Condensate feed pump power
CCP	Condenser cooling pump power
SCC	Superconducting coil power
NPS	Number of power supplies
PSVOLT	Power supply voltage
PSKA	Power supply current (kA)
BUSLM	Bus length (m)
NBKRS	Number of dc circuit breakers
NDR	Number of dump resistors
EDRMJ	Maximum energy dissipated in a dump resistor (MJ)
PDRMW	Maximum power to a dump resistor (MW)

Facility power and the diesel generator backup power are provided at the 2.4 kV level. There is a trend towards using only two medium voltages today, namely, 4.16 kV and 13.8 kV. It may be desirable to change from 2.4 kV to 4.16 kV, as proposed for FPD-II.

ELECTRICAL POWER CONVERSION SYSTEMS

The electrical power conversion system includes all the power supplies for the magnets and power injection systems for the plasma, coil protection equipment, and the cables and bussing. Table 4-16 contains key magnet power conversion system data for FPD-I. The magnet design was not well enough established during the early study to determine the coil currents. Coil currents were based on typical currents used in the MARS magnets.[2] These MARS currents are much lower than the magnet design currents established later for FPD-II. As a result, the bussing and coil protection cost for FPD-I are substantially less than for FPD-II. Energy requirements were calculated for the central cell and axicell coils. For end cell magnets, the energy requirements were extrapolated from similar data for MARS.

TRITIUM SYSTEMS

The features of a fusion reactor like FPD-I that are important for the design of the tritium systems are: (1) the amount of fusion power and the fractional burn; (2) the use of neutral beams or pellet fuelers for fueling; (3) the presence of a blanket module with or without a power train; and (4) the size of fuel storage requirements.

The size of the fuel processing and storage system depends on the fusion power, the fractional burn, and the length of the burn. These input parameters and the tritium and deuterium mass flow rates that result are shown in Table 4-17 for two different fueling options--positive neutral beams and pellets. The overall efficiency of positive neutral beams ranges from 0.2 to 0.3; therefore, the total tritium input ranges from 22 to 33 g/hour or 7 to 10 kg during a burn cycle of 300 hours. The fueling rate for pellet fuelers may range from 3 to 10 pellets/s with ∿100% waste at each of these rates.

Table 4-16. The FPD-II magnet power conversion data.

Magnet group	NPS[a]	PSVOLT	PSKA	BUSLM	NBKRS	NDR	EDRMJ	PDRMW
Central cell-7	1	30	6	150	5	16	175	2.2
Choke insert-2	1	1	±220	100	0	0	0	0
Choke bkgrd-2	2	30	9	100	4	8	500	3.0
Transition 1-2	2	12	6.5	100	4	8	100	1.6
Anchor cell-4	2	12	6.5	120	4	8	100	1.6
Plug cell-4	2	12	6.5	140	4	8	120	2.0
Transition 2-2	2	12	7.0	160	4	8	75	1.8
Recircularize-2	2	12	7.0	180	4	8	75	1.8

[a]For mnemonic definitions see Table 4-15.

The total tritium input ranges from 13 to 38 g/hour; the minimum rate
corresponds to a supply rate of 4 kg/cycle. At the lower throughput, the
pellet fueler has an advantage over neutral beams for the following reason.
First, since two hours of tritium fuel is stored to ensure constant fueling
during operation, higher fueling rates result in higher inventories. Second,
processing units will contain higher tritium inventories at the higher rates.
Using the throughput rates in Table 4-17, tritium inventories in the test cell
and other processing areas are determined. These are shown in Table 4-18. A
system with an inventory of 200 g could be used to handle both options.

The units supplied in the processing area include uranium storage beds, a
fuel cleanup unit, a cryogenic distillation unit, a waste gas recovery system,
a solid waste disposal system plus all controls, monitors, analytical
equipment and necessary secondary confinement, and processing systems needed
to support the system. The units are sized based on Tritium Systems Test
Assembly (TSTA) reference units; they are located in a tritium processing
building.

Table 4-17. Tritium and deuterium mass flow rates for FPD-I.

Input parameters	Value
Burn time (h)	300 (12.5 d)
Plant availability	0.25
Power (MW)	360
Current to central cell (kA) or to test cell	0.235
Current to end cell (kA)	0.007
Cycles/year	7.3
Tritium fraction	0.5
Fractional burn	0.17

Processing variables	Value
Tritium burnup (g/h)	2.3
Deuterium burnup (g/h)	1.5
Tritium to plasma (g/h)	6.6
Deuterium to plasma (g/h)	4.4

Fueling options	Beams[a]	Pellets[b]
Tritium waste (g/h)	15.4 → 26.5	6.6 → 31.5
Total tritium input (g/h)	22 → 33	13.2 → 38.1
(kg/d)	0.5 → 0.8	0.3 → 0.9
(kg/cycle)	6.6 → 9.9	4.0 → 11.4
(kg/y)	48 → 72	29.2 → 83.2
Deuterium waste (g/h)	10.3 → 17.8	4.4 → 21
Deuterium end cell (g/h)	2.6 → 3.8	2.6 → 3.8
Total deuterium input (g/h)	17.4 → 25.9	11.4 → 29.2
(kg/d)	0.4 → 0.6	0.3 → 0.7
(kg/cycle)	5.2 → 7.8	3.4 → 8.8
(kg/y)	38 → 57	25 → 64

[a] Beam efficiencies (+) 20-30%, (-) 7-10%.
[b] Waste will range from 100% to 300%. The maximum assumes a rate of
10 pellets/s rather than 3 pellets/s (base case).

4-77

Table 4-18. Tritium inventories (g) in FPD-I.

Option	Beams	Pellet
Location		
Structure[a]	<30	<30
Beam pump[b]	2.5 → 4.2	--
Surge tank	2.5 → 4.2	--
Pellet fueler	--	10
Blanket	1	3
Blanket recovery	3	1
Total test cell	39 → 42	44
Storage[c]	44 → 66	26 → 76
Pellet preparation	--	13 → 38
Fuel cleanup	45 → 48	43 → 50
Cryogenic distillation	55 → 58	53 → 59
Total processing	144 → 172	135 → 223
Total	183 → 214	179 → 267

[a] Dissolved tritium in all components.
[b] Cycled 1/6 every 10 minutes.
[c] Two hours of fueling.

The blanket system is assumed to supply all tritium burned (∿5 kg/year) and all tritium lost to decay, released or lost to waste in processing. The amount lost to decay (<20 g/year) depends on the plant inventory. The amount lost to waste depends on the efficiencies of the multiple processing systems. The assumptions made are that losses will be ≤0.1% of the amount processed or ≤85 g/year. The required breeding ratio is then 1.03.

The processing system to remove tritium from the LiPb blanket includes a tritium removal system, a tritium purification system to remove gamma impurities, a tritium control system for the power train coupled to the blanket, an impurity removal system for the LiPb plus auxiliary equipment, dump tanks, etc. This equipment is located in the hot cell.

Four different atmospheric tritium recovery (ATR) systems are provided
for the four tritium areas--test cell, hot cell, tritium building, and heat
exchanger building. The units are sized for the air volumes processed and the
processing time selected (5 days). The areas have minimum internal volumes of
$\sim 5 \times 10^4$ m^3, $\sim 2 \times 10^4$ m^3, $\sim 1.6 \times 10^4$ m^3, and $\sim 3.2 \times 10^4$ m^3. A throughput
rate of 0.5 vol%/min is needed to achieve cleanup in 5 days. This corresponds
to 250 m^3/min, 100 m^3/min, 80 m^3/min, and 160 m^3/min, respectively.

A tritiated water recovery unit is provided. It serves to remove tritium
from any water system that becomes contaminated, and it is also used to
concentrate the tritiated water collected by the different ATR systems. Water
systems that may become contaminated are those that serve beam dumps, halo
plates, direct converter units, etc. The unit has the potential for reducing
tritium waste from water systems by a factor of 10^4.

MAINTENANCE REQUIREMENTS AND OPERATING AVAILABILITY

MAINTENANCE REQUIREMENTS

The maintenance requirements for FPD-I are based on the earlier work done
for the Technology Demonstration Facility (TDF)[14] and the MFTF-α+T
facility.[15] These requirements were used to guide the development of the
FPD-I configuration in the areas of shield design, component location, and
access. The primary thrust of these requirements is that contact operations
are permitted on the device, 24 hours after shutdown, provided the plasma
chamber is unopened and all shielding is in place. The biological shield is
designed to limit activation to 0.5 mrem/hour one day after shutdown. This is
in accordance with DOE Order 5480.1, Chapter XI, "Requirements for Radiation
Protection," which stipulates that a design objective of one-fifth the maximum
permissible dose to radiation workers will meet the ALARA requirement of
1 rem/year. Under these conditions, workers may spend up to 2000 hours/year
(40 hours/week) near the device. This enables personnel to routinely perform
hands-on inspection, disassembly of connections, maintenance equipment setup,
and supervision of maintenance activities in the reactor cell prior to any
device disassembly.

Maintenance operations that require opening the plasma chamber must be
performed remotely because of the high gamma radiation within the shield

boundary. These operations use proven remote-equipment technology in the areas of manipulator handling and viewing.

Component installations are modularized and arranged so that independent disassembly and removal may be accomplished wherever practical using overhead lifting. In addition, reasonable access on the device and within the reactor cell is provided to accommodate lifting fixtures and remote equipment. An example of this access is the overhead access into the end cell to vertically remove C coils or the choke coil set as independent modules. The end cell access cover is estimated to weight 85 tonnes (without water) the C coils weigh <85 tonnes, and the choke coil set weighs 130 tonnes (without shielding). Each of these components weighs less than the main crane capacity of 250 tonnes. Table 4-19 is a listing of major component weights.

Table 4-19. Major component weights
for FPD.

Component	Weight (tonnes)
Central cell module A	155
Central cell module B	110
End cell access cover	235[a]
Central cell solenoids	40
Halo scraper/direct converter	10
Transition coil (T1)	78
Transition coil (T2)	56
Recircularizing coil	15
Choke coil set (without shield)	129
Anchor coil (A1, A2)	56
Plug coil (P1, P2)	66

[a]FPD I; the cover for FPD II weighs
85 tonnes.

In-vessel inspection will precede operations that require opening the plasma chamber. The numerous locations along the length of FPD (approximately every 10 meters) with air-lock interfaces will allow full viewing of the components internal to the plasma chamber, without the requirement of venting. A more detailed discussion can be found in Ref. 15.

Several other maintenance requirements are noteworthy, even though they do not impact the configuration design: (1) personnel and maintenance equipment are not permitted in the reactor cell during device operation. (2) Prior to, and during maintenance operations, power supplies are shutdown and coils are de-energized. (3) Superconducting coils may be kept at cryogenic temperatures for maintenance operations that do not require venting the plasma chamber.

OPERATING AVAILABILITY

The operating life for FPD is ten years with an availability objective of 25%, defined as a percentage of total calendar time. If the operations plan used for MFTF-α+T[1] is assumed for FPD, the annual allocation of time is as shown in Table 4-20.

Table 4-20. Time allocation for FPD.

Allocation	% of Total	Hours
Average operating time of the device	25	2190
Scheduled downtime; 2 weeks/month, 5 days/week, 2 shifts/day	23	1920
Potentially available but not operating (PABNO); all remaining calendar time	52	4550[a]

[a]This time is available for device operation or maintenance.

We assume that the operating time for the device occurs within a 5-to-6-day week with also two working shifts similar to that of scheduled downtime. We also assume that the scheduled downtime averages two weeks per month but may occur at irregular intervals, depending upon the mean time between failure

(MTBF) and mean time to replacement (MTTR) of components. All remaining time
(PABNO) consists of the third daily shift and weekends and is approximately
one-half of the calendar year. The PABNO time can be considered the reserve
for unscheduled maintenance operations, thermal cycling of the superconducting
coils and plasma chamber reconditioning, and additional device operation
beyond the availability objective.

Component Replacements

Several major components have been identified as requiring scheduled
replacements. These components are listed in Table 4-21 along with estimates
of their MTBF[15] and the total number of replacements required, assuming
2190 hours/year of device operations. All others are considered to be
lifetime components, but with varying degrees of risk. Only those replacements

Table 4-21. Replacement scheme for components.

Component	MTBF[a] (hour)	No. of replacements
Choke coils	2200	8-10
Ion sources	900	20-24
Ion dumps	1800	10-12
Cryopanels	4400	5
Windows	1600	12-14

[a]Mean time between failures.

in the neutral beam system, and possibly the replacement of diagnostics, do
not require venting the plasma chamber. Therefore, all other operations are
assumed to require thermal cycling of the superconducting coils.

The coils are designed to accommodate 120 warmup/cooldown cycles over the
ten year life of the device, and Batzer et al. estimates that each cycle
requires six weeks of downtime.[15] Clearly, it is not possible to
accommodate 120 cycles during the device lifetime. An estimate of the number

of cycles can be made by assuming that the scheduled downtime plus the PABNO time is available for cycling if some maintenance activities can be accomplished in parallel. In addition, we assume that plasma chamber detritiation and reconditioning also occur simultaneously; therefore, 6470 hours are potentially available for an upper limit of six thermal cycles per year.

PLANT FACILITIES

The plant for FPD-I includes features common to any experimental fusion facility as well as features unique to mirror fusion. The various elements of the plant are designed and arranged to achieve a smoothly functioning and economic arrangement. Much of the conceptual design effort is focused on high cost facilities, whereas a less detailed definition is given for the remaining facilities. This effort has resulted in an estimate of the approximate sizes and an identification of the general characteristics of the major facilities. Although all elements of the facilities are accounted for in the cost estimate, only the principal elements are summarized in the following paragraphs.

SITE PLAN

A representative location for FPD-type devices is identified within the Lawrence Livermore National Laboratory (LLNL) complex at Livermore, California, shown in Fig. 4-31. This figure shows the relative location of FPD with respect to other LLNL facilities. Good access, ease of construction, and utilization of LLNL facilities to the maximum practical extent were considered in identifying the FPD location.

PLANT ARRANGEMENT

The relative location of all major buildings and facilities are shown in Fig. 4-32. This layout represents a compact arrangement to minimize buildings and systems costs, which are affected by the choice of layout. Common building walls and floor mat, short piping and ducting, and common use of support systems are examples of cost-reducing measures used in the plant arrangement. An additional feature used is the separation of nuclear grade

4-83
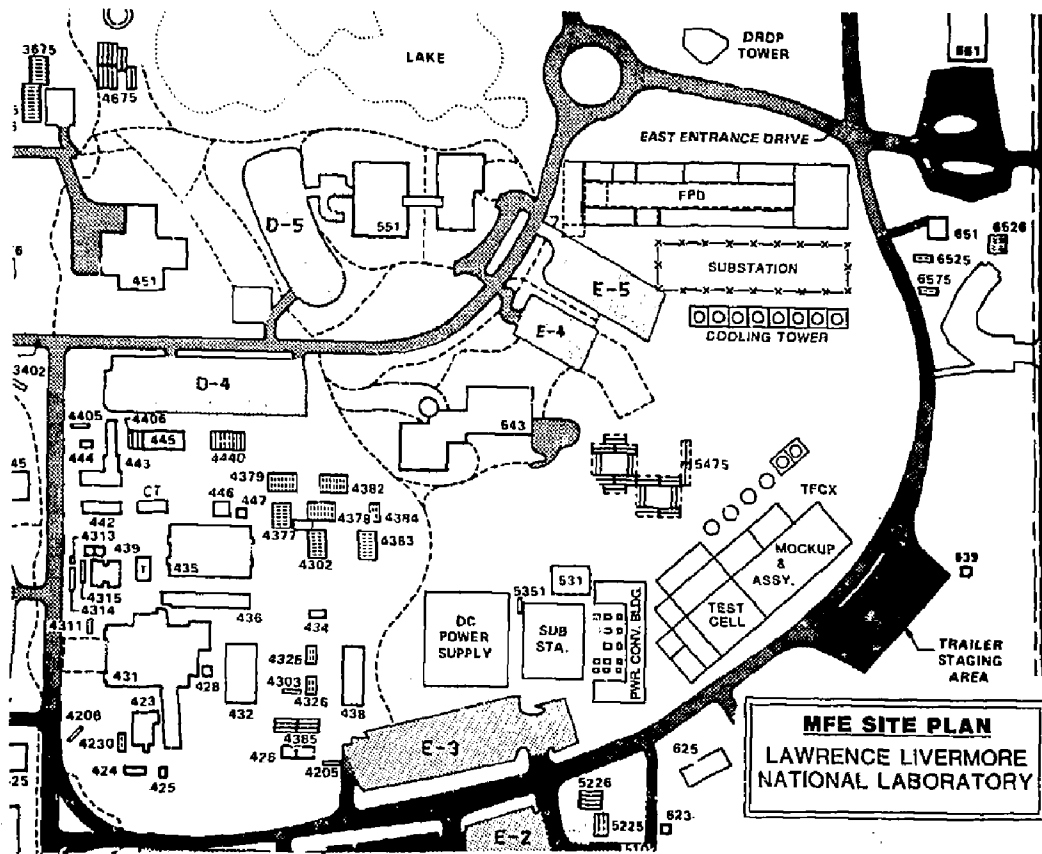
Figure 4-31. The Magnetic Fusion Energy (MFE) site plan at Lawrence Livermore National Laboratory.
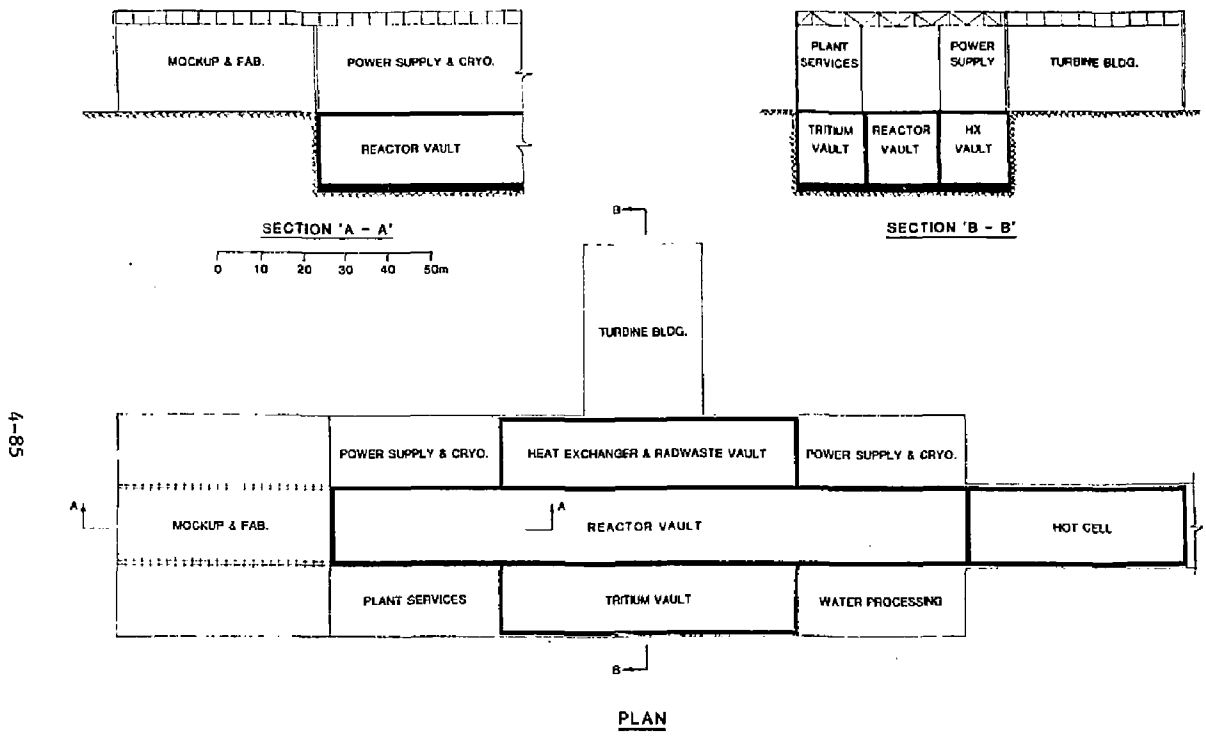
Figure 4-32. The FPD-I building arrangement.

and non-nuclear grade systems and structures so that the non-nuclear grade
system and structures may be constructed at a much lower cost. If these two
grades are not separated, the entire plant needs to be nuclear grade, as are
the present fission plants; thus, the nuclear grade facilities of FPD are
clustered together to provide the desired separation.

Some of the supporting structures are not shown in Figs. 4-30 and 4-31
because corresponding existing LLNL facilities are adequate for these purposes
(e.g., control building).

All plant buildings, structures, and systems are designed to meet
Department of Energy (DOE) and other appropriate safety and environmental
requirements.

Reactor Vault

Because the reactor vault is the most important and expensive of all the
buildings, a design concept trade off involving this building was conducted
with attention paid to: (1) underground vs above ground construction, and
(2) horizontal vs vertical methods of reactor module replacement, affecting
the width and height of the building. Based on economic and technical
considerations, we selected an underground reactor building using the vertical
method of module replacement (Fig. 4-31).

A unique feature of the reactor building shown in Fig. 4-33 is the
overhead transporter concept. In this concept, the main crane (500 tonne) is
located in the transporter, which is external to the reactor building. The
external transporter leaves the reactor building much shorter than if the
crane were located inside the building. To remove a reactor module during a
maintenance operation, the transporter is placed directly over the module. A
smaller crane (75 tonne) inside the transporter removes the T-shaped roof
beams to allow the lifting of the reactor module with the help of the larger
crane. After the module is lifted, the roof beams are replaced and the module
is transported to the hot cell. In this cell, a similar procedure is used to
lower the module.

A safety concern in this concept is the leakage of tritium from the
reactor vault into the transporter and then to the space outside the
transporter. To mitigate this concern, the space directly above the reactor

4-86

20

15

150

16

Beam Dump

Hot Cell

SECTION 'A–A'

0 5 10 15 20m

C

Transporter

D

B

A

A

16

C

D

B

PLAN
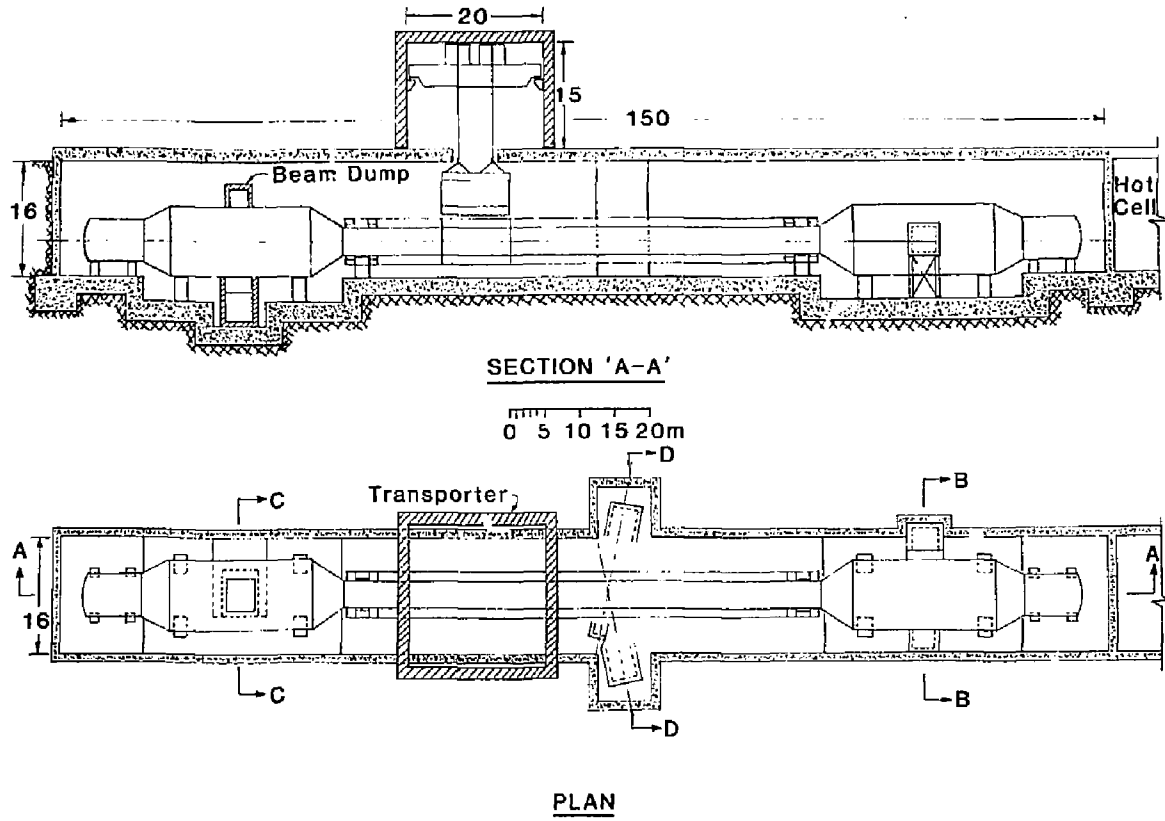
Figure 4-33. The FPD-I reactor building--trench style.

vault (i.e., the tranporter passageway) is made gas-tight to reduce the
leakage of tritium into the environment. Moreover, a subatmospheric pressure
will be maintained in this space.

Other Major Buildings

Other major buildings and structures that are provided for FPD-I plant
include: hot cell, tritium vault, heat exchanger and radwaste vault, power
supply and cryogenics building; fabrication, assembly and mockup building;
plant services building; water processing building; control building; turbine
building; cooling tower; and miscellaneous structures.

Mechanical Systems

The heat transport system for FPD-I transports heat from the reactor
(blanket, reflector, direct converter, halo scraper) to the steam generator.
Total thermal power is 422 MW. A steam turbine power conversion system
generates 164 MW gross electric power. The heat rejection system rejects
258 MW through a mechanical draft wet cooling tower (Fig. 4-34). An additional
80 MW is rejected from the auxiliary cooling systems.

In addition to the major system described above, a large number of other
mechanical systems are needed to support the operation of FPD-I. Some of
these systems are:

- Auxiliary cooling system,
- Emergency cooling system,
- Radwaste handling system,
- Liquid metal (LiPb) processing system,
- Water supply systems,
- Air supply systems,
- Gas systems,
- Heating, ventilation, and air conditioning systems,
- Radiation monitoring system,
- Fire protection system,
- Plant security system.
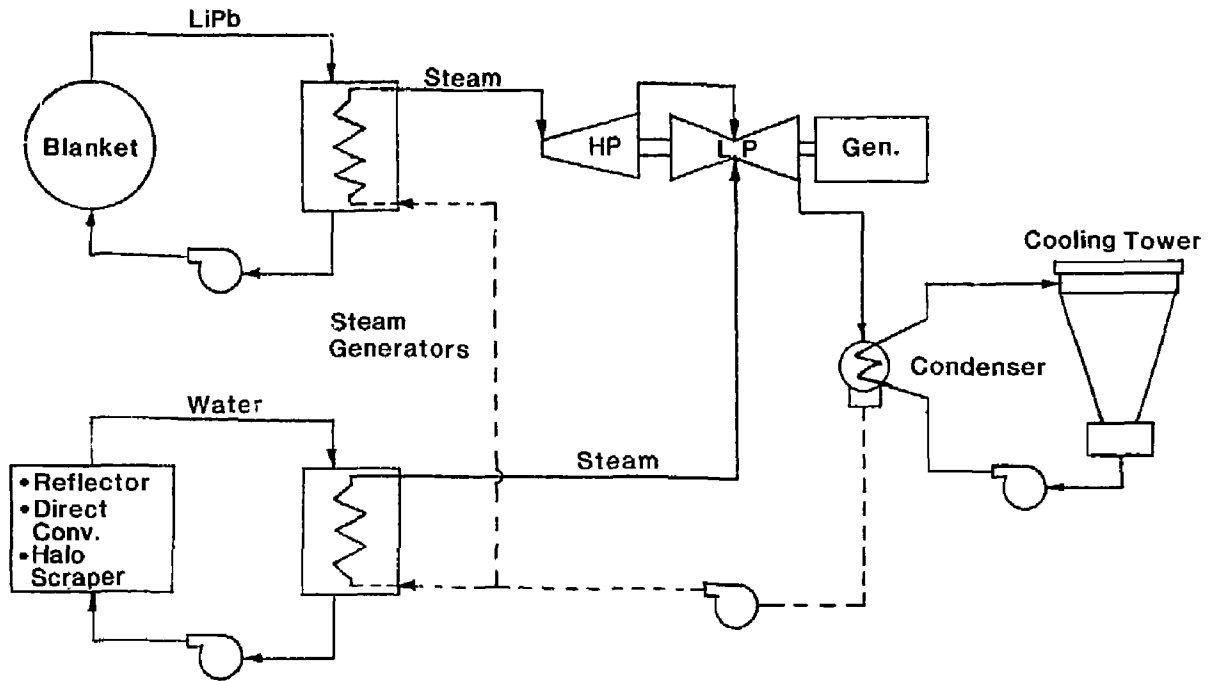
Figure 4-34. The FPD-I heat transport and power conversion system.

REFERENCES

1. W. D. Nelson et al., MFTF-α+T Progress Report, Oak Ridge National Laboratory, Oak Ridge, TN, ORNL/FEDC-83/9 (to be published).

2. B. G. Logan et al., Mirror Advanced Reactor Study (MARS), Final Report, Lawrence Livermore National Laboratory, Livermore, CA, UCRL-53480 (1984).

3. W. S. Cooper and R. V. Pyle, The National Negative-Ion-Based Neutral Beam Development Plan, Lawrence Berkeley Laboratory, Berkeley, CA, PUB-464 (1983).

4. B. S. Brown, "Radiation Effects in Superconducting Fusion Magnet Materials," J. Nuc. Mater. 97, 1 (1981).

5. M. Soell, "Influence of Radiation Damage on Maximum Attainable Magnetic Field for Toroidal Fusion Magnet Systems," J. Nuc. Mater. 72, 168 (1978).

6. R. A. VanKonynenburg, et al., "Fusion Neutron Damage in Superconductors and Magnet Stabilizers," J. Nuc. Mater. 103 & 104, 739 (1981).

7. B. S. Brown and T. H. Blewitt, "Critical Current Density Changes in Irradiated Nb_3Sn," J. Nuc. Mater. 80, 18 (1979).

8. C. L. Snead, et al., "High-energy-neutron Damage in Nb_3Sn: Changes in Critical Properties, and Damage-energy Analysis," J. Nuc. Mater. 103 & 104, 749 (1981).

9. C. E. Klaburde, et al., "The Effects of Irradiation on the Normal Metal of Composite Superconductor: A Comparison of Copper and Aluminum," J. Nuc. Mater. 85 & 86, 185 (1979).

10. J. M. Williams et al., "The Effects of Irradiation on the Copper Normal Metal of a Composite Superconductor," IEEE Trans. Magn. 15, 731 (1979).

11. S. Tokamura and T. Kato, "Effects of Low Temperature Irradiation and other Materials for Superconducting Magnets," J. Nuc. Mater. 103 & 104, 729 (1981).

12. M. W. Guinan, "Radiation Effects Limits on Copper Superconducting Magnets," Lawrence Livermore National Laboratory, Livermore, CA, UCID-19800 (1983).

13. R. R. Gitman, Jr., "Organic Insulators and the Copper Stabilizer for Fusion Reactor Magnets," in Proc. of International Conference on Neutron Irradiation Effects, Argonne National Laboratory, Argonne, IL, November 9-12, 1981.

14. R. R. Coltman, Jr. et al., Radiation Effects on Organic Insulators for Superconducting Magnets, Oak Ridge National Laboratory, Oak Ridge, TN, ORNL/TM-7077 (1979).

15. T. H. Batzer et al., A Tandem Mirror Technology Demonstration Facility, Lawrence Livermore National Laboratory, Livermore, CA, UCID-19328 (1983).

Section 5
FPD-II

5.0 FPD-II

THE FPD-II CONFIGURATION OVERVIEW

The second option for the Fusion Power Demonstration, FPD-II, has a central cell length of 96-m measured from the centerline of one choke coil to the other. This increased length together with an improved end plug design increases the fusion power to 480 MW. Without a deuterium-tritium (DT) axicell for nuclear testing, this ignited plasma concept would be capable of supplying ∿200 MW net electric power. Like the FPD-I design, the use of tritium-breeding liquid lead-lithium blanket modules make this reactor self-sufficient in tritium. Thus, this device should be a true fusion power demonstration reactor.

The overall configuration to FPD-II is presented in Fig. 5-1. The baseline design features of this design include a nuclear testing station or DT-axicell, central cell modules similar to those in FPD-I that use the semicontinuous solenoid concept, and end cells configured similar to those in FPD-I.

The DT-axicell arrangement, although based on the Mirror Fusion Test Facility α+T (MFTF-α+T)[1] configuration, was developed for the more demanding FPD-II goal. This goal requires more test area at significantly higher wall loading. The mechanical arrangement of FPD-II features a 2-m-long nuclear-test module (vs 1-m-long for FPD-I) to which 4-5 MW/m^2 of neutron power can be applied. The beam power that is needed to reach this wall loading requires the mechanical arrangement shown in Fig. 5-2.

The axicell consists of two superconducting background coils (CS1), two copper choke coils (CCC1), one copper field-enhancing coil (CSO), nuclear shielding, test module, vacuum vessel, and support structure. The CSO coils are an integral part of the test module. The choke coils (CCC1) are supported by the nuclear shield (Fig. 5-3). To remove a CCC1 coil, the test module and magnet hatch must be removed; then the CCC1 coil and surrounding shield are transported in the axial direction to clear the nuclear shield in the bore of the CS1 coils. Finally, the CS1 coil is removed vertically through the magnet hatch.

(a)

PELLET INJECTOR CENTRAL CELL MODULE DT-AXICELL BEAM DUMP

END CELL

NUCLEAR SHIELDING ICRH 24T CHOKE COIL BEAM DUMP

CENTER CELL
NEUTRAL BEAM SLOSHING ION BEAM PT 'b' ECRH PT 'a' ECRH

(b)

END CELL 'C' COILS BLANKET TEST MODULE ACCESS HATCH

Meters

HALO SCRAPER BLANKET MODULE

DIRECT CONVERTOR LiPb COOLANT
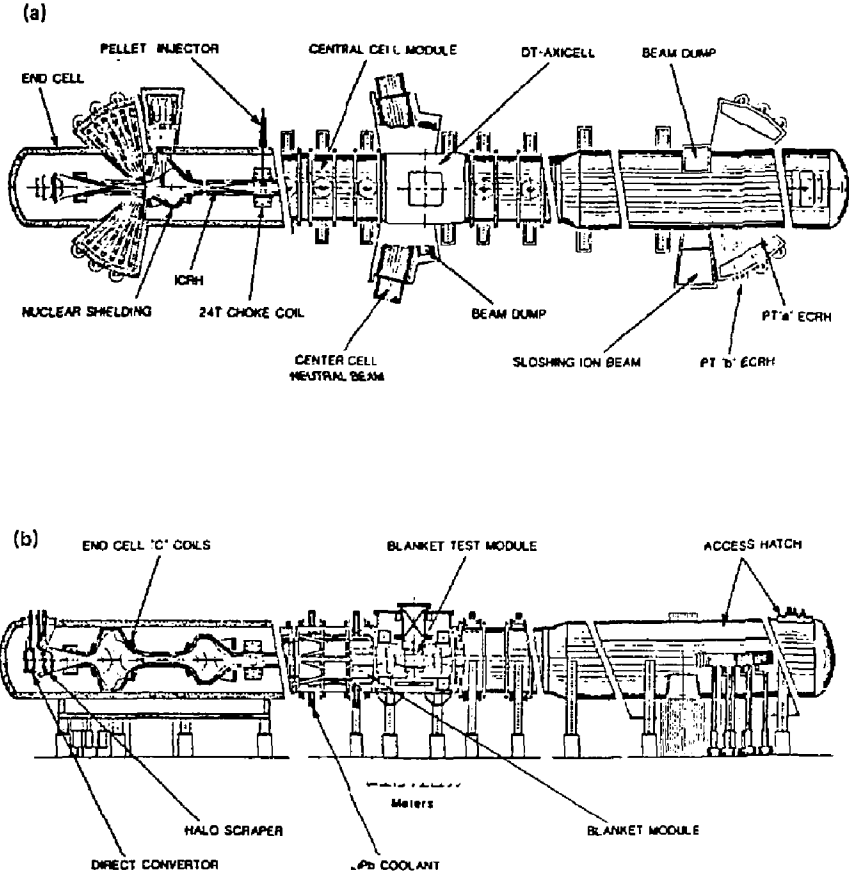
Figure 5-1. (a) FPD-II plan view; (b) FPD-II elevation view.
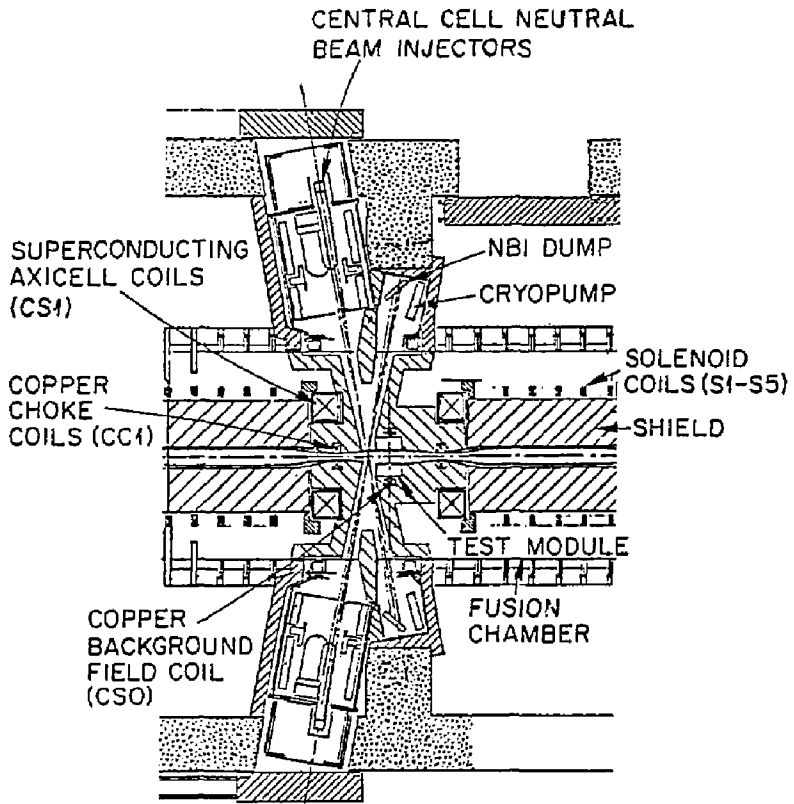
Figure 5-2. The ion-cyclotron resonant heating (ICRH) launcher design.

MAGNET HATCH   TEST MODULE

BACKGROUND COIL
(CS1)

SHIELDING

CHOKE COIL
(CCC1)

VACUUM VESSEL

SUPPORT STRUCTURE

FIELD ENHANCING COIL (CS0)
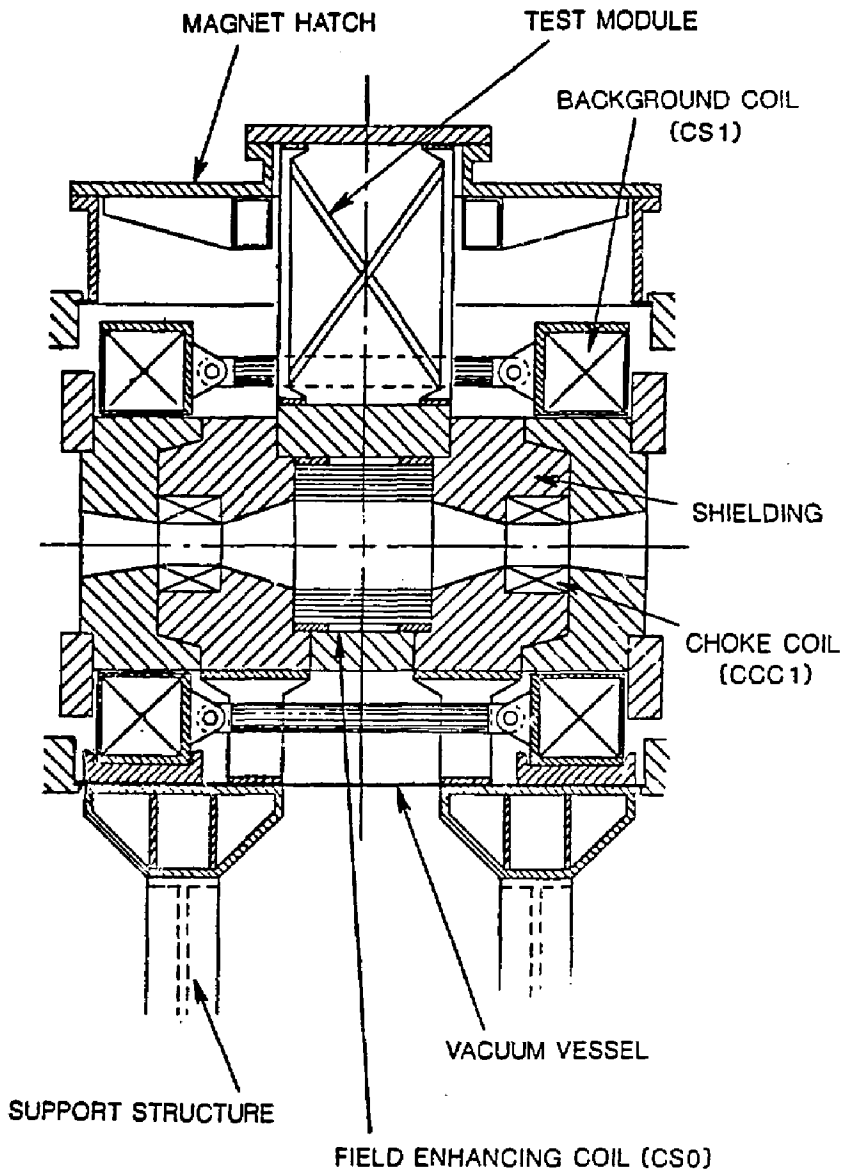
Figure 5-3. The FPD-II DT-axicell configuration.

The axicell vacuum vessel is a cylindrical structure with external stiffeners and two top-located access hatches (Fig. 5-4). Because the test module may be subject to frequent removal, it is furnished with a separate hatch. This large magnet hatch is also used to remove the other coils and shielding.

The axicell nuclear shield consists of a steel ball and water design that satisfies the shutdown dose-rate requirement of 0.5 mrem/hour, 24 hours after shutdown for a 5 MW/m^2 wall loading.

For the FPD-II design, the central cell is configured (Fig. 5-4) using eight full-length modules and two half-length modules that are mated to the choke coils in a manner similar to the FPD-I design. Recent study shows that the portion of the central cell adjacent to the DT-axicell must be configured so that a length of the solenoid can be permanently axially connected to the DT-axicell background coils. This connection is necessary because, like the choke coil area, large axial forces also exist between these coils as in the choke coil region. This minor modification can be easily incorporated in the design.

The central cell module for FPD-II is similar to that for FPD-I with the exception that the portion of nuclear shielding located within the bore of the solenoid coil is sufficient to lower the shutdown dose rate to an acceptable level. Therefore, a double-walled vessel with a water shield is not employed; instead, a single-walled externally ring-stiffened shell is provided in a manner reminiscent of the Mirror Fusion Test Facility-B (MFTF-B) (Fig. 5-5).

The end cell configuration is also similar to that of FPD-I with several significant improvements. First, the end cell biological shield is reduced in size significantly because of the reduced neutron source allowing the use of an end-cell double-walled vessel of only 0.6 m thick. Second, the reduced ICRH-subsystem power requirements allow the use of a rigid waveguide that simplifies the integration of this subsystem; therefore, it is unnecessary to incorporate a four-loop antenna. Third, the point b ECRH subsystem, while still requiring a quasi-optical approach to the transport and launcher, uses 10 active and 2 on-line spare gyrotrons (vs 12 and 2, respectively in FPD-I). This approach makes it easier to provide the clearances required for the surrounding nuclear shielding and permits the use of a less costly nuclear
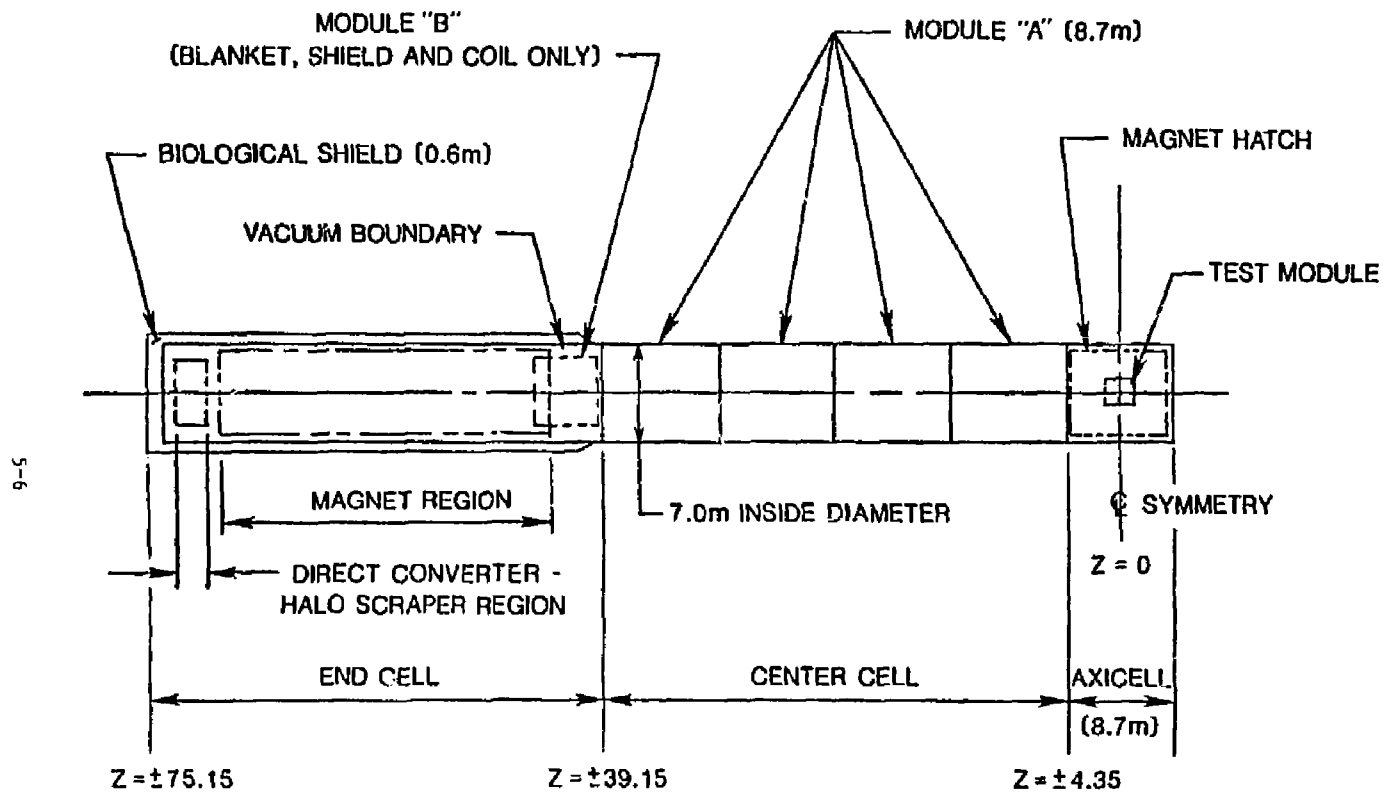
Figure 5-4. The FPD-II modular configuration.
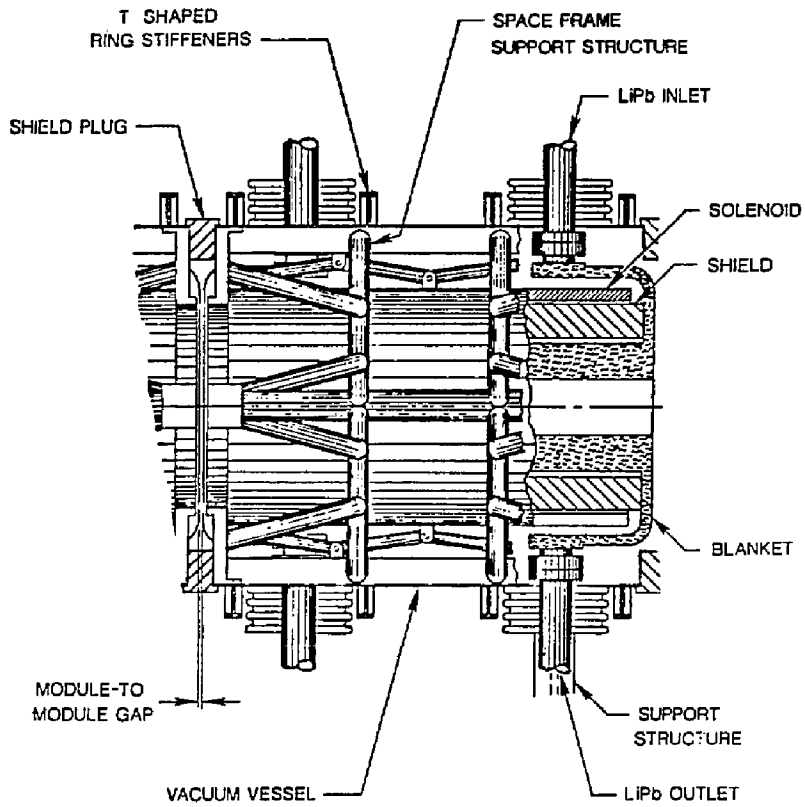
Figure 5-5. The FPD-11 central cell module.

shield design around that portion of the access not directly in the throat of the C coils. Fourth, reduced sloshing-ion-beam power requirements together with improved target point to coil geometry for FPD-II (the angle to the z axis being relaxed to permit 90° injection) allowed us to design a much improved mechanical arrangement (Fig. 5-6). The four sources are in a fan arrangement, two in-line along the axis of the machine, such that two beams cross each other at the target point arrayed in the circumferential direction. This reduction to two beams arrayed circumferentially vs three for FPD-I, allows more space for nuclear shielding within the throat of the C coils. Together with the significant reduction in neutron source strength in the end cell, this design provides improved coil protection and lowered nuclear heat load to the refrigeration system.

In addition, we moved the point of pellet fueling injection so that it does not pass through the insert choke coil, but is located instead toward the central cell side of the choke coil.

In this section, we provide more detail for the FPD-II direct-converter and halo-scraper arrangement making significant progress in the definition of this subsystem. We have confirmed that these are lifetime components. The integration of the direct converter and halo dump into the design is accomplished in a manner similar to the FPD-I design, employing a vertical lifting approach through a dedicated hatch. This allows for ease of installation, is compatible with the overall device maintenance/installation philosophy, shortens the reactor building, and improves our ability to replace subsystems or upgrade to a new concept, if necessary or desirable.

The FPD-II configuration is an improved design primarily because of a significantly better end-cell plug design that reduces the end-cell nuclear-source strength and heating-system power requirements. The central cell module design is also improved, requiring only a single-walled vacuum vessel. While the physics design of the DT-axicell was being optimized, the mechanical configuration approach was confirmed by our studies on the impact of a much higher (4-5 vs 2 MW/m^2) wall loading on the nuclear test-station concept.
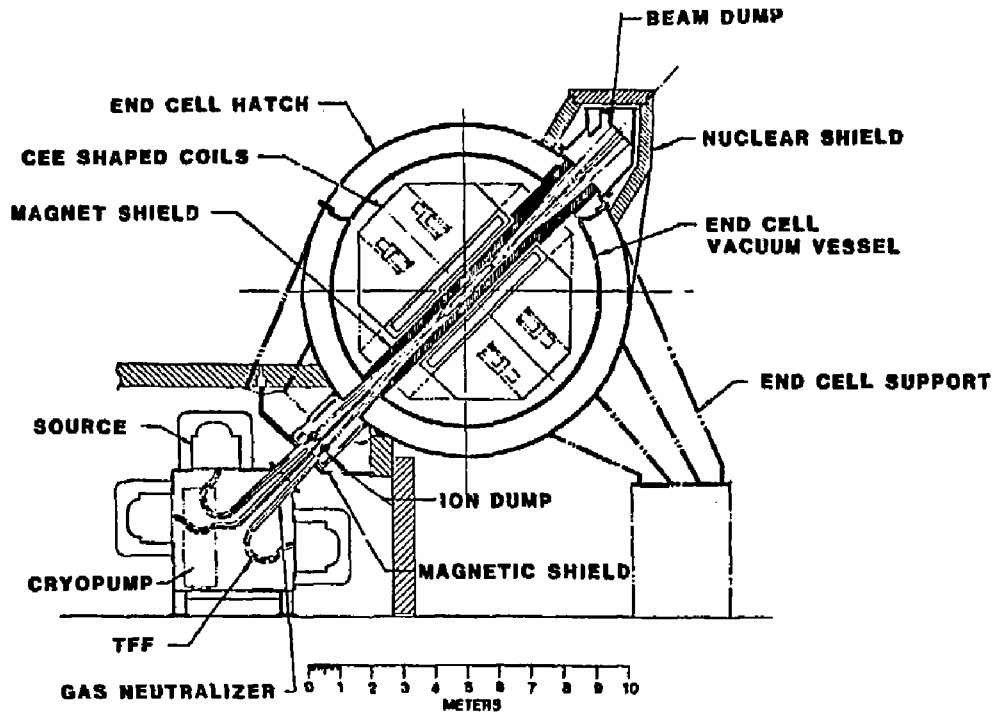
Figure 5-6. Negative-ion sloshing-beam configuration.

POSITIVE-ION-BASED NEUTRAL-BEAM SYSTEM

The primary purpose of the axicell neutral-beam system is to maintain the high temperature and density and hence the high wall loading needed for the blanket test module. This system also fuels the device, therefore the injected species must be of a 50/50 mix of deuterium (D) and tritium (T). Nearly 25 MW of beam power is required at an average energy of 80 keV corresponding to 310.8 A. The injection path is 15° from the normal to the z-axis to achieve good mirror trapping, but still offset in the orthogonal plane to allow injection from both sides of the axicell with clearance from beam dumps.

The D and T beamlines differ because: (1) the neutralization efficiency has an inverse mass dependence for a given energy; (2) the heavier tritium specie has a slightly better species mix; and (3) the extracted current and accelerator grid conductance both decrease as the inverse square root of the mass for given source dimensions. However, in most respects, the two beamline configurations are similar and are based on the Technology Demonstration Facility (TDF)[2] and MFTF-α+T[1] central-cell beamline design concepts. The average energy for these devices can be specified in two ways: (1) D and T species both having an average energy of 80 keV corresponding to a 100-keV D beam and a 90-keV T beam; or (2) average all injected particles to define an 80-keV D beamline and a 120-keV T beamline. The latter method was chosen here because the total beamline efficiency was higher and less sources were required.

Tables 5-1 through 5-5 summarize the requirements, the basic beamline configuration, and the key system parameters; blowups of the axicell and the beamlines are shown in Figs. 5-7 and 5-8. Individual source currents for the D and T beamlines are 71.0 A and 59.3 A, respectively. The D system configuration is identical to MFTF-α+T with four sources in the beamline (3 operating/1 redundant) as depicted in Figs. 5-9 and 5-10. Lower extracted T currents for the same source result in an extra tritium source in the D-system beamline (4 operating/1 redundant). Consequently, the T-ion bending

Table 5-1. Axicell beamline requirements.

Requirements	Value
Delivered power (MW)	24.86
Averaged ion energy (keV)	80
Delivered current (A)	310.8
Injection angle (from ⊥ to z-axis) (deg)	15

Table 5-2. Axicell beamline configurations for TDF and MFTF-α+T.

	D-beamline	T-beamline
Beam energy (keV)	80	120
Delivered power (MW)	9.39	15.39
Full energy (MW)	7.13	13.04
Half energy (MW)	1.74	2.07
Third energy (MW)	0.54	0.28
Line power (MW)	23	38.25
Injector efficiency (%)	40.5	41.1
Diameter		
Vacuum vessel (m)	3.25	4.0
Beamline (m)	3.95	4.8
Length (m)	11.5	11.5
Number of sources	3/1	4/1
(operating/redundant)		
Beam footprint at plasma axis (cm^2)	8.3 x 8.3	8.3 x 8.3
Total cryogen requirements		
LH_3 (ℓ/hour)	75	75
LH_2 (ℓ/hour)	304	304

Table 5-3. Axicell beamline source for Oak Ridge National Laboratory (ORNL) long-pulse three-grid accelerator with circular apertures.

	D-beamline	T-beamline
Source current (A)	71.0	59.3
Species mix	0.82/0.14/0.04	0.88/0.01/0.02
Cross section (cm^2)	16 x 40	16 x 40
Divergence (deg)	0.5 x 0.5	0.5 x 0.5

Table 5-4. Axicell beamline neutralizer for a low-conductance, tapered, water-cooled rectangular duct.

Target thickness (95% equilibrium neutralization) (cm^2)	7.68×10^{15}
Length (m)	1.5
Cross section	
$a_1 \times b_1$ (cm^2)	16 x 44
$a_2 \times b_2$ (cm^2)	16 x 35

Table 5-5. Axicell beamline drift duct (a tapered, water-cooled, rectangular duct).

	D-beamline	T-beamline
Length (m)	2.24	2.24
Cross section		
$a_1 \times b_1$ (cm^2)	60 x 35	90 x 35
$a_2 \times b_2$ (cm^2)	35 x 19	43 x 19

CENTRAL CELL NEUTRAL
BEAM INJECTORS

SUPERCONDUCTING
AXICELL COILS
(CS1)

NBI DUMP

CRYOPUMP

SOLENOID
COILS (S1-S5)

SHIELD

COPPER
CHOKE
COILS (CC1)

TEST MODULE

COPPER
BACKGROUND
FIELD COIL
(CS0)

FUSION
CHAMBER
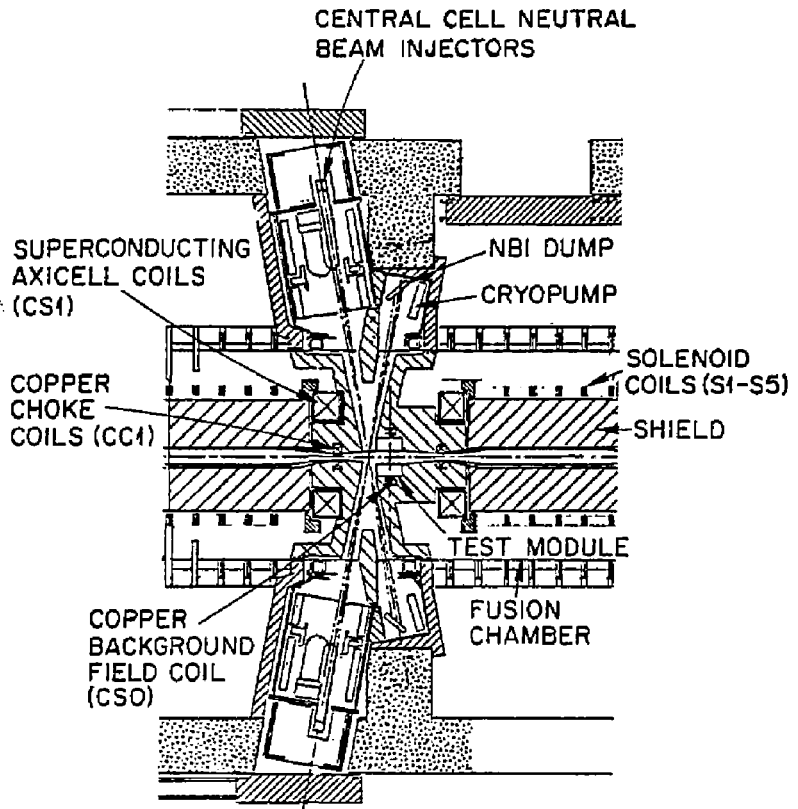
Figure 5-7. The central-cell reactor-like insert in MFTF-α+T.
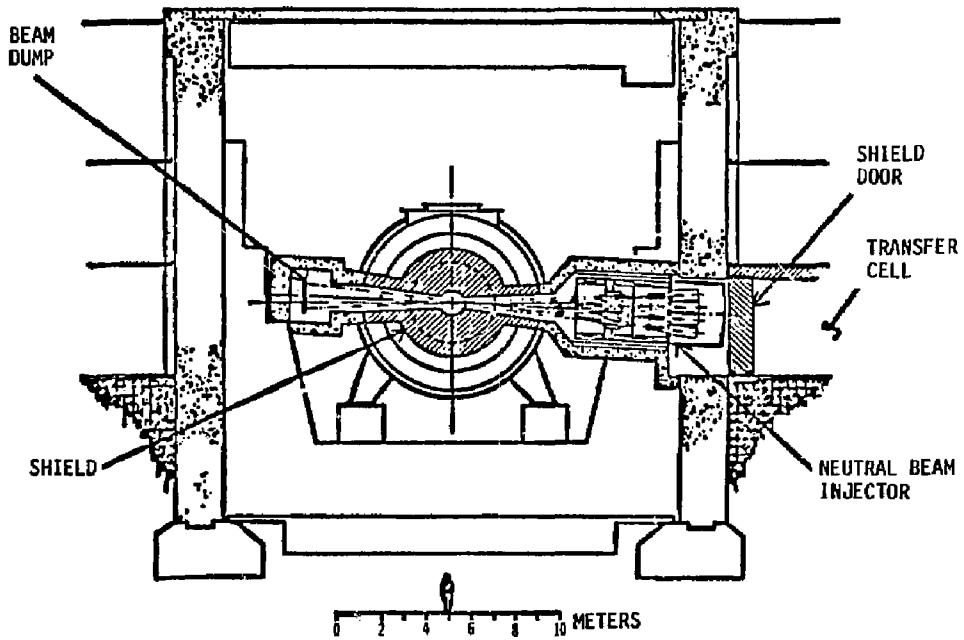
Figure 5-8. Elevation through the central cell.
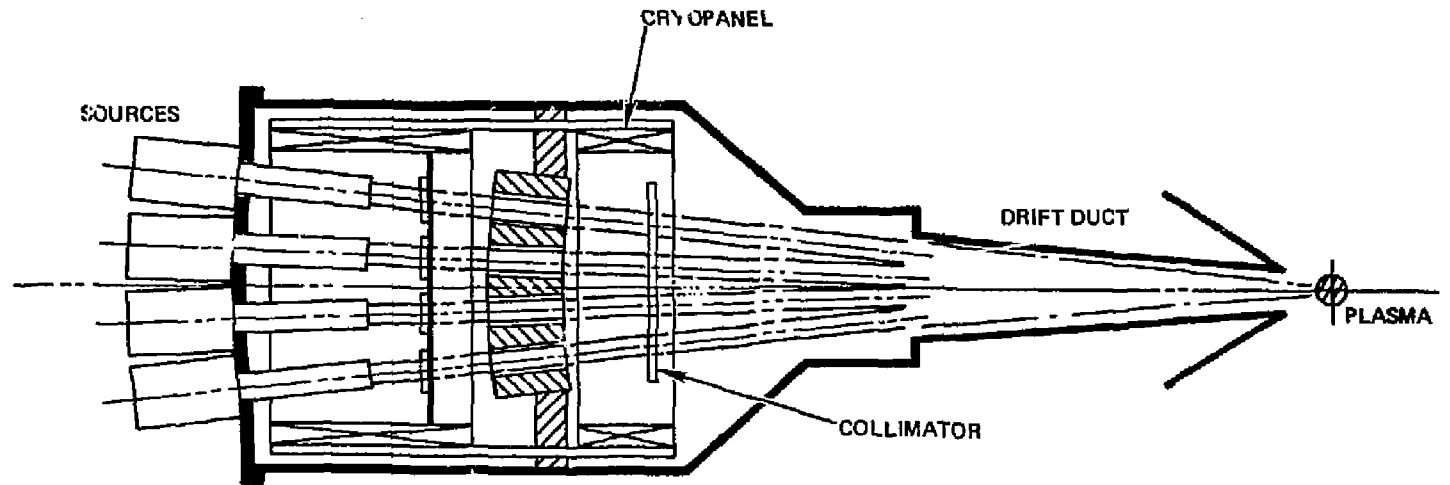
Figure 5-9. Beamline layout.
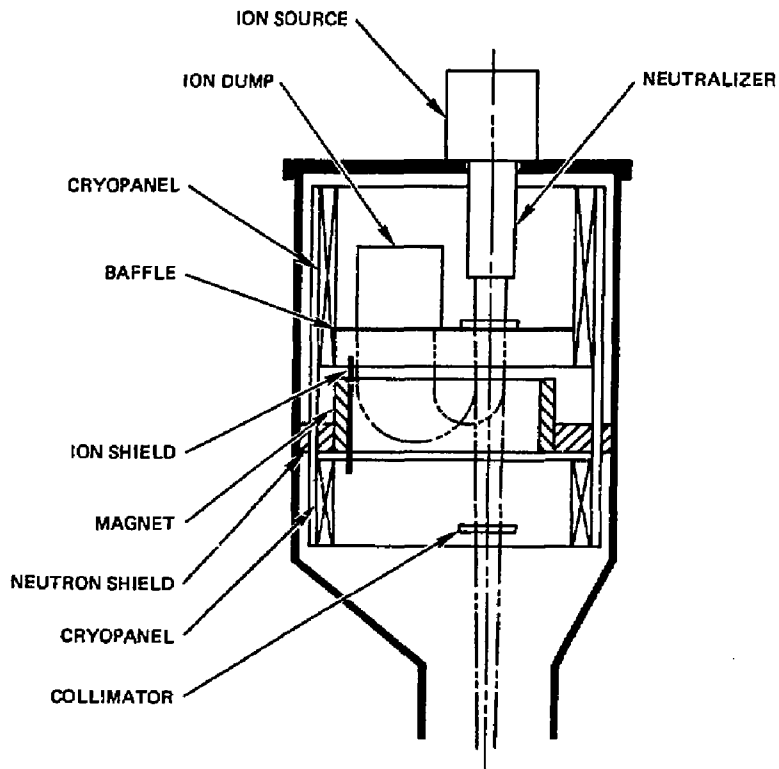
Figure 5-10. Arrangement of beamline components.

magnet requires an extra slot; plus the drift duct, the vacuum vessel, and the shields are larger than those for the deuterium beamline.

Figures 5-11 and 5-12 summarize the power flow for the D and T beamlines, respectively. The beam accelerators in each beamline are powered by a single converter/transformer through protection and regulation circuitry; sources in a beamline also have a common power supply. Each ion bending magnet has its own small power unit (i.e., <50 kW). Very high powers must be dissipated in the ion dumps; we may need to directly convert a portion of this power to extend what may be an unacceptably short lifetime of the ion dump. Finally, the efficiency for the entire axicell neutral-beam system is 40.7%; the system pulls 61.25 MW of line power.

DT AXICELL MAGNETS

The axicell magnet system consists of five circular coils--three normal copper coils and two superconducting coils. These five coils provide the axial field for this region and satisfy the other system requirements.

System Function Summary

The DT axicell is a test section that has a uniform neutron wall loading over the length of the test module. This axicell confines the plasma under ignition conditions with relatively high $<\beta>_{axicell}$.

Requirement Summary

The length of the DT axicell is 5 m, defined by 15-T peaks in the mirror field to satisfy the physics requirements of the TPD machine. Key physics requirements are 5-T magnetic field on axis at $z = 0$ in the test space; $\sim$15-T choke field at the ends of the axicell ($z = \pm2.5$) for ion confinement.

The sizes and locations of magnets must be compatible with various configurational constraints. These constraints include adequate access for the heating system (neutral beams); access to the test space; and enough clear bore to accommodate the plasma and plasma halo.
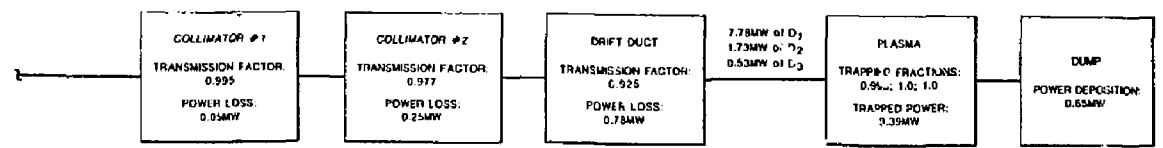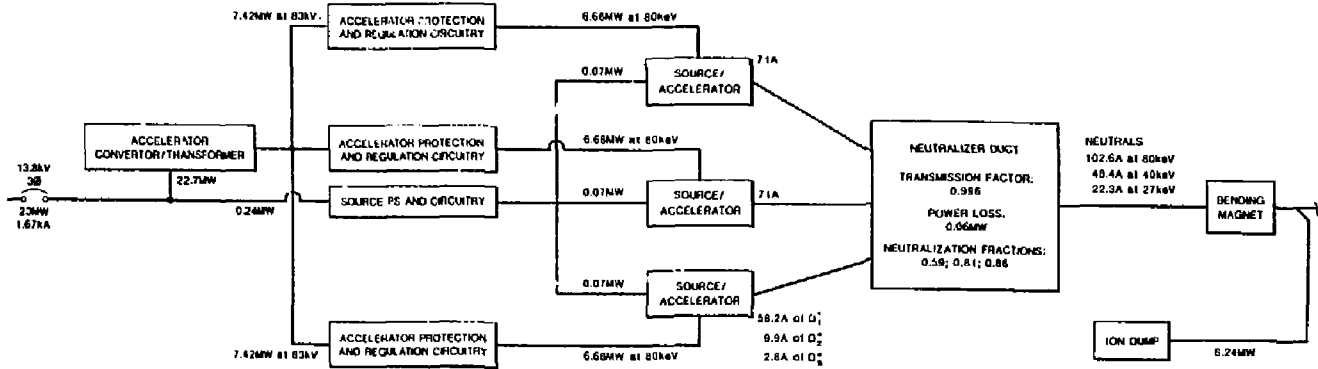
Figure 5-11.   Current and power flow for the axicell deuterium beamline.
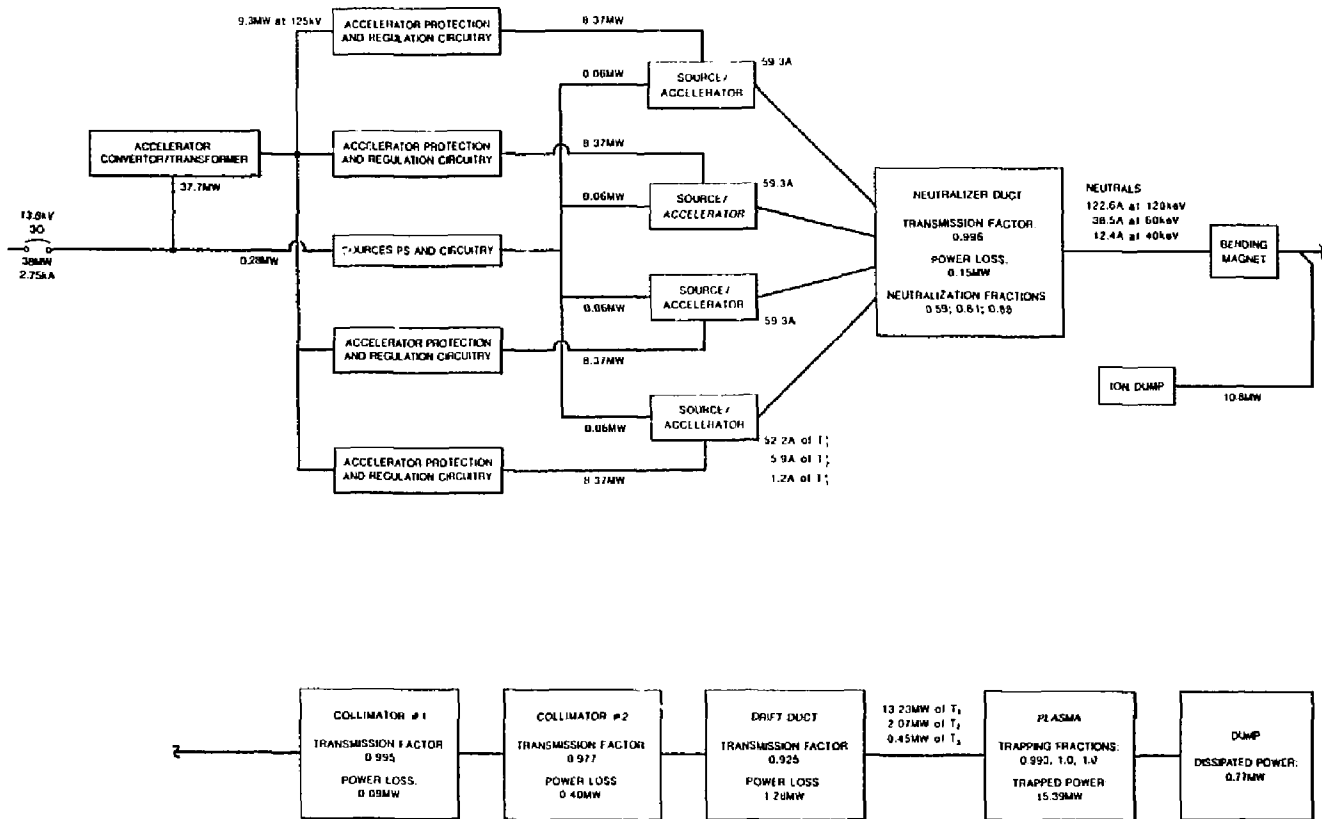
Figure 5-12. Current and power flow for the axicell tritium beamline.

Magnet Layout

The configuration of the axicell magnets is shown in Fig. 5-13 and the key design parameters are listed in Table 5-6. The superconducting coils (CS1) in conjunction with the normal copper coil (CS0) provide 5-T background magnetic field at the midplane (z = 0). Under the copper choke coils (CCC1), the peak field is 15 T at z = ±2.5 m.

The peak fields at the windings of choke coils and CS0 coil are 15 and 5 T, respectively. These coils employ internally-cooled copper plates. The main design constraint on these coils is removal of the resistive and nuclear heat loads. These coils are designed to withstand the radial and axial loads of normal FPD operation. The CS0 coil is removed, along with the test module for access to the test space.

The CS1 background field coils are superconducting. The peak field at the winding is 12 T. The winding layout and key design parameters for these coils are given in Table 5-7. These CS1 coils are similar to the coils required in the DT cell of the MFTF-α+T. A Nb_3Sn force-cooled conductor (shown in Fig. 5-14, similar to the conductor used in the Westinghouse Large Coil Project (LCP) coil, is utilized in these coils. The winding is pancake wound (three to four conductors are wound in parallel). The splices, outlet LHe manifolding, and leads are located at the outer perimeter of the coil. The LHe inlet is provided at the inner surface of the winding with no splices made at this location. With this winding concept and cooling scheme, the winding current density of $\sim$2000 A/cm^2 is feasible. These coils are discharged with a center-tap for keeping the dump voltage at $\sim$1500 V and for limiting peak winding temperature rise to $\sim$200 K.

Conclusion

The design of normal copper coils and superconducting coils needed for a DT axicell is feasible. Some development work is required for the Nb_3Sn force-cooled conductor. This task has also been identified as needed in the Tokamak Fusion Core Experiment (TFCX) project.

BEAMLINE

CENTRAL CELL MODULE

BACKGROUND
COIL (CS1)

CHOKE COIL
(CCC1)

TEST MODULE

TEST MODULE COIL
(CS0)

BEAM DUMP
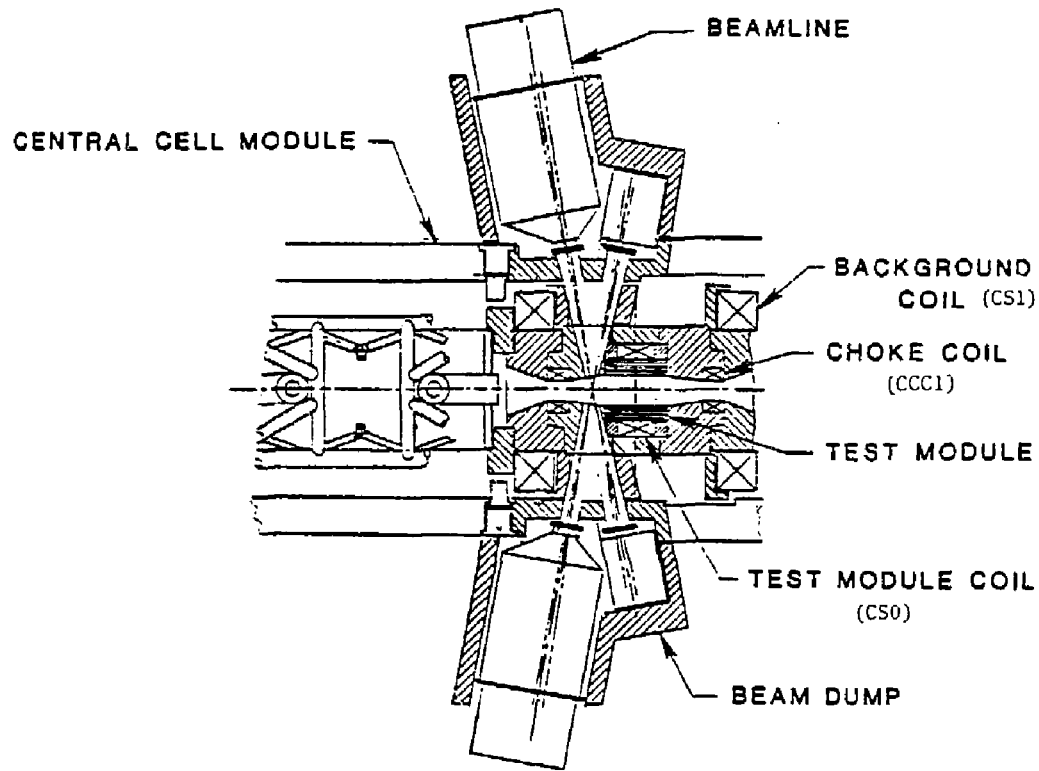
Figure 5-13. The DT axicell coil configuration.

Table 5-6. Key design parameters for the axicell magnets.

Coil	Mean axial position (m)	Mean radial position (m)	Axial build Δz(m)	Radial build ΔR(m)	Winding current density (A/cm^2)	MA-turns	Peak field (T)
CCC1	+2.50	0.50	0.90	0.38	2450	8.38	15
CS0	0.00	1.20	1.00	0.09	2400	2.16	5
CS1	+3.15	2.50	1.15	1.15	2000	26.45	12

Table 5-7. The CS1 coil design parameters.

Parameter	Value
Electromagnetic	
Operating current (kA)	12
Winding current density (A/cm^2)	2000
Geometric	
Total number of turns	2204
Number of pancakes	46
Number of turns/pancake	48
Coil length (cm)	108.2
Coil depth (cm)	112.9
Cryogenic	
LHe inlet temperature (K)	4.0
LHe inlet pressure (atm)	5
LHe outlet temperature (K)	5.0
LHe outlet pressure (atm)	3
Peak nuclear heating rate (mW/cm^3)	<1
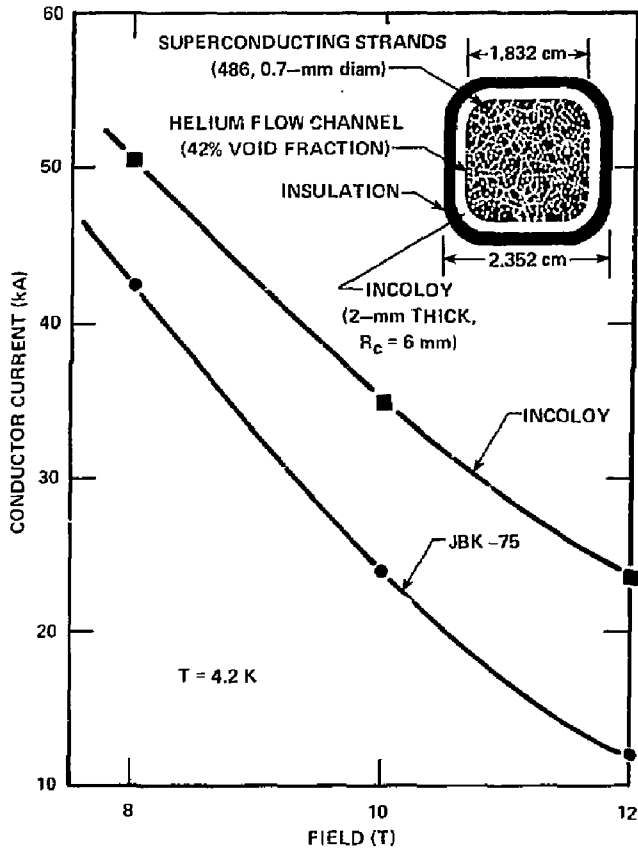
Figure 5-14. The Nb$_3$Sn-conductor critical current as a function of magnetic field.

SHIELDING AND VACUUM CONTAINMENT

The DT axicell is located symmetrically at about z = 0, as shown in Fig. 5-15. The cylindrical axicell is 8.7-m long and has an inside diameter of 7.0 m. The central cell A modules are the same length and can be interchanged with the axicell. The major axicell components described in this section are the vacuum vessel and the shielding.

Vacuum Vessel

The vacuum vessel is a single-walled, externally stiffened structure with two top-located hatches (Fig. 5-16). The small hatch is an integral part of the test module. The test module consists of the hatch cover, test module, field-enhancing coil (CSO), shielding, and support structure. The test module is supported from the large magnet hatch (Fig. 5-17). The magnet-hatch size allows for removal of all other components. The typical hatch vacuum seal is shown in Fig. 5-17.

The test module can be removed vertically, together with the CSO coil, without disturbing the other components. To remove the remainder of the coil shielding, the test module must be removed first. This sequence provides space for axial translation of the shielding/choke-coil (CCC1) module so that the test module can be removed vertically. The CCC1 coil is supported by the surrounding nuclear shield. To remove a background coil (CS1), all of the adjacent shielding in the coil bore must first be removed; then, the innercoil cold structure can be disconnected, which allows vertical removal of the coil.

Nuclear Shield

The nuclear shield thickness in the axicell is an equivalent of 97 cm, taking credit for the coils and test module where applicable. The shield thickness is based on the shutdown dose-rate requirement and a neutron wall loading of 5 MW/m^2. The shield composition is 87-cm steel/water (60% steel, 40% H$_2$O), 5-cm B$_4$C, followed by 5-cm lead. The steel/water shield consists of a steel container filled with a fixed-size steel ball that results in the
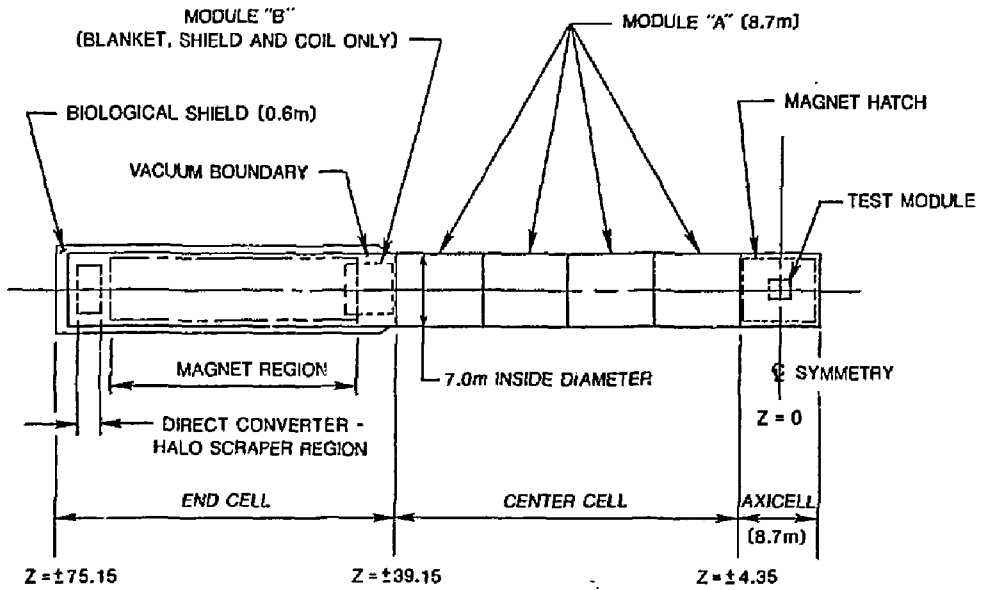
Figure 5-15. The FPD-II modular configuration.
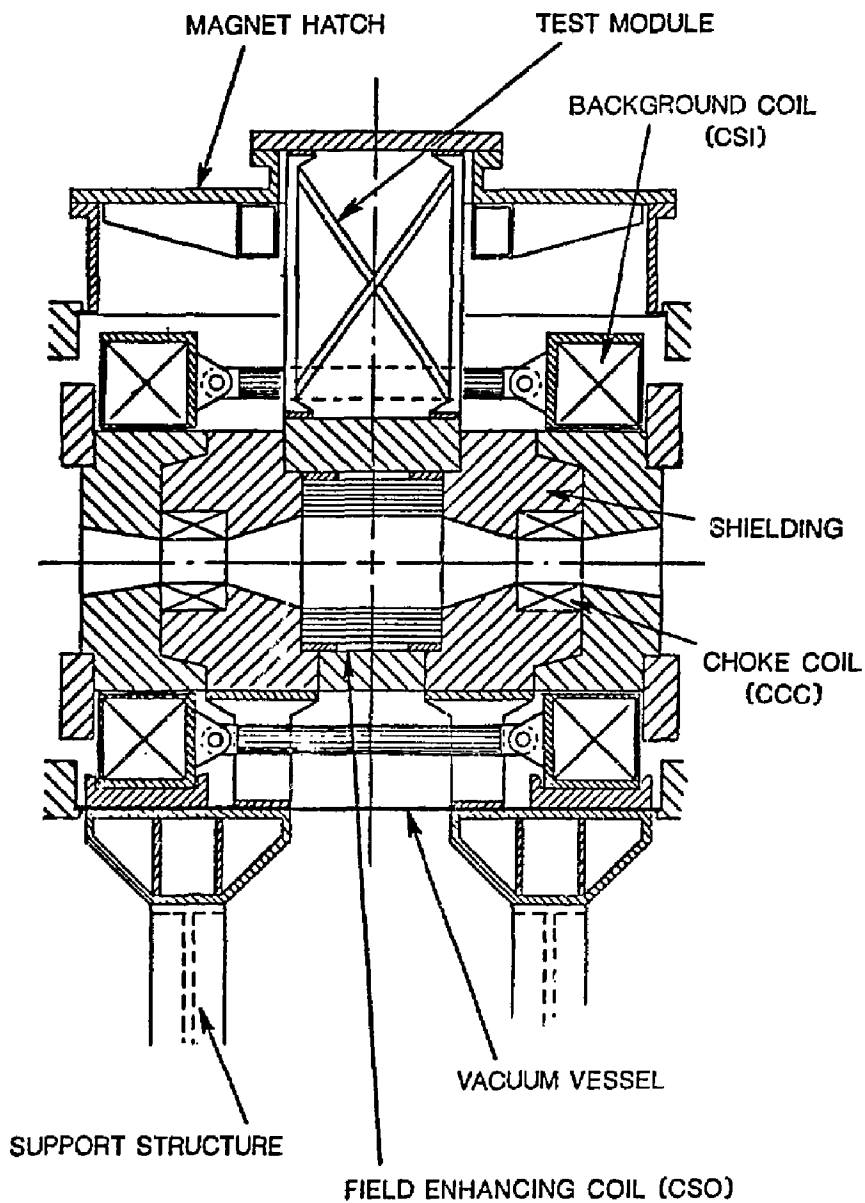
Figure 5-16. The FPD-II DT axicell configuration.
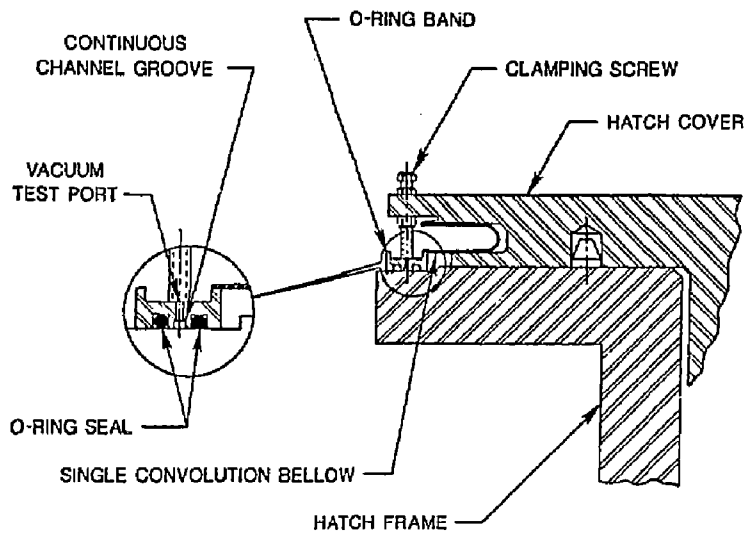
Figure 5-17. The FPD-11 axicell-hatch vacuum seal.

60/40% steel/H_2O ratio. The 5-cm B_4C shield consists of a 20% steel
container, 20% cooling H_2O, and 60% B_4C, with a packing density of 70%
(0.7). A 5-cm Pb shield is attached to the B_4C.

SUPPORT STRUCTURE

Two support legs, each located under the CS1 coil, are provided to
transmit all loads to reinforced concrete piers.

CENTRAL CELL

CENTRAL CELL MAGNETS

The central cell magnet system consists of eight full-size and two
half-size solenoidal modules. Each module has correction coils integral with
solenoid winding for reducing magnetic-field ripple caused by axial separation
between adjacent modules. A DT axicell (discussed earlier in this section) is
located at mid-point of the central cell.

The central-cell magnet modules are similar in size to those for FPD-I.
Design feasibility is discussed in Sec. 4. The active length of the central
cell is 92 m. Effective lengths of the full and half-size modules are 8.7 m
and 5.85 m, respectively. Axial gap between adjacent modules is 1 m.

SHIELDING AND VACUUM CONTAINMENT

The modularization of the central cell is shown in Fig. 5-15. The
central cell consists of eight A modules and two B modules. The A modules are
self-contained assemblies, whereas the B modules are without an individual
vacuum vessel. The B-module vacuum vessel is integrated into the end cell to
provide sufficient end cell length to incorporate access hatches and end
transitions. Each central cell module consists of (outward from plasma) a
$Li_{17}Pb_{83}$ (LiPb) blanket/reflector, shield, solenoid coil, space-frame
support structure, and vacuum vessel. The A modules are 8.7-m long and the B
modules are 6.85-m long. Each A module can be independently, vertically

removed for maintenance. Prior to a B module removal, the adjacent A module must be removed and the B module transferred in the z direction. Figure 5-18 shows a typical A-module configuration.

The central-cell module design enables a buildup assembly sequence, Fig. 5-19. The assembly sequence starts with the space frame mounted in an assembly jig. The solenoid coil is installed, followed by the shield and the blanket. Alternatively, the blankets can be installed after the subassembly is installed inside the vacuum vessel. This design allows for checks and tests at each assembly step. The blankets are supported from the shield. Enough space is allowed between the components for thermal growth. Figure 5-20 shows a more detailed module-to-module seal concept.

Vacuum Vessel

A typical central-cell vacuum vessel is cylindrical (7.0-m inside diameter), with external T-shaped ring stiffeners (Fig. 5-18). The ring stiffeners are connected by longitudinal stiffeners. The vacuum vessel reacts to all loads induced by the internal components.

Shielding

The shield thickness is sized to meet the shutdown dose rate of 0.5 mrem/hour, 24 hours after shutdown. The shield thickness required below the solenoid coils is 58 cm. This shield consists of 53 cm of steel/water and 5 cm of B_4C. The steel/water shield is a mixture of 60% steel and 40% H_2O. The steel shield consists of the container that is filled with one size of steel balls (approximately 60%). The remaining volume, $\sim$40%, is filled with H_2O. The 5-cm B_4C shield is mounted on the outside of the steel/H_2O shield. The B_4C shield consists of 20% steel (container), 20% cooling water, and 60% B_4C, with a density of 70% (0.7). The shield plugs (Fig. 5-18) are the equivalent of 85-cm thick (80-cm steel/water, 5-cm B_4C), the same composition as the remainder of the shield.
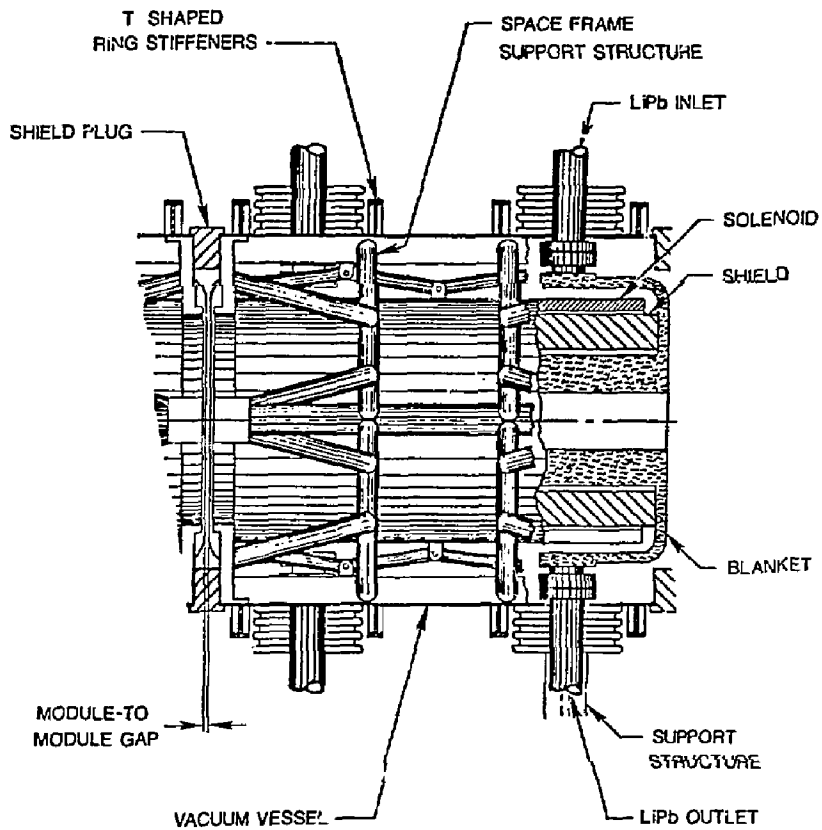
Figure 5-18. The FPD-II central cell module.

COLD MASS SUPPORTS

BLANKET MODULE

NUCLEAR SHIELD

SOLENOID COIL

8.7 METERS

LIQUID LIPb
COOLANT MANIFOLD

CENTRAL CELL
VACUUM VESSEL

B   B

A

A

SUPPORT RAIL INTERFACE

VIEW A-A

VIEW B-B
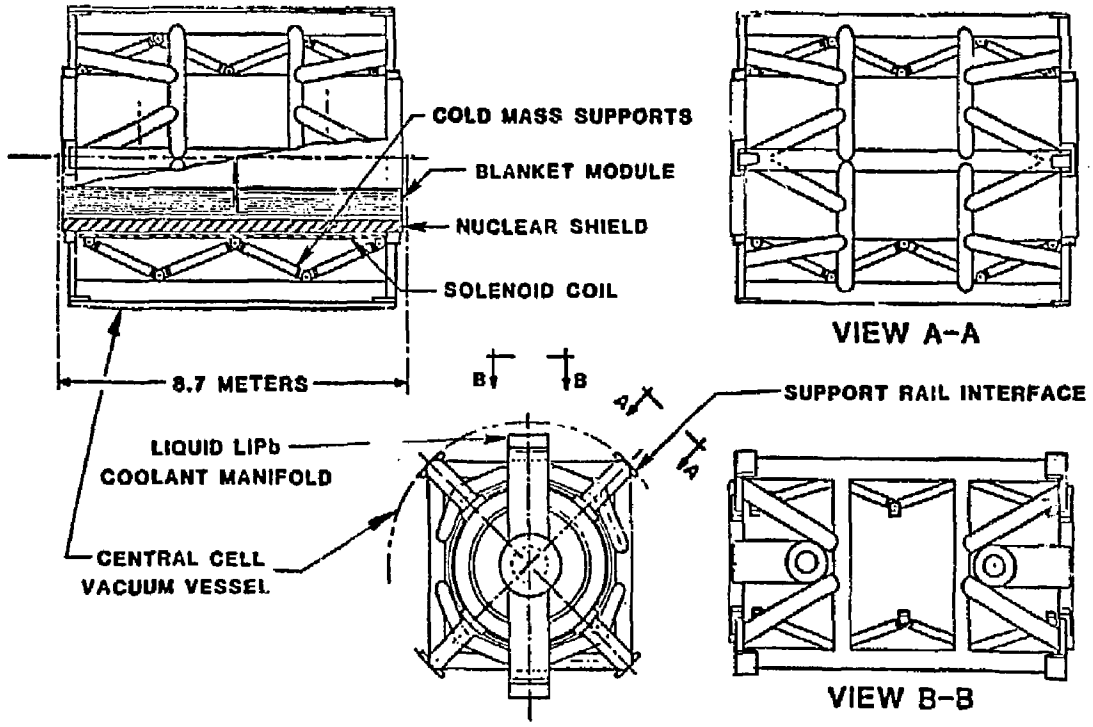
Figure 5-19. The central-cell component assembly.
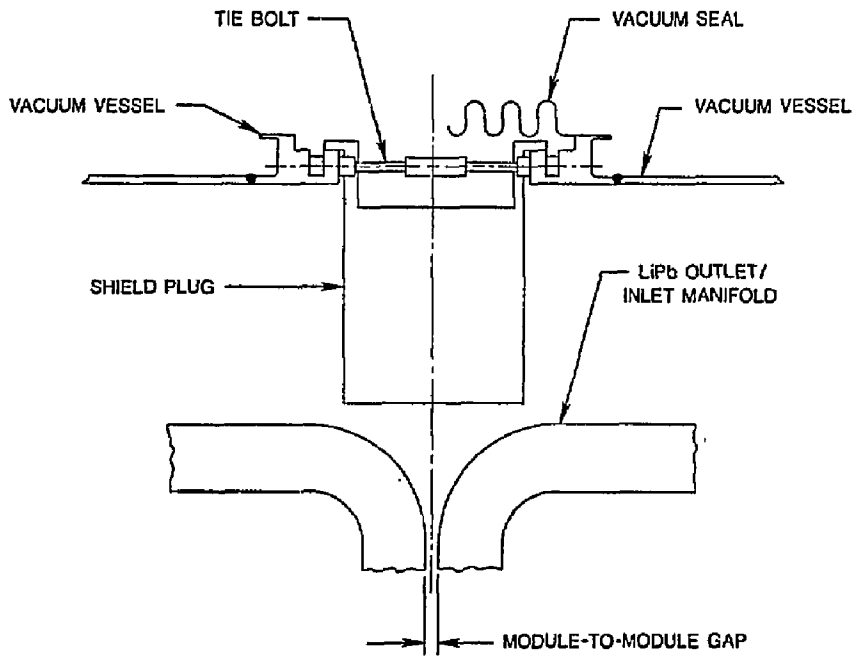
Figure 5-20. Module-to-module seal.

SUPPORT STRUCTURE

Each of the A modules has two sets of support legs. The support legs transmit all of the module loads to reinforced-concrete piers.

END CELL

MAGNETS

The end-cell magnet system consists of two transition, two plug, two anchor-type C coils, and one recircularizing coil. All the C-type coils have essentially the same configuration, dimensions, current density, operating current, and peak fields. The T1 coil has a unique separation of the winding pack into thirds in its minor radius region toward the choke coil. The recircularizing coil is the last coil in the end cell and the configuration is similar to MFTF-α+T.

System Function Summary

The magnet system is sized and arranged to provide the on-axis magnetic field required for plasma performance. In addition, the end cells provide machine plugging and magnetohydrodynamic (MHD) stability.

Requirement Summary

On-Axis Field. The axial-field profile in the end cell region is shown in Fig. 5-21. The peak field on the C-coil conductor is 10 T, and the maximum centerline field is 7.5 T at z = $\pm$51 and 56 m. The minimum end-plug field is 2.5 T at z = 57 m. In addition to these on-axis field requirements, the plasma leaving the end-plug regions must be circular to accommodate a circular direct converter.

Access and Clearance Requirements. Access between and location of end cell magnets must be compatible with the plasma heating systems. These systems are: 475-kW negative-ion neutral-beam injector at z = $\pm$56.62 m, 71-MHz ion-cyclotron resonant heating (ICRH) associated with resonances at z = $\pm$59.3 m.
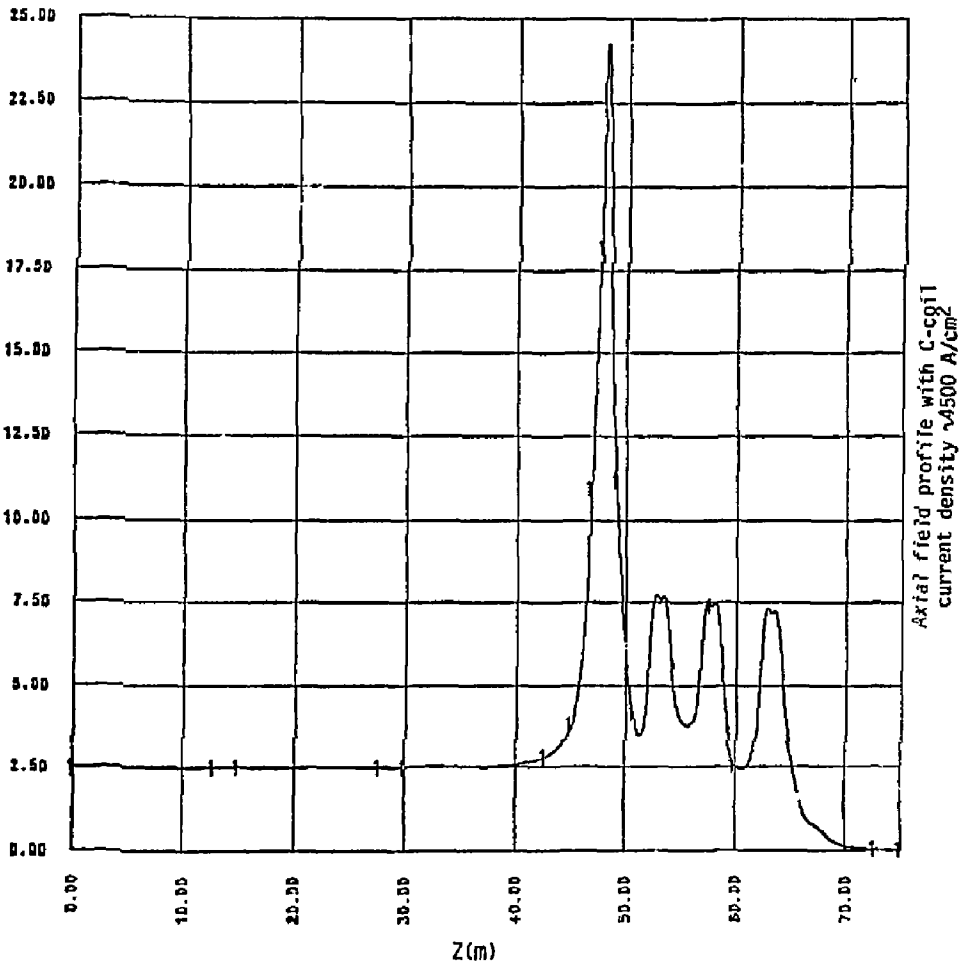
Figure 5-21. Axial-field profile with C-coil current density at ∿4500 A/cm^2.

Design Life and Number of Cycles. The design life and number of cycles for the end-cell magnet system are the same as for the overall system. Design life is 10 years of operation at a 10% duty factor. The superconducting magnets in the end cell are designed to withstand 120 cooldown/warmup cycles and 12,000 charging/discharging cycles at operating temperature.

Maintainability. The end cell magnets are to be designed for the life of the machine; however, realistic magnet replacement schemes must be identified during conceptual design.

End Cell Magnets

Magnet Configuration and Design. The configuration for the FPD-II end-cell system is shown in Fig. 5-22. Locations, dimensions, currents, current densities, and fields associated with this configuration are shown in Table 5-8. This coil-set concept meets the requirements stated earlier in this section.

The conductor selected for the C coil is a modified LCP Nb_3Sn forced-flow conductor. The modifications assumed in this application address the need for higher current density ($\sim 4,500$ A/cm^2) and removal of up to 5 mW/cm^3 of nuclear heating. The modifications assumed to achieve these objectives are as follows:

Current Density
- Using an incoloy conduit material,
- Reacting at 700 C after winding,
- After reacting, Epoxy impregnation.

Nuclear Heating Removal
- . Using larger helium cross-sectional area,
- Having a 3-K inlet temperature for supercritical LHe.

The winding concept assumes double pancakes with three conductors in parallel.
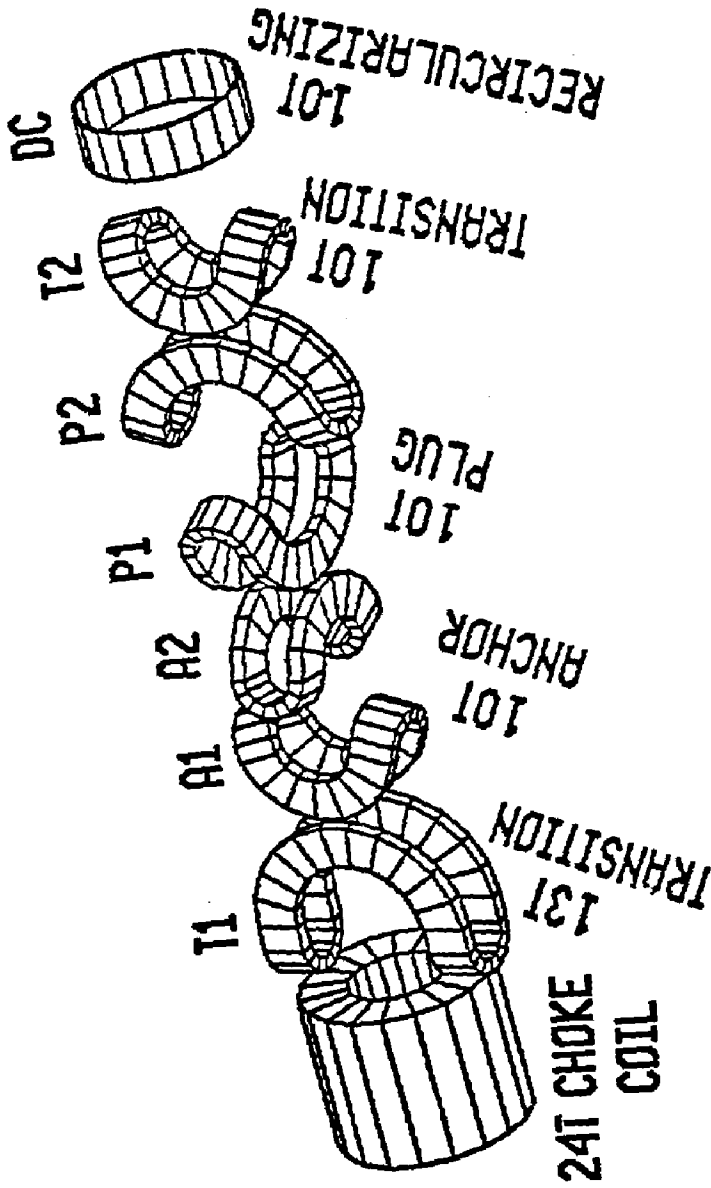
Figure 5-22. End cell configuration. The FPD design discussion is based on the P2 and T2 magnet pair.

Table 5-8.   End plug coil parameters for FPD-II (model coil set--C83).

Coils	z_m (m)	$R_{major}/$ R_{minor} (m)	Δz (m)	ΔR (m)	λj (A/cm^2)	Coil current (MA)	Peak field (T)
T2	64.85	1.2/0.6	0.81	0.27	4553	10.0	9.73
P2	60.98	1.7/0.6	0.81	0.27	4530	9.96	9.95
P1	59.96	1.7/0.6	0.81	0.27	4530	9.96	10.00
A2	56.10	1.2/0.6	0.81	0.27	4553	10.00	10.20
A1	54.74	1.2/0.6	0.81	0.27	4553	10.00	10.40
T1	50.88	1.7/0.6	0.81	ᵃ ᵃᵃ	4530	9.96	10.00

Figure 5-23 shows the cross section of a typical C coil in the end cell
system. We selected the inner plate thickness of 5 cm to provide space for
30 cm (per side) of nuclear radiation shielding and an LN$_2$ cold wall in the
bore of the magnets. The other plate thicknesses along with the 5.08-cm inner
plate provide support for the magnetic loads from the conductor pack. These
magnetic loads produce primary membrane and both primary and secondary bending
stress in the coil case. Significant reinforcing is required to resist both
lobe-separating forces. Spacing within the reinforcing structural members is
determined by local bending stress conditions. The use of the external
stiffening avoids the use of excessively thick plate sections to carry the
large loads associated with these coils. The coil material is assumed to be
304-LN stainless steel with a 4-K yield strength of 100 ksi.

The 1-T recircularizing coil can be designed with the forced-flow or pool-
boiling conductor. The final coil design will be the conduit that results in
the lowest combined cryogenic, electrical, magnet system cost. A pool-boiling
coil is assumed for this FPD predesign and costing effort.
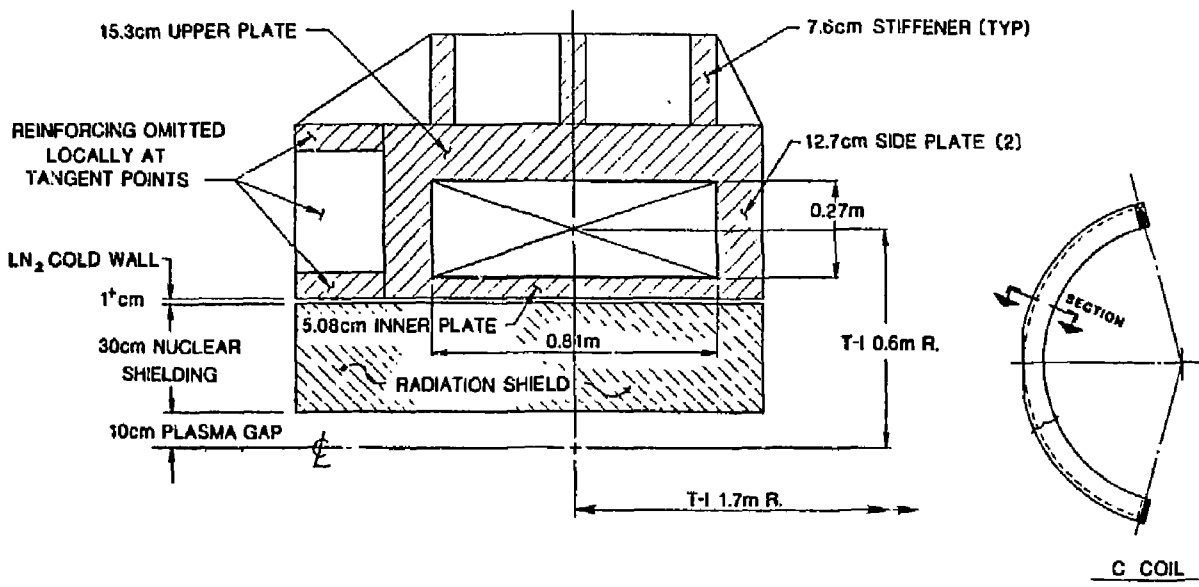
Figure 5-23. Typical C-coil cross section.

Conclusions

Tne end coil system concept is achievable using the force-cooled conductor
concept proposed by the Massachusetts Institute of Technology. This
force-cooled conductor is also specified for TFCX; research and development
tasks have been identified for qualifying this conductor for operating at 10 T.

Structural/design considerations in the end-cell C coils represent a
significant, but believable, extrapolation from MFTF-A and MFTF-B experience.
Finally, the low-field recircularizing coil is well within the limits of
current superconducting coil technology.

END-CELL PLASMA HEATING SYSTEMS

Four end-cell plasma heating systems perform various functions in FPD-II:
an anchor ICRH system creates high beta; a high-energy negative-ion-based
neutral beam (NINB) system and two electron-cyclotron resonant heating (ECRH)
systems form the thermal barrier and central-cell ion-confining potential in
the plug. End-cell heating requirements for FPD-II are listed in Table 5-9;
where the table contains two sets of data, the first set corresponds to the
nonaxicell case, and the second set to the axicell case.

The key differences between the FPD-I heating requirements (see Sec. 4)
and the FPD-II requirements are:

1. Lower ECRH and ICRH powers;
2. Lower betas in both the anchor and the plug;
3. Changes in all trapping fractions except for the potential-peak
   ECRH system.

The rf powers decrease in FPD-II because the new magnet set is more compact
and thus the heating volume decreases. In addition, a decrease in axial
confinement is required to limit the trapped-ion current in the transition
during axicell beam operation, which further relaxes the rf power
requirements. The lower betas decrease the complexity of the rf systems
because the frequency shift during startup decreases. The higher heating

Table 5-9. The end-cell heating requirements for FPD-II. (When there are two sets of power and current requirements, the first value corresponds to the nonaxicell case and the second value, in parenthesis, to the axicell case.)

	Anchor ICRH	Sloshing NINB	Potential-peak ECRH	Thermal-barrier ECRH
Heat locations –	--	a'	a	b
$-z_{axis}$ (m)	±54.25 & ±56.6	±58.78	±61.63	±60.5
Absorbed power (MW)	0.26 (0.21)	1.37 (0.47)	0.35 (0.19)	11.09 (10.57)
Trapping fraction	0.6 x 0.5	0.29	0.85	0.7
Delivered power (MW)	0.87 (0.7)	4.71 (1.62)	0.41 (0.23)	15.85 (15.0)
Vacuum frequency (Hz)	76.0×10^6	--	84.0×10^9	70.0×10^9
Heating frequency (Hz)	71.0×10^6	--	68.0×10^9	52.0×10^9
Delivered current (A)	--	9.91 (4.99)	--	--
Beam energy (keV)	--	475 (325)	--	--
Injection angle(deg)	--	90	--	--

frequencies in FPD-II also improve ECRH optics (lower-beam divergences) and offer versatility in the anchor-ICRH-launcher design (e.g., waveguides). The trapping fraction of the NINB increases because of the inclusion of multistep ionization processes and alphas. On the other hand, trapping fractions for the ICRH system and the thermal barrier ECRH system are lowered in FPD-II because of uncertainty in wave physics. The ICRH change has little adverse effect because the power level is low; the ECRH trapping fraction is decreased to 0.70. This decrease adds ~4 MW and thus one more gyrotron to each transport system, which would not be required if a trapping fraction of 0.85 were used.

The main impact that axicell operation has on end-cell heating systems is in the sloshing-beam NINB system. The power to the NINB decreases from 4.71 to 1.62 MW; the delivered current decrease is not as large because the

injection energy for the axicell case drops from 475 to 325 keV. The ECRH and ICRH systems are defined for axicell operation, but are capable of delivering slightly greater powers when there is no axicell insert. The neutral beam system is sized for the nonaxicell case (4.71 MW, 475 keV system); the operational characteristics for the axicell case are discussed later in this section.

ECRH Systems

The thermal-barrier ECRH system delivers 7.5 MW at 52 GHz into each plug at point b, $z = \pm 60.5$ m. As in the FPD-I device, 1-MW gyrotrons are assumed to be available and a quasi-optical transmission system is used for the thermal-barrier system at point b. Because of the low power requirement for the potential-peak system at point a (115 kW per plug), a waveguide transmission system is more compact and more practical to use than a quasi-optical transport system.

The system for point b is of the same configuration that was outlined in Sec. 4 in Fig. 4-3 and depicted in Figs. 4-11 and 4-12. The FPD-II ECRH configuration is shown in Fig. 5-24 and the quasi-optical transport system parameters for the 52-GHz system are listed in Table 5-10. Two transport modules are located in the plug regions, each with five operating beams and one redundant launcher. Because the magnet set is rotated at 45°, the beams pass between the yin-yang magnet pair through the major radius gaps with the transport modules centered about the x-z plane on each side of the plug.

Also denoted in Fig. 5-24 is the potential-peak ECRH system; this low power system comprises 200-kW gyrotrons and a waveguide transmission system. A block diagram of the transmission line is shown in Fig. 5-25. To avoid potential problems associated with window failures (e.g., SF_6 or window-coolant leaks into the plasma chamber), a vacuum waveguide was chosen for FPD-II, but power handling capabilities and arcing issues in a radiation environment still need to be quantified.

The ECRH-system power flow and key system parameters are summarized in Fig. 5-26. The power for this pair of systems at each end cell is provided by a single converter/transformer unit rated at 25 MW and 83 kV, which feeds

ECRH TRANSPORT SYSTEM
VACUUM CHAMBER

REFLECTOR

WAVEGUIDE

NEGATIVE ION
BEAMLINE

GYROTRON,
MAGNET,
AND SHIELD

"σ" SYSTEM

SOCKET & TANK

NINB SOURCES

SHIELDING

PLAN

ELEVATION
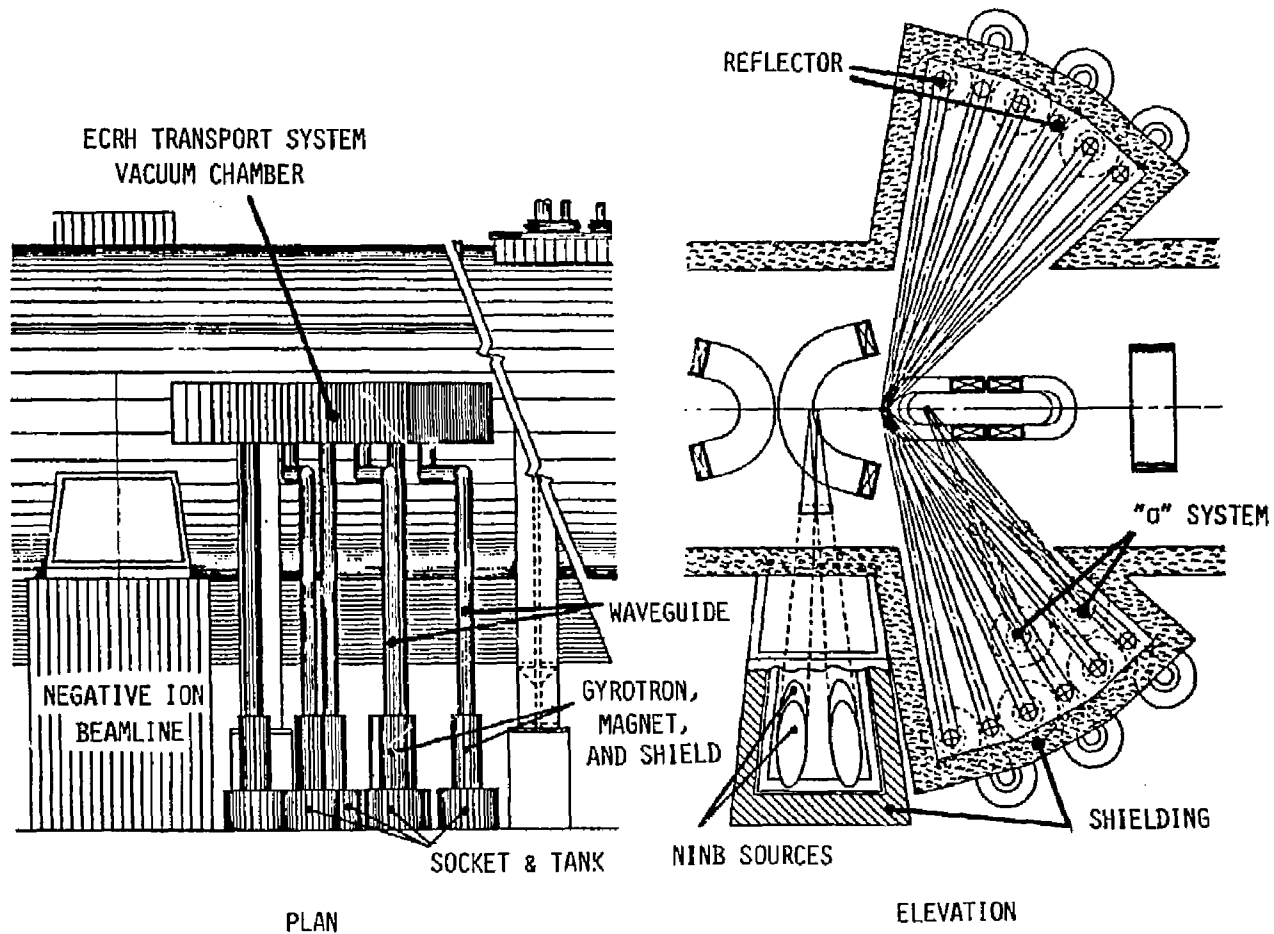
Figure 5-24. End plug and ECRH system configuration.

Table 5-10. Thermal barrier quasi-optical
system parameters.

Type	Offset-conical horn/ paraboloid reflector
Conical angle (deg)	17
Cone height, h (cm)	56.45
Paraboloid focal length, f (cm)	30.19
Mirror diameter, D_m (cm)	54.0
Initial beam diameter, D_0 (cm)	41.65
Distance to point b, X_0 (m)	8.5
Beam diameter at point b, $D(X_0)$ (cm)	15.0
Distance to magnets, X (m)	7.25
Maximum beam diameter in magnet region, $D(X)$ (cm)	19.0
Number of transport systems/end	2
Number of beam launchers/ transport system	6 (5 operating/ 1 redundant)
Launcher transmission efficiency (%)	96
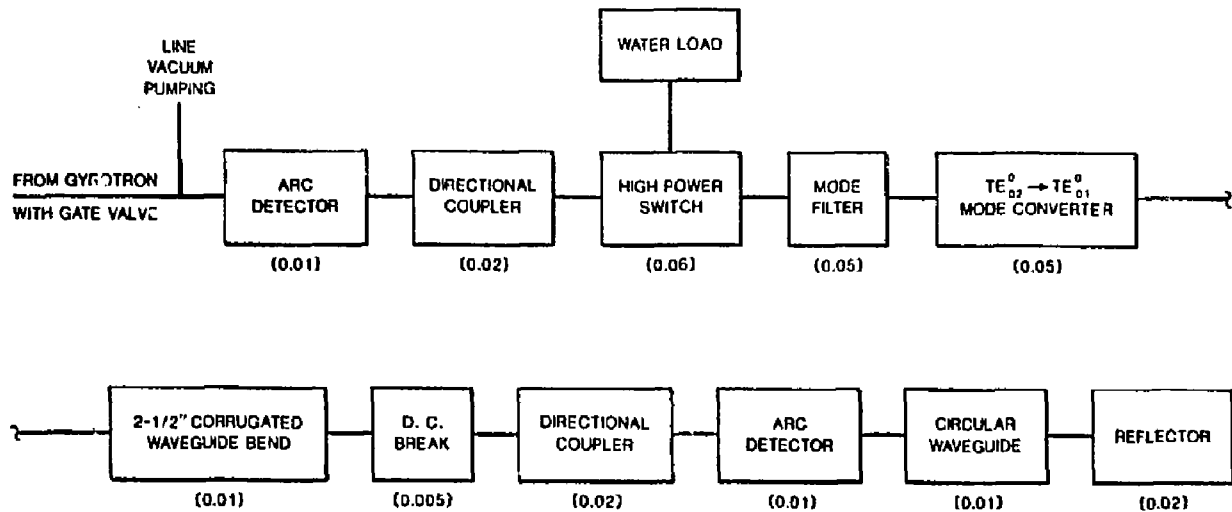
Figure 5-25. Potential-peak ECRH-waveguide transmission system. The parenthesis indicate fractional power loss in component. Total transmission efficiency--70.8%.

- POWER FLOW
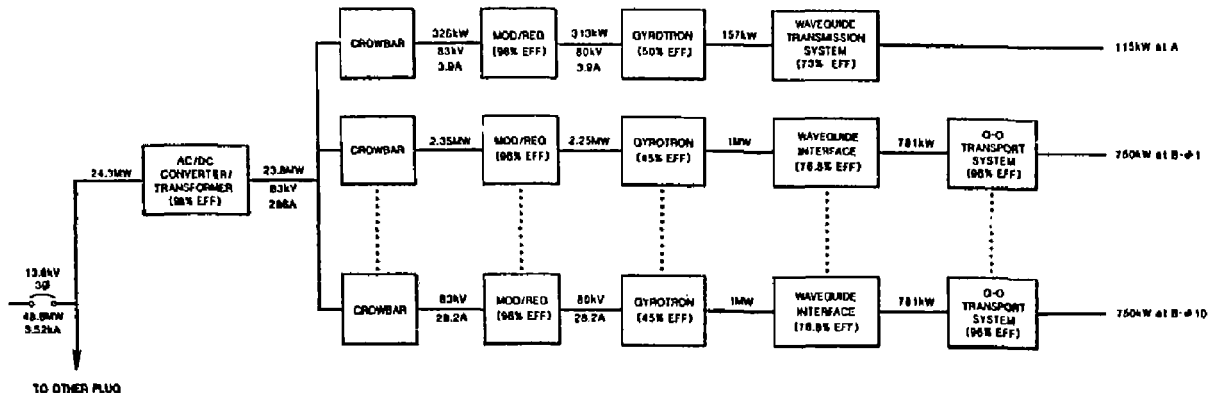
- KEY SYSTEM PARAMETERS

  - Total System Efficiency: 31.3%

  - Line Power: 48.6MW

  - LHe Requirements (for Gyrotron): 22 l/hr

  - LN$_2$ Requirements (for Gyrotron): 11 l/hr

  - Coolant Water Requirements: 7,225gpm

Figure 5-26. The FPD-II ECRH power flow.

eleven parallel protection and regulation networks. Each network supplies a
gyrotron and consists of a crowbar protection circuit, a modulator/regulator
series tube, and a disconnect ground switch. The 1-MW gyrotrons are assumed
to operate at a lower efficiency than the 200-kW tubes because of possible
mode competition in the larger collector cavities that are expected for the
higher power. The total ECRH-line requirement is 48.6 MW and the system
efficiency is 31.3%.

Anchor ICRH System

The anchor ICRH system must deliver 435 kW to each anchor when operating
without the blanket test module and 350 kW during axicell operation. Lower
beta in the FPD-II anchor results in a higher heating frequency, 71 MHz, than
the 54 MHz that was required in previous studies (e.g., Mirror Advanced
Reactor Study (MARS),[3] MFTF-α+T,[1] and FPD-I); because of this higher
frequency, waveguides become a viable alternative to an antenna launcher.

Although the coupling physics of a waveguide launcher in the ICRH
frequency range is not quantified yet, its engineering benefits in fusion-
reactor applications, when compared with loop antennas, have been espoused for
a number of years and include:

1. Removes much of the launcher from the harsh plasma-edge environment
   and thus prolongs the launcher's lifetime;
2. Is easier to maintain;
3. Has more power-handling capability.

An antenna launcher was used in the FPD-I configuration because at 54 MHz the
waveguides were too large without the fourth or fifth harmonic heating. Here,
the $\geq$30% increase in frequency allows use of single-ridged waveguides of
widths <1.0 m at the second deuterium harmonic and ~60 cm for the third
harmonic. Figure 5-27 contains a schematic of a single-ridged guide and
dimensions for several harmonics for a 15-Ω waveguide impedance.
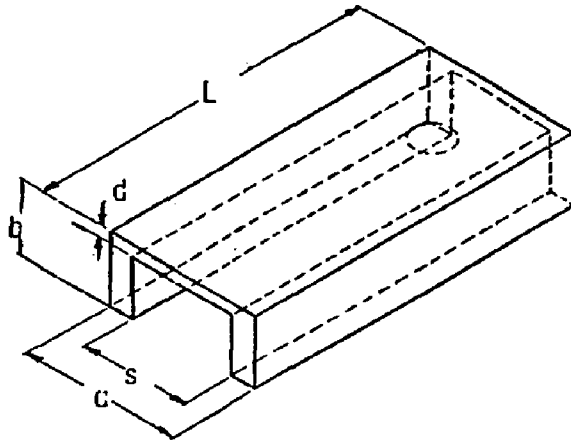
Harmonic	f_{heat} [MHz]	a [cm]	b [cm]	s [cm]	d [cm]	L [cm]
2	71.1	95.2	21.4	71.4	1.61	4.29
3	106.7	63.4	14.3	47.6	1.07	2.86
4	142.2	47.6	10.7	35.7	0.8	3.10

Figure 5-27. Ridged-waveguide harmonic heating alternatives.

The remainder of the anchor ICRH system is considered of standard design and is shown in Fig. 5-28. A summary of the entire system follows:

- Configuration: two launchers per anchor
  (1 operating/1 redundant)
- Launcher: single-ridged waveguide
  Waveguide power: 350 kW
  Efficiency: 97%
- Transmission system: mainly 6-1/8 in.
  Coaxial + step transformer and two stub tuning systems
  Efficiency: 82.4%
  Coolant loops
  No. 1: Launcher back to stub tuner No. 2
    7 gpm while operating
    4 gpm while dormant
  No. 2: Remainder--4 gpm while operating
- Transmitter: multistage
  Two power supplies: FPA--675 kW, 20 kV
    Driver--10 kW, 7 kV
  Efficiency: 59.3%
  Coolant loop: 150 gpm
- Performance:
  Total line power: 1.48 MW
  System efficiency: 47.5%
  Total water coolant requirements: 330 gpm.

Power levels in this summary are for the axicell operating scenario. Rather than the three-stub tuning system used in the FPD-1 antenna system, the third stub is replaced by a 50-Ω → 15-Ω coaxial-step-impedance transformer. The power source is a multistage amplifier chain and at 71 MHz the Eimac X-2170/8973 tetrode is the appropriate final power amplifier. Even though this system has a relatively low power requirement, the waveguide and tetrode are both capable of handling 1 MW so that for little additional cost, the purchase of 1.5-MW power supply offers a margin of surplus capability in the
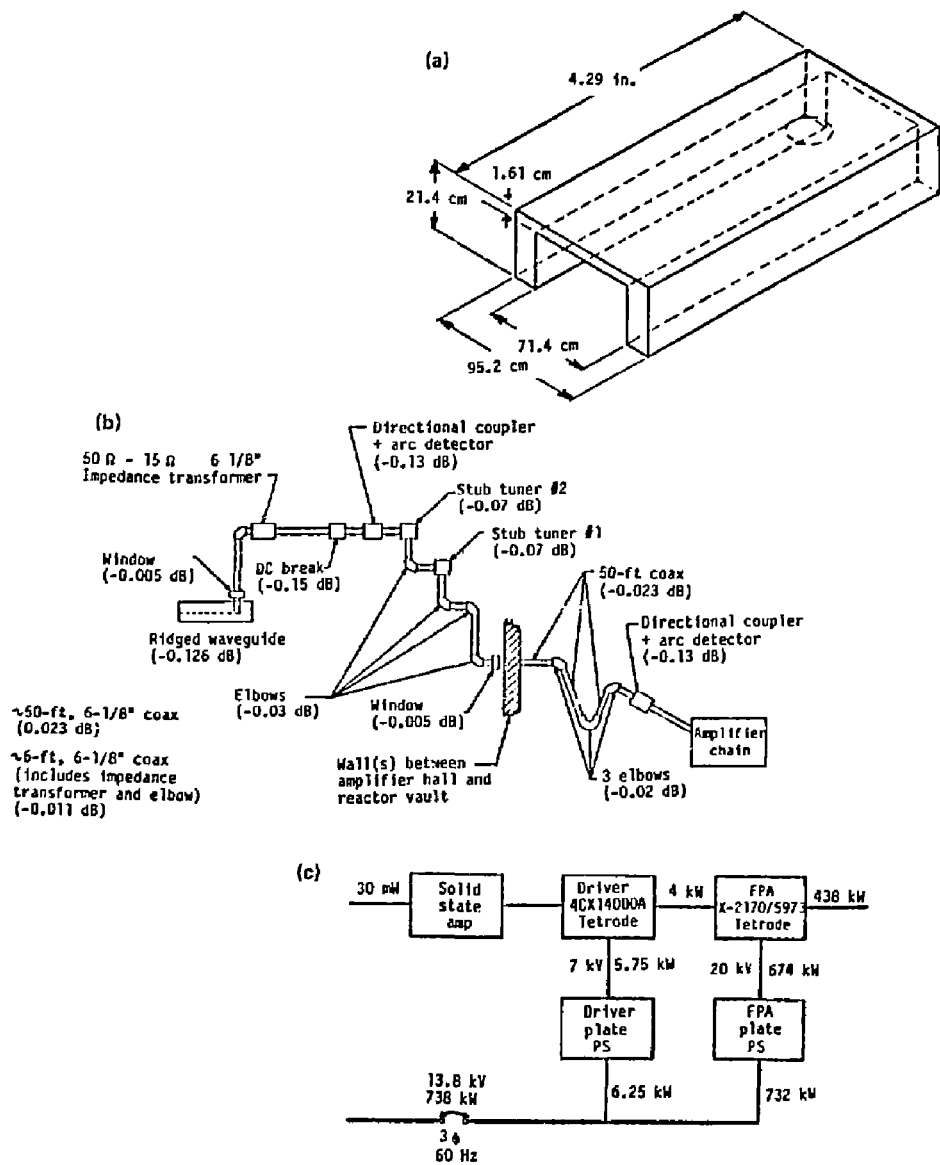
Figure 5-28. The FPD-II ICRH system description. (a) Single-ridged waveguide launcher; (b) mainly 6-1/8-in. transmission system; (c) multistage transmitter.

event that wave-coupling and ion-trapping efficiencies are lower than assumed. The total line power for the system during axicell operation is 1.48 MW corresponding to a 47.5% system efficiency. Without the axicell, the line power increases to 1.85 MW.

Negative-Ion Neutral-Beam System

The neutral beams that create the sloshing-ion distribution in the plugs are the heating systems most effected by whether or not there is an operating axicell. Without the axicell, 2.35 MW (4.95 A at 475 keV) is injected into each plug; whereas the power, current, and beam energy decrease to 800 kW, 2.5 A, and 325 keV, respectively, when the axicell is in operation. The system summarized below corresponds to the more demanding requirements, but we will also discuss the system implications associated with axicell operation.

- Configuration:
    One beamline per plug;
    Four sources per beamline (3 operating/1 redundant);
    Sources arranged in a 2 x 2 array.
- 4.0-A Lawrence Berkeley Laboratory type self-extraction source at -475 kV, 2 x 68 cm^2 ribbon beam;
    RF plasma generator in magnetic multipole bucket containment;
    Forced cesium diffusion through converter plate;
    Small transverse magnetic fields to divert electrons;
    Standard 80-kV single-slot pre-accelerator;
    Gas efficiency: 12% + total gas flow (3 sources): 8.8 T ℓ/s.
- Transverse field focusing (TFF) transport and high-voltage accelerator:
    80-kV TFF-transport section [low energy beam transport (LEBT)] at -395 kV with multistage differential pumping $\div$ 9.0 m^2 cryopumps;
    Four-stage TFF high-voltage accelerator (-305 kV, -220 kV, -135 kV, -50 keV);
    High energy beam transport (HEBT) section;
    TFF focusing voltages range from ±25 to ±50 kV;
    Divergence: 0.45° x 1°;
    Pressure 1 x 10^{-5} Torr.

- Gas jet neutralizer with a Poulsen-type plug nozzle:

    Optimum gas thickness: 6.5×10^{15} cm^{-2};

    Average pressure in pump chamber: 5×10^{-4} Torr;

    Approximate dimensions: $2 \times 1.75 \times 1.75$ m;

    Cryopanels: 15 m^2.

- Ion magnet/dump region:

    Pressure 1.0×10^{-5} Torr;

    2.0 m^2 cryopumps.

The beamline configuration has much in common with the FPD-I NINB system described in Sec. 4, in particular, the source and TFF configurations shown in Sec. 4 in Figs. 4-17 and 4-18. The source current capability is more in line with the Negative-Ion Development Program's goal of 6 A/m (Ref. 4) leading to a slightly larger source (2×68 cm^2), but a factor of two increase in source current (4 A). The gas load per source also doubles to 2.9 ℓ/s; the cryopanel area requirements in the LEBT section are 7.5 m^2 with 50% LEBT grid transmissivity and 20% recycling factor.

The key departure from past designs is the use of a gas-jet neutralizer in FPD-II. This concept incorporates a Poulsen-type nozzle that was previously used to minimize flow of alkali vapor metal along negative-ion beamlines.[5] Although much more analysis is required on deuterium-jet neutralizers, they do not require advanced technology, should entail only a modest development effort, and have a number of advantages when compared with conventional gas-cell neutralizers. These advantages include:

1. A shorter magnetic shield is used, which results in a decrease in the beamline weights, and costs are less (beamlines are easier to maintain).

2. The gas curtain separates the ion beam from the neutral-beam region.

3. The jets help pump the beamline.

4. The jets prevent the gas in the pumping chamber from freely flowing back into the beamline.

5. The jets permit a reduction of ion losses by a lower beamline background gas pressure.

6. The jets do not appear to represent a significant cost increase.

Figure 5-29 represents the jet neutralizer concept. The cryopump chamber is quite large, but can be outside the main beamline vacuum and magnetic shielding envelope. The cryopanel area in the pump chamber is 15 m^2.

Figure 5-30 is the current and power flow of a beamline and Fig. 5-31 is the beamline in the end cell configuration. The current efficiency is 41.25%, whereas the power efficiency is 45.36%; the difference occurs because most the current is lost at low energies. The line power requirement for the entire system is then 10.4 MW.

To operate the beamlines during axicell operation, the following changes in the beamline are required: (1) the number of operating sources decreases from three to two; (2) the individual source current decreases almost 30% to 3.13 A; and (3) the last two stages of the TFF high-voltage accelerator are converted to nonaccelerating TFF transport sections, and the acceleration potential in the HEBT is raised 10 kV. The system line power required during this phase is 3.5 MW.

DRIFT PUMPING

Requirements

Table 5-11 summarizes the FPD-II drift pumping system requirements. Each of the parameters is described in Sec. 4. Note that the plug cell has two populations: one for the so-called "cold" ions and another for the "sloshing" ions. The combination of reduced bandwidth (10% as compared with 66%) and fewer frequencies ($\sim$45 compared with 110) makes the implementation much more attractive than that of the FPD-I.

Another parameter, which eases the design problem, is the large (>10:1) reduction in flux for the transition; this results in a reduction in coil current and therefore power amplifier size.

Configuration

The same basic concept is planned here as in the FPD-I and MFTF-α+T. There are 13 channels for the transition and 46 (22 cold and 24 sloshing)
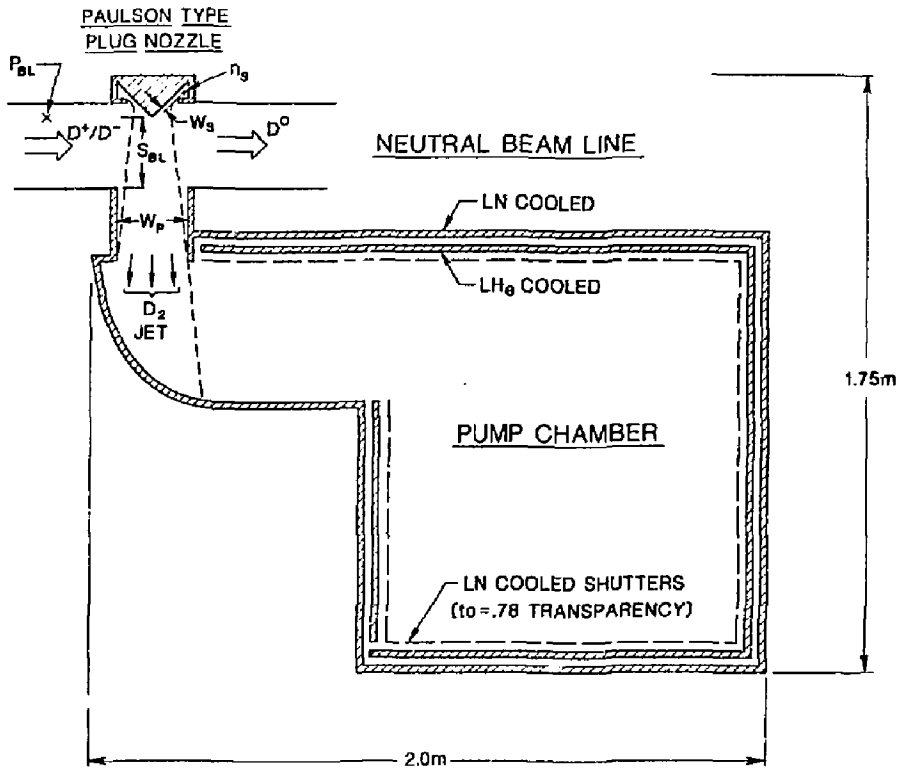
Figure 5-29. Deuterium gas jet neutralizer concept.
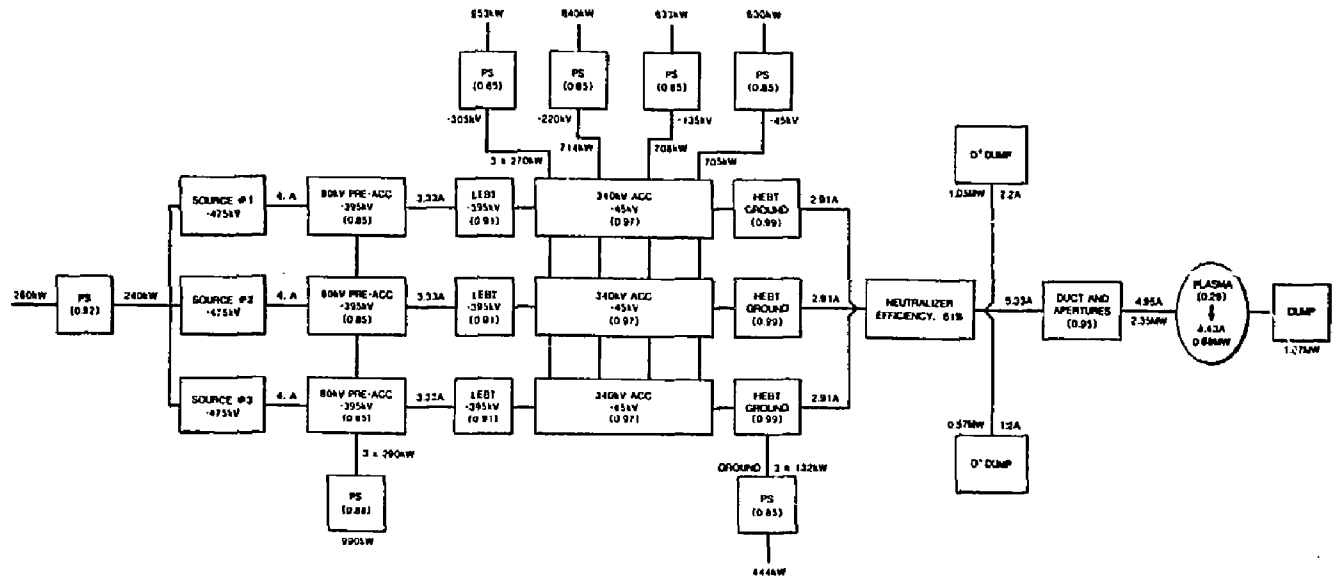
CURRENT EFFICIENCY: 41.25%
POWER EFFICIENCY: 45.36%

Figure 5-30. Sloshing beam current and power flow (the fractions in parenthesis correspond to current transmission fraction).

END CELL HATCH

NUCLEAR SHIELD HATCH

"C" SHAPED COILS

BEAM DUMP

DUMP

NEUTRALIZER

END CELL
SUPPORT

JET

TFF

COIL SUPPORT
STRUCTURE

NUCLEAR SHIELD DOOR

SOURCE
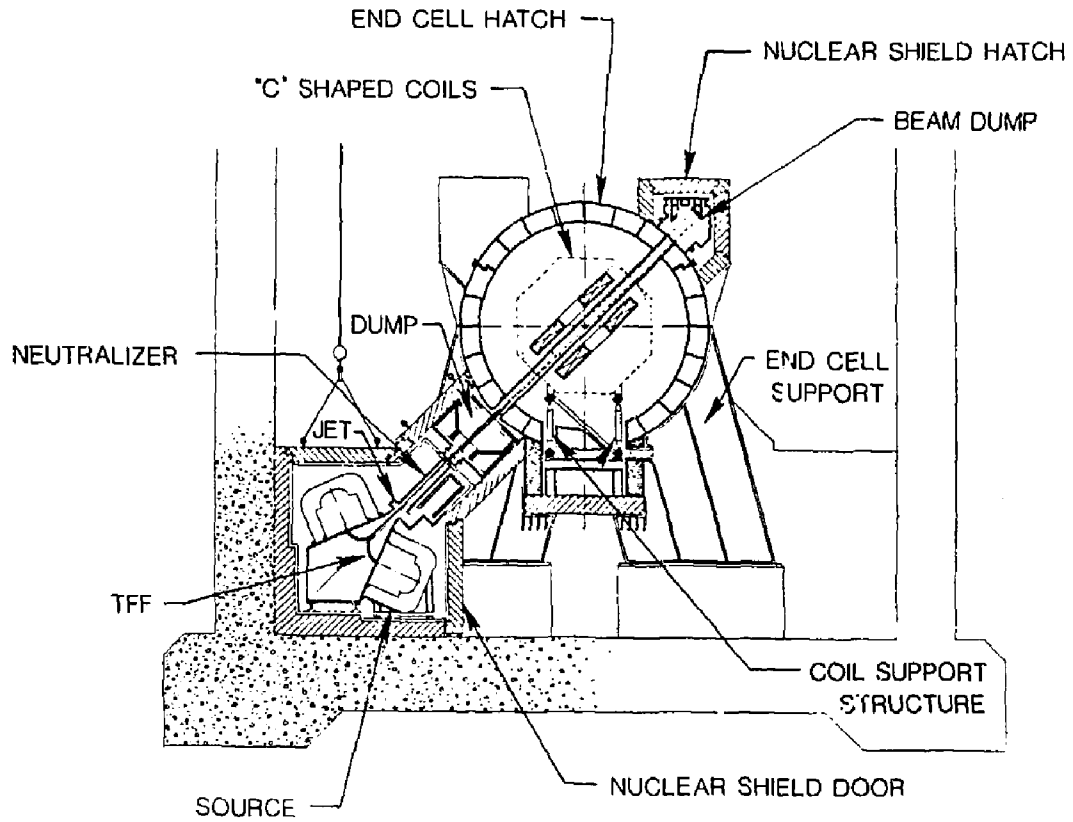
Figure 5-31. End plug and sloshing beamline configuration.

Table 5-11. The FPD-II drift-pump requirements.[a]

| Transition cell | Parameter | Plug cell | |
		Cold	Sloshing
106.63	Center frequency (kHz)	827.6	1328.9
37.3	$\Delta f/f$ bandwidth (%)	10	10
39.78	Δf bandwidth (kHz)	82.76	132.89
13	No. of frequencies	41	48
0.00538	Perturbation flux (Wb)	0.00349	0.00349

[a]Assumptions: • MARS-like coil

      - hairpin shape

      - scaled

   • Eddy current loading

      - scaled from MFTF-α+T

channels for the plug cell. We plan to have 2 tones per channel to cover the total of 89 (41 + 48) frequencies for the plug. For further details, refer to Sec. 4 or the MFTF-α+T study report.[1]

Performance

Table 5-12 shows the results of the performance analysis. The coil currents were estimated to be:

$$I_c = 1.3 \text{ kA}\quad \text{transition}$$

and

$$= 0.9 \text{ kA}\quad \text{plug.}$$

Table 5-12. Performance.

Transition cell	Parameter	Plug cell	
		Cold	Sloshing
	Coil:		
4	Inductance (μH)	4	4
8.3	Resistance (mΩ)	23.0	42.3
303	Inherent Q	901	789
1.8	Load resistance (mΩ)	5.2	9.5
246	Loaded Q	72`	645
15.0	Power (kW)	17.6	32.2
3.4	Power, I_c (kW)	3.9	7.2
	Transmitter:		
13	No. of channels	21	24
10.2	Power output (kW)	7.5	9.3
0.54	Channel bandwidth %	0.48	0.42
1	Tones/channel	2	2
13.7	Transmission and matching efficiency	13.6	17.2
16.7	Prime power (kW)	12.3	5.8

Again, the analysis procedure is the same as used in the MFTF-α+T study.[1] Because the flux requirement is modest, the power requirement is small compared with FPD-I. The details of the design are summarized in Table 5-1? The values are given in microfarads and microhenries for the capacit and inductors, respectively. For this design, the plug system suppli   spectrum capable of covering the 10% bandwidth. Hence any form of modulation (noise, cw sweep, or tone) can be used. The efficiencies, in terms of wat of prime power to amperes of circulating current, are 45, 65, and 86 for the transition, plug (cold), and plug (sloshing) systems, respectively. This is goo efficiency compared with the MFTF-α+T, where the ratio was 170.

Table 5-13. Component values.

| Component[a] | Transition | Plug | |
		Cold	Sloshing
C_1(µF)	0.00096	0.0023	0.000907
C_2(µF)	0.00016	0.00002	0.000010
C_3(µF)	0.01150	0.00039	0.000239
C_4(µF)	0.00033	0.00160	0.001012
L_1(µH)	16	8	8
L_2(µH)	14,060	2,030	1,400
L_3(µH)	228.9	97.1	60.1
L_4(µH)	690.8	23.1	14.3
Tube	4CX5000R	4CX5000R	4CX5000R

[a]Refer to Fig. 4-22 in Sec. 4.

Future Work

Breaking up the spectrum into bands improved the implementation of the plug system, but the system still has 46 channels driving a single pair of coils. Further reductions in bandwidth are desirable. It would be worthwhile to investigate limitations on the Q of the drift pump coil because the coil limits the intrinsic bandwidth. Refer to Sec. 4 for other future efforts.

HALO SCRAPER/DIRECT CONVERTER

We designed a halo pump and direct converter for FPD-II for which design parameters are more fully described than those for FPD-I. The true cross-sectional shape of the plasma determines the shape of the various elements in the FPD-II direct converter. We also considered the effect of the changed magnets set (A-18 to C-53) on the design of the FPD-II direct converter.

Design Assumptions

To minimize costs, the FPD-II direct converter produces only low-grade throw-away thermal energy. The return water-coolant temperature is set at 80°C (inlet temperature is 30°C). We assume that the plasma cross-sectional shape does not change with changes in the machine operating power level. This assumption simplifies the design process until we can determine from our studies the effects on the direct converter of plasma shape and power distribution resulting from variations in machine operating power.

Design Description

The FPD-II direct-converter design is based on the C-53 magnet set. A recent iteration of the magnet design resulted in the C-83 magnet set—we have not assessed the impact of this change at this time.

The plasma cross-sectional shape obtained from the C-53 magnet set is an irregular four-pointed star. We tried to eliminate the "lobing" of the star at the four points and to make the shape more regular. Some modification of the shape was possible by changing the cross section, the mean radius, and the current density of the recircularizing solenoid. Because it is not possible to completely recircularize the plasma by changing only the recircularizing solenoid, the amount of recircularization necessary depends on a cost tradeoff between the increasing magnet size and the fabrication complication of irregularly shaped converter elements. For the purpose of this design, we changed the recircularizing solenoid to obtain a regular shape for the leading edge of the halo scraper and the interface between the halo scraper and the halo dump. Figure 5-32 shows the plasma shape with a modified recircularizing coil.

To minimize the direct-converter cost, the elements of the converter are spread axially. The halo-scraper assembly is positioned close to the recircularizing solenoid, but allows enough space for adequate diffusion of the neutral particles and does not exceed the peak power density of a zirconium-copper halo scraper. Good spacing between the halo assembly and the collector assembly is necessary to allow independent assembly and disassembly.

HALO DUMP
HALO SCRAPER
OUTER COLLECTOR
INNER COLLECTOR

Z = 66.00

Z = 67.00

Z = 68.00
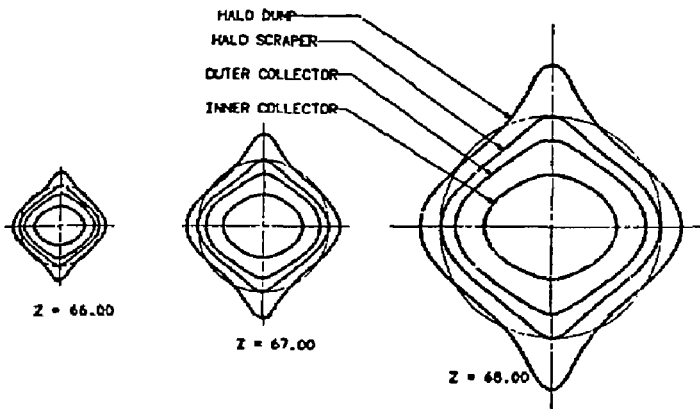
Figure 5-32. The C-53 magnet set plasma shape in the area of the FPD-11 direct converter.

To simplify machining, the actively cooled elements in the halo scraper are defined as conical surfaces. These surfaces allow constant width cooling grooves to be milled in a straight, radial direction. Where possible, the circumferential edges have been simplified (e.g., the inner edge of the outer collector shadows the inner collector allowing the edge of the inner collector to be simplified).

The separate assemblies of the halo and the collector are mounted from the vacuum vessel. The assemblies can be removed separately (Fig. 5-33). The plug for the halo scraper is sized to permit removal of the recircularizing solenoid.

The power distribution to the various elements of the direct converter is shown in Table 5-14. Table 5-15 lists the details of the cooled surfaces for

5-60
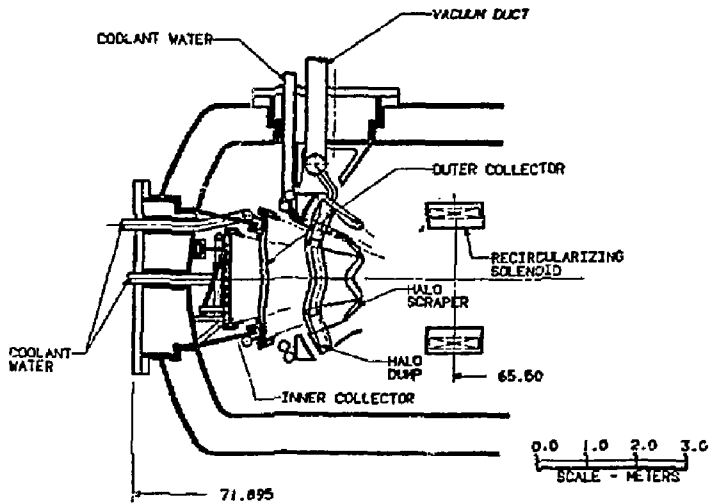
Figure 5-33. The FPD-II direct converter.

Table 5-14. Power distribution (MW both ends).

	Thermal (MW)	Electric (MW)
Halo dump	19.0	0.0
Halo scraper	7.2	0.0
Outer collector	4.3	4.2
Inner collector	21.4	37.0
Total	51.9	41.2

Total power = 93.1 MW

Table 5-15. Direct converter thermal design.

	Inner collector	Outer collector	Halo scraper	Halo dump
Heat flux (design) (MW/m^2)	1.78	0.62	1.49	2.07
Coolant flow rate (gpm)	810	163	990	990
Coolant pressure (psi)	620	620	620	620
Coolant pumping power (kW)	67	20.5	76	76
Coolant velocity (m/s)	7.2	3.3	10	6
Surface temperature, copper(°C)	127	124	148	195
Surface temperature, TZM (°C)	236	162	239	321
Coolant channels				
Width x depth (cm)	0.7 x 0.3	1.3 x 0.3	0.7 x 0.4	1.16 x 0.4
Number of sectors	3	8	8	8
Channels per sector	112	70	112	112
Channels per channel path	1	7	4	4

the water-cooled zirconium copper and TZM designs of the direct converter.
Reduced tritium permeation is possible if the cooled surfaces are fabricated
from TZM but the cost would be greater than the zirconium-copper design.
Figure 5-34 depicts the coolant channels for the halo scraper—the coolant
channels for the other elements of the direct converter are similar.
Table 5-15 gives the channel dimensions.

Helium was considered as a coolant, but was not selected for three main
reasons:

1. High pumping power required,
2. High capital cost of the pumping equipment,
3. Tritium extraction system required.

HALO SCRAPER SEGMENT

SCRAPER ANGLE TO PLASMA = 28°
MATERIAL = ZIRCONIUM COPPER
NO. OF SEGMENTS = 8
SEGMENT HEADER PIPE SIZE = 7.6 CM
HEADER PIPE SIZE = 20.0 CM
WATER COOLING

.40
1.00
.27
.70

A
A

PLASMA FACE

SECTION AA
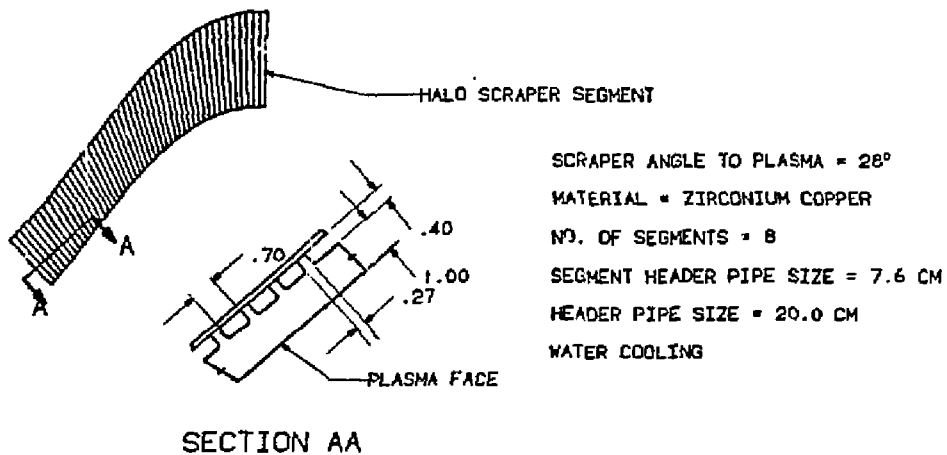
Figure 5-34.   The FPD-II direct converter/halo scraper coolant channels.

Costs

Table 5-16 summarizes the costs of the two direct converter options considered for FPD-II with a comparison to MARS.

SHIELDING AND VACUUM CONTAINMENT

The end cell region, Fig. 5-35, is a double-walled vacuum-vessel/ biological shield that contains the end cell coils, direct converter, and halo scraper. The vessel has an inside diameter of 7.0 m and a length of 40.0 m. Each end cell has a direct-converter/halo-scraper hatch and a large magnet-access hatch. The configuration in Fig. 5-35, allows for vertical removal of all the cell components. In addition, the vacuum vessel provides interface connections for the negative-ion sloshing beam, ICRH and electron-cyclotron resonant heating (ECRH) rf systems, and the drift pumping coils.

VACUUM VESSEL/BIOLOGICAL SHIELD

The end-cell vacuum vessel consists of two concentric, cylindrical
shells forming an annular volume for the water shielding. The inner and outer
shells are connected by radial bulkheads, as shown in Fig. 5-35. The inner
and outer shell spacing is 0.6 m, based on biological shield requirements.
Figure 5-36 shows the magnet cold-structure support box integrated into the
cylindrical vacuum vessel. The removable top hatches are framed by a beam
structure. Both the magnet hatch and vacuum vessel have longitudinal
stiffeners connecting the two shells and the bulkheads. The hatches are
sealed with a single-convolution, welded bellows.

MAGNET SHIELD

In addition to the biological shield, the end cell also has a magnet
shield. The function of the magnet shield is to protect the coils from
excessive heating and radiation damage. The shield consists of a 30-cm

Table 5-16. Costs in 1984 dollars, including materials,
fabrication, and installation.

	MARS, TZM (M$)[a]	FPD-II, TZM (M$)	FPD-II, Copper (M$)
Piping and supports	1.63	0.52	0.26
Halo	4.13	1.46	0.29
Collector	4.0	1.22	0.24
Total	9.76	3.20	0.79

[a]Millions of dollars.
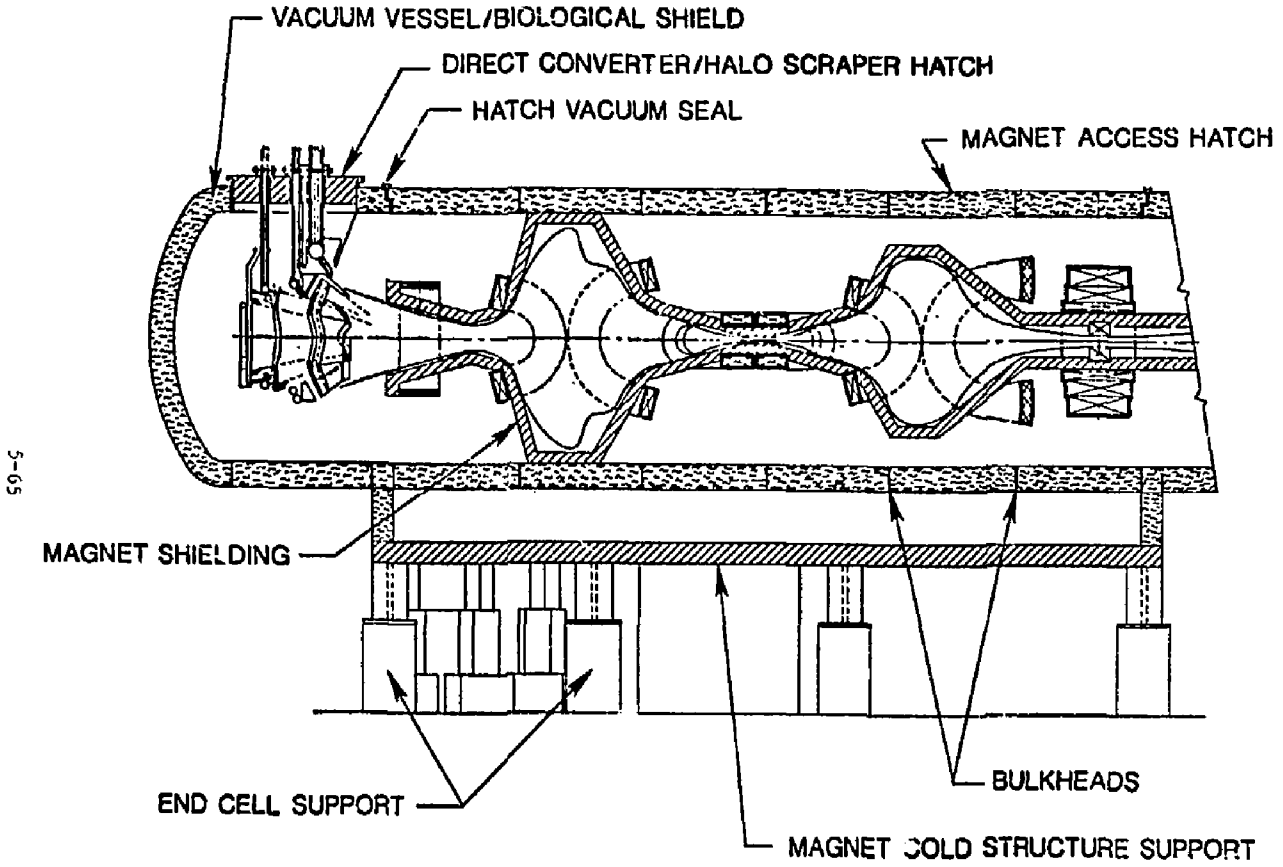
Figure 5-35. The FPD-II end-cell configuration.
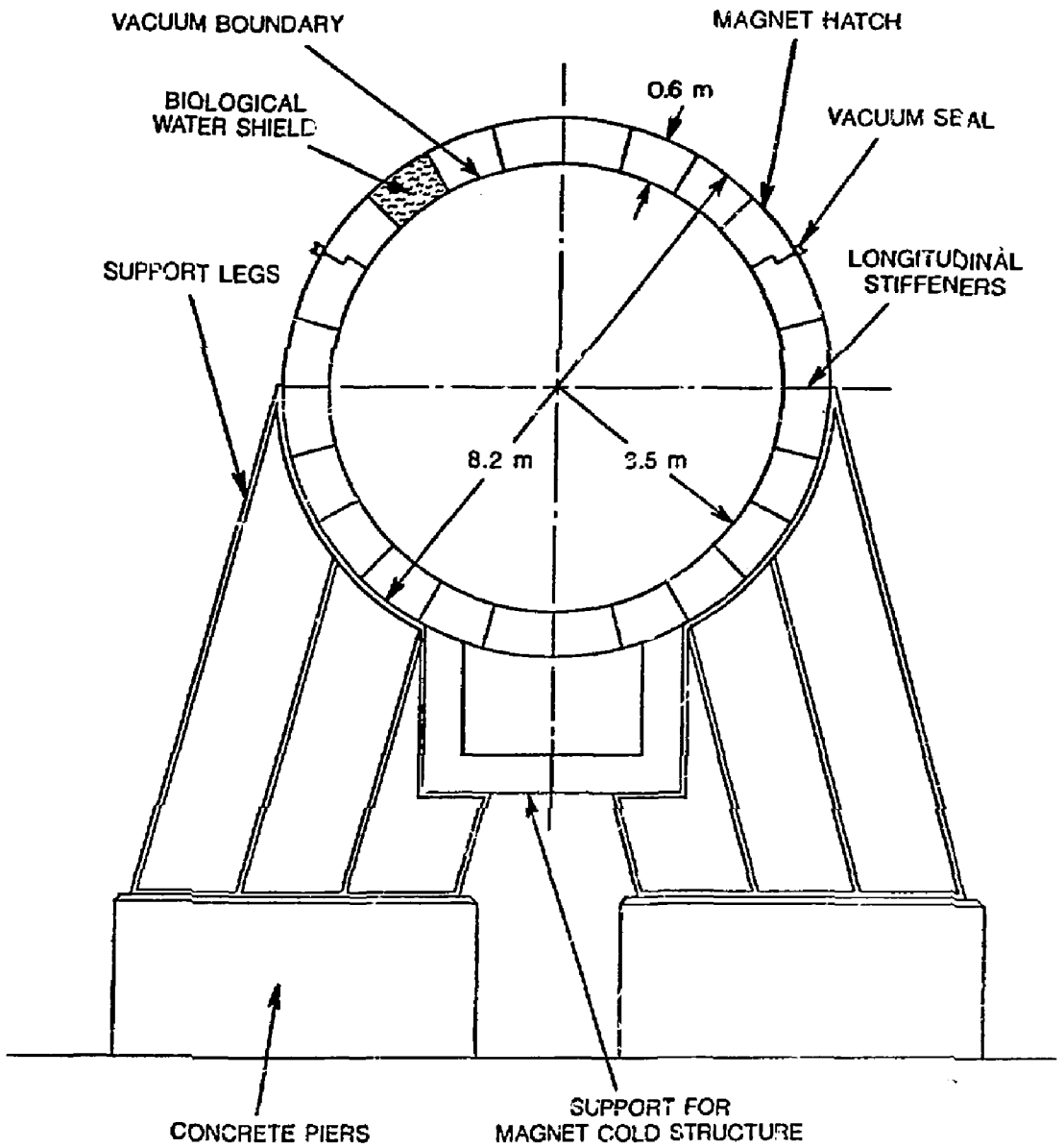
Figure 5-36. The FPD-11 end-cell vacuum vessel.

steel/water shield (80% steel, 20% H_2O) and 5-cm B_4C shield. The steel/H_2O shield design is the layered plate concept with cooling grooves. The water maintains the shield temperature at a maximum of $200^{\circ}C$. The steel/water shield is followed by the actively cooled B_4C shield. The B_4C shield composition by volume is 20% steel for the container vessel, 20% H_2O coolant, and 60% B_4C, with a density of 0.7. The shield is located at the plasma periphery, (Fig. 5-35). In the area of the choke coil, the thickness is increased to meet local requirements.

SUPPORT STRUCTURE

Each end cell has four sets of support legs, Fig. 5-36. The support legs constrain the end cell in the vertical and lateral directions, but allows axial motion for thermal expansion.

C-COIL NUCLEONICS: ONE-DIMENSIONAL ESTIMATE

INTRODUCTION

The shielding needed to limit neutron heating and damage in the C-coils to acceptable levels strongly influences end-cell size, and thus the size and cost of the entire machine. Our objective is to minimize total cost of the machine by varying the size of the end-cell C-coils in order to provide the optimum space between the coils and plasma for shielding. A procedure proposed to accomplish this objective is outlined later under this topic (see Ref. LLNL-FPD-84-018 in the Appendix).

RADIATION LIMITS

In LLNL-FPD-84-016 (see the Appendix), we originally set the maximum allowed radiation exposures in the superconducting coils at the following values:

- 10^{11} rads in the insulation.
- 10^{18} n/cm^2 ($E_n > 0.1$ MeV) in NbTi (for a 20% drop in critical current, 70% of which is annealable at room temperature).
- 4×10^{18} n/cm^2 ($E_n > 0.1$ MeV) in Nb$_3$Sn.

In LLNL-FPD-84-48 (see the Appendix), we revised the following fast ($E > 0.1$ MeV) neutron-fluence limits to allow for more design flexibility:

- 10^{20} to 10^{21} n/cm^2 range for NbTi with an accompanying 25% lower critical current.
- 1 to 4×10^{19} n/cm^2 range for Nb$_3$Sn, believed achievable.

These higher limits are speculative.

Because of the time and expense involved in detailed 3-D analysis of the end cell, we developed the following 1-D method to assess various configurations:

1. Calculate the heating and damage rates in the superconducting coils vs the shield thickness using 1-D slab geometry.

2. Calculate 14-MeV neutron energy currents (wall loading) in 1-D slab or cylindrical geometry using coil and plasma geometries, and plasma source strength.

3. Combine steps 1 and 2 to obtain a 1-D estimate of peak heating and damage rates.

4. Integrate the plasma neutron line source as a function of z, in regions where source strength is significant and shield space is limited.

5. Combine steps 1 and 4 to estimate the total heating in the C-coils (our major assumption is that axial neutron transport is not significant.)

As a first step, the heating and damage rates vs shield thickness were calculated in 1-D slab geometry using both the ONEDANT code and a 30-neutron plus 12-gamma XSLIB data library based on ENDF/B-V. This code and its data

library were developed at Los Alamos National Laboratory and used at the University of Wisconsin for the MARS project.[3]

The configuration used to calculate radiation levels in the coil vs shield thickness is shown in Fig. 5-37. The shield consists of a thick zone of W(70 v/o) + H_2O (10 v/o) + boric acid (1 v/o) + FE 1422 (10 v/o) followed by a thin zone ($\sim$4 cm) where TiH_2 replaces the W. This shield was devised in a preliminary optimization study (see Ref. LLNL-FPD-84-45 in the Appendix). Heating levels, neutron flux (E > 0.1 MeV) and dose rates in the coil vs shield thickness at a wall loading of 1.0 MW/m^2 are given in Figs. 5-38 and 5-39. The total heating calculation includes both the coil and its case: approximately 36% occurs in the case and 64% in the winding pack.

The second step in the 1-D method is to estimate wall loading at coil locations, where source strength and geometry combine with limited shield space to yield significant heating and/or damage rates.

To illustrate this process we are using the C83 end-cell coil set for FPD-II as an example. Figure 5-40 has both a 0 and a 90° cut through C83 showing C-coil winding packs and the hot and halo plasma boundaries (inner and outer lines, respectively) as they thread through the end-cell coils. The fusion neutron volumetric source strength along the centerline of C83 is shown in Fig. 5-41. Examining Figs. 5-40 and 5-41 together show that geometry and source strength combine to give four points where relatively high coil-radiation levels may occur in the C-coils. Starting at the innermost C-coil (T1[*] at z $\simeq$ 50 m) and working outward, the first point occurs in the second coil at z $\simeq$ 53.3 m. At this point a local maximum in the volumetric source strength (2.6 x 10^{11} n/s) and an approximately 4-cm half-thickness plasma fan (see Fig. 5-42 for blowup of the geometry) combine to give a 1-D wall loading on the coil of 0.023 MW/m^2. The space between the coil and the halo plasma is approximately 40 cm (Fig. 5-42). Subtracting 15 cm for the coil case and insulation leaves 25 cm for shielding. With 25 cm of shielding and a wall loading of 0.023 MW/m^2, peak local heating and other radiation levels in the coil at this point are (Figs. 5-38 and 5-39):

---

*Transition coil 1.

FIRST WALL
(80% STEEL, 20% H$_2$O)

107

PLASMA

131 ————— HALO
134 ◄—— FIRST WALL
135

SHIELD
(79% W / TiH, Pb, 10% H$_2$O,
1% BORIC ACID 10%, FE 1422)

S.C. COIL

165
166 SS LAYER

THERMAL INSUL.
(LOW DEN. AL.)

168.6
169.6 LN RAD SHIELD

172.3
COIL CASE
(80% STEEL, 20% He)

175.3
POLYIMIDE
176.3
WINDING CASE
STEEL
178.3
POLYIMIDE
179.3
1 cm S.C. COIL
180.3
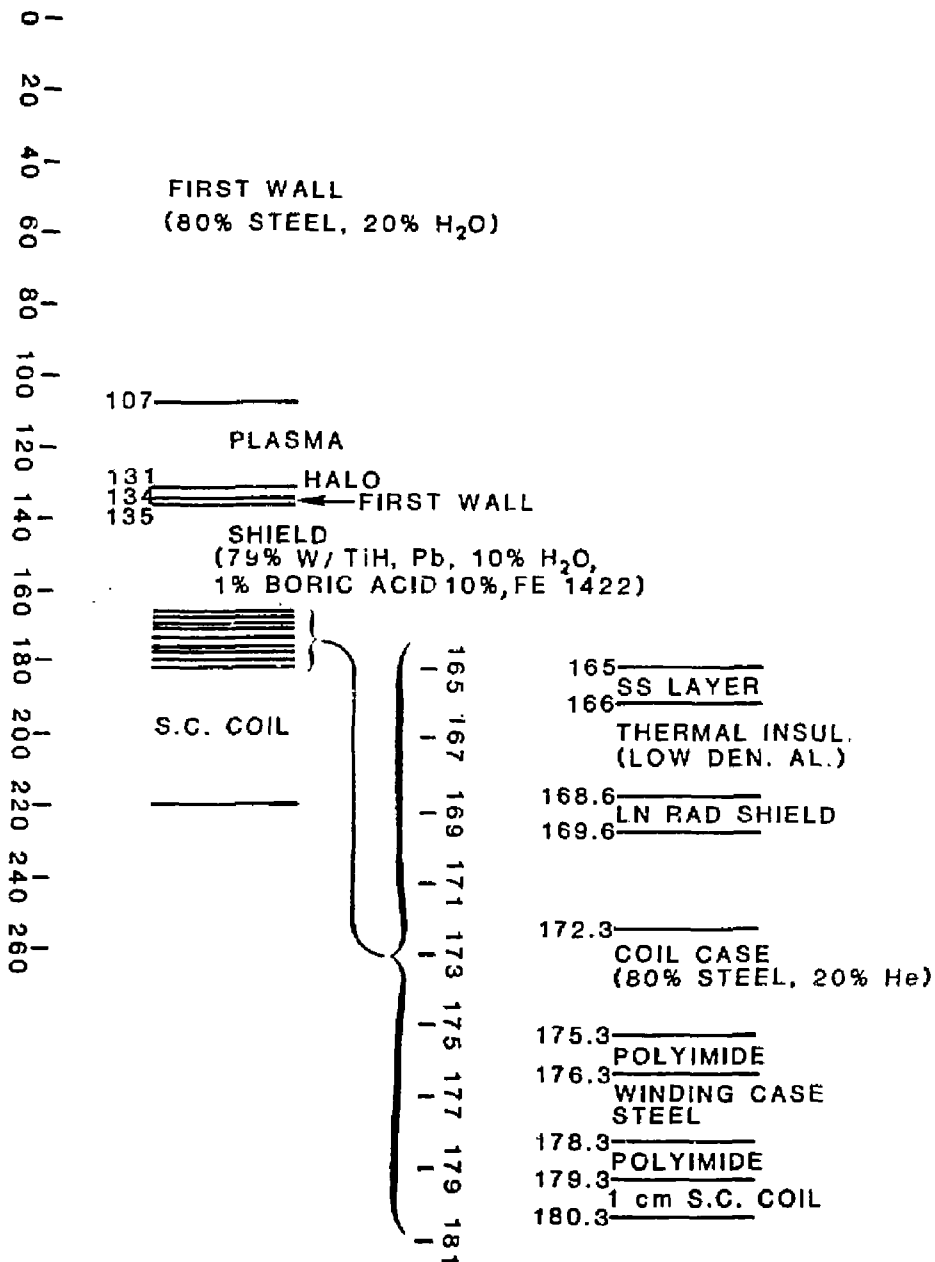
Figure 5-37. The 1-D slab model.
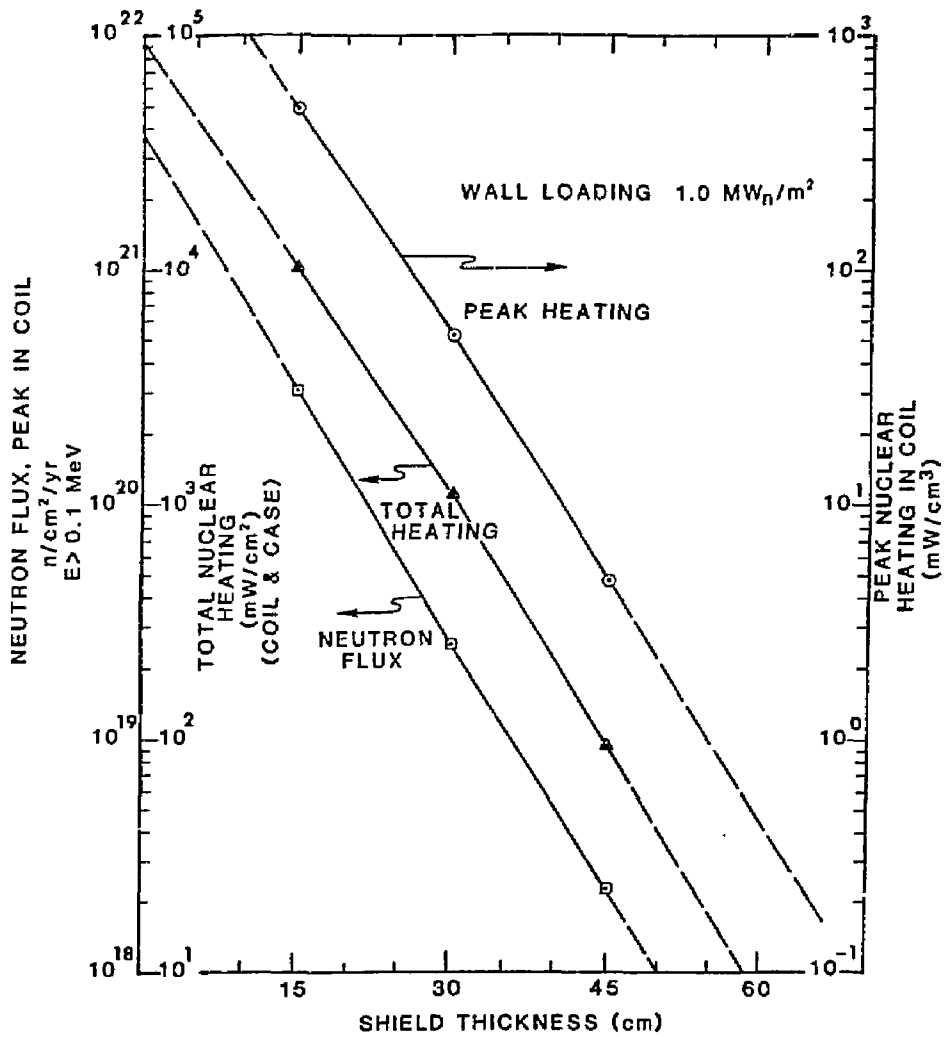
Figure 5-38.   Neutron flux and heating vs shield thickness.
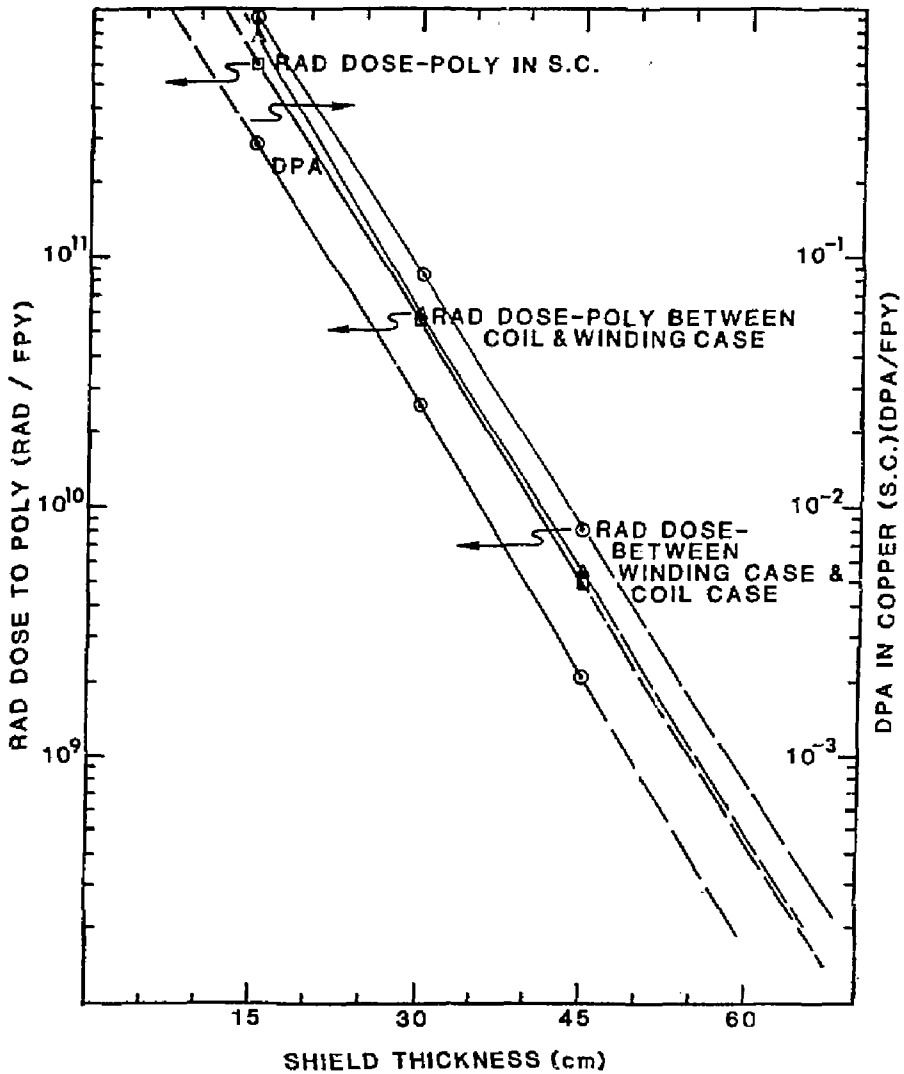
Figure 5-39.   Insulator dose rates and Cu-dpa vs shield thickness.

FPD   MODEL C83
GRID 1, T= 0.000

08:46:55 C 08/25/84
(GTL:0,0,0,0,0,0)

FPD   MODEL C83
GRID 6, T= 90.000

08:46:55 C 08/25/84
(GTL:0,0,0,0,0,0)
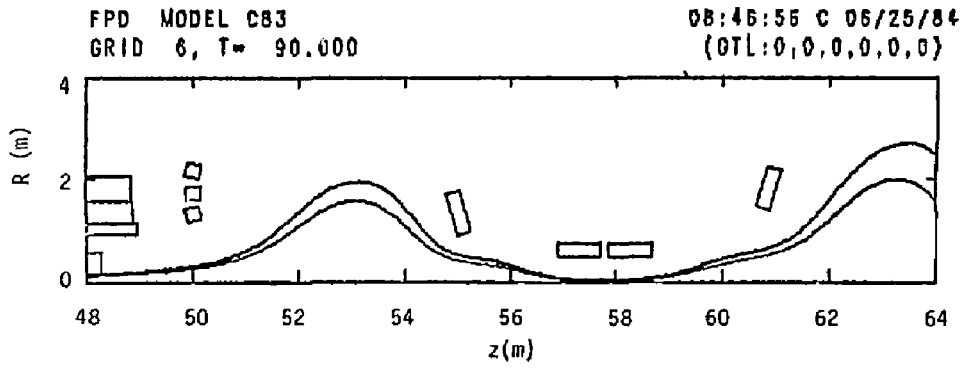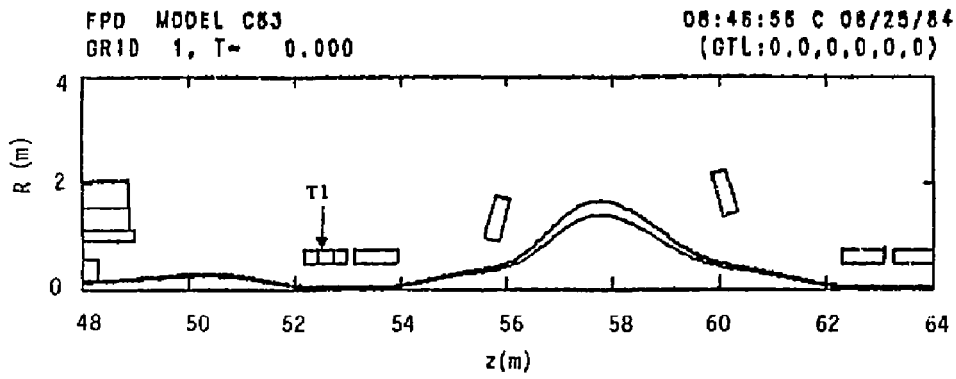
Figure 5-40.   The FPD end-cell configuration C-83.
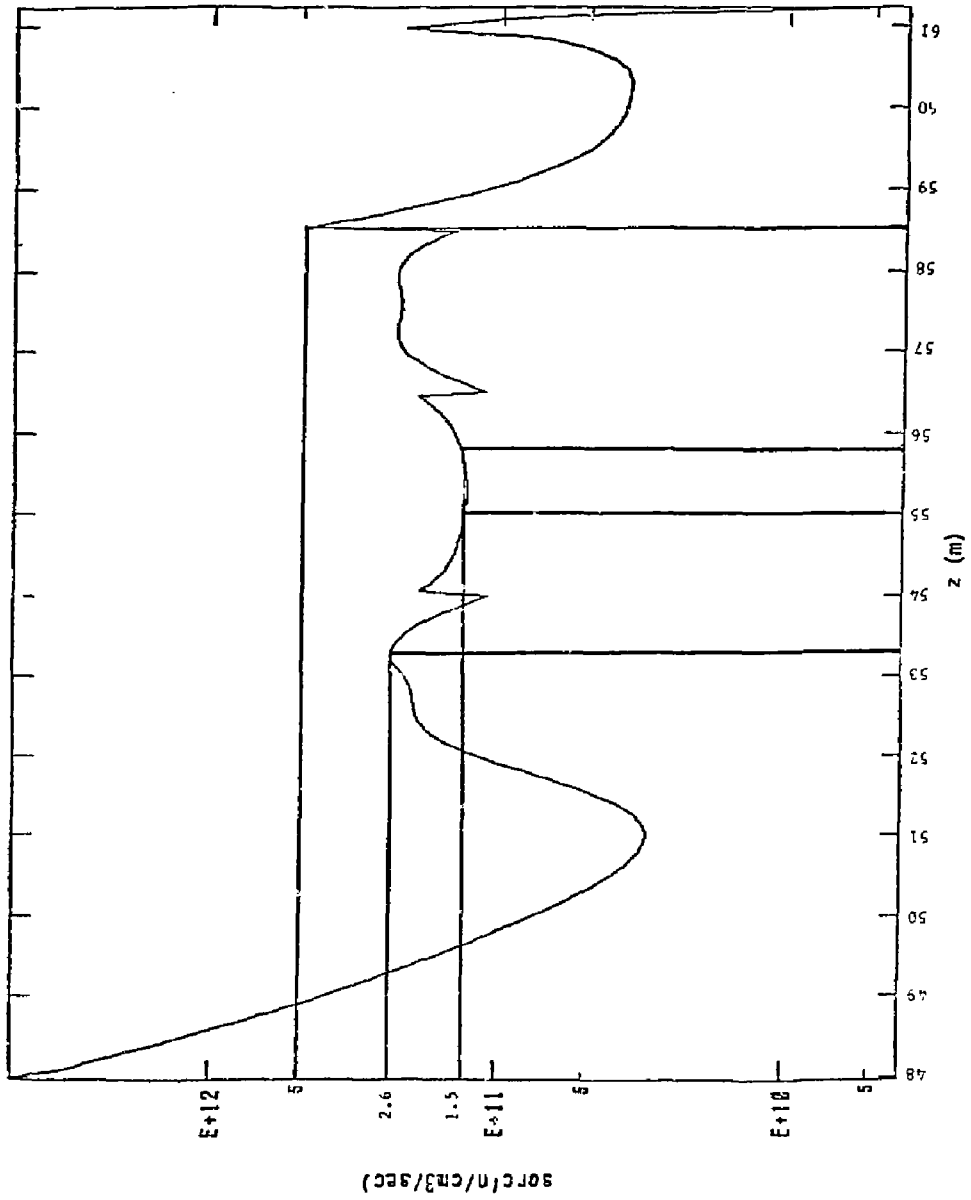
Figure 5-41. End cell (C-83) volumetric source vs z.
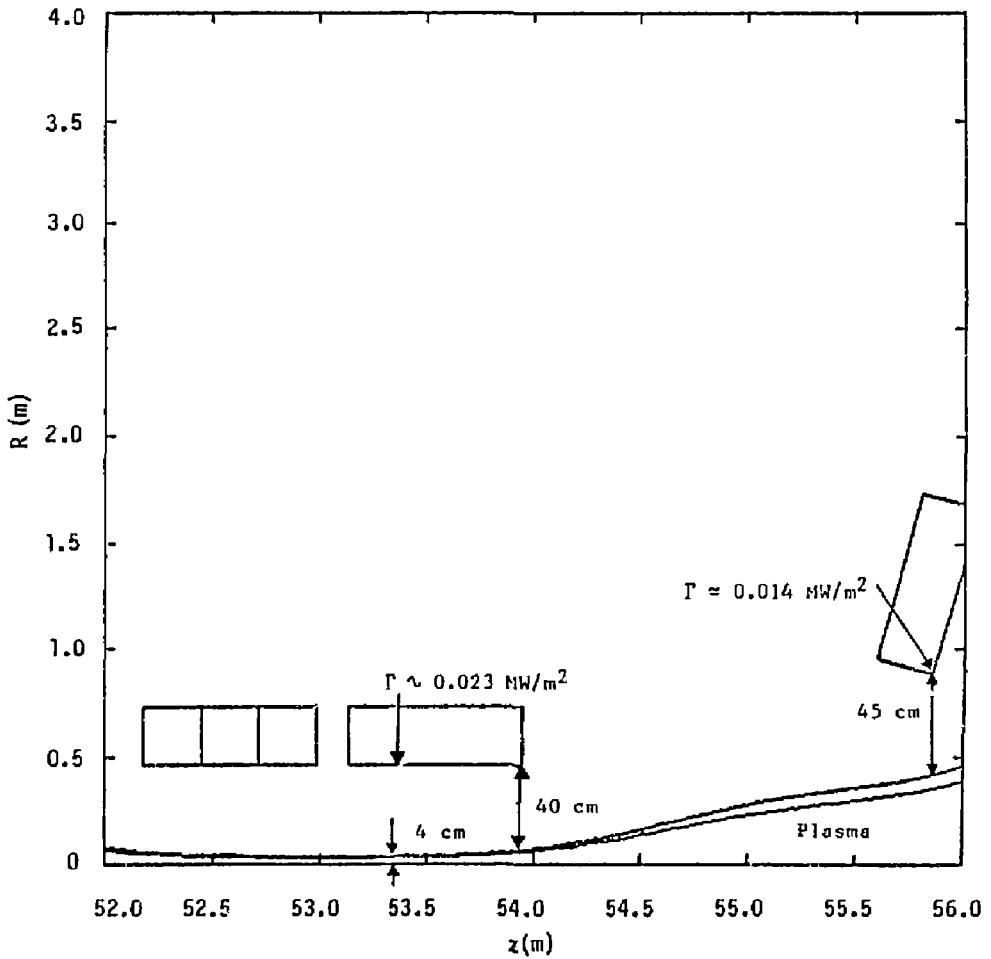
Figure 5-42.   End cell (C-83) configuration (z = 52 to 56 m).

- Peak heating (P) = 2.5 mW/cm^3.
- Peak flux [ϕ (E > 0.1 MeV)] = 1.3 x 10^{18} $n/cm^2 \cdot yr$.
- Peak rad dose to insulators = 4.6 x 10^9 rads/yr.
- Peak displacements per atom (dpa) in Cu = 0.0013/yr.

The next two points at which local maxima in coil radiation levels may occur are at the inner corners of the minor radia turns of the anchor coils (z = 55 m and 55.8 m, respectively). At these points the plasma is nearly circular, therefore, a cylindrical 1-D geometry is used to calculate wall loading. The line source strength at these two points is 3.4 x 10^{16} n/m·s (Fig. 5-43); therefore, the wall loading at the coil at these two points is 0.014 MW/m^2. The space available for shielding is 30 cm. The lower wall loading plus 5 cm more shielding at these points, compared with the first point, result in heating and damage rates 70% less than at the first point.

The fourth point at which a local maximum in coil radiation levels occurs is on the centerline of the first plug C-coil at z = 58.6 m. Here volumetric source strength has a sharp peak of 5 x 10^{11} $n/cm^3 \cdot s$ (Fig. 5-41) and the space for shielding is only approximately 23 cm (Fig. 5-44). Using a 1-D slab model, the wall loading at this point is 0.056 MW/m^2. This wall loading coupled with space for only 23 cm of shielding, results in the peak 1-D heating and damage rates listed below.

- Peak heating = 8.4 mW/cm^3.
- ϕ_n (E > 0.1 MeV) = 4.5 x 10^{18} $n/cm^2 \cdot yr$.
- Rad dose to insulator = 9.5 x 10^9 rads/yr.
- The dpa in Cu = .0045/yr.

Because the source at this point has a sharp peak in z, the wall loading and resulting radiation levels are overpredicted by the 1-D method. Nevertheless, based on this analysis, we predict this point to have the highest radiation levels in this C-coil set.

In addition to local peak heating and damage rates in the coil, total neutron-induced heating in the entire C-coil set and the cryogenic cases is also important because of the cost of cryo-refrigeration. To estimate this
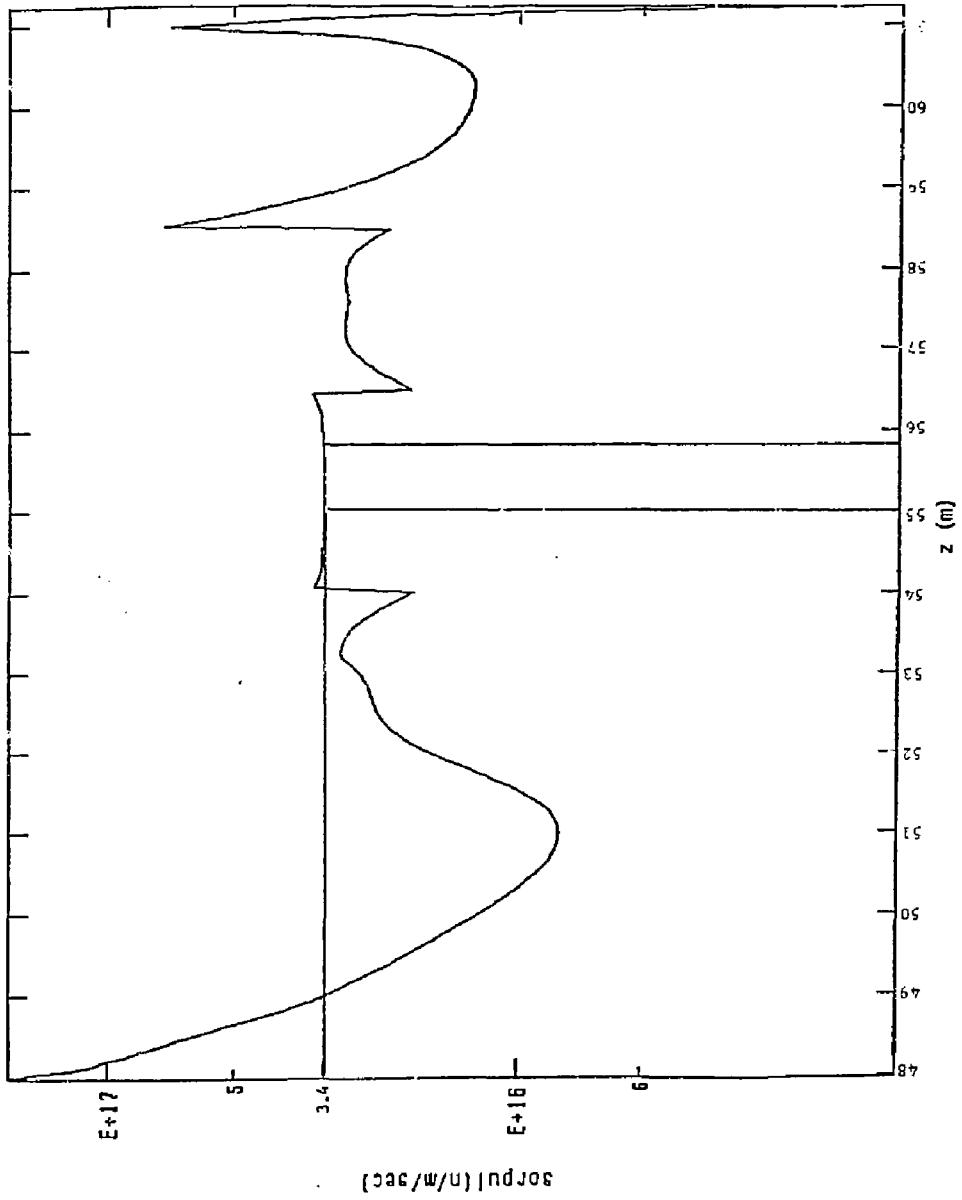
Figure 5-43. End cell (C-83) line source vs z.
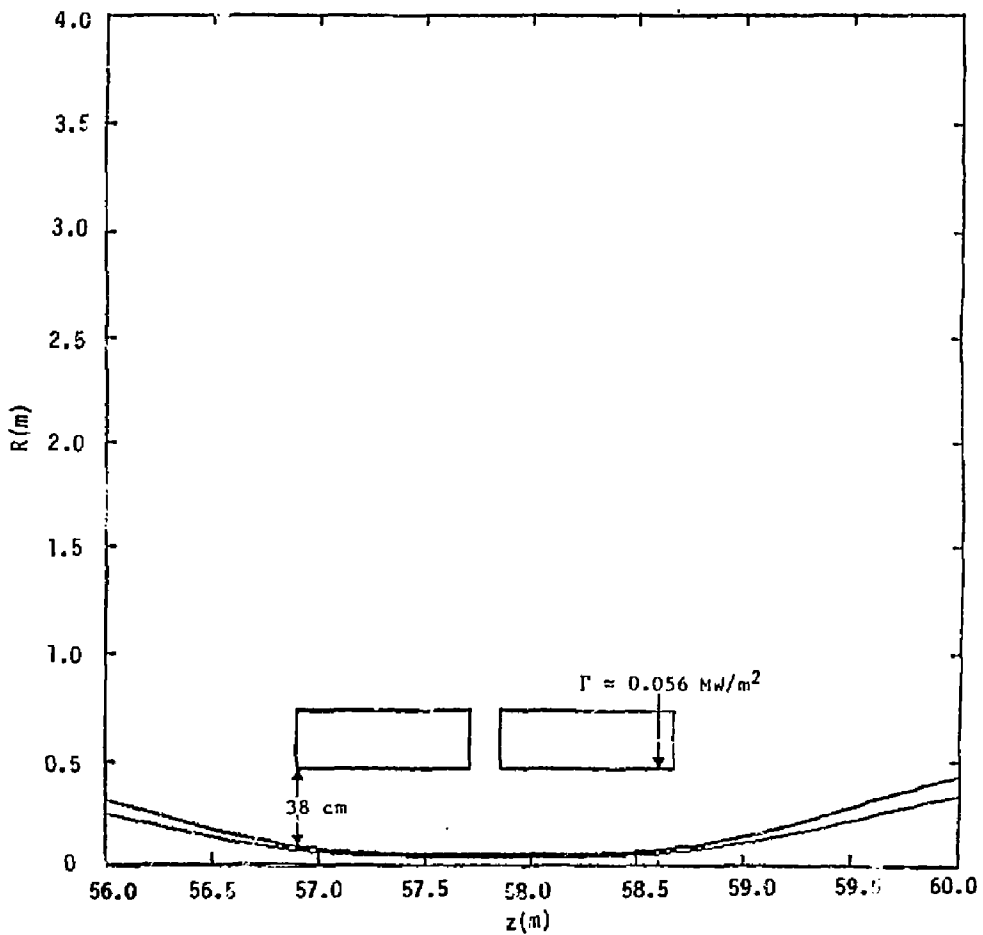
Figure 5-44.   End cell (C-83) configuration (z = 56 to 60 m).

total heating, the end-cell line source is integrated over z in those regions where shielding space is limited (Fig. 5-45). These regional sources are then attenuated by the allowable shield thicknesses in each region. For this case (C83), the first region is taken to extend from $z \simeq 52$ m to $z = 54$ m. The source in this region is 4.1×10^{16} n/s and the shielding space is 25 cm. The attenuation factor with a 25-cm shield is 0.023 (Fig. 5-38); therefore, total coil plus case heating is 2.2 kW. The second region is from $z \simeq 56.7$ to $z \simeq 58.7$, and by the same methods, heating is 4.4 kW. Thus, the total of both regions in both ends is approximately 13 kW. Although these two regions should account for most of the C-coil heating, there are areas outside these regions where coil heating will also occur. To accommodate this additional heating in a crude way, total C-coil heating is assumed to be twice the two-region 1-D result. Therefore, the total heating in the C83 C-coil set is estimated to be 26 kW. This energy is assumed to split--with approximately 36% in the windings and approximately 64% in the case--as occurred in the ONEDANT calculation.

The 1-D methodology just described was applied to a series of end C-coil magnet sets starting with A18 (the original FPD-1 configuration) and culminating with C83 (the FPD-II configuration). The results of these series of 1-D analyses are summarized in Table 5-17.

Note that both the A18 and C83 peak neutron flux levels will exceed the *original* limits for NbTi (1×10^{18} n/cm^2) and Nb$_3$Sn (4×10^{18} n/cm^2) before 5 full power years of operation are reached, but that they are well below the revised, more speculative limits of 10^{20} to 10^{21} for NbTi and within the 1 to 4×10^{19} range for Nb$_3$Sn. The insulator dose limit of 10^{11} rads is not reached in either case.

We emphasize that these 1-D results are only crude estimates used to help guide end-cell optimization. The attractive candidates must be analyzed with 3-D methods to adequately account for the complicated geometries involved.

PROPOSED END CELL DESIGN AND OPTIMIZATION PROCEDURE

The proposed end cell design and optimization procedure follows:

1. Specify design objectives and criteria.
2. Assume (or modify) coil set parameters and check to see if feasible.
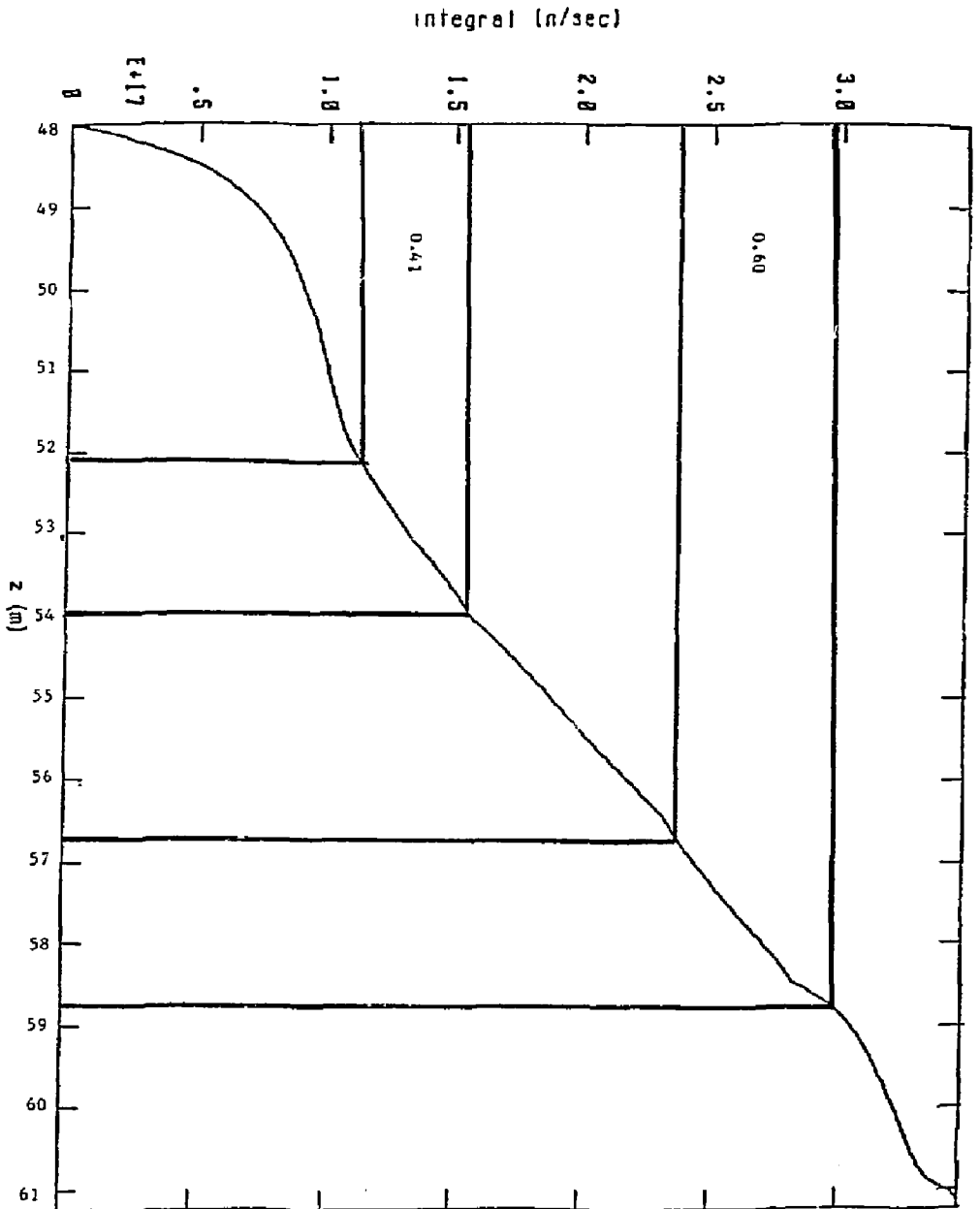
Figure 5-45. Integral of end-cell source vs z.

Table 5-17. Summary of 1-D analysis for five different C-coil types.

Coil set	Halo thickness at choke coil	Total heating[a] (kW)	Peak heating[b] (mW/cm^3)	Peak neutron flux[a] (n/cm^2 FPY[c] $E_n > 0.1$ MeV)
A18	5 cm	5.2	2.5	1.2×10^{18}
	$2 \rho_\alpha$	6.2	7.5	3.6×10^{18}
C31	$2 \rho_\alpha$	19	190	1.2×10^{20}
C51	5 cm	32	3.2	1.8×10^{18}
	$2 \rho_\alpha$	42	8.1	4.5×10^{18}
C61	5 cm	13	0.8	3.7×10^{17}
	$2 \rho_\alpha$	14	1.7	7.8×10^{17}
C83	$2 \rho_\alpha$	26	8.4	4.5×10^{18}

[a]At hot spot in winding.

[b]$\sim64\%$ winding; $\sim36\%$ case.

[c]Full power years.

3. Calculate plasma shapes and stability and conductor fields. If okay, proceed to step 4.

4. Calculate fusion neutron source distribution.

5. Perform 1-D estimate of neutron heating and damage rates in coils with W and Fe shields.

6. Check coil radiation levels. If okay, proceed to step 7.

7. Estimate 3-D calculation of coil heating and damage.

8. Check coil radiation levels. If still okay, proceed to step 9.

9. Design and then estimate end cell cost, including refrigeration.

10. Modify and iterate coil set configuration or objectives, where possible, to minimize cost.

Details of Optimization Procedure

In Step 1, acceptable field configurations are specified by Lawrence Livermore National Laboratory (LLNL) along with basic superconducting coil design criteria such as J vs B and acceptable radiation damage rates specified by the LLNL Fusion Engineering Design Center (FEDC).

In Step 2 various coil sets are laid out (or modified) and analyzed in Step 3 to see if they produce acceptable plasma configurations and conductor fields. Steps 2 and 3 are repeated as necessary to get acceptable and consistent coil sets (LLNL).

In Step 4 fusion neutron source distribution(s) are calculated with the acceptable magnetic field configuration from Step 3 (LLNL).

In Step 5 the coil set and plasma geometries and the neutron source distributions from Steps 2, 3 and 4 are used to perform an initial 1-D estimate for peak heating the radiation fluxes and for damage rates in the coils with various shielding types (W vs Fe) in the available space between the coils and the halo plasma boundary (LLNL and/or FEDC).

In Step 6 the estimated coil radiation levels from Step 5 are compared to criteria (from Step 1) to see if they are within acceptable levels. If they are not acceptable, Step 2 is repeated and the configuration of coil set is modified to better accommodate the shielding needs (thicker shields where fluxes are too high and thinner shields as appropriate) (LLNL and/or FEDC).

In Step 7 cases that pass Step 6 are subjected to a much more rigorous (and costly) 3-D analysis of coil heating and damage rates (FEDC).

In Step 8 radiation levels from Step 7 are compared to the radiation limit and other criteria to confirm whether the coil/shield configurations are still acceptable.

In Step 9 coil/shield configurations that pass Step 8 are designed to the level necessary to judge whether they are technically credible. Their costs are also estimated [LLNL/FEDC/General Dynamics (GD)].

In Step 10 insight gained in the earlier steps is used to modify coil set configurations to reduce cost (LLNL/FEDC/GD).

TRITIUM PERMEATION

Tritium permeation through components subjected to energetic tritium bombardment is considered a potentially serious problem for future fusion reactors. High tritium concentrations in the region near the plasma-side surface are reached by implantation of the energetic tritium. The tritium diffuses to either the plasma-side surface, where it undergoes relatively slow recombination and release from the surface as a molecule; or to the coolant-side surface, where it enters the coolant. If the permeation rate to the coolant is significant, processing of the coolant is required to maintain the tritium concentration at a tolerable level.

We investigated tritium permeation through the halo scraper and direct converter components to establish whether or not processing of the water coolant is required. We used a one-dimensional, transient, finite difference model of the copper structure to determine: the tritium permeation rate, the total tritium concentration in the water coolant, and the tritium inventory in the structure during the lifetime of FPD. We included the impact of pulsed operation in this study, however, predictions assuming continuous burn roughly agree with those using pulsed operation. We assumed that each burn pulse consisted of 300 hours of burn (the longest burn expected for FPD) followed by 900 hours of dwell time before the next burn.

The results of the above study are summarized in Table 5-18. The total amount of tritium in the halo scraper and direct converter coolant system is only 52 kCi. By estimating the water volume in this coolant system at 12 m^3, the end-of-life tritium concentration in the coolant, assuming no processing, is 4.3 kCi/m^3. This is well below the 16 kCi/m^3 present in the operating CANDU heavy-water reactors. The inventory in the halo scraper and direct converter components is also quite low. Therefore, processing of the water coolant is unnecessary; the water could simply be barrelled and transported for disposal.

Table 5-18. Tritium permeation rates and inventory in direct converter/halo scraper components.

Component	Maximum permeation rate	Total tritium in coolant[a]	Tritium inventory in structure
	Ci/day	Ci	Ci
Halo scraper	14	2.7×10^4	7.3×10^3
Outer collector	2.4	4.0×10^3	1.4×10^3
Inner collector	12	2.1×10^4	6.7×10^3
Total	28	5.2×10^4	1.5×10^4

[a]Assumes no removal by processing but does account for radioactive decay.

MATERIALS

A significant difference, in selecting materials for FPD-II, compared with FPD-I, is the higher neutron wall load in the axicell. The neutron wall loading of 5 MW/m^2 and lifetime operation at an integrated wall load of 12.5 MW·y/m^2 impose challenging requirements on the first wall and blanket structural material of FPD-II. In steel material this exposure will produce a displacement damage level of approximately 130 dpa and transmutation reaction product gases of 1400 to 2000 atomic ppm He and 6000 atomic ppm H. (The exact values will depend on the detail of blanket design and steel composition.) Few data are available on the effect of this irradiation level on the properties of candidate structural materials, therefore, the design must allow for axicell replacement during the operating life of the reactor. However, there is some data to indicate that either a ferritic/martensitic steel or an austenitic stainless steel may be adequate for service to 12.5 MW·y/m^2 in a MARS-like blanket module.

Some data suggest that the ferritic/martensitic steels may be resistant to swelling up to neutron fluences producing >100 dpa. However, the data are for irradiations producing little helium and coverage of irradiation temperature is incomplete. Data at somewhat lower fluences suggest that tensile strength will not be degraded, but that tensile elongation will be reduced to low but usable levels. Irradiation creep rates will be known in a few years, and can be accommodated in design. The shift in the ductile-to-brittle transition temperature (DBTT) that results from irradiation of ferritic steels is a concern. Available data hint that the ferritic steel 9 Cr-1 Mo might be a better choice than HT-9 (12 Cr-1 Mo) because the lower initial DBTT can result in a DBTT after extended service that is still below the reactor shutdown temperature.

The austenitic stainless-steel type 316 would swell excessively in the fluence required in the axicell. However, advanced austenitic steels have been developed for swelling resistance and these steels may prove adequate for service to 12 MW·y/m^2. If the swelling resistance proves adequate, irradiation creep during service and reduced tensile ductility will impose limitations that can be accommodated in the design.

Current activities of the Fusion Reactor Materials Program are directed at qualifying alloys for service under conditions that are anticipated for the axicell. The pace of the program is such that the data relevant to axicell conditions is now becoming avilable. As a result, the final choice of a structural alloy for the axicell should be reviewed regularly, to ensure that the best candidate material is used.

Most other material issues in the FPD-II configuration are similar to FPD-I (see Sec. 4).

ELECTRICAL SYSTEMS

The electrical systems include the electric plant equipment of the ac power system, the power conversion for the confinement magnets, the power conversion for the microwave and neutral beam injector (NBI) systems, and the instrumentation and control systems.

THE AC POWER SYSTEM

The ac power system includes all the switch gear, transformers, and distribution of power to the electrical loads identified in Table 5-19; the table also includes the busing and fault protection for the turbine generator and direct converters, and the inverters of the direct conversion system. Referring to Table 5-19, the total recycle power needed for FPD-II is 128 MW without the axicell and 243 MW with the axicell. The total electrical power output is 40 MW from direct converters and 205 MW from the turbine generator. Engineering Q_e, defined as the power generated divided by the power consumed by the plant, is 1.9 without the axicell and 1.0 with the axicell.

Table 5-19. Estimate of FPD-II electrical power generation and loads.

Power generation or load description	Electric power (MW)	
	Input	Output
Central-cell neutral-beam injectors	0(62)	
Central-cell ICRH power	0	
Plug-cell neutral-beam injectors	6(4)	
Anchor-cell ICRH	2(2)	
Anchor- and plug-cell drift pumps	2(2)	
Plug-cell ECRH	50(50)	
Resistive coil power	23(78)	
Cryogenic system power	25(25)	
Cooling system and vacuum system power	10(10)	
Superconducting-coil power systems	3(3)	
Fuel processing and tritium cleanup	7(7)	
Direct converters		40
Turbine generator		205
Total (with axicell)	128 (243)	245

Figure 5-46 is a simplified block diagram of the power distribution system. The main 230-kV substation provides all of the 13.8-kV power during startup. After the plant is on line, the direct converters and turbine generator supplies more power than that consumed without the axicell. A net power of 117 MW is delivered to the utility line. With the axicell, the power generated is nearly equal to the power consumed.

A small 30-MV·A substation provides better regulated power to the 4.16-kV loads. The 4.16-kV substations may selectively receive power from either the 230- or 115-kV substations. The 4.16-kV substations provide power to eight 2-MW load-control centers. Two 4.16-kV diesel generators provide backup power to selected critical loads if a power failure occurs.

Figure 5-47 is a one-line diagram of the FPD-II power-distribution system. Mnemonics used on the diagram are defined in Table 5-20. Medium voltage power is provided by the power-distribution system at 13.8 kV and 4.16 kV, the preferred voltages in use today. The substation would also be adequate for TFCX-S, the superconducting coil tokamak now being considered as a next generation machine. If TFCX-S and FPD-II were located at the same site, both machines could be operated from the same substations alternately, but not concurrently. In Fig. 5-47, note that 4.16 kV is available from three sources: the 230-kV substation, the 115-kV substation, and the diesel generator units. The turbine-generator 4500-A continuous-duty circuit breakers are custom built but commercially available. Isolation switches are provided at the 230/13.8-kV transformers, but the only main transformer circuit breakers are on the high-voltage side. Faults that may develop on the two main 13.8-kV buses will trip the high voltage circuit breakers which have more than sufficient interrupt capacity.

The 115/4.16-kV substation, not shown in Fig. 5-47, consists of a three-winding transformer that has switch gear and lightning protection on the high-voltage side. Each 4.16-kV winding provides power to three 2-MW load-control centers and are connected to the main system with breakers 18 and 19 shown in Fig. 5-47.
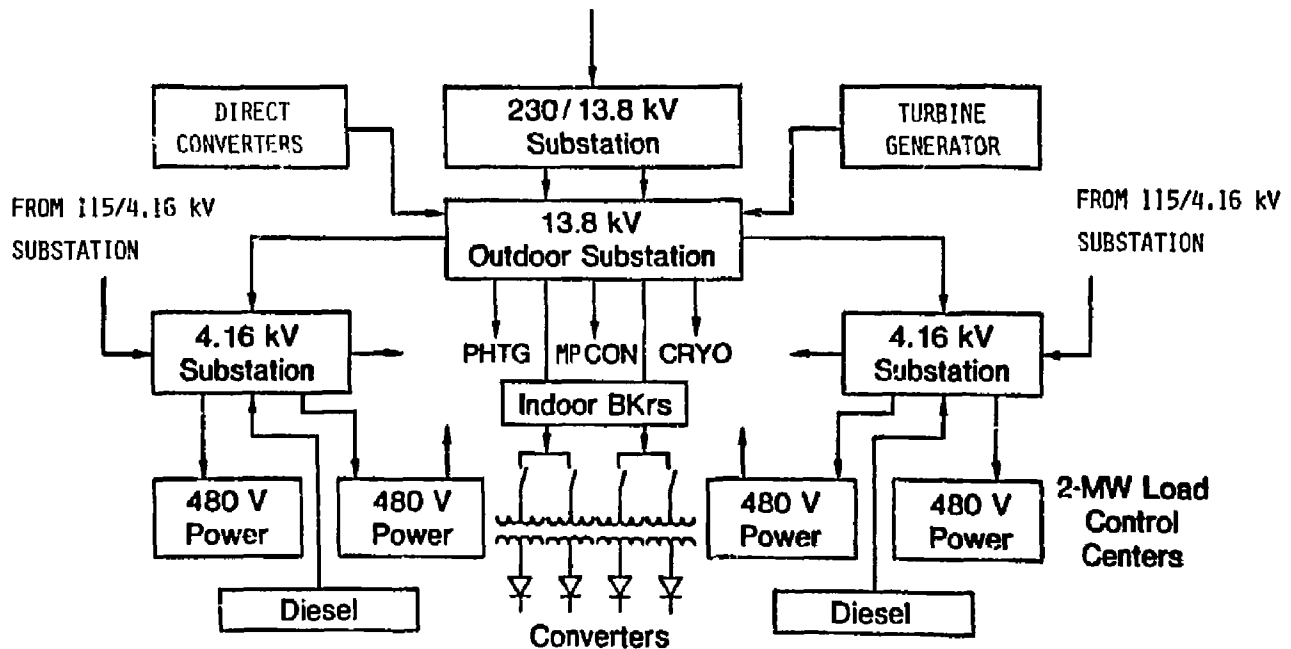
Figure 5-46. Simplified block diagram of the FPD-II power-distribution system.
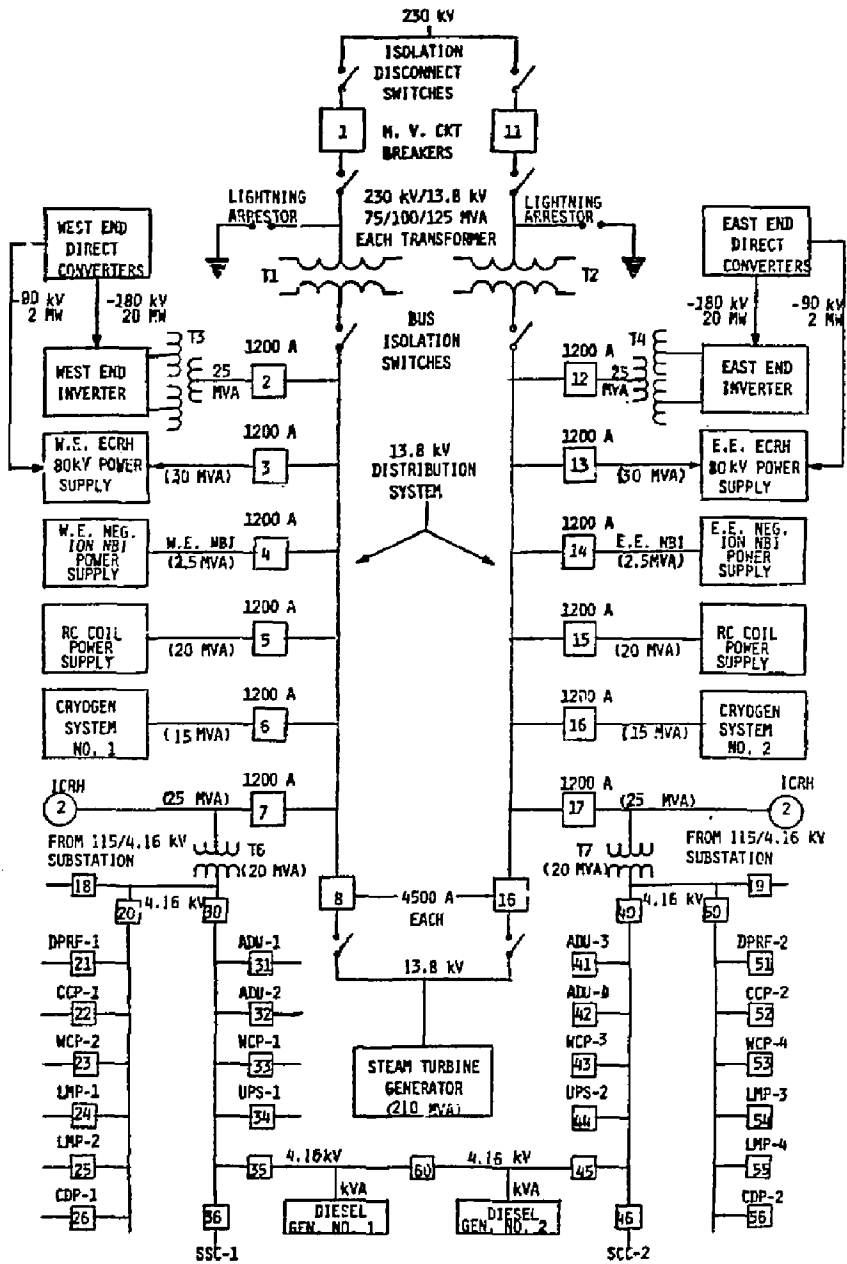
Figure 5-47. One-line diagram of the FPD-II power-distribution system.

Table 5-20. Mnemonic definitions.

Mnemonic	Description
DPRF	Drift pump rf power
ADU	Atmospheric detritiation unit power
WCP	Water cooling pump power
LMP	Liquid metal pump power
UPS	Uninterruptible power supply
CFP	Condensate feed pump power
CCP	Condenser cooling pump power
SCC	Superconducting coil power
NPS	Number of power supplies
PSVOLT	Power supply voltage
PSKA	Power supply current (kA)
BUSLM	Bus length (m)
NBKRS	Number of dc circuit breakers
NDR	Number of dump resistors
EDRMJ	Maximum energy dissipated in a dump resistor (MJ)
PDRMW	Maximum power to a dump resistor (MW)

ELECTRICAL POWER CONVERSION SYSTEMS

The electrical power-conversion systems include the following:

1. All the power supplies for the magnets, and power injection systems
   for the plasma;
2. The coil-protection equipment,
3. The cables and bussing.

Table 5-21 contains the key magnet power-conversion data for FPD-II both
with and without the axicell option. Mnemonics in the column headings of the
table are defined in Table 5-20. The first column of Table 5-21 refers to the
characteristic configurations for the magnet power conversion for the group.
These configurations are shown in Figs. 5-48 through 5-52.

Table 5-21. The FPD-II magnet power conversion data.[a]

Type	Magnet group	NPS	PSVOLT	PSKA	BUSLM	NBKRS	NDR	EDRMJ	PDRMW
A	Central cell-8	1	20	60	200	5	16	150	30
B	Central cell-2	1	1C	60	120	2	4	55	15
D,E	Choke insert-2	1	+120	100	150	0	0	0	0
C	Choke background-2	2	30	9	100	4	8	39C	4.4
B	Transition-1-2	2	12	25	100	4	8	60	12
B	Anchor cell-4	2	12	25	120	4	8	240	12
B	Plug cell-4	2	12	25	140	4	8	240	12
B	Transition-2-2	2	12	25	160	4	8	45	12
B	Recircularize-2	2	12	25	180	4	8	65	12
D	Axicell choke-2	1	+190	130	100	0	0	0	0
C	Axicell background-2	2	30	12	100	4	8	500	12
E	Axicell center-1	1	165	80	100	0	0	0	0

[a]For mnemonic definitions see Table 5-20.
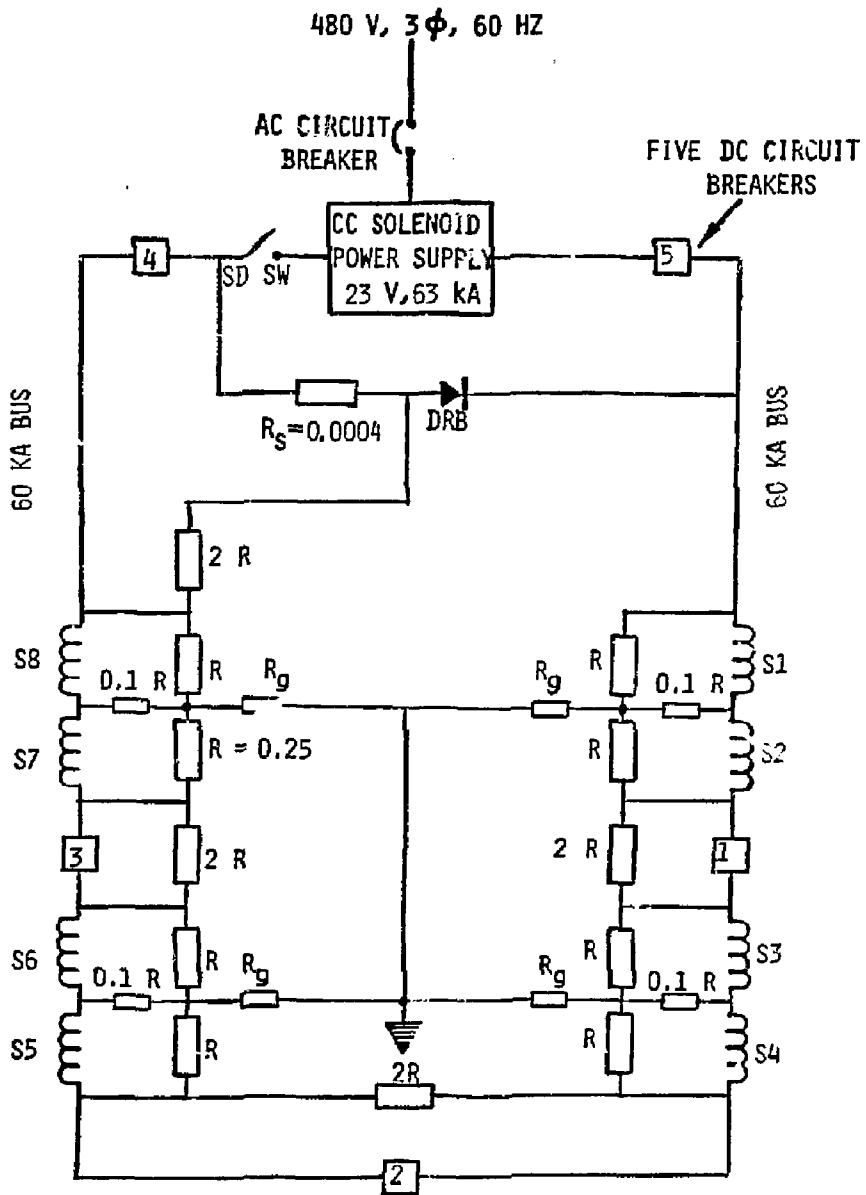
Figure 5-48. Power-conversion system for the central cell solenoid magnets. (Type-A circuit)
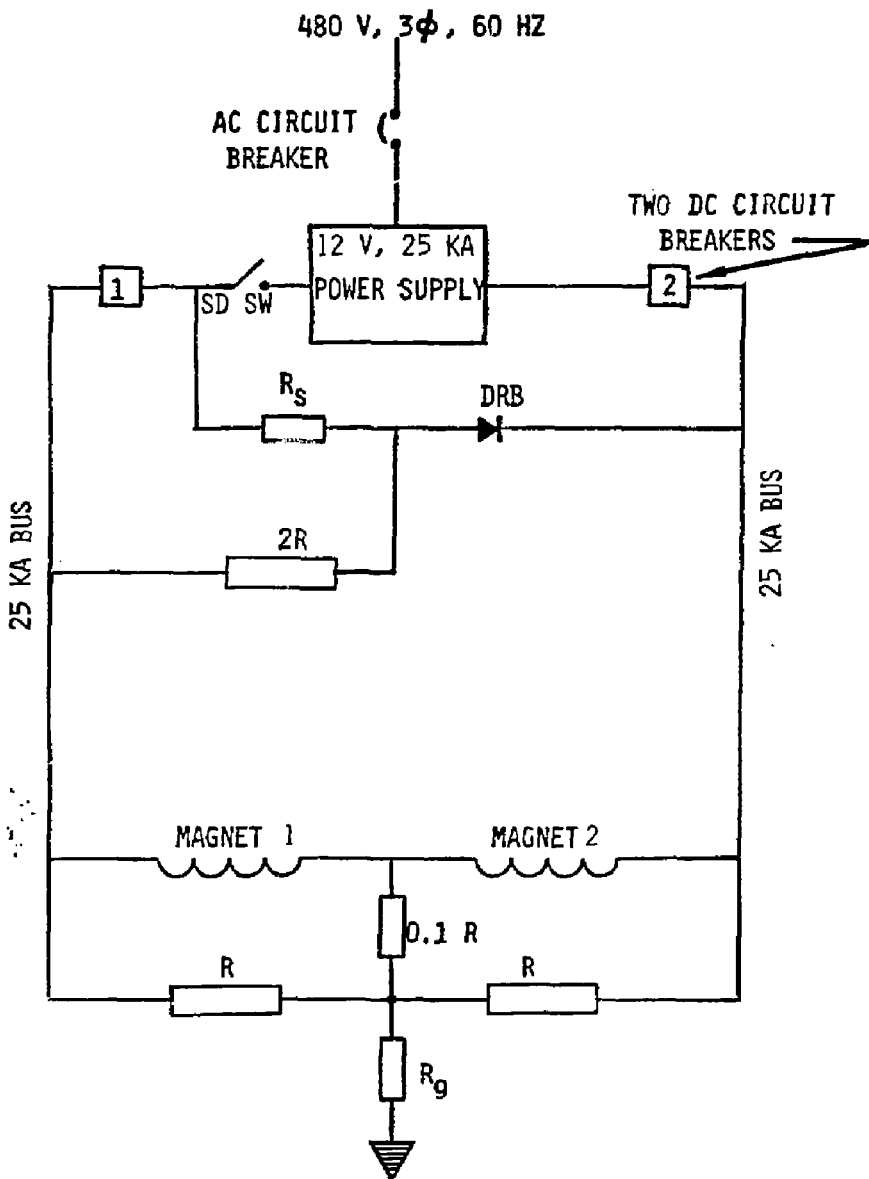
Figure 5-49. Type-B power-conversion system.
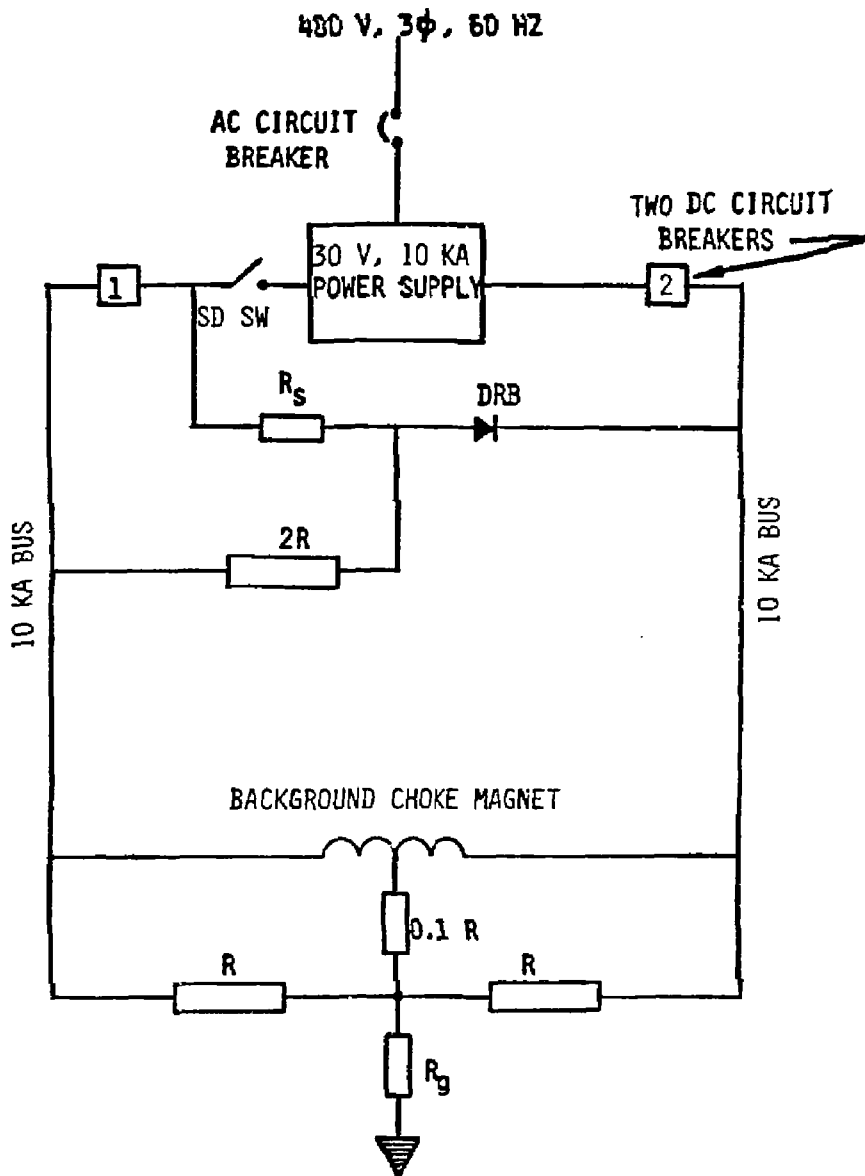
Figure 5-50. Type-C power-conversion system.
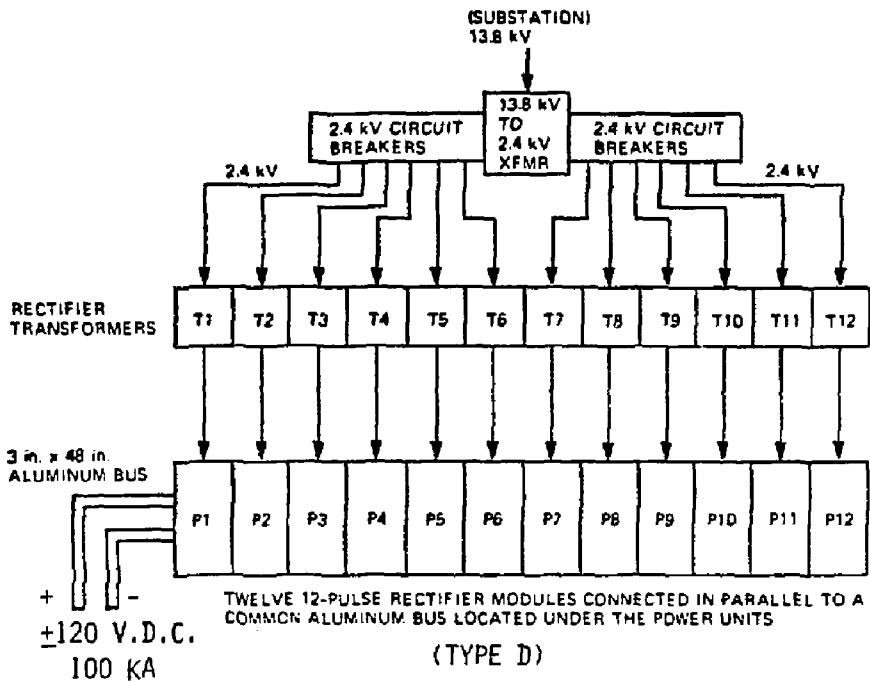
Figure 5-51. Type-D power-conversion system.

Figure 5-52. Type-E power-conversion system.

The type-A circuit (Fig. 5-48) shows the 16 dump resistors for the 8 main solenoid coils connected in series. There are five large dc circuit breakers for interrupting the 60-kA coil current if quench conditions are detected. The pneumatically operated slow-dump switch SD-SW has very low voltage across it because of the low-resistant-shunt slow-dump resistor R_s. The busing cross section is ten times higher than that used in the MARS study.[3] Figures 5-49 and 5-50 show the type B and C power conversion systems that apply to the two coil and single coil groupings of Table 5-21. The only difference is that the background choke coils are so large (high energy) that they must have a center tap and separate dump resistors to protect them if a quench occurs.

Figures 5-51 and 5-52 depict power supply construction for the resistive coils, which require substantial power at high current and moderate voltages. For the lower power coils, such as the axicell center coil and main solenoid choke coils, it may be desirable to reduce the ac line voltage to 2.4 kV to reduce the cost of the circuit breakers and rectifier transformers (Fig. 5-49). For the higher power axicell choke coils, the direct connection to the 13.8-kV line via the auto transformer (shown in Fig. 5-52) may be more flexible or cost effective. In either case, the very large currents require large cross-section busing as shown in the figures. Copper busing will reduce the cross section by 50%, but is generally more expensive than aluminum. Joining the slabs together, however, may favor the use of copper busing.

The power conversion equipment for the plasma-heating systems consists of numerous converter/transformer units and all associated switch gear. Because the heating-system sources all require tight voltage regulation, twelve-pulse converters are used. The converters include all the surge arresters, reactors, filters, breakers, and preinsertion resistors that are required to smooth and condition the dc signal and protect sensitive elements of the unit (e.g., the thyristor valves). The larger ac-dc converter units are as follows:

- 38-MW, 126-kV, 300-A unit for the axicell tritium beamline (1);
- 25-MW, 83-kV, 300-A units for the ECRH systems (2);
- 23-MW, 83-kV, 277-A unit for the axicell deuterium beamline (1).

The two ICRH units are small, 1.5 MW at 20 kV, and the multiple units for the sloshing beam system are all <1 MW with voltages ranging from 45 to 475 kV.

INSTRUMENTATION AND CONTROL

We had insufficient time to address the instrumentation and control (I&C) issues for FPD-I and FPD-II in other than a precursory survey. The I&C for FPD-I and -II should be about the same. The I&C cost estimate considers four basic groups:

1. Plant process I&C,
2. Safety I&C,
3. Plasma diagnostics,
4. Supervisory-level data processing.

Each of these categories has both software and hardware aspects.

The plant process I&C includes all the data acquisition, local computers, and data transfer links to the supervisory level computers. The safety I&C includes all sensors, data acquisition, hardware controls, and computers needed for safety monitoring and for preventing plant startup and operation under adverse conditions. The safety I&C is a highly reliable system that is independent of all other systems. Plasma diagnostics include all the plasma diagnostic systems, data acquisition, and lower level computers dedicated to the diagnostics. The supervisory level data processing includes all the large scale data processors and their support peripherals found in the control room. This system also includes the dedicated data links to other general purpose data processors located in other facilities. All groups have console displays.

The software and hardware I&C cost should be comparable to that for MFTF-B or Tokamak Fusion Test Reactor (TFTR). However, more plant-process I&C is needed for monitoring the direct-converters, shield, blanket, and halo-dump modules. The safety system must be augmented to include all tritium facilities and fueling systems. However, only the essential plasma diagnostics for monitoring and controlling the machine are included in the

cost estimate. (There is very little space available for interfacing plasma diagnostics for physic experiments.) We assume that other predecessor machines will provide the plasma physics data.

The axicell addition requires add.tional I&C for the high-flux blanket and shield modules as well as the additional magnets and neutral beam injectors. For cost estimating purposes, approximately 30% was added to the process I&C.

TRITIUM SYSTEMS

In designing the tritium systems for a fusion reactor like FPD-II, we need to consider four important areas: (1) the use of neutral beams or pellet fuelers for fueling; (2) the presence of a blanket module with or without a power train; and (3) fuel storage requirements; and (4) the fusion power and the fractional burn.

The tritium and deuterium mass flow rates for FPD-II are shown in Table 5-22 for two different fueling options--positive neutral beams and pellets. The efficiency of positive neutral beams ranges from 0.2 to 0.3; therefore, the total tritium input ranges from 40 to 60 g/hour or 4 to 6 kg during a burn of 100 hours (length of the longest cycle). The fueling rate for pellet fuelers may range from 3 to 10 pellets/second with ∿100% waste at each of these rates. At steady state ∿3 pellets/second would be fueled. This corresponds to a tritium input of 14 to 21 g/hour or 1.4 to 2.1 kg/cycle.

The pellet fueler has two advantages over neutral beams. First, since two hours of tritium fuel is stored to ensure constant fueling during operation, a lower fueling rate results in a lower inventory. Second, processing units contain lower tritium inventories at a lower rate.

The tritium inventories in the test cell and other processing areas at the throughput rates cited are shown in Table 5-23. For beam fueling, the total inventory is ∿230 to 290 g. For pellet fueling, it is 180 to 210 g. With an inventory of 250 g, both options could be handled by the same system.

The units supplied in the processing area include uranium storage beds, a fuel cleanup unit, a cryogenic distillation unit, a waste gas recovery system, a solid waste disposal system, plus all controls, monitors, analytical

Table 5-22. Tritium and deuterium mass flow rates for FPD-II.

Input Parameters	Value
Burn time (h)	100
Plant availability	0.25
Power (MW)	479
Current to central cell (kA)	0.249
Current to end cell (kA)	0.009
Current to test cell (kA)	<0.431[a]
Cycles/yr	21.9
Tritium fraction	0.5

Processing variables at steady state for two options	Neutral beam[b]	Pellet[c]
Fractional burn	0.13	0.22
Tritium burnup (g/h)	3.1	3.1
Deuterium burnup (g/h)	2.0	2.0
Tritium to plasma (g/h)	12.1	7.0
Deuterium to plasma (g/h)	8.1	4.7
Tritium waste (g/h)	28 → 48	7 → 14.0
Total tritium input (g/h)	40 → 60	14 → 21.0
(kg/d)	0.97 → 1.5	0.3 → 0.5
(kg/cycle)	4.0 → 6.1	1.4 → 2.1
(kg/yr)	89 → 133	31 → 46
Deuterium waste (g/h)	19 → 33	4.7 → 9.4
Deuterium end cell (g/h)	3.7 → 5.3	3.7 → 5.3
Total deuterium input (g/h)	31 → 46	13.1 → 19.4
(kg/d)	0.74 → 1.1	0.31 → 0.47
(kg/cycle)	3.1 → 4.6	1.3 → 1.9
(kg/yr)	67 → 101	29 → 42

[a]For a test cell ∿3.5 m long.
[b]Beam efficiencies (+)20-30%, (-)7-10%.
[c]Waste will range from 100% to 300%. The beam case is 3 pellets/s. When the reactor is started, up to 10 pellets/s may be required.

Table 5-23. Tritium inventories (g) in FPD-II for two options.

Option	Beams	Pellet
Structure[a]	<30	<30
Beam pump[b]	4.5 → 7.8	--
Surge tank	4.5 → 7.8	--
Pellet fueler	--	10[c]
Blanket	3.8	3.8
Blanket recovery	1	1
Total test cell/heat exchanger	43 → 50	45
Storage[d]	80 → 120	28 → 42
Pellet preparation	--	14 → 21
Fuel cleanup	50 → 55	43 → 45
Cryogenic distillation	60 → 65	53 → 55
Total processing	190 → 240	138 → 163
Total	233 → 290	183 → 208

[a]Dissolved tritium in all components.

[b]Cycled 1/6 every 10 min.

[c]This inventory is a minimum. For an extruder, the
inventory is at least 20 g.

[d]Two hours of fueling.

equipment, and necessary secondary confinement and processing systems needed
to support the system. The units are sized based on Tritium Systems Test
Assembly (TSTA) reference units. They are located in a tritium processing
building separate from the test cell.

The blanket system is assumed to supply all of the tritium burnt
($\sim$6.7 kg/year) and also all of the tritium lost to decay, to environmental
releases or to waste in processing. The amount lost to decay (14 g/year)
depends on the plant inventory ($\sim$250 g). The amount lost to waste depends
on the efficiencies of the multiple processing systems. We assume that losses
will be $\leq$0.1% of the amount processed or $\leq$130 g/year with a required
breeding ratio of 1.03.

The processing system used to remove tritium from the LiPb blanket
includes a tritium removal system, a tritium purification system to remove
gamma impurities, a tritium control system for the power train coupled to the
blanket, an impurity removal system for the LiPb, plus auxiliary equipment,
dump tanks, etc. This equipment is located in the hot cell.

Four different atmospheric tritium recovery systems (ATR) are provided
for the four main tritium areas--test cell, hot cell, tritium building, and
heat exchanger building. The units are sized for the air volumes processed
and the processing time selected (5 days). The respective buildings have
internal volumes of $\sim 6.1 \times 10^4$ m^3, $\sim 2.4 \times 10^4$ m^3, $\sim 1.6 \times 10^4$ m^3, and
$\sim 4.3 \times 10^4$ m^3. A throughput rate of 0.5 vol%/min is needed to achieve
cleanup in 5 days. This corresponds to units of 305 m^3/min, 120 m^3/min,
80 m^3/min, and 215 m^3/min, respectively. The test cell and heat exchanger
units are coupled to serve as backups for each other. The system for the
tritium building is a separate system as is the hot cell unit. The
transporter unit is handled by part of the heat exchanger system. The air in
the large upper building above the test cell in which the transporter is
located is cleaned by the combination of the hot cell and test cell systems.

A tritiated water recovery unit is also provided for FPD-II. It serves
to remove tritium from any water system that becomes contaminated and it also
is used to concentrate the tritiated water collected by the different ATR
systems. Water systems that may become contaminated are those that serve beam
dumps, halo plates, direct converter units, etc. The tritiated-water recovery
unit has the potential of reducing tritium waste from the water systems by a
factor of 10^4.

The overall tritium system for FPD-II described here is similar to that
for the FPD-I design. The tritium mass flow rate for fueling FPD-II by pellet
is slightly higher than FPD-I's because, although the fusion power increased,
the fractional burn expected also increased. The fueling for FPD-II by beams
is approximately twice that needed for FPD-I because greater beam power is
needed in the FPD-II design. The blanket for FPD-II must produce ~ 2 kg more
tritium fuel each year than the blanket in FPD-I to replace the greater amount
of tritium burnt.

MAINTENANCE REQUIREMENTS AND OPERATING AVAILABILITY

The maintenance requirements and operating availability for FPD-II are identical to those discussed in Sec. 4 for FPD-I, except for the addition of the DT axicell. The axicell is located at $z = 0$ and consists of a test module with an integral solenoid coil (CSO), and a shield module with integral choke coils (CCC1). These components are removable through the access port located over the test module. The present design of the axicell requires the removal of test module before the choke coils can be removed. This is a developmental concern since the test module may be a lifetime component, while the choke coils may require annual replacements. Additional configuration development is required to achieve independent replacement of the coils.

Figure 5-53 shows the disassembly of the axicell based on the design developed for MFTF-α+T (see Ref. 1 for a more detailed discussion of this component and its modular subassemblies).

PLANT FACILITIES

We have used the same approach in designing the plant facilities for FPD-II as we used in FPD-I. However, the overall plant arrangement is modified to reflect the absence of a thermal-power conversion system (Fig. 5-54). In FPD-II, all of the thermal power generated is transported to an intermediate cooling-water loop and is rejected to the environment through a cooling-tower loop consisting of a mechanical-draft wet cooling tower (Fig. 5-55). The intermediate loop is provided to reduce migration of tritium and corrosion products to the environment. The total thermal power rejected is approximately 765 MWt. All other FPD-II facilities are similar to the FPD-I facilities with the differences specified in the cost estimate.

COST ANALYSIS

The total capital costs estimated for the FPD-II device are shown in summary form in Table 5-24. This estimate is in millions of mid-1984 dollars and has the following qualifications:
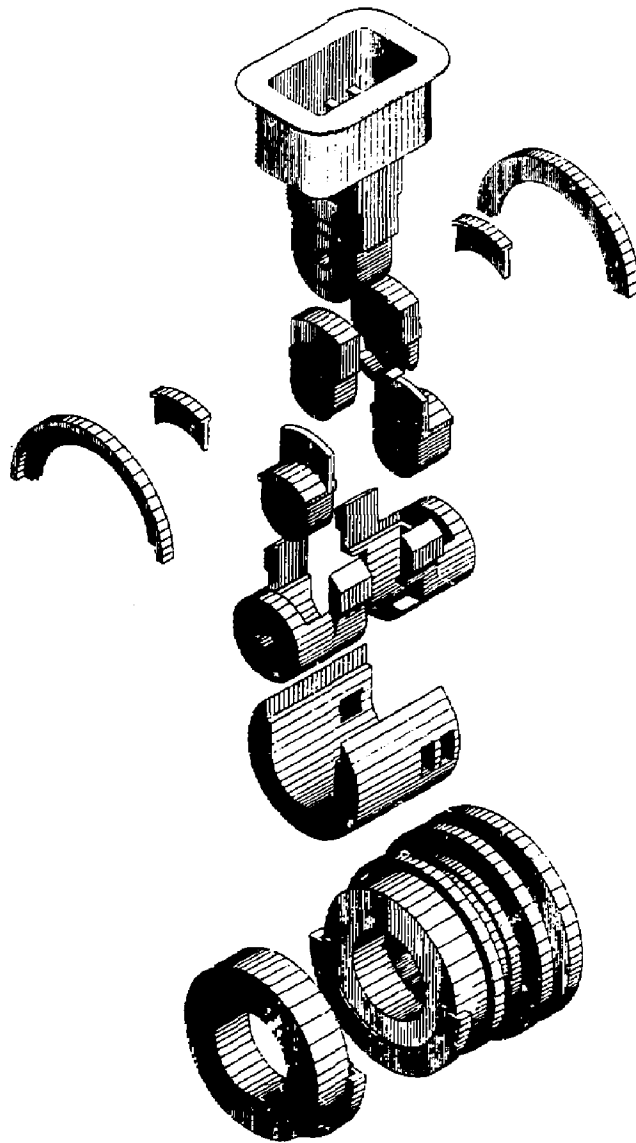
Figure 5-53. Disassembly of the DT axicell based on the MFTF-α+T design.

Transporter

SECTION 'A-A'

SECTION 'B-B'

B

A

A

| Mockup & Assy. | Cryo Plant | Power Supplies | Plant Services |
| | | | |

Decon.

| | | Heat Exch. Cell | Tritium Cell | Hot Cell |

Diesl. Gen.

Radwaste Cell

B

PLAN

0   20   40m
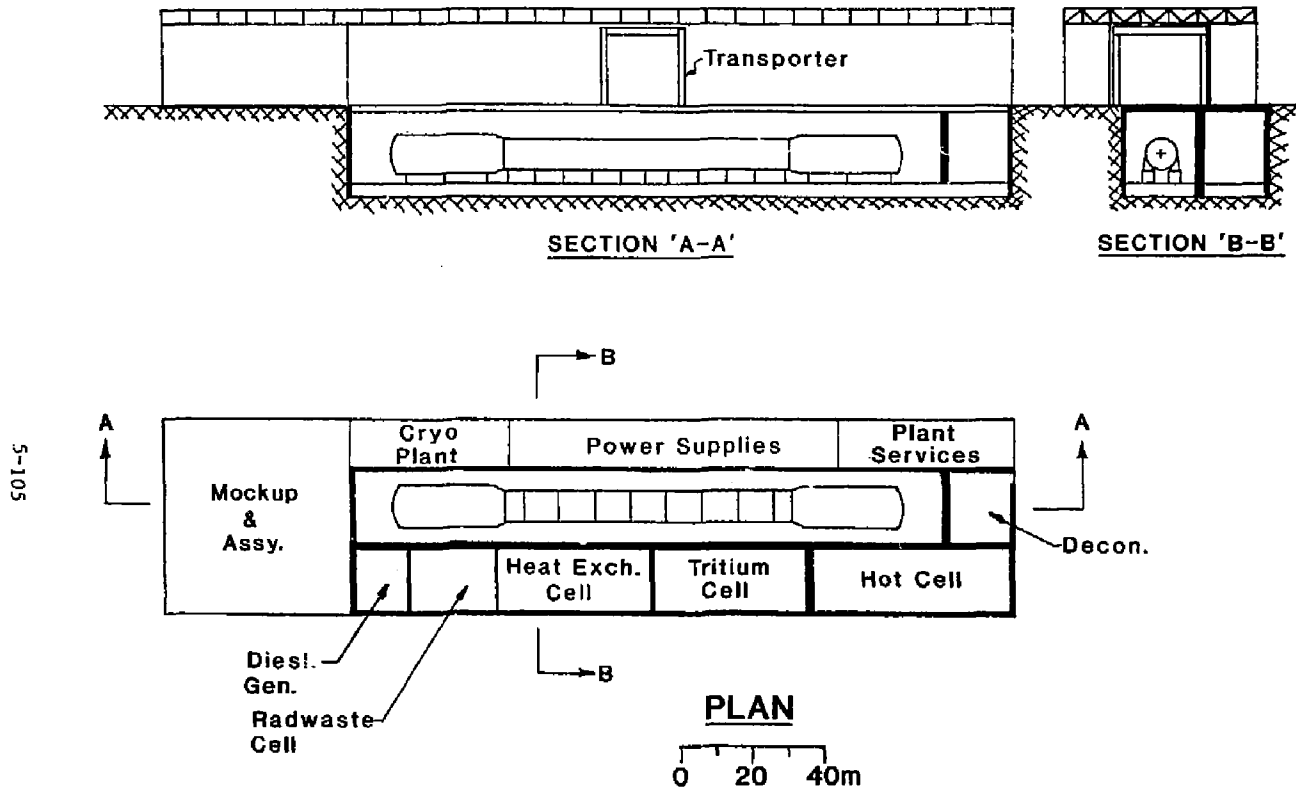
Figure 5-54. The FPD-II plant arrangement. Option 1: vertical module replacement.
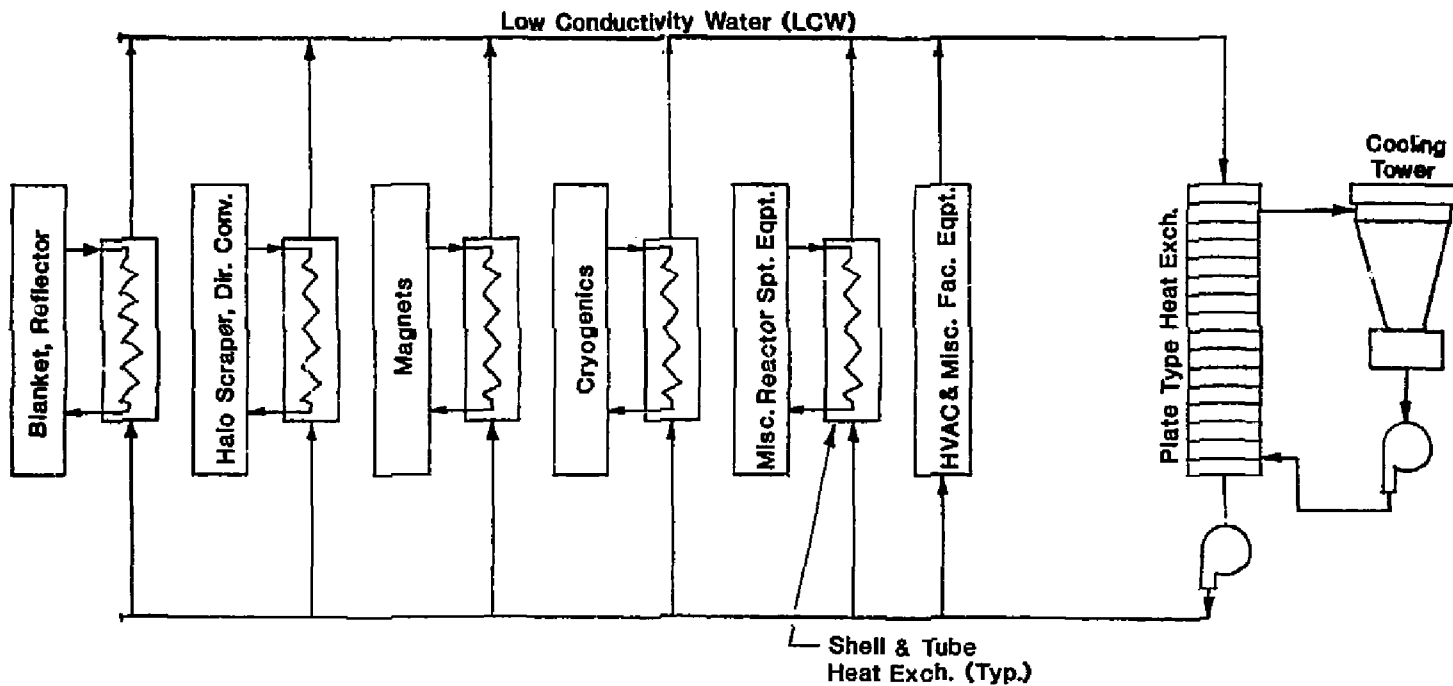
Figure 5-55. The FPD-II heat transport system.

Table 5-24. FPD-II capital cost summary
(1984 millions of dollars).

Direct cost	1,372.3
Indirect cost	480.3
Subtotal	1,852.6
Contingency	555.8
Total capital cost	2,408.4

• The device will be constructed on an undeveloped national laboratory
site.

• The device will be constructed by a prime contractor who is
responsible to the national laboratory for engineering, procurement,
and construction.

The costs of each FPD-II component/subsystem were estimated by the
engineers and organizations responsible for the design and specification of
that particular component/subsystem. We developed a cost-data-collection
methodology to ensure that all components and subsystems were included in the
cost estimate and to ensure that all cost data had a common basis. The FPD-I
work breakdown structure was initially arranged to correspond to the standard
mandatory accounts for fusion cost estimates, which is being developed at FEDC
based on earlier work by Battelle.[6] The engineer or organization
responsible for each account developed the work breakdown below the mandatory
level. Responsible engineers/organizations were provided with component cost
forms that were used to transmit cost data to the FEDC Cost Engineering
group. Components and subsystems were costed by using supplier quotes, by
analogy with a similar component or subsystem, or by cost estimating
relationships that attempt to predict the cost based on the required
performance and quantity to be purchased as correlated to historical cost data.

The FPD-II cost estimate differs from the FPD-I estimate because of the following factors:

- Better design definition exists for some components and subsystems;
- Design changes from FPD-I have occurred;
- Deletions and/or additions were made to the estimate.

A detailed breakdown of the FPD-II capital cost elements is presented in Table 5-25. Capital costs are composed of direct costs, indirect costs, and contingency costs. The direct costs shown in Table 5-25 include component engineering costs, equipment costs, and installation costs associated with the permanent facilities, systems, and equipment. These costs are defined as follows:

- Component Engineering Costs--Cost associated with design and verification testing of first-of-a-kind components.
- Equipment Cost--Cost associated with purchase/fabrication of equipment, which includes tooling, fabrication, Q/A, management, fabrication engineering, acceptance testing, and packaging and shipping.
- Costs--Cost of manual labor involved directly in erection of permanent plant facilities, systems, and equipment.

Indirect costs, shown in Table 5-25, are those costs that cannot be directly identified with specific permanent plant facilities, systems, and equipment; these costs include the following:

- Construction Services and Equipment Cost--Temporary facilities, construction equipment/supplies, taxes, and fees.
- Home Office Engineering and Services Cost--Plant and reactor systems engineering, procurement, cost and scheduling, Q/A, and construction management.
- Field Office Engineering and Services Cost--Field office operation, job supervision, Q/A, testing, and startup.
- Owner's Cost--Project management, engineering, Q/A, taxes, training, and inventories and spares.

Table 5-25. The FPD-II capital costs (1984 millions of dollars).

Account No.	Account title	Costs (1984 M$)		
20	Land and land rights	0		
21	Structures and site facilities	127.0		
211	Site improvements/facilities		5.0	
212	Reactor building		30.0	
213	Turbine building		0	
214	Reactor maintenance buildings		28.0	
215	Tritium building		12.5	
216	Electrical equipment buildings		8.0	
217	Other buildings and structures		43.5	
22	Reactor plant equipment	1183.9		
221	Reactor systems		268.0	
221.1	First wall			0
221.2	Blanket system			96.4
221.3	Shielding			89.5
221.4	Reactor structure			77.1
221.5	Energy and particle removal/ control			5.0
222	Magnet systems		339.3	
222.1	Central cell solenoids			76.6
222.2	Choke coils			30.4
222.3	Transition coils			58.2
222.4	Anchor coils			47.6
222.5	Plug coils			56.0
222.6	Recircularizer coils			5.8
222.7	Recircularizer solenoids			0
222.8	Axicell coils			64.2
222.9	Thermal shielding			0.5
223	Power injection systems		109.9	
223.1	ECRH system			46.7
223.2	ICRH system			4.1
223.3	LHRH system			0
223.4	Neutral beam injection system			59.1

Table 5-25. (Continued.)

Account No.	Account title	Costs (1984 M$)	
224	Vacuum systems	0.5	
224.1	Plasma chamber		0.5
224.2	External vacuum vessel		0
224.3	Secondary systems		0
225	Power conditioning systems	72.7	
225.1	Magnet system power conditioning		39.3
225.2	Power injection system power conditioning		27.3
225.3	Energy and particle removal/ control power conditioning		6.1
225.4	Energy storage system		0
226	Heat transport system	105.6	
226.1	Blanket heat transport system		38.8
226.2	Shield heat transport system		0.1
226.3	Cryogenic coding system		35.6
226.4	Water cooling system		30.7
226.5	Gas cooling system		0.5
227	Fuel handling	152.4	
227.1	Fuel injection systems		7.7
227.2	Fuel processing and purification		19.2
227.3	Storage and receiving		5.2
227.4	Atmospheric recovery systems		26.3
227.5	Water recovery systems		7.7
227.6	Blanket recovery systems		86.3
228	Instrumentation/control (I&C)	71.4	
228.1	Process I&C		21.4
228.2	Safety instrumentation		3.4
228.3	Diagnostics		27.2
228.4	Data processing		20.4

Table 5-25. (Continued.)

Account No.	Account title	Costs (1984 M$)	
229	Maintenance equipment	64.0	
229.1	Manipulator systems		10.8
229.2	Transport systems		19.1
229.3	Inspection/viewing/testing systems		10.2
229.4	Remote cutting/welding/machine tools		3.9
229.5	Mockup equipment		11.8
229.6	Miscellaneous tools		3.6
229.7	Decontamination Equipment		1.1
229.8	Radwaste treatment/disposal		3.5
23	Turbine plant equipment	0	
231	Turbine generators	0	
232	Main steam system	0	
233	Condensing system	0	
234	Feed water heating	0	
235	Other turbine plant equipment	0	
236	Turbine plant I&C	0	
24	Electric plant equipment	37.6	
241	Switchgear	9.1	
242	Station service equipment	8.3	
243	Switchboards	4.3	
244	Protective equipment	4.5	
245	Electrical structure and wiring Containers	0	
246	Power and control wiring	11.4	
25	Miscellaneous Plant Equipment	11.0	
251	Transportation and lifting equipment	5.0	
252	Air and water service systems	3.0	
253	Communications equipment	2.0	
254	Furnishings and fixtures	1.0	
255	Bulk materials	0	
26	Heat rejection systems	12.8	
	Total direct cost	1372.3	

Table 5-25. (Continued.)

Account No.	Account title	Costs (1984 M$)
91	Construction services and equipment	137.2
92	Home office engineering and services	205.8
93	Field office engineering and services	68.6
94	Owner's cost	68.6
	Total indirect cost	480.3
	Subtotal	1852.6
	Contingency	555.8
	Total capital cost	2408.4

These indirect costs were included in the estimate as a percent of direct cost. Allowances used were 10% for construction services, 20% for home office engineering, and 5% each for field office engineering and owner's cost.

Contingency is an allowance for the uncertainty that exists within the conceptual design in quantity, pricing, or productivity and is under the control of the engineer/constructor and within the defined scope of the project. Contingency has been included in the estimate at 30% of the direct cost.

REFERENCES

1. W. D. Nelson et al., MFTF-α+T Progress Report, Oak Ridge National Laboratory, Oak Ridge, TN, ORNL/FEDC-83/9 (to be published).

2. A Tandem Mirror Technology Demonstration Facility, Lawrence Livermore National Laboratory, Livermore, CA, UCID-19328 (1983).

3. B. G. Logan et al., Mirror Advanced Reactor Study (MARS), Final Report, Lawrence Livermore National Laboratory, Livermore, CA, UCRL-53480 (1984).

4. W. S. Cooper and R. V. Pyle, The National Negative-Ion-Based Neutral Beam Development Plan, Lawrence Berkeley Laboratory, Berkeley, CA, PUB-464 (1983).

5. P. Poulsen and E. B. Hooper, Jr., "Large Area Negative Ion Source for High Voltage Neutral Beams," in Proc. of 8th Symp. on Engineering Problems of Fusion Research, 1979, IEEE Pub. No. 79CH1441-5-NPS, p. 696.

6. S. C. Schulte, W. E. Bickford, C. E. Willingham, S. K. Ghose, and M. G. Walker, Fusion Reactor Design Studies--Standard Unit Costs and Cost Scaling Rules, Pacific Northwest Laroratory, Richland, WA, PNL-2987 (1979).

Section 6
STUDYING THE CRITICAL TECHNOLOGY ISSUES

6.0 STUDYING THE CRITICAL TECHNOLOGY ISSUES

All advanced fusion reactor concepts include projections of current technology. In order that hardware performance not limit the progress of physics research, present-day experiments are based on state-of-the-art technology. Consequently, technological advances are directed by the dollars one can afford to invest in that hardware needed to reach certain physics milestones rather than by interest in developing the entire field of technology.

We recognized from the outset that to operate an FPD experiment in the late 1990s, we needed to foster technological change in several key areas. Although the MARS study by LLNL and the fusion power community evaluated the technological growth necessary for full-scale electricity production, we had to adjust the schedule of technology development on FPD because it is a less ambitious project than MARS.

CRITICAL ISSUES MEETINGS

In 1983, we compiled a list of all critical issues we could anticipate for FPD (Table 6-1) and organized a series of meetings based on the 20 issues found. (These roughly coincided with our monthly FPD design progress meetings.) Invitations were extended to members of the U.S. fusion community working on related technology. The format and proposed objectives of each workshop are shown in Table 6-2.

Only one planned workshop was not scheduled for FY84: remote maintenance. We needed a firm mechanical configuration to bear the scrutiny of a remote-handling review, and that design was not final. However, close attention to assembly and maintenance had guided each design iteration to date. (Once our Phase III design is reasonably firm, we plan to hold a final meeting on this critical issue.)

After each critical issue meeting we distributed the minutes of the meeting with appropriate comments and summary. The average attendance was about 30--75% from the FPD project group and 25% consultants from other DOE laboratories and university research teams.

Table 6-1. Critical issues for FPD.

System		Issue
Magnets	1.	Shielding of end plug coils to minimize size and cost
	2.	*-II requirements with cost impact
Neutral beam injection	3.	Photodetachment neutralizer
	4.	Superconducting magnetic shield
	5.	Transverse-field-focus beam transport
	6.	Beam dump
Drift pump coils	7.	Power supplies
	S.	Neutron shield = semiconductor = high magnetic permeability
Gyrotrons for ECRH	9.	1-MW tubes by 1995
	10.	Mirror quality and aiming
Direct converter	11.	Halo pumping and ion disposal
	12.	Plate cooling
	13.	Neutron activation
ICRH	14.	Antenna or waveguide with horn
Fuel pellet injection	15.	Rail-gun velocity increase
	16.	Location relative to choke coil
Liquid-metal blanket	17.	Corrosion and MHD pressure drop
Siting	18.	Tritium inventory
	19.	Component activation
Repair	20.	Design for remote maintenance

Table 6-2.   Critical issue workshop format.

_____

Agenda

1.   Present and compare design ideas.

2.   Criticize and/or support.

3.   Agree on design approach for FPD.

4.   Devise test methods and schedule for FPD.

5.   Assign design responsibility for FPD.

Objectives

1.   Agree on basic design approach.

2.   Specify design goals.

3.   Define FY84 depth of study.

4.   Who will pursue this study?

5.   What issues will (s)he address?

6.   When will the work be complete?

_____

CONCLUSIONS

The critical issue meetings were all productive. Attendees concurred that the currents and voltages required for FPD seemed technically feasible. They recommended an increase in funding for beam technology to ensure attainment of timely milestones. Participants found no "black boxes" representing unknown research problems.

It was the consensus that the weakest area of current knowledge is pellet fueling. Present physics calculations indicate the need for pellet velocities of tens of kilometers per second. However, rail guns can deliver barely 3 km/s, and these have yet to be operated in a rapid-fire, reliable fashion. Finally, attendees noted that we must improve our ability to predict plasma-pellet heat-transfer needs as well as fashion experiments to increase pellet velocity or add sabots to protect the pellets.

In the Appendix we include the memorandums that discuss in detail our findings concerning these critical issues.

Section 7
SITING AND SAFETY

7.0 SITING AND SAFETY

INTRODUCTION

In addition to the specifics of FPD siting and safety, we also consider two sets of general siting and safety criteria in this section. The first set consists of general site-selection criteria that seem to be universally applicable to large, fusion power machines, including the FPD machine. The second set comprises general reactor design criteria, which, if followed, will appreciably mitigate potential problems with siting and safety.

GENERAL SITE-SELECTION CRITERIA

1. <u>Relationship of the facility to population centers and density.</u> No conflict should exist between the operation of the fusion facility during its lifetime and the master plan for development in the vicinity.

2. <u>Electrical power sources.</u> Adequate electrical power should be available without requiring new substations and power lines.

3. <u>Heat disposal.</u> Heat disposal should be readily provided by using cooling towers, rivers, lakes, or oceans, and should create little or no adverse environmental effects.

4. <u>Hot cell facility.</u> An area of the site should be dedicated to a hot cell facility for processing radioactive materials and parts.

5. <u>On-site disposal of radioactive waste.</u> If possible, radioactive waste should be disposed of on site; therefore, the site must meet the NRC Class A requirements for near surface burial as outlined in the Code of Federal Regulations, 10CFR61. These waste materials include the following:

    a. Operational wastes--machine parts that need regular replacement, expended material, protective clothing, rags, sludge, solvents, etc.

    b. Decommissioning wastes--all of the above, plus activated machine components.

6. Off-site disposal of radioactive waste. If radioactive materials cannot be disposed of on site, off-site disposal areas must be identified and be readily accessible. Material to be disposed of will be the same as in 5 above. The following transport concerns must be addressed:
   a. Transportation routes must be identified.
   b. Alternate routes must be found when local ordinances restrict the transport of radioactive materials.

7. Seismic safety. The seismic safety criteria used in the design must be consistent with the local seismic requirements.

8. Tornado hazards. Tornado hazards must be considered in the design of the buildings and the facilities.

9. Flood hazards. Flood hazards must be taken into account in facility design.

10. Air traffic. Proximity to airports and flight paths may require additional precautions against possible effects of airplane crashes.

11. Fence-line radioactive dose rates. The projected radioactive dose rates at the fence line must conform to existing and proposed Department of Energy (DOE) and Environmental Protection Agency (EPA) regulations. If property buffer zones are needed, it must be possible to acquire them.

12. Radioactive material inventories. Inventories of radioactive materials on site may be limited by special hydrology, unusual leach rates, and unusual nuclide migration rates.

GENERAL REACTOR DESIGN CRITERIA

1. Hands-on maintenance. We cannot anticipate all possible failure modes and necessary maintenance procedures; therefore, where possible, hands-on maintenance capability should be emphasized in the design. ·Hands-on maintenance will be possible only in selected places outside of the outer-machine shield.

2. Materials for hands-on maintenance. In regions where hands-on maintenance is highly desirable, materials that will "cool" quickly if activated should be used, making general access easier and simplifying remote handling when necessary.

3. Remote maintenance. Most of FPD requires remote maintenance and remote handling capability, therefore, remote maintenance should be major consideration from the start in the design studies.

4. Materials for near-surface burial. Materials must be used that, when activated, can be handled and disposed of by near-surface burial.

5. Reactor design for decommissioning. Design the reactor for easy decommissioning (e.g., make the components modular so that highly activated parts can be easily separated from the rest of the machine).

6. Water contamination. No routine release of radioactivity should be allowed to surface or near surface water.

7. Volatile materials. In regions of high activation, use of materials that easily become volatile in accident situations should be avoided.

SUMMARY OF REGULATIONS

In addition to the above general criteria, we operate in an environment of regulations reflecting society's choices regarding the handling of hazards and hazardous materials. The following brief summary reflects the kinds of regulations that pertain to the siting and safety of FPD.

RADIOACTIVITY

The Lawrence Livermore National Laboratory (LLNL) is regulated in its handling of radioactive material by the DOE and the EPA. The current DOE regulations are contained largely in "Requirements for Radiation Protection", DOE Order 5480.1, Chapter XI. There are no current EPA regulations governing radioactive dose rates; however, the EPA has proposed regulations for the off-site dose rates ("Clean Air Act, Radiological Emissions Standards", Federal Register, April 6, 1983). These regulations apply to routine operations, not accident situations. The LLNL exposure limits for on-site personnel and routine operations, as listed in the LLNL Health and Safety Manual Section 33, are based on the DOE Order 5480.1, Chapter XI. The exposure limits are the same as those stated in the NRC 10CFR20 and are the recommendations of the National Council on Radiation Protection (NCRP) and the International Protection (ICRP). The exposure limits are as follows:

1. Whole body, head and trunk, bone marrow, gonads, and lens of the eye shall not exceed 3 rem/quarter or 5 rem/year.

2. Skin of whole body exposure to beta of E greater than 700 keV, or x or gamma of E greater than 10 keV, shall not exceed 5 rem/quarter or 15 rem/year.

3. Hands, feet, or ankles shall not exceed 25 rem/quarter or 75 rem/year.

These dose limits are the maximum permitted during routine operations; however, the exposure policy of DOE and LLNL is to keep radiation exposures as low as reasonably achievable (ALARA). ALARA is subject to many definitions, but a draft on ALARA submitted to DOE by Kathren and Selby of Pacific Northwest Laboratory in April, 1980 states:[1]

"Both costs and dose reductions are difficult to evaluate and there may be significant variability in the perception and acceptance of risk by individuals and society. In general, dose reductions that cost less than $2000 per person-rem of dose spared are probably always cost-beneficial, while costs in excess of $60,000 per person-rem of dose spared are probably not cost-beneficial. In the absence of sound cost figures, an ALARA program cannot rely upon cost-benefit analysis. In such cases, the criterion must be whether or not dose reduction is reasonably achievable, given the limits of economics and practicality."

In the past, DOE has set the ALARA limit at 1/5 of the limits presented above (i.e., the design limit for DOE is whole body 0.6 rem/quarter or 1 rem/year). The policy at LLNL is to design to half the DOE limit--300 mrem/quarter or 500 mrem/year. It is also LLNL policy that the casual passerby (walking by the building) shall not be exposed to more than 0.25 mrem/hour. Off-site limits are controlled by the EPA. In the "Clean Air Act, Radiological Emissions Standards", the EPA proposes radiation dose guidelines of 10 mrem/year whole body, and 30 mrem/year to any organ for any member of the public residing at the site boundary. This dose limit for the general public includes radiation doses from all airborne radioactivity. For fusion experiments, the limit includes any dose received from released tritium, from neutron activation products from the air in the experimental area, plus any

other radiation dose sources that may be connected with the experiment. The dose limit does not necessarily include the "sky shine" or radiation that escapes the shielding around the experimental facility. In our judgement all the above sources will be included in future proposals and should be allowed for in the design process. At the time of the publication of EPA's proposed regulations, the effective date was set for September 1, 1983; although the regulations were not made effective on that date, it is clear that something like these standards will be adopted in the future. The proposed EPA dose limits are consistent with those imposed on the fission industry. The current NRC site boundary limits for an operating reactor are 5 mrem/year for whole body and 15 mrem/year for organs.

Accident scenarios are handled differently from routine operations. The NRC regulation, as published in 10CFR100, sets the off-site dose from a maximum credible accident in a power reactor at 25 rem. The DOE draft, "Non-reactor Nuclear Facilities: Standards and Criteria Guide," dated February 1981 speaks of a type 3 accident. This is an occurrence that may occur infrequently during the lifetime ($10^{-3} < P < 10^{-1}$/year). In this draft, the off-site dose limit for the type 3 accident is 5 rem. However, at LLNL, past practice suggests that this limit is too high. For an occurrence that might happen as often as 10^{-1}/year, the limit should be about 500 mrem. Again, to put this into context, a release of 120 g of tritium from the 30 m stack of the LLNL tritium facility is calculated to give rise to about 3 to 4 rem to a person residing at the fence line during passage of the cloud. A ground level to 10 m high release of 35 g of tritium is calculated to give about the same dose.

SEISMIC REQUIREMENTS

The following seismic criteria represent those criteria that will probably be developed for use in the FPD design.

OPERABILITY

1. Accomplish a thorough structural analysis and design or testing program to ensure that the integrity and operability of the Seismic Category I structures, systems, and components are maintained for

7-5

the Design Basis Earthquake (DBE) condition. Seismic Category I
structures, systems, and components shall be designed to remain
functional* during and after the DBE.

2. Ensure the integrity and/or operability of those Seismic Category I
   structures, systems, and components that are essential to assure
   shutdown capability, to maintain a safe shutdown condition, and to
   prevent or mitigate the consequences of accidents, which could
   result in potential off-site exposures.

3. List and categorize structures, systems, and components in the
   following four safety classifications: high-hazard, moderate-
   hazard, low-hazard, no-hazard status. Guidelines for classification
   shall be provided by LLNL. Each safety classification has its own
   DBE Excitation Criteria.

4. Evaluate nonseismic Category I structures, systems, and components
   on a case-by-case basis. Nonseismic Category I items shall be
   designed using LLNL's no-hazard Standard Facility Criteria. Failure
   of Non-Category I items and Category I items must not cause failure
   of any Category I items in successively higher levels of the DBE
   requirements (i.e., an item in a lower safety classification must
   not cause failure of an item in a higher safety classification).

5. Include, but do not limit, hazardous and nonhazardous structures,
   systems and components to building structure, piping, electrical
   conduit, mechanical systems, electrical systems, associated support
   systems, etc.

SEISMIC EXCITATION

1. Define the DBE input ground motion for each structure, system or
   component configuration by specifying the maximum horizontal ground
   acceleration (PGA) and the horizontal ground response spectra. The
   maximum vertical ground acceleration is two-thirds of the maximum

---

*Following the guidelines in 10CFR100, functional can be defined as perfor-
mance sufficient to limit the maximum off-site dose to 25 rem. Practice at
LLNL, however, has been to strive for lower exposure, even in the event of a
DBE. A number that seems consistent with past practice at LLNL is to limit
the maximum off-site dose to 500 mrem. We suggest that FPD be designed to
this performance level.

horizontal ground acceleration. The response values of the vertical ground-response spectra are equal to two-thirds of the response values for the horizontal ground-response spectra. The LLNL DBE ground-response spectra with a peak ground acceleration is normalized to 1.0 g.

2. Assume that the DBE horizontal ground motion occurs in any orientation within the horizontal ground-motion plane for the given structure. In addition, consider that the horizontal ground motion acts simultaneously with the vertical ground motion (two-directional excitations).

3. Include the following two steps in the high-hazard seismic-excitation and design requirements. LLNL requires that all high-hazard structures, systems, and components (Seismic Category I items) go through a two-step design process. The first step consists of evaluation and design in the elastic range of response, using a dynamic-response spectrum analysis with the LLNL ground-response spectra and a corresponding peak ground acceleration (PGA) of 0.5 g (DBE) applied simultaneously with a vertical PGA of $\pm$0.33 g. Engineering evaluations and design are accomplished by using Uniform Building Code (UBC) analysis methods in addition to UBC strength allowables. Connection evaluation and design accounts for an additional load factor of 1.5; the connection design/evaluation uses forces that are 1.5 times greater than those resulting from 0.5 g (DBE). The second step of the design process takes the components into the inelastic range and checks the integrity of the Seismic Category I items against forces resulting from an earthquake with horizontal PGA of 0.8 g applied simultaneously with a vertical PGA of $\pm$ 0.53 g. For this design check, the item must remain functional during and after the earthquake.

4. Include the following two steps in the moderate-hazard seismic-excitation and design requirements. LLNL requires that all moderate-hazard structures, systems, and components (Seismic Category I items) go through a two-step design process. The first step consists of evaluation and design in the elastic range of response, using a dynamic response spectrum analysis with the LLNL ground-response spectra and a corresponding peak ground acceleration (PGA) of 0.25 g

(DBE) applied simultaneously with a vertical PGA of +0.17 g.
Engineering evaluations and design are accomplished by using UBC
analysis methods along with UBC strength allowables. Connection
evaluation and design accounts for an additional load factor of 1.5;
the connection design/evaluation uses forces that are 1.5 times
greater than those resulting from the 0.25 g (DBE). The second step
of the design process takes the components into the inelastic range
and checks the integrity of the Seismic Category I items against
forces resulting from an earthquake with horizontal PGA of 0.5 g
applied simultaneously with a vertical PGA of +0.33 g. For this
design check, the item must remain functional during and after the
earthquake.

5. Include the following in the low-hazard and no-hazard (conventional
buildings) seismic-excitation and design requirements.

   a. One- and two-story buildings and structures: current UBC
   requirements are upgraded for a building seismic-lateral-load
   coefficient of 0.25 W (static). If UBC seismic requirements are
   more stringent, UBC seismic requirements shall control.
   Connection evaluation and design, resulting from seismic forces,
   shall account for an additional load factor of 1.5 (i.e.,
   connection design/evaluation loads = 1.5 x 0.25 W Loads).
   Analysis procedures, design procedures, and material strength
   allowables shall meet the requirements of the latest edition of
   the UBC. Lateral forces on structural and nonstructural
   components shall be designed to meet the basic performance
   requirements of the UBC.

   b. Buildings and structures greater than two stories: these
   buildings and structures shall meet the seismic design
   requirements for one- and two-story buildings and structures,
   and shall be evaluated and designed using the LLNL ground-
   response spectra with a corresponding horizontal PGA of 0.5 g
   applied simultaneously with a vertical PGA of +0.33 g.
   Engineering evaluations and design shall be accomplished by the
   use of inelastic analysis methods combined with inelastic stress
   allowables. Little regard shall be given to the condition of
   the building following the DBE. Primary concern is to ensure

7-8

prevention of building collapse, thereby allowing the building occupants to egress safely following an earthquake of major intensity on site. Lateral forces on structural and nonstructural components shall be designed to meet the basic performance requirements of the building structure.

c. All buildings and structures with significant cross-axis coupling and/or torsional response: the design of buildings and structures placed within this category shall meet the requirements of 5b above.

SPECIFIC FPD SITING AND SAFETY CONSIDERATIONS

In addition to the above general requirements, there are specific safety and siting considerations that are appropriate for FPD.

TRITIUM USE

After surveying the special hazards of using tritium in the FPD facility, we are confident that proper design will allow adequate containment. DOE has placed requirements on the construction of plutonium buildings (DOE 6430, Part 2), but there is no comparable document setting forth requirements for tritium buildings. However, engineers designing new tritium facilities may need to consider a "design basis accident" in their plans. The DOE Division of Environmental Safety and Health (ES&H) is preparing a document describing tritium building criteria. As far as legal requirements are concerned, the site boundary is the fence line. The NRC requirements for fission reactors state that, under normal operations, a person presumed to be residing on the fence line continuously should not receive more than 500 mrem/year. DOE requires that normal operations should be designed to limit this dose to 170 mrem/year. To give guidance in the case of accidents, the NRC has defined an "Extraordinary Nuclear Occurrence," which covers external exposure, ingestion, inhalation, plus the food and water dose routes. This type of accident occurs when a person residing in an unrestricted off-site area receives a whole-body dose that exceeds 20 rem. This whole-body dose can be received at the time of the nuclear occurrence or over a longer period of

7-9

time. In an "Extraordinary Nuclear Occurrence", the NRC establishes the conditions for the "waivers of defense" proposed for incorporation in indemnity agreements, insurance policies, and in contracts furnished as proof of financial protection. The NRC definition of an "Extraordinary Nuclear Occurrence" carries no express or implied inference that such a dose may or may not be hazardous to the person receiving it. To put this in context, the present LLNL tritium facility has a design capability whereby release of a mega-Curie of tritiated water [HTO (104 grams of tritium)] in a worst-case situation will give rise to 3 rem at the fence line.

The Tritium Systems Test Assembly (TSTA) project at Los Alamos National Laboratory is wrestling with the question of accountability requirements, (set by DOE at ± 0.01 gram). For the 800-gram tritium inventory expected in FPD, DOE accountability requirements expect an accuracy of 12.5 ppm. This accuracy is considered unachievable because of a number of losses, (e.g., permeation into the structure and into the water coolant). Personnel at TSTA have not found adequate equipment or methods to deal with this question.

Presently, the FPD facility is projected to have about 800 grams of tritium in the entire facility, with about 40 grams vulnerable in FPD itself. However, we are investigating alternative schemes for reducing the total amount of tritium. One scheme is prompt recycling of the tritium exhausted out through the halo. This tritium, plus the included deuterium, could be purged of heavy ions and hydrogen and then recycled back to the pellet injector along with make-up tritium from the blanket breeder. Such a conceptual system could significantly reduce the size of the tritium handling facility and, at the same time, it could reduce the total amount of tritium circulating.

MATERIAL ACTIVATION

Calculations of neutron-induced activation are proceeding, but the results obtained to date indicate that the FPD facility can be designed and constructed to operate within existing guidelines and can be decommissioned after its useful life. Calculations are continuing in the area of activation relevant to hands-on maintenance. Early results indicate that components, which are exposed to neutron fluxes equivalent to "first wall," will have to be handled

remotely from the beginning of the experimental program. Other areas may have low enough fluxes that some contact maintenance will be possible, at least early in the experimental program. Calculations of radionuclide inventory are underway. The important time regimes for central cell activities are as follows:

- Immediately after shutdown, when afterheat levels will be greatest;
- Twenty-four hours after shutdown, when some of the activities will contribute significantly to the radiation inside the vault;
- Months after shutdown, when major replacements might be undertaken;
- Years after shutdown, during decommissioning;
- Decades after shutdown, for waste storage considerations.

The moderate wall loading for FPD (0.85 MW/m^2) in the long solenoid section, plus the high wall loading (4 to 5 MW/m^2) in the 3-m-long central test section, are reduced by the rather low-load factor (30%). Hence, for activation products with half-lives of several months or more, this scenario is equivalent to steady-state operation at 0.25-MW/m^2 wall loading for the long solenoid section and 1.5 MW/m^2 for the central test section. Afterheat in the first wall steel immediately after shutdown will be about half that of Starfire,[2] or about 0.4 W/cm^3, but will decay much more rapidly than in Starfire. The copper insert coil will activate, presenting problems both in handling and in waste disposal. The activity will be dominated by the 5.3-year Co(60), produced by the (n,a) reaction in Cu(63), and will determine the shielding and handling techniques needed to replace this coil. The $Li_{17}Pb_{83}$ (LiPb) used as a coolant in the blanket and first wall will activate in the neutron flux. Depending on actual residence time in the high-neutron-flux regions and on the operating level and also on the availability of the FPD facility, the contact-surface dose rate for cooling loops containing the LiPb could be several to many rem/hour. In addition, the LiPb will entrain corrosion products as it circulates. Some of these corrosion products may be already activated before entrainment while others will activate as the LiPb circulates through the high-neutron-flux regions of FPD. This indicates that remote maintenance should be planned for the LiPb loops from the beginning. Accident scenarios involving LiPb should be investigated in the future.

Liquid nitrogen is used in the superinsulation for several magnets (e.g., the transition and yin-yang coils). We calculated the C(14) production in liquid nitrogen at the yin-yang coils (assuming a 14-MeV neutron source strength of 1×10^{13} $n/cm^2 \cdot s$ at this location and no additional shielding on the coils); the result was a C(14) production rate of 0.1 microCi/liter/year. To determine whether or not this production rate is a problem, we will need to study the neutron activation of nitrogen at all points in the cooling loop and also make some assumptions about the nitrogen leak rate to the environment. The N(13) (10-min halflife) resulting from activation of the liquid nitrogen may be a hazard in the event of a massive leak under accident conditions.

DECOMMISSIONING

Long-term activation is thought to be a decommissioning rather than a waste storage problem. The total operating time of the solenoid cells (about 1.25-MW year/m^2) and of the test section (5- to 7-MW year/m^2) is not likely to produce large inventories of very long-lived nuclides; furthermore, we are not addressing a whole series of machines, but one isolated test bed. Decommissioning handling problems, if they occur 5 to 10 years after shutdown, are likely to be heavily influenced by the presence of Co(60) activity, just as in light-water reactors. This Co(60) originates from Cu(63), Co(59), and Ni(60). Because Co(60) is a hard-gamma emitter, its presence will probably dictate the shielding needed during decommissioning. Careful choice of structural materials can result in all radioactive waste being classified as Class C (suitable for near surface burial). If this is the case, a site selection that allows on-site disposal of the waste can be extremely important because packaging and transportation problems will be minimized. Decommissioning will involve all of the techniques developed for dealing with fission reactors. In particular, it will require a custodial period for the FPD facility to allow the induced radioactivity to decay to levels that will permit disassembly and disposal. This period has been estimated to be between 5 and 10 years. During this time, maintenance must be performed on the facility to protect it against deterioration and accidents. Once actual decommissioning begins, the larger radioactive components must be disassembled to allow packaging for disposal. This may involve the use of a plasma torch, pools, and all the other techniques developed for fission systems. If the levels are low enough,

near-surface burial may be possible; if not, the waste must be packaged as high-level waste. In either case, decommissioning of FPD, like any other DT fusion device, will provide a major challenge.

CONCLUSION

Siting and safety criteria for FPD are generally logical and straight-forward. Careful attention to these criteria early in the design process can result in a simpler machine that satisfies the constraints listed here and results in a better overall system that is easier to operate, maintain and decommission.

REFERENCES

1. R. L. Kathren, J. M. Selby, E. J. Vallario, <u>A Guide to Reducing Radiation Exposure to as Low as Reasonably Achievable (ALARA)</u>, U.S. Department of Energy, Washington, DC (1980).

2. <u>Starfire -- A Commercial Tokamak Fusion Power Plant Study</u>, Argonne National Laboratory, Argonne, IL, ANL/FPP-80-1 (1980).

Section 8
TANDEM MIRROR REACTOR SYSTEMS CODE (TMRSC)

8.0 TANDEM MIRROR REACTOR SYSTEMS CODE (TMRSC)

INTRODUCTION

We are developing a computer code for a tandem mirror reactor that will allow us to provide self-consistent configuration, performance, and cost analyses as a function of plasma, magnetic, and engineering parameters. With the first version of the TMRSC, we will model a configuration similar to MARS[1] and FPD,[2] which incorporates the central cell and end cell that are shown schematically in Fig. 8-1. The end cell consists of a choke coil, a C-coil transition region, an anchor C-coil set, a plug C-coil set, and a recircularizing C coil. The thermal barrier in this configuration is located in the plug.

The modules comprising the TMRSC are being provided by various sources within the fusion community; the physics, magnetics, magnet, and facility modules are the responsibility of Lawrence Livermore National Laboratory (LLNL). Neutronics, shielding, and tritium modules are being modeled by Argonne National Laboratory (ANL). Blanket thermal hydraulics, heat transport/power conversion, cryogenics, direct converter, and plasma heating systems are being provided by TRW. Magnet electrical, ac power, vacuum vessel, fueling, maintenance equipment, and instrumentation and control (I&C) modules are being modeled by Oak Ridge National Laboratory--Fusion Engineering Design Center (FEDC). The integration of the modules into the TMRSC is the responsibility of the FEDC.

FLOW DIAGRAM

The flow diagram for the TMRSC Code is shown in Fig. 8-2. The code consists of separate modules, each describing a reactor component or system connected by a driver. Three feedback loops are indicated by dashed lines. These loops are necessary due to the strong coupling between the plasma physics, the magnetics, neutronics, and magnet design parameters.

In TMRSC, we use a calculational procedure that starts at the plasma center line of the central cell and proceeds radially (Fig. 8-3). The central cell length and plasma radius are determined primarily from the desired fusion power, on-axis magnetic-field beta, and plasma temperature. The central cell
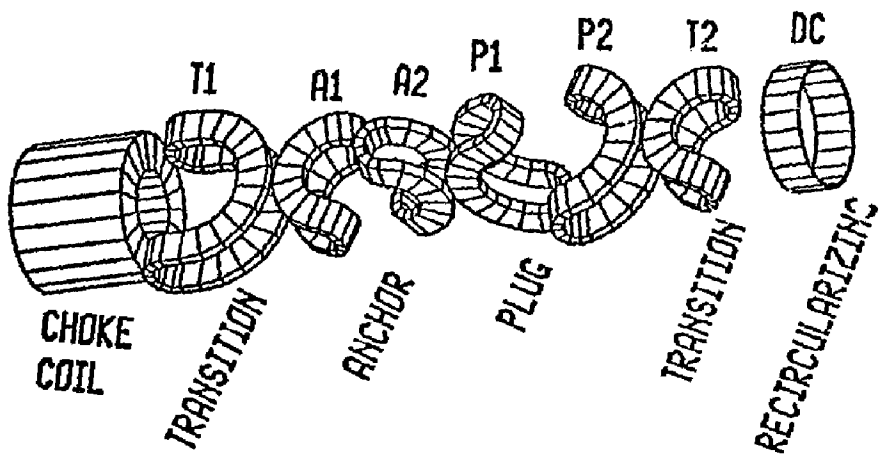
Figure 8-1. End cell configuration.

```
┌─────────┐    ┌──────────────┐    ╱POWER ╲  YES  ┌───────────────┐    ┌──────────────┐    ┌──────────────┐
│  INPUT  │───►│   PHYSICS    │───►◄ REACTOR? ►───►│ BLANKET & SHIELD│──►│ CENTER CELL &│──►│ CHOKE SHIELD │
└─────────┘    │  (TMR BAR)   │    ╲       ╱       └───────────────┘    │ CHOKE MAGNETICS│  └──────────────┘
               └──────────────┘       │ NO                             └──────────────┘
                                      ▼
                            ┌──────────────┐
                            │  FIRST WALL  │
                            │   & SHIELD   │
                            └──────────────┘
```

Revise betas & end cell lengths

Revise case thickness

```
┌──────────┐    ┌──────────┐  YES  ╱PHYSICS╲    ┌──────────────┐  YES  ╱ CASE ╲    ┌──────────────┐
│AUXILIARY │◄───│ END CELL │◄──────◄ VALID? ►◄──│   END CELL    │◄─────◄ SPACE ►◄──│ CENTER CELL & │
│ PHYSICS  │    │ MAGNETS  │       ╲       ╱    │MAGNETICS/MHD │       ╲ OK?  ╱    │ CHOKE MAGNETS │
└──────────┘    └──────────┘        │NO         └──────────────┘        │NO        └──────────────┘
```

Revise "C" coil minor radius

```
┌──────────────┐    ╱ SHIELD╲  YES  ┌──────────────┐    ┌──────────────┐    ┌──────────────┐    ┌──────────┐
│END CELL SHIELD│──►◄ SPACE  ►─────►│   DIRECT     │───►│ PLASMA HEATING│──►│ VACUUM VESSEL │──►│ FUELING  │
└──────────────┘    ╲ OK?   ╱       │  CONVERTER   │    └──────────────┘    └──────────────┘    └──────────┘
                     NO             └──────────────┘
```

```
┌──────────────┐    ┌──────────────┐  YES  ╱ POWER ╲    ┌──────────────┐    ┌──────────────┐    ┌──────────────┐
│HEAT TRANSPORT│    │HEAT TRANSPORT│◄──────◄REACTOR?►◄──│   THERMAL    │◄──│  CRYO SYSTEM  │◄──│   MAGNET     │
└──────────────┘    │  & POWER     │       ╲       ╱    │ HYDRAULICS   │    └──────────────┘    │  ELECTRICAL  │
                    │ CONVERSION   │        │NO         └──────────────┘                        └──────────────┘
                    └──────────────┘
```

```
┌──────────────┐    ┌──────────────┐    ┌──────────────┐    ┌──────────┐    ┌──────────┐
│  FACILITIES  │───►│   TRITIUM    │───►│ MAINTENANCE  │───►│ AC POWER │───►│  I & C   │
└──────────────┘    │  PROCESSING  │    │  EQUIPMENT   │    └──────────┘    └──────────┘
                    └──────────────┘    └──────────────┘

                                        ┌──────────┐    ┌──────────────┐
                                        │  OUTPUT  │◄───│ COST SUMMARY │
                                        └──────────┘    └──────────────┘
```

Figure 8-2. Tandem mirror reactor systems code flow diagram.
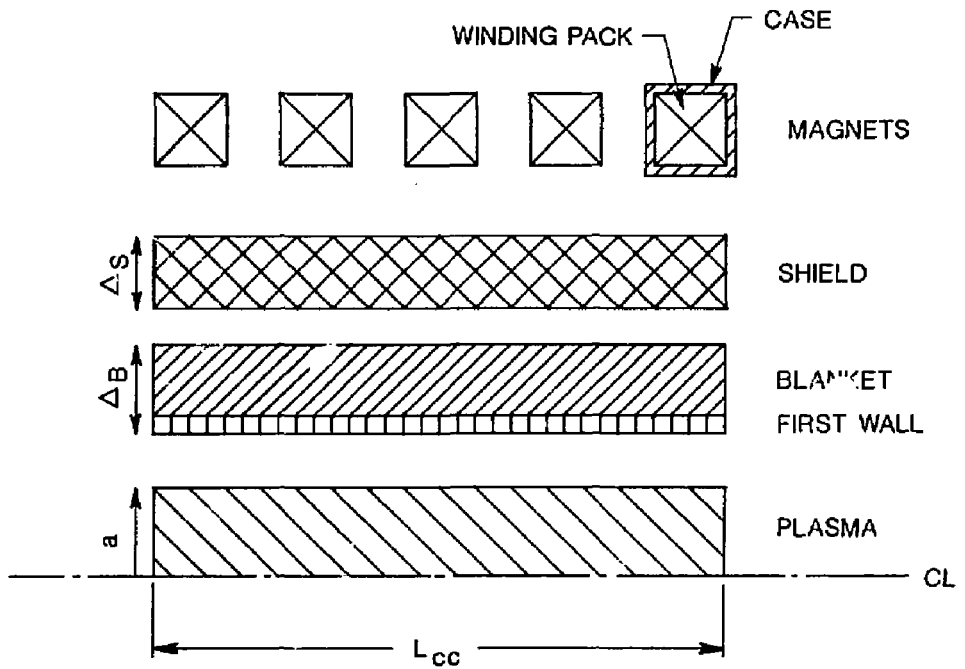
Figure 8-3. Central cell configuration.

blanket thickness is determined consistent with the desired energy multiplication and tritium breeding ratio. The shield thickness is set consistent with nuclear response limits in the superconducting solenoidal coils. The central-cell solenoidal-coil radius is then determined from the summation of the plasma radius, blanket and shield thickness, and assembly gaps. The coil current and the conductor area for the solenoidal coils are determined as a function of the coil radius, desired on-axis magnetic field, and allowable coil-current density.

The code proceeds to step axially to the choke coil and end cell regions. The plasma radius at the choke coil is a function of the desired magnetic field on the choke-coil axis and the need to pass the central cell magnetic flux. (An option exists to specify the choke-coil plasma radius and calculate the central-cell plasma radius.) The choke coil (superconducting portion plus copper insert portion) is sized, after determining the plasma radius at the choke coil, based on the required currents and the allowable current densities. The TMRSC code also accounts for the space required for shielding of the choke coil.

The C-coil radii in the end cells are consistent with the plasma boundary, the desired on-axis magnetic field, shielding requirements, desired sweep angle, and allowable current densities. Axial positions of the coils are chosen to be consistent with recircularizing the flux in the anchor and plug wells and reducing to zero the average geodesic curvature. As previously noted, a feedback loop assures compatibility between coil geometry, neutronics, magnetics, and plasma stability.

Modules downstream of the iteration loops are executed in a once-through manner according to the sequence shown in Fig. 8-2.

MODULE DESCRIPTIONS

PHYSICS

The physics module of TMRSC solves multiple nonlinear linked equations to compute the steady-state plasma power and particle balance, and the plasma supplemental heating requirements for tandem mirror reactors. The code maintains quasi-neutrality at several cardinal points in the end cell region, and determines volumes, densities, potentials, and fusion-power values.

Options to find minimum length, maximum power, or maximum Q are also available. Finally, the central cell may be specified as ignited or driven.

NEUTRONICS

Five blanket options and three shield designs are available in the neutronics module of TMRSC. Tritium breeding ratios, energy deposition, and nuclear response in the coils are determined consistent with the neutron wall loading, and material composition and thickness. End cell shielding is based on the neutron source strength. Costs of the blanket and shield are also estimated with this module.

BLANKET THERMAL HYDRAULICS

The blanket thermal hydraulics module in TMRSC is used to determine coolant inlet and outlet temperature, pressure drops, pumping power, lifetime estimates, and structural temperatures for liquid-metal and gas-cooled components.

MAGNETICS

Magnetics for the central cell, solenoidal coils, the choke coil, and the end-cell C coils are determined by the TMRSC magnetics module. Required currents are computed based on the magnetic-field profile, the coil radii, and the axial location of the coil. The central cell coils may be discrete coils or a current sheet. Conductor current density and coil-dimension or coil-aspect ratio are input items. The end-cell C coils are sized and positioned to provide (1) the desired magnetic field profile; (2) flux tube circularity in the magnetic wells; and (3) zero average geodesic curvature. This module runs the EFFI magnetic field code and the TEBASCO (tandem equilibrium and stability) code. Allowable value of beta in the central cell, anchor, and plug are determined consistent with magnetohydrodynamic (MHD) equilibrium and stability. These values of beta are coupled to the plasma physics through an external feedback loop.

MAGNET

Central-cell and end-cell magnets are modeled by the magnet module of
TMRSC. Magnet designs must be consistent with limitations of current density,
maximum field, cryostability, and fluence for various conductor types.
Coil-case thickness is based on allowable stress. Cost for each magnet is
also estimated by this module.

NEUTRON SOURCE (AUXILIARY PHYSICS)

The neutron source module of TMRSC calculates the neutron source strength
in the end cells (needed to determine shielding requirements); and frequency
requirements for the plasma rf heating and drift pumping systems [electron-
cyclotron resonant heating (ECRH), lower-hybrid resonant heating (LHRH),
ion-cyclotron resonant heating (ICRH)]. This module also determines the
magnetic flux, heat flux, magnetic-field profile, and net electrical power
associated with the direct converter.

DIRECT CONVERTER

The direct converter is based on a gridless design, and consists of four
concentric collectors at each end. Radial drift pumping forces most of the
ions in the plasma onto the halo, which is kept at ground potential by the two
outer collectors. Electrons flow axially through the middle of the magnet set
and are deposited on the two inner collectors, which are biased on the order
of -100 kV. Direct electrical power is produced by the electrons; heat
deposited by the ions and alphas can be recovered by a thermal cycle.

The direct converter module of TMRSC calculates the collector area
required for each of the four regions based on a maximum energy flux allowed
(input parameter). The electrical power produced, effective radii of the
collectors, length of the direct converter, and the size of the enclosing
vacuum tank are also calculated by this module. The thermal power is
determined by the heat-transport module. Costs are computed based on
collector area for each region, direct electrical power for inverting
equipment, and vacuum pumping requirements.

PLASMA HEATING

The plasma-heating module of TMRSC sizes rf heating or neutral heating systems to supply the required supplemental heating to the plasma in the central cell or end cell regions. The rf systems compute required circulating power, efficiency, cost, and component sizes consistent with available space for access and required power at the launcher. The negative-ion neutral-beam module computes the circulating power, efficiency, cost, and the number of sources and associated currents to deliver the required power to the plasma. Heating-system-component characteristics, such as power supplies, amplifier, waveguide, launchers, and neutralizers are also determined by this module. Positive-ion heating systems are not currently included in this module but may be added later.

The rf systems for drift pumping application are also included in this module. The purpose of the drift-pump system is to remove ions by the process of induced radial drifts, which have become trapped in the end cells as they pass to the potential peaks. There are two coils in each end to pump different groups of ions, and each is located where the radial extent of the plasma in the double-ellipse fan transition is maximized (one between the transition coil and the anchor coil, the other between the anchor coil and the plug coil). This model is based on the MARS system and produces a perturbation field normal to the ambient B field. The physics requirements of ion pumping speed, frequency, and geometry are used to calculate the required rf frequency, the required current in the coils, and the number and width of individual driver frequencies. The coil inductance and voltage are computed from the specified coil geometry, and the dissipated power is determined based on the Q of the circuit. Ohmic losses and total power consumption are also calculated by this module.

VACUUM VESSEL

A vacuum vessel exterior to the solenoidal coils, end-cell C coils, and direct converter is sized and costed by the vacuum-vessel module of TMRSC.

AC POWER

The ac-power-system-code module of TMRSC calculates characteristic design
and cost data for the electrical power systems needed to operate the reactor.
This module identifies and computes the cost for major equipment such as
circuit breakers, switches, transformers, lightning arresters, diesel
generators, load control centers, and power feeders. This module does not
include the turbine generator nor the dc direct converter in the end cells,
but it does include the switch gear and dc to ac inverters that interface with
the main substation. An electrical power summary is also generated by this
module.

MAGNET ELECTRICAL

The magnet electrical module of TMRSC computes design and cost data for
the power supplies and coil protection equipment of the central cell and end
cell magnets. Specifically, design and cost data for power supplies, bussing,
load centers, dump resistors, dc current breakers, and associated local
controls and instrumentation are determined by this module.

INSTRUMENTATION AND CONTROL (I&C)

The I&C module of TMRSC determines the costs of process I&C, plasma
diagnostic instrumentation, data transmission, data processing, and consoles
located in the control building. The cost of each I&C process and diagnostic
includes both hardware and software.

In this module, I&C are defined as the supervisory control and data
system located in the main control building, plus the associated data links to
local I&C. This module does not include the local process control and instru-
mentation located in the proximity of the reactor vault.

MAINTENANCE EQUIPMENT

The maintenance equipment module of TMRSC consists of a compiled list of
reactor cell and hot cell equipment with unit costs. The user chooses the
appropriate equipment for a particular device configuration from the

comprehensive listing. The equipment either scales with reactor parameters or is fixed in size and cost.

FACILITY

The facility module of TMRSC estimates the size and cost of buildings based on reactor size, thermal power from the blanket and other components, gross electrical power output, and number and capacity of each turbine generator. Facilities considered include reactor building, hot-cell building, tritium building, steam-generator building, power-supply building, cryogenics building, and central building. Also, the costs of radwaste systems equipment, miscellaneous reactor and balance of plant equipment, and special materials are estimated in this module.

CODE STATUS

Approximately 80% of the modules have been received from the various authors within the fusion community who are contributing to this effort. The integration effort is approximately 20% complete. The target date for the first version of the integrated systems code is October 1, 1984.

REFERENCES

1. B. G. Logan, <u>Mirror Advanced Reactor Study (MARS) Final Report</u>, Lawrence Livermore National Laboratory, Livermore, CA, UCRL-53480 (1984).

2. C. D. Henning et al., <u>Fusion Power Demonstration: Baseline Report</u>, Lawrence Livermore National Laboratory, Livermore, CA, UCID-19975 (1984).

Appendix

Appendix

A MIRROR MACHINE WITH OCTUPOLE END PLUGS

TO: Distribution
FROM: John Perkins
SUBJECT: A Mirror Ignition Machine With Octupole Er'd Plugs

1. Summary

      For the past year or so, the Fusion Power Demonstration (FPD) project
at LLNL has been developing the definition of a mirror ETR with end cells
based on the MARS configuration. A major goal of the project has been to
def.ne the minimum length for ignition of an optimized (i.e. lowest cost)
system. However, due to the long transition lengths of the MARS-mode end-
cell configuration coupled with updated Fokker-Planck calculations of end-
cell trapping rates, a mirror ETR based on the MARS magnet configuration
cannot achieve ignition with a central cell length less than about 90 m.
      Accordingly, during the past month, effort has been devoted to FPD
with an octupole end plug. Initial results from these activities look very
encouraging and optimization studies indicate that the octupole version of
FPD will achieve ignition with a central cell length of ∿ 30 m. With
each end plug magnet length of only ∿ 8 m and a total machine length of
∿ 63 m, this suggests that a mirror ignition device operating with
octupole end-plugs is potentially capable of being sited in building 431.
The principle parameters of both the MARS-mode and octupole-mode of FPD
are compared in Table 1. Note that the total machine length for the
ocutpole-mode is only ∿ 63 m compared with ∿ 147 m for the MARS-mode.

Table 1. A comparison of the FPD ignition machine with MARS and octupole end plugs. Both are minimum length machines. (A more detailed parameter list for the octupole-mode is given in Table 2).

	MARS-node	Octupole-mode
Center cell length[a] L_c (m)	90	30
End cell magnet length (m)	19.4	8
Total machine length[b] (m)	∿ 147	∿ 63
Central cell plasma radius r_c (m)	0.46	0.45
Fusion Power (MW)	479	156
Q	36.7	7.0
Q_{eng}[d]	∿ 2.2	<1
Neutron wall loading (MW/m^2)	1.0	1.0
Total ECRH power[c]	11.4	21.7

[a]Effective lengths--physical lengths (choke to choke) are 96 and 35 m, respectively.

[b]6 m has been added at each end to allow for direct converters, halo dumps, and vacuum end tanks.

[c]Includes both core plasma and mantle for octupole-mode.

[d]Engineering Q; i.e., gross electrical power divided by recirculating electrical power.

The two big advantages of the octupole version of FPD are of course cheaper end cell magnets and shorter ignition lengths. The one big disadvantage is access. Within this compact end plug system, we require the integration of seven major subsystems, namely (1) core-plasma barrier ECRH, (2) core-plasma potential peak ECRH, (3) mantle ECRH (4) sloshing ion beams, (5) drift pump coils, (6) inner recirculating octupole coils, and (7) neutron shielding. In this regard, future studies may indicate that the minimum length for ignition may not be the principle design requirement. Rather access conditions in the octupole may dictate the central cell ignition length by defining a minimum volume end-cell magnet configuration.

2. Parameter Scaling Studies

Initial parametric scaling studies have been performed on the octupole version of FPD. Here we are interested in the optimum central cell plasma radius r_c and plug beta β_p which result in the shortest length ignition machine, while minimizing the total plug ECRH power (i.e. ECRH power for both the core plasma and the mantle). Minimizing the ECRH power is an important consideration in the octupole plug where space is at a premium.

The TMR power balance code "TMRBAR" was employed for these scaling studies. The code has been updated to model the hot electron mantle. ECRH power requirements are computed for both the plug core plasma and the outer mantle region.

Requirements on beta profiles across the core and mantle regions are determined by satisfying line-averaged interchange stability requirements, thus requiring details of field curvatures through the central cell and end cells.

The following sections present an overview of the major features of the octupole scaling studies.

3. Effect of Central Cell Plasma Radius on Ignition Length

Figure 1 shows the minimum central cell length for ignition L_c as a function of the central cell plasma radius r_c for the octupole version of FPD; the beta of the plug core plasma $<\beta_p>$ is shown as a parameter. A central cell field of 2.5 T was used in all these parametric trades because analysis of the previous MARS-mode FPD configuration showed that L_c minimizes for a central cell field of ~ 2.5 T and we expect this optimum field to be essentially independent of end cell type.

From Fig. 1 we see that, at any given $<\beta_p>$, there is an optimum value of r_c around 0.55 m for which the central cell ignition length is minimized. This can be ascribed to the fact that at larger values of r_c, end cell trapping rates drive the system to longer values of L_c, while at smaller r_c a longer L_c also results due to reduced alpha particle energy deposition in the center cell. Now as r_c increases at constant B_c, the central cell flux ($\pi r_c^2 B_c (1-<\beta_c>)^{1/2}$) increases accordingly.

Fig. 1. VARIATION OF MINIMUM LENGTH FOR IGNITION WITH CENTRAL CELL PLASMA RADIUS

$\langle \beta_P \rangle = 0.55$

$\langle \beta_P \rangle = 0.45$

$\langle \beta_P \rangle = 0.35$

$\langle \beta_P \rangle = 0.25$

$\langle \beta_P \rangle = 0.15$

CENTRAL CELL IGNITION LENGTH L_c (m)

CENTRAL CELL RADIUS (m)

A-5
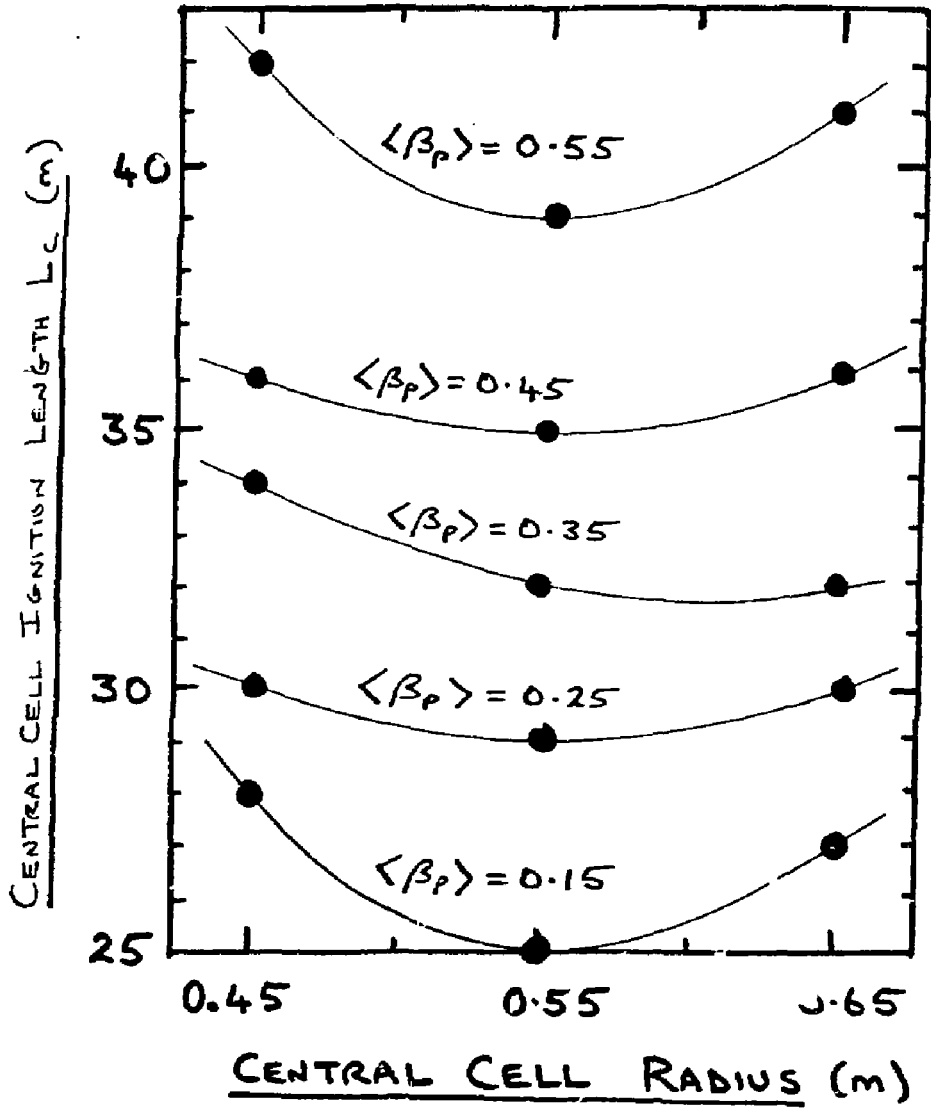
Mapping this flux through the end-cell magnets with conductor fields maintained near maximum desirable values, necessitates larger end-cell coil radii. Figure 2 illustrates the dependence of the FPD octupole magnet dimensions on the central cell plasma radius. Maintenance of a given end-cell mirror ratio with larger coil radii requires larger mirror lengths (analogous to solenoidal ripple where a constant $\Delta B/B$ is obtained for a constant ratio of solenoid radius to solenoid spacing). However, larger end cell mirror lengths result in longer end cell trapping lengths (i.e. the length between the central cell mirror peak and the end cell potential peak). This, in turn, results in correspondingly larger end cell trapping rates. Since central cell ignition requires that alpha heating essentially supports the radial losses incurred by trapping in and pumping out of the end cell region, central cell lengths determined only by end-cell trapping would minimize for very small central cell radii.
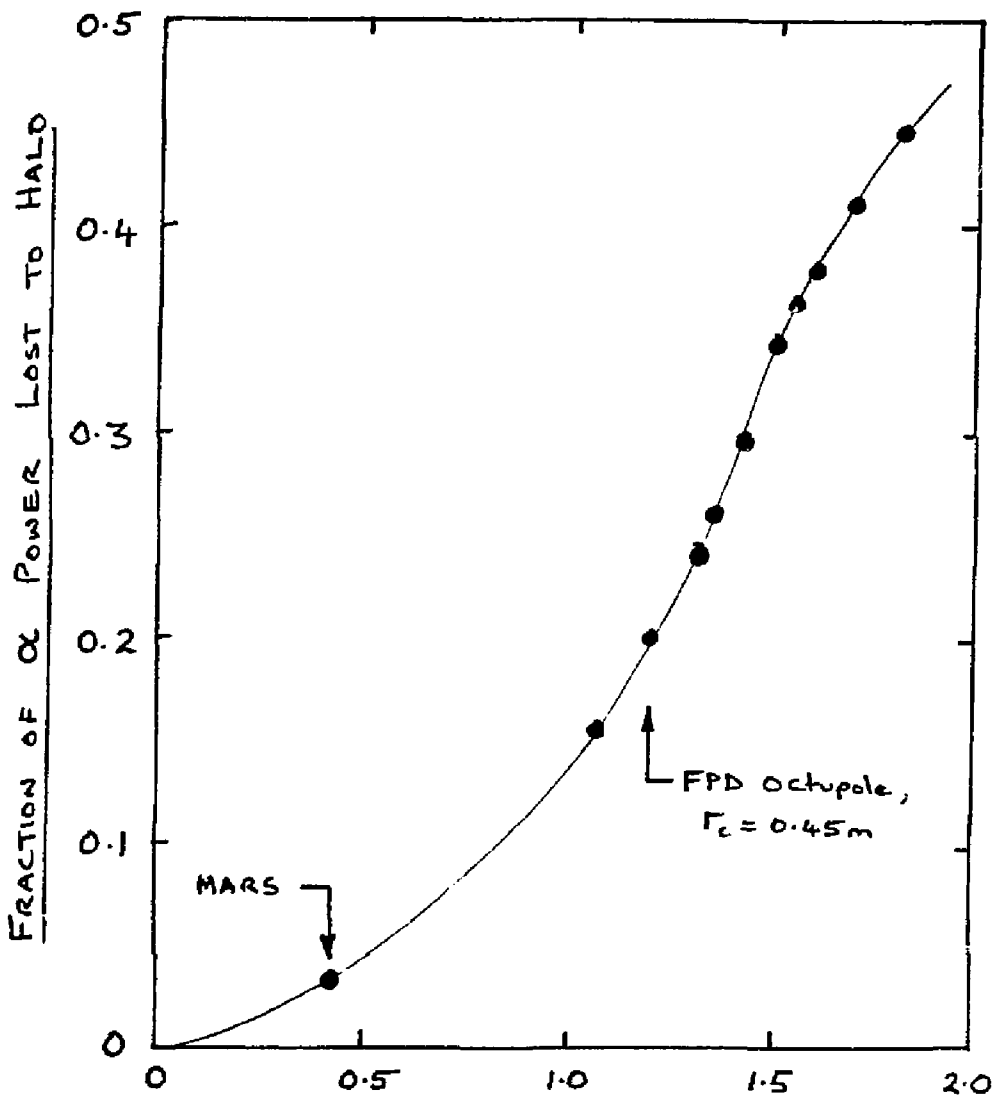
Unfortunately, our relatively low B_c of 2.5 T and high $<\beta_c>$ of 60% imply large alpha particle orbits. Hence, a decreasing central cell radius results in a greater fraction of the fusion alpha energy escaping the plasma and being deposited in the halo. Figure 3 illustrates this effect where the fraction of the central cell alpha power deposited in the halo outside the plasma is plotted as a function of a parameter p which incorporates the dependence of r_c, B_c and $<\beta_c>$ as shown. As will be shown in Sec. 4 later, the optimum version of FPD-octupole has $r_c = 0.45$ m. It is interesting to note that at this plasma radius, our ETR attains its "optimized" ignition length by discarding $\sim 20\%$ of its central cell alpha heating power to the halo!

4. ECRH Power in the Mantle

Now from Fig. 1, with $<\beta_p> = 0.15$ and $r_c = 0.55$ m, a minimum length for ignition of 25 m is theoretically achievable. However, it is also necessary to assess the total ECRH requirements ($P_{ECRH,core} + P_{ECRH,mantle}$) in the end cell. Although for a given β_p and r_c, the ECRH power requirements for the core plasma are fixed from power balance considerations, we are somewhat free to select the mantle hot electron energy to minimize the mantle ECRH power. This is so since the MHD interchange criterion only defines the beta profile through the mantle allowing hot electron energy and corresponding density to be selected externally.

Fig. 2   FPD OCTUPOLE-MODE MAGNET CONFIGURATION

Octupole coil (1·5 T midplane)

Outer mirror coil (6·75 T)

25 T Center cell Solenoid

24 T choke coil

L_1

L_2

R

C.cell plasma radius r_c (m)	L_1(m)	L_2(m)	K
0.45	7.59	4.22	1.27
0.55	9	5	1.5
0.65	10.42	5.79	1.74

$$P = \left\{ \Gamma_c \, B_c \, \sqrt{1 - \tfrac{1}{2} \hat{\beta}_c} \right\}^{-1}$$

Γ_c = c.cell plasma radius, B_c = c.cell vac. field
$\hat{\beta}_c$ = c.cell on-axis beta.

Fig. 3   EFFECT OF FINITE ALPHA GYRORADII
ON ALPHA POWER LOSS TO HALO

As an illustration, Fig. 4 plots the mantle ECRH power as a function of the mantle hot electron energy for three values of plug beta $<\beta_p>$ in the core plasma; this figure is for the mantle beta conditions determined by a center cell radius of 0.45 m. As expected, a hot electron energy E_{hot} can be selected to minimize $P_{ECRH,mantle}$; low values of E_{hot} result in high $P_{ECRH,mantle}$ due to scattering and drag losses while high values of E_{hot} also result in higher ECRH power due to synchrotron losses.

Therefore, for each central cell radius r_c and each plug beta $<\beta_p>$ in Fig. 1. we can now select a mantle hot electron energy to minimize the total end cell ECRH power. This minimized power is shown in Fig. 5 as a function the radius r_c of the central cell plasma with $<\beta_c>$ as a parameter.

5. FPD-octupole Baseline Selection

Selecting the FPD-octupole baseline via Figs. 1 and 5 illustrates the Catch-22 situation, i.e. a low plug beta $<\beta_p>$ results in a short central cell length for ignition in Fig. 1 but requires a high total ECRH power in the end cell in Fig. 5. For example, with r_c = 0.55 m and $<\beta_p>$ = 0.15, an ignition length of 25 m is obtained. However, this requires ∿ 68 MW of ECRH power with resulting low system Q (∿ 2.7) and ECRH access problems in the octupole plug.

Accordingly, our current baseline employs a central cell radius of 0.45 m with $<\beta_p>$ = 0.25. Although this results in a larger minimum ignition length of 30 m, the total ECRH power requirements are only ∿ 22 MW.

Table 2 provides an extended list of system parameters for the FPD ocutupole. Note that the neutron wall loading is 1 MW m^{-2} which is reasonably respectable for blanket and technology testing. Note also that the system Q is only 7, an indication that the system is capable of igniting with a short central cell length and, therefore, small total fusion power.

It should be noted that, unlike the MARS-mode of FPD, the octupole version with these parameters is unlikely to generate net electrical power, having an engineering Q (gross electrical power divided by recirculating electric power) of less than unity. By contrast, because of the long minimum ignition length requirement in the MARS mode of FPD, it was impossible to obtain a baseline design with Q_{eng} less than two!

Fig. 4 VARIATION OF MANTLE ECRH POWER WITH MANTLE HOT ELECTRON ENERGY.

$(r_c = 0.45\,m)$

$\langle \beta_p \rangle = 0.55$

$\langle \beta_p \rangle = 0.35$

$\langle \beta_p \rangle = 0.15$

← Minima
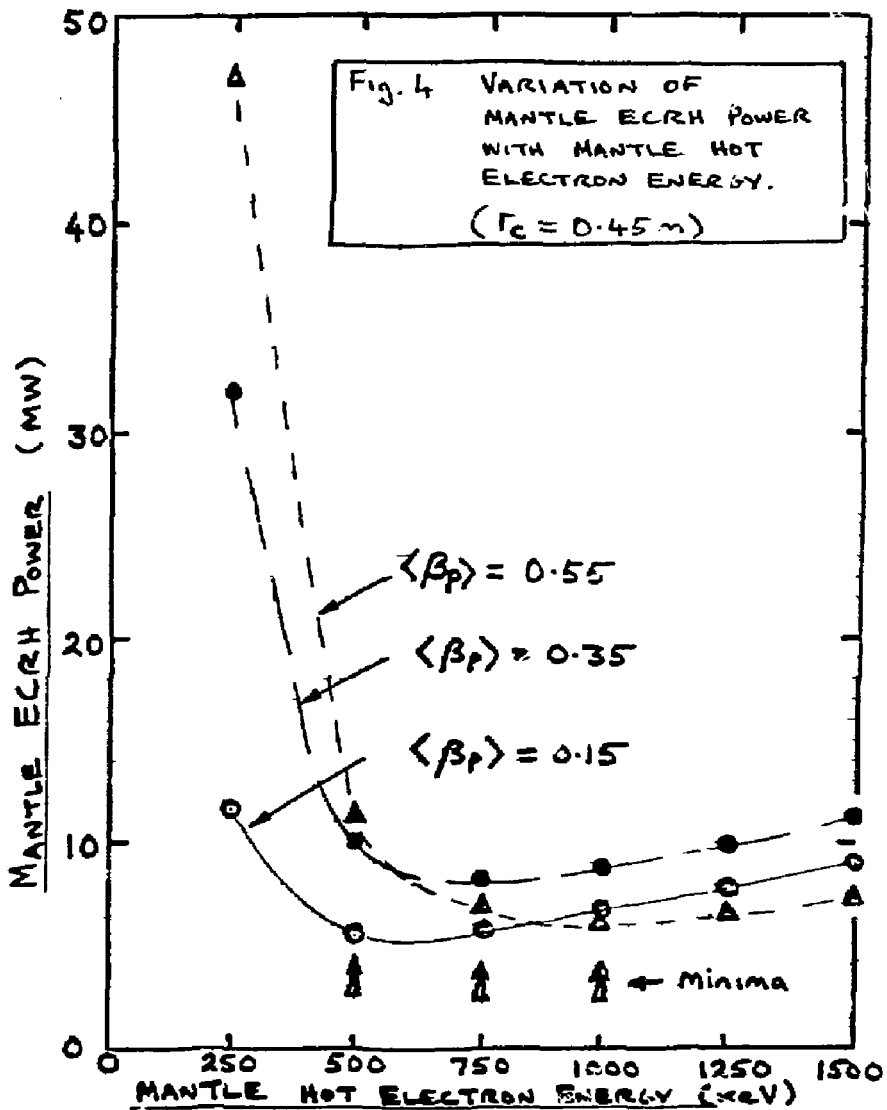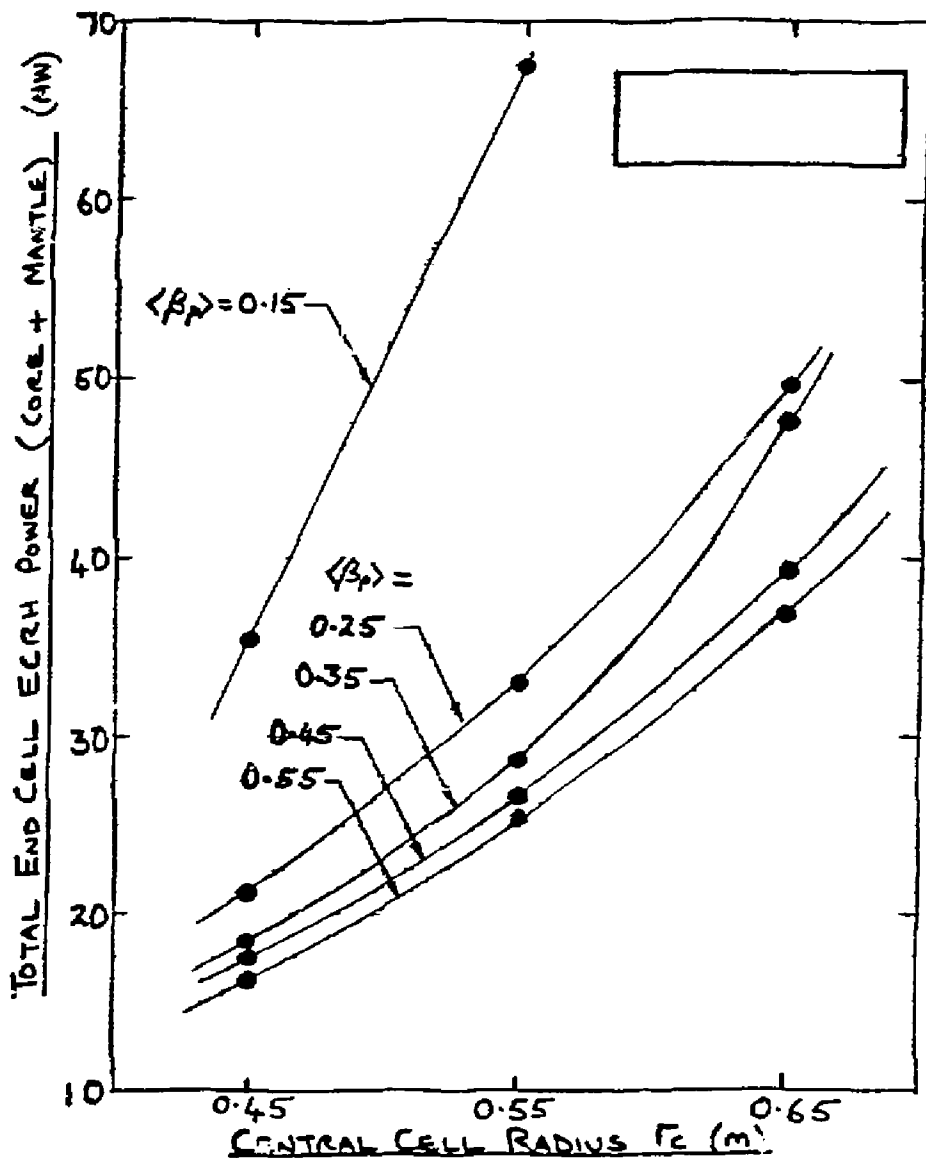
Fig. 5 VARIATION OF TOTAL
END CELL ECRH POWER
(CORE PLASMA PLUS MANTLE)
WITH CENTRAL CELL
PLASMA RADIUS.

A-II

Table 2. Preliminary parameters for FPD-octupole.

_____

General

    Fusion power (MW)   156
    Neutron wall loading (MW/m^2)   1.0
    Q (overall)   7.0
    Q (core plasma only)   10.5
    Q_{eng} <1
    Required cold fuelling current (A)   102
    Overall machine length (m)   ∿ 63

Central Cell

    Effective length (m)   30
    Physical length[a] (m)   35
    B_c (T)   2.5
    Plasma radius (m)   0.45
    First wall radius (m)   0.67
    $<\beta_c>$ 0.6

Choke coil

    B_{choke} (T)   24
    Coil inner radius (m)   0.14
    plasma radius (m)   0.116

End cell

    Total end cell magnet length[b] (m)   ∿ 8
    Core ECRH power, barrier (MW)   13.8
    Core ECRH power, potential peak (MW)   0.46
    Mantle ECRH power (MW)   7.4
    Sloshing ion beam energy (keV)   475
    Sloshing ion beam power (MW)   0.61
    Total heating power (MW)   22.3
    $<\beta_p>$ 0.25
    $<\beta_{mantle}>$ 0.45
    Mantle not electron energy (keV)   750
    End cell trapping current (A)   79.2

_____

[a]Choke to choke.

[b]Choke coil to outer mirror.

Clearly, a net power producing ETR based on the octupole could be obtained by simply increasing the central cell length in the current design above 30 m until the fusion power is large enough to give $Q_{eng} = 1$. However this is not the most desirable method of achieving this result. In fact, rather than allowing the fusion power, wall loading and Q to float (downwards) to achieve an absolute minimum length, minimum cost, ignition machine as we have done above, we would fix the fusion power at some reasonably high level where we would be confident of obtaining $Q_{eng} \sim 1$ and solve for the corresponding length. In this latter case, the optimum central cell field and plasma radius would differ from the 2.5 T and 0.5 m values above, and the resulting machine would be considerably more expensive than the present minimum length ignition baseline. Such considerations are being applied to the scaling studies for MINIMARS now in progress where we require $Q_{eng} > 4$.

Work is continuing on the FPD-octupole design in three main areas, namely (1) improved plasma engineering and magnetics modeling, (2) integration of plasma heating systems in the octupole plug and (3) evaluation of system costs.

YIN-YANG SHIELDING

MEMORANDUM
LLNL-FPD-84-15

TO: FPD Distribution
FROM: Dave Dorn
SUBJECT: Yin/Yang Shielding for the FPD

    A series of calculations have been done on shielding for the Yin/Yang
coils in the FPD. The actual configuration for a typical calculation is
detailed in Figure 1. The calculations were done on the LASL code ONEDANT
in 1-D slab geometry with the data file from Laila El-Guebaly at the
University of Wisconsin.

    This set of calculations differs from previous ones we have done in
that, within a given thickness of shield, performance was optimized as a
function of thickness of TiH_2 substituted for part of the W shield at
the back. Table 1 shows the numerical results of these calculations.
Figures 2-4 show the results of this optimization, in graphical form, for
shield thicknesss of 15 cm, 30 cm and 45 cm. Coupled with the 14.3 cm
thickness of case and insulation to the super conducting windings, these
shields give total distance to the plasma chamber of 29.3 cm, 44.3 cm and
59.3 cm for the three. The calculations were done assuming a first wall
neutron loading of $1MW/m^2$.

    Broad optima were found at the following splits between W and TiH_2:

Shield Thickness	W Thickness	TiH_2 Thickness
15 cm	11 cm	4 cm
30 cm	24 cm	6 cm
45 cm	41 cm	4 cm

Performance indicators for these three cases are tabulated in Tables 2 and 3 and are plotted in Figures 5 and 6.

While in this particular configuration, substitution of the W by TiH_2 clearly reduces the neutron fluence for energies over 0.1 Mev, it does little to mitigate the nuclear heating. In order to investigate the possibility of helping in this area, another several calculations were run in which some of the tungsten was removed and a comparable thickness of Pb was added at the back of the shield. Table 4 lists the results. While the total nuclear heating can be reduced in this way, other important parameters rise. We will need to consider the entire system performance to determine the optimum shield.

Finally, Table 5 shows the distribution of nuclear heating in the SC case, winding pack, and magnet itself for a typical shield (30 cm shield made up of 24 cm W and 5 cm TiH_2). It may be that HeI can be used for cooling in the case while HeII can be used in the winding pack and SC magnet itself. This should appreciably affect the economics of the helium refrigeration system and may shift the optimum to a higher nuclear heating level.

Table 1. Performance Indicators
For Shield of W/TiH$_2$

Shield	W/TiH$_2$	ht n	ht g	ht t	HT n	HT g	HT T	n fluence
15 cm	W	7.6e1	4.4e2	5.2e2	2.2e3	7.4e3	9.6e3	5.4e20
15 cm	13/2	5.9e1	4.2e2	4.8e2	1.8e3	7.9e3	9.7e3	3.6e20
15 cm	11/4	5.2e1	4.3e2	4.8e2	1.5e3	8.4e3	1.0e4	3.0e20
15 cm	TiH$_2$	6.2e1	5.9e2	6.5e2	1.7e3	1.1e4	1.3e4	3.5e20
30 cm	W	7.6e0	4.7e1	5.4e1	2.2e2	7.8e2	1.0e3	5.2e19
30 cm	27/3	4.9e0	4.5e1	5.0e1	1.5e2	8.7e2	1.0e3	2.8e19
30 cm	26/6	4.2e0	4.8e1	5.2e1	1.2e2	9.4e2	1.1e3	2.4e19
30 cm	21/9	4.2e0	5.2e1	5.6e1	1.1e2	1.0e3	1.1e3	2.3e19
30 cm	TiH$_2$	7.9e0	1.0e2	1.1e2	2.0e2	1.9e3	2.1e3	4.4e19
45 cm	W	6.9e-1	4.4e0	5.1e0	2.0e1	7.2e1	9.3e1	4.6e18
45 cm	41/4	3.9e-1	4.3e0	4.7e0	1.2e1	8.5e1	9.7e1	2.3e18
45 cm	36/9	3.5e-1	5.0e0	5.4e0	9.7e0	9.7e1	1.1e2	2.0e18
45 cm	31/14	4.0e-1	6.0e0	6.4e0	1.1e1	1.1e2	1.2e2	2.2e18
45 cm	TiH$_2$	1.1e0	1.8e1	1.9e1	2.7e1	3.2e2	3.5e2	5.9e18

where: ht n is peak SC heating due to neutrons (mW/cm^3)
ht g is peak SC heating due to gammas (mW/cm^3)
ht t is sum of ht n and ht g
HT n is total SC coil & case heating due to neutrons (mW/cm^2)
HT g is total SC coil & case heating due to gammas (mW/cm^2)
HT T is sum of HT n and HT g
n fluence is the neutron fluence in the first cm of SC (n/cm^2-FPY)

Table 2. - Performance Indicators
For Optimal Shields

Shield	W/TiH$_2$	ht n	ht g	ht t	HT n	HT g	HT T	n fluence
15 cm	11/4	5.2e1	4.3e2	4.8e2	1.5e3	8.4e3	1.0e4	3.0e20
30 cm	26/6	4.2e0	4.8e1	5.2e1	1.2e2	9.4e2	1.1e3	2.4e19
45 cm	41/4	3.9e-1	4.3e0	4.7e0	1.2e1	8.5e1	9.7e1	2.3e18

where: ht n is peak SC heating due to neutrons (mW/cm^3)

ht g is peak SC heating due to gammas (mW/cm^3)

ht t is sum of ht n and ht g

HT n is total SC coil & case heating due to neutrons (mW/cm^2)

HT g is total SC coil & case heating due to gammas (mW/cm^2)

HT T is sum of HT n and HT g

n fluence is the neutron fluence in the first cm of SC (n/cm^2-FPY)

Table 3. - Performance Indicators
Radiation Dose to Polyimide (rads/FPY) and DPA in Cu

Shield	W/TiH$_2$	case	pack	SC coil	DPA in Cu
15 cm	11/4	9.5e11	7.9e11	6.2e11	2.9e-1
30 cm	24/6	8.9e10	6.0e10	5.5e10	2.4e-2
45 cm	41/4	8.0e9	5.4e9	4.9e9	2.1e-3

where: case is the dose in the poly between case and winding pack

pack is the dose in the poly between winding pack and SC

SC coil is the dose in the poly in the SC coil

DPA is the displacements per atom per FPY in Cu in SC coil

Table 4. - Performance Indicators (Pb)
For 30 cm $W/TiH_2/Pb$ Shield, (24-Pb)/6 (mW)
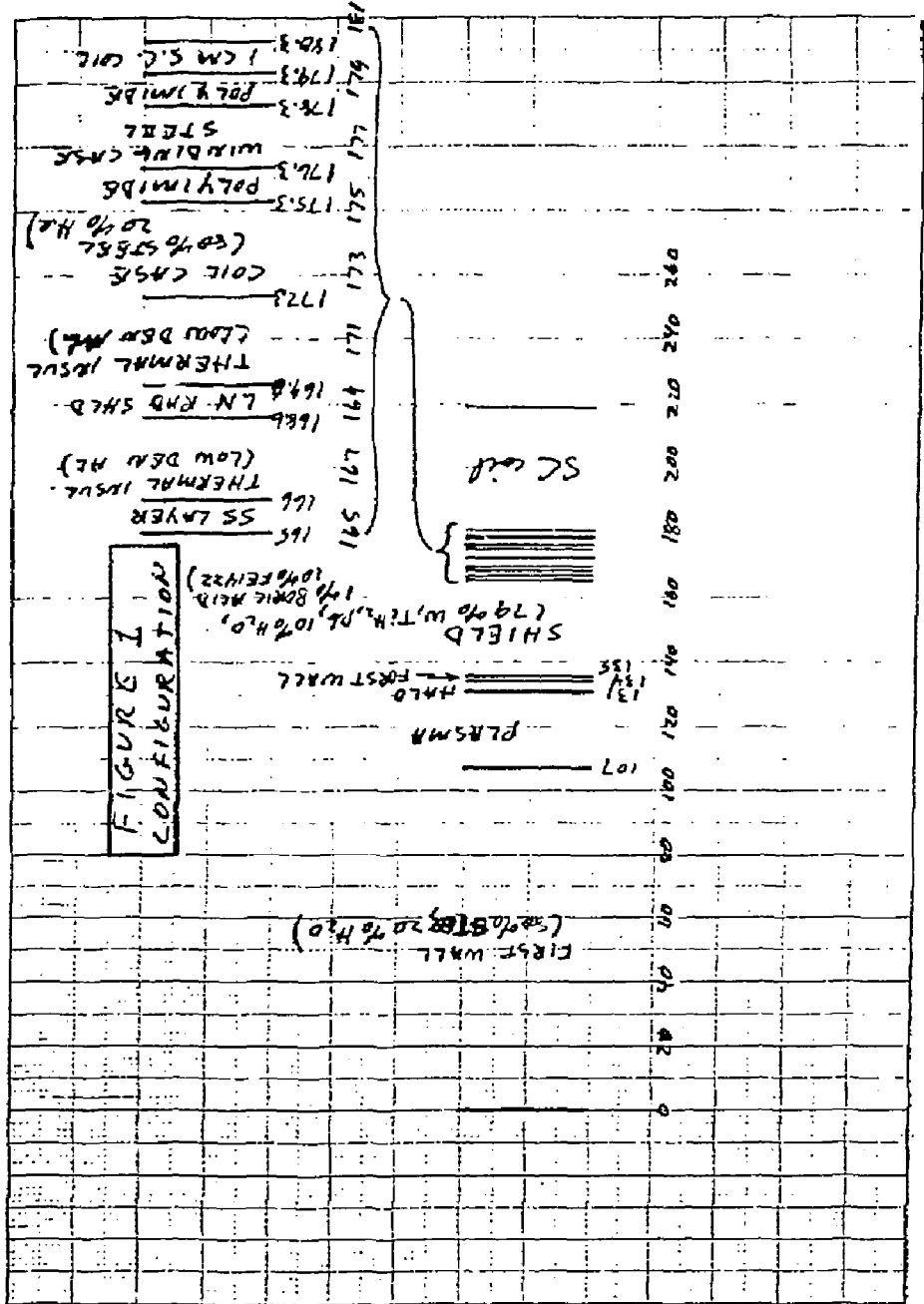
Shield	Pb	ht n	ht g	ht t	HT n	HT g	HT T	n fluence
30 cm	0 cm	4.2e0	4.8e1	5.2e1	1.2e2	9.4e2	1.1e3	2.4e19
30 cm	2 cm	4.9e0	3.9e1	4.4e1	1.4e2	7.2e2	8.7e2	2.9e19
30 cm	4 cm	5.8e0	3.8e1	4.4e1	1.7e2	6.9e2	8.6e2	3.6e19
30 cm	6 cm	6.9e0	4.1e1	4.8e1	2.0e2	7.5e2	9.5e2	4.5e19

where: ht n is peak SC heating due to neutrons (mW/cm^3)

ht g is peak SC heating due to gammas (mW/cm^3)

ht t is sum of ht n and ht g

HT n is total SC coil & case heating due to neutrons (mW/cm^2)

HT g is total SC coil & case heating due to gammas (mW/cm^2)

HT T is sum of HT n and HT g

n fluence is the neutron fluence in the first cm of SC $(n/cm^2$-FPY)

Table 5. - Heating Distribution for 30 cm Shield, 24/6
Total Heating in SC coil Assembly $(mW/cm^2$ of coil)

Component	HT n	HT g	HT T
Coil Case	1.6e1	3.9e2	4.1e2
Poly	3.5e1	2.3e1	5.8e1
Winding Case	8.0e0	1.6e2	1.7e2
Poly	2.2e1	1.3e1	3.5e1
SC coil (1 cm)	4.0e0	4.8e1	5.2e1
Rest of SC	3.5e1	3.1e2	3.5e2
TOTAL	1.2e2	9.4e2	1.1e3

where: HT n is nuclear heating due to neutrons (mW/cm^2)

HT g is nuclear heating due to gammas (mW/cm^2)

HT T is sum of HT n and HT g

A-19

FIGURE 2

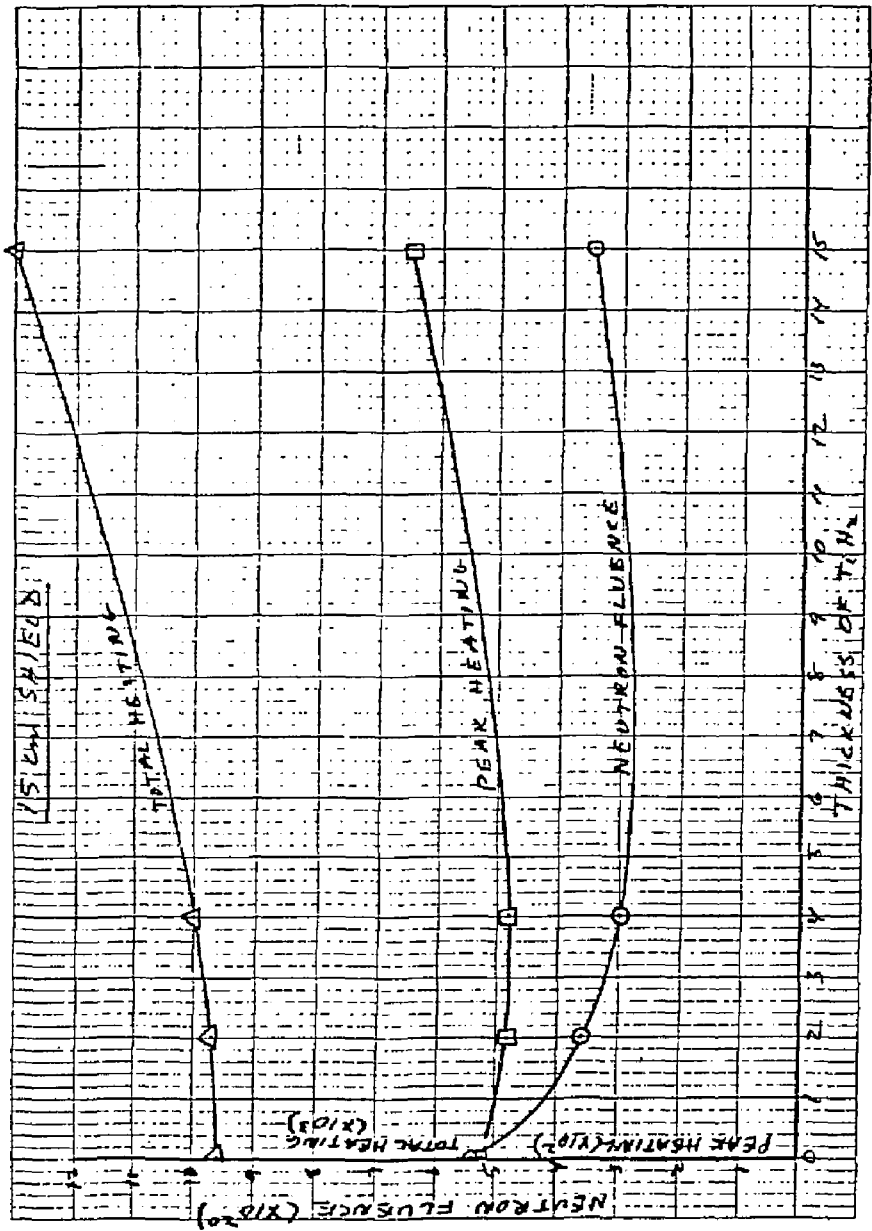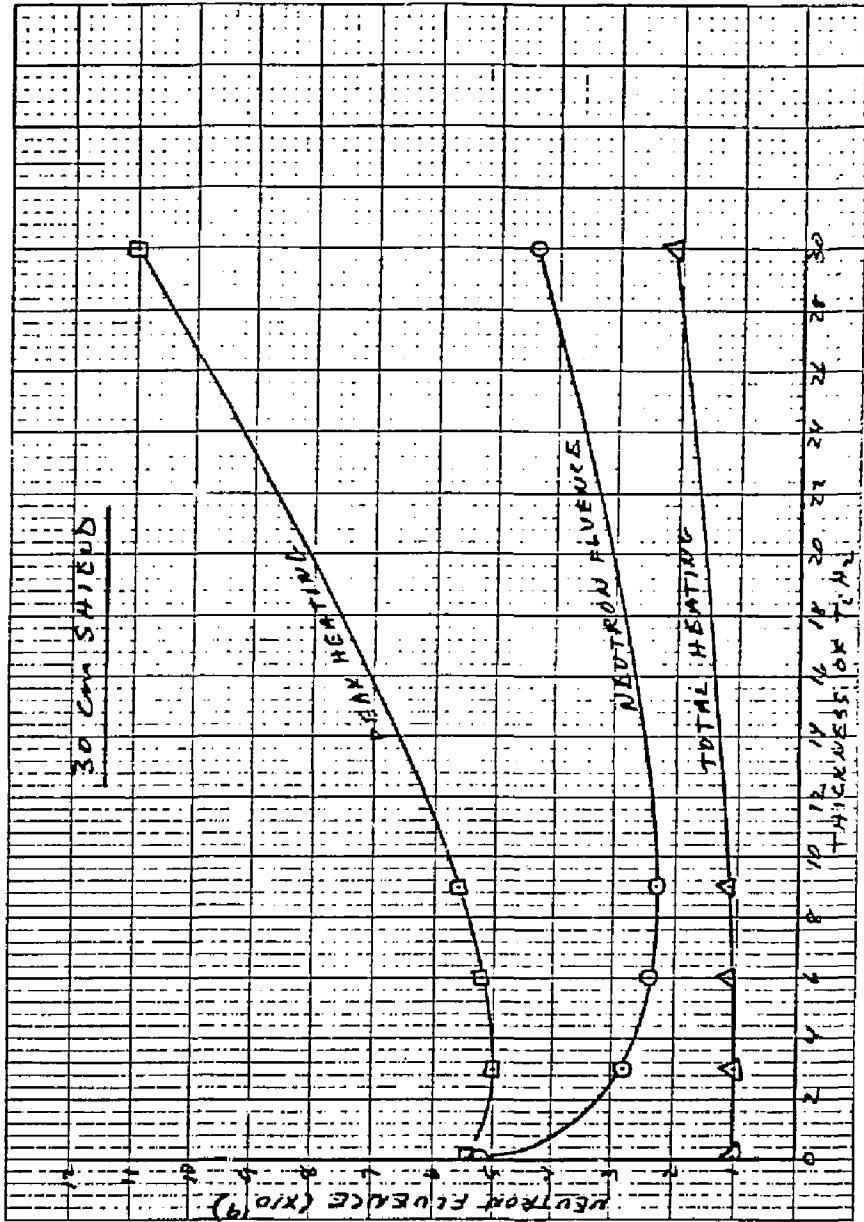A-21

FIGURE 3

30 cm SHIELD

X-RAY HEATING

NEUTRON FLUENCE

TOTAL HEATING

THICKNESS OR TIME

NEUTRON FLUENCE (x10¹⁹)

A-22

FIGURE 4

FIGURE 5

SHIELD THICKNESS (CM)

A-24

FIGURE 6

A-25
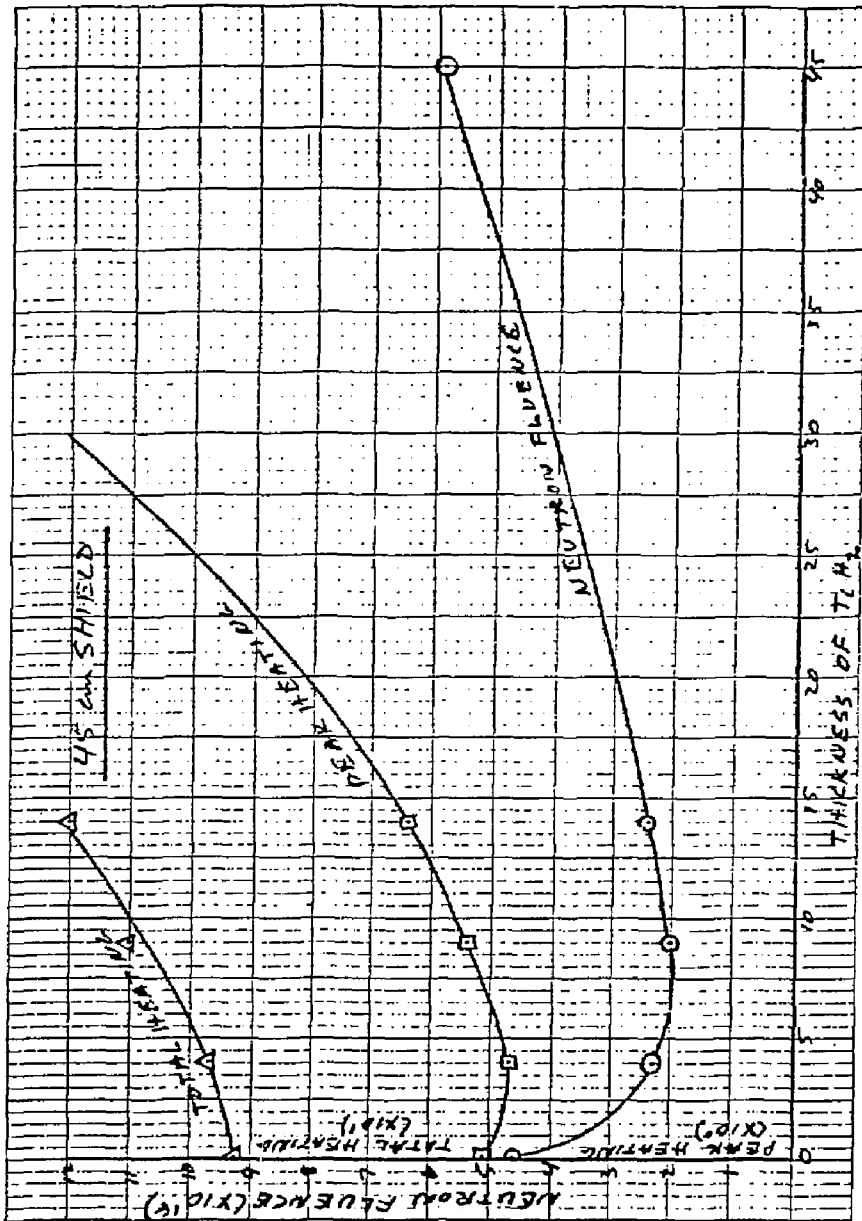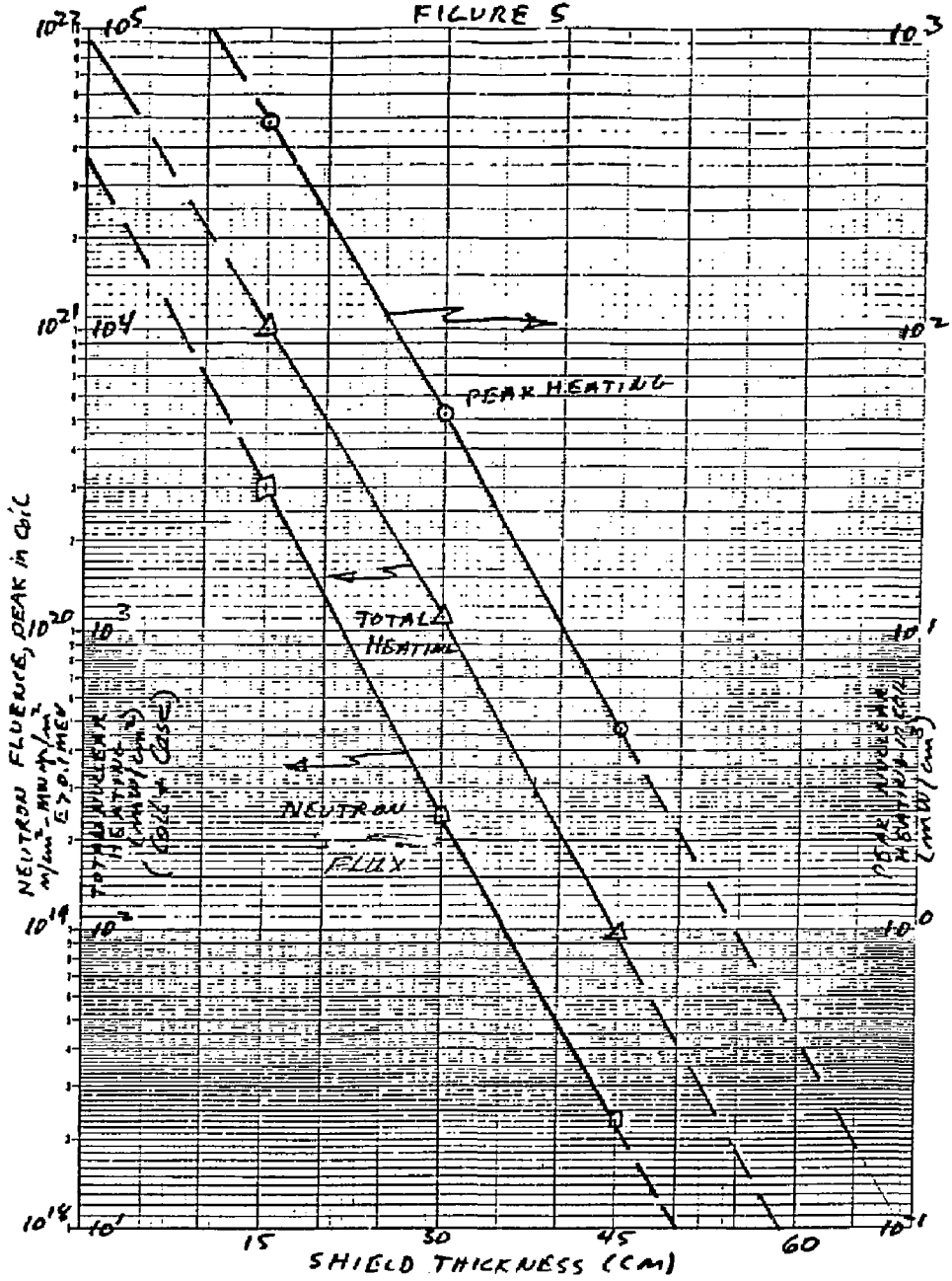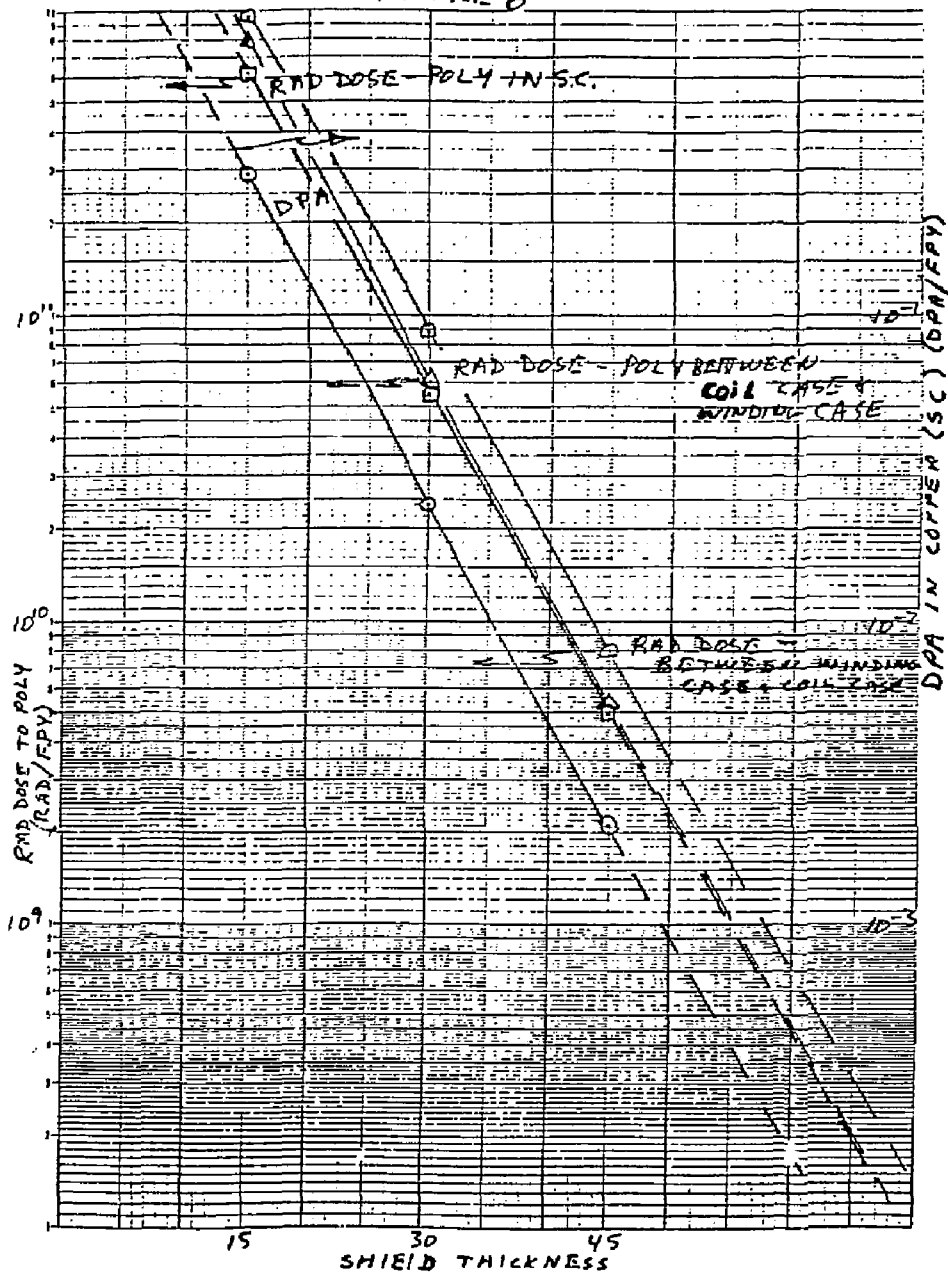
NEUTRON FLUENCE DESIGN LIMIT FOR SUPERCONDUCTING MAGNETS

MEMORANDUM

TO: Distribution   LLNL-FPD-84-48
                                               March 20, 1984
FROM: J. D. Lee

SUBJECT: Neutron Fluence Design Limit for SC Magnets

    This subject was reconsidered at an informal meeting held at the FEDC on
February 22, 1984.

    For reference, this subject was formally considered at the Magnet
Critical Issues meeting held December 5th in Philadelphia and reported by Neef
in LLNL-FPD-84-016. Recommendations made included:

    o   Radiation limit to electrical insulation - 10^{11} rads maximum (at a
        max. compressive stress of 30,000 psi).

    o   Radiation limit to superconductor

        -   for NbTi - 10^{18} fast (E > 0.1 MeV) neutrons/cm^2 will
            result in a 20% decrease in critical current. Annealing at
            room temperature will regain 70% of that 20%.

        -   for Nb$_3$Sn - 4×10^{18} fast neutrons/cm^2 will result in a
            20% increase in critical current. A greater fluence then
            causes a fairly rapid decrease in critical current, so use
            4×10^{18} neutrons/cm^2 as an upper limit.

    At the February 22nd meeting we discussed adopting a more general
criteria that trades off fluence and magnet design parameters.
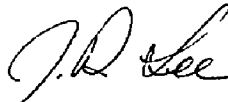
    NbTi - Based on discussions with Mike Guinan, there appears to be
    evidence the degradation of the critical current in NbTi saturates at
    $\sim$ 25% of its initial value in the 6 to 10×10^{18} n/cm fluence range
    (see Fig. 1). Likewise, the resistivity increase in Cu may saturate at
    $\sim$ 330 nΩcm at a fluence of $\sim 10^{19}$ n/cm. Mike thinks that the
    conductor fluence limit may result from low cycle fatigue in the Cu,
    occurring at a fluence in the 10^{20}-10^{21} range.

    Nb$_3$Sn - Unlike NbTi the drop in J$_c$ in Nb$_3$Sn is not expected to
    saturate. But there is hope the fluence limit can be increased into the
    $1-4 \times 10^{19}$ range before J$_c$ drops to an unacceptable low value (see
    Fig. 2). Data must be developed to support this hope.

A-27

In summary we should consider increasing the fluence limit in NbTi and
Nb_3Sn while decreasing their current densities accordingly. There may be an
optimum in the fluence vs current density tradeoff. This optimum (lowest cost
system) could be searched for by examining a number of coil sets in which the
minimum available space between the helo plasma and the coil pack varies
between 30 and 60 cm. Peak conductor and total coil heating should also be
included in such a trade study.

I have collected a number of references on this subject but we need more
input from the SC materials community on radiation effects, especially on
Nb_3Sn.

J. D. Lee

JDL:lc
Attachments
2084z

References:

1.   C. L. Snead, Jr. and T. Luhman, "Radiation Damage and Stress Effects in
     Superconductors: Materials for High-Field Applications," Brookhaven
     National Laboratory, BNL-33230.

2.   P. Hahn, B. S. Brown, H. W. Weber and M. W. Guinan, "Spallation and 14
     MeV Neutron Irradiation of Stabilized NbTi Superconductors," Argonne
     National Laboratory, IP-II-7 (1983).

3.   M. W. Guinan and R. A. Van Konynenburg, "Fusion Neutron Effects on
     Magnetoresistivity of Copper Stabilizer Materials," Lawrence Livermore
     National Laboratory, UCRL-90134 (1983).

4.   C. D. Henning, E. N. C. Dalder, J. R. Miller and L. J. Perkins,
     "Superconducting (Radiation Hardened) Magnets for Mirror Fusion Devices,"
     Lawrence Livermore National Laboratory, UCRL-90092 (1983).

5.   F. Nardai, H. W. Weber and R. K. Maix, "Neutron Irradiation of a Broad
     Spectrum of NbTi Superconductors," Cryogenics (April 1981).

6.   H. Attaya, et. al., "Blanket and Shielding Considerations for Advanced
     Tokamak Reactor Concepts," University of Wisconsin, UWFDM-562 (1983).
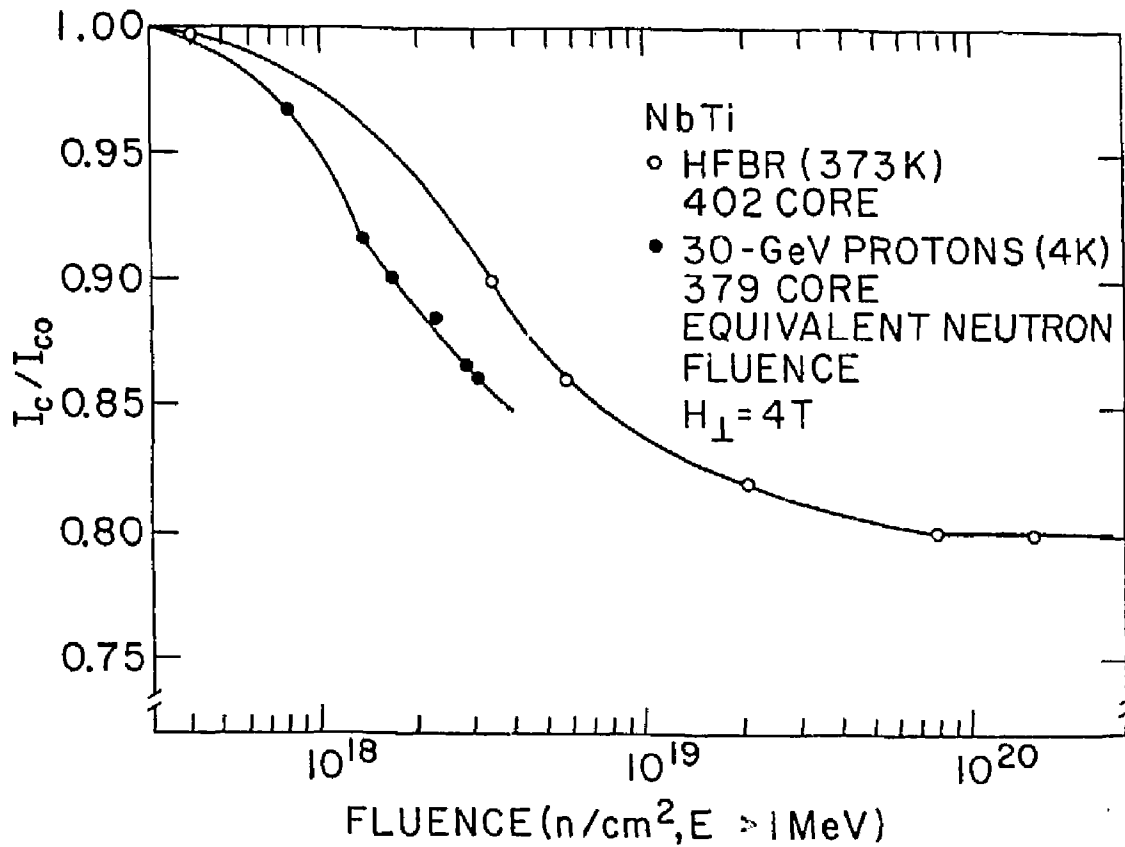
Ref 1   Fig. 2 (from Ref 1)

Fig. 2 (from Ref 1)

Ref 1

CRITICAL ISSUES

TO: Distribution

FROM: William S. Neef, Jr., L-644

SUBJECT: Report on the Critical Issue Meeting on the Direct Converter
           held at the Fusion Engineering Design Center on June 14, 1984

The monthly FPD progress meeting was held at Oak Ridge, Tennessee in
June. The Direct Converter discussion was held the second day and
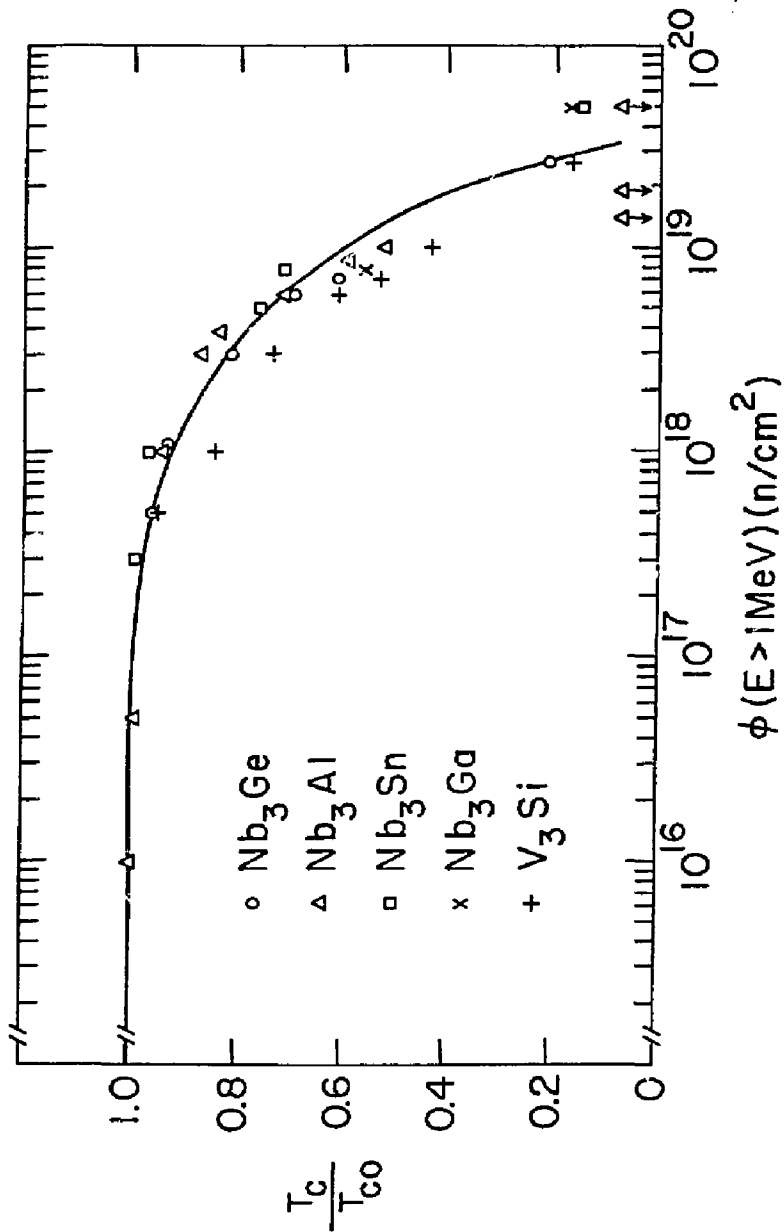occupied the full morning. Presentations were made by B. Barr of LLNL,
M. Petravic of PPPL, and T. Luzzi and I. Clarkson of GAC.

B. Barr reported on theoretical work that he and M. Gilmore at LLNL
are pursuing concerning radial potential profile. The plug voltage is
assumed "flat" and one gyroradius has been assumed as the radial distance
for voltage reduction in the halo. The current design has 18 MW of ion
power in the halo - hence being dissipated on the halo scraper at the halo
pump inlet. Barr's viewgraphs are included with this report.

Dr. Petravic from Princeton is a member of the physics group
designing divertors and limiters for their tokamaks. In their case 10 eV
plasma may hit the first wall of a limiter. At that energy erosion of a
tungsten surface is not a problem. In their designs incident power can be
less than 500 watts/cm^2 so cooling can be accomplished in a
straightforward manner. They do observe hot spots and note that they are
stationary (ie, they do not "dance around" on the limiter).

For diverters he distinguished between high recycling regions and low
recycling regions and said they would probably be separated on future
designs by some physical barrier.

Grumman's presentation emphasized three main issues; 1) the geometry
of the exit flux is neither circular or elliptical and may require unusual
plate configurations to achieve radial voltage control, and 2) the water
cooling of said plates requires complex header configurations. The
voltage stand-off of separate segments has not been designed as yet, and
3) water velocity of 10 meters per second is required for plate cooling
and may lead to an erosion problem if any cavitation is present.

One issue not yet addressed is the end-of-life disposal of the
central plate which sees a considerable neutron flux. These neutrons
"beam" from the central cell. Our neutronics analysis has not given
integrated values for this flux. It will be available soon. The material
choice to control tritium permeation will be strongly influenced by the
activation and disposal problem. Luzzi and Clarkson's viewgraphs are
included with this report.

A-32

The concensus was that very good progress has been made in direct
converter design. Problem areas are well understood if not completely
solved. We will have a credible design ready for FPD and subsequent
Tandem Mirror Reactors.

Bill

W. S. Neef, Jr.
Advanced Mirror Studies

1741v
WSN:tan

cc: V/G Package - Barr
     V/G Package - Grumman

MEMORANDUM

TO: Distribution   LLNL-FPD-84-017

FROM: W. S. Neef, Jr.   December 15, 1983

SUBJECT: Report on the FPD Critical Issue Meeting on Drift Pump Coils,
         December 13, 1983

We thank you for your participation in the Drift Pump Workshop. It was requested that we send out the names and addresses for all attendees and you will find that attached to this memo.

~~Copies of all the viewgraphs presented during the meeting are also included for your reference.~~

The following list of critical issues related to drift pumping is the one generated during the afternoon portion of the meeting. Responsible organizations and/or individuals are listed as we agreed during the meeting.

Design for FPD Drift Pumps

1. $B_\perp$ vs $B_\parallel$ physics study.   LLNL, Byers

2. Modeling the geometry for eddy current   (Turner at ANL)
    calculation.   Metzler at FEDC

3. Side-by-side coil arrangement $(z \pm \Delta z)$
    each with fewer driving frequencies –   Metzler at FEDC
    study coil current and efficiency.

4. Use of ferrites for neutron shielding near   Neef at LLNL
    DP coil (possible to improve antenna Q).

5. Circuit efficiency and cost for the $B_\perp$
    method - as a function of current. Use   Metzler at FEDC
    MARS parameters and vary coil current
    from 2000 to 20,000 A.

6. Antenna fatigue damping of mechanical   Neef at LLNL
    vibration (for drift ω as well as bounce ω).

7. Neutron shielding of nearby superconductor.   LLNL Neef & Lee
                                                          FEDC Gohar

8. Physics Q effects – ability to heat cold   LLNL Perkins
    particles.

9. Charge-exchange particle bombardment   LLNL Perkins
    heating if coil is exposed.

10. Choice of shielding material PbO, WC,   (ORNL Wiffin)
    WO$_3$, W in transformer core form, etc.   FEDC Metzler
                                                    LLNL Neef

11. It was suggested by Don Smith that we   FEDC Metzler
    look into "kicker" magnets in synchrotrons   LLNL Neef
    since they use iron cores and are
    geometrically similar.

A scheduled date for completion of this drift-pump design is mid-March 1984.

W. S. Neef, Jr.
Advanced Mirror Systems Group

WSN:lc
1915z

MEMORANDUM

TO: Distribution   LLNL-FPD-84-016

FROM: W. S. Neef, Jr.   December 15, 1983

SUBJECT: Results from FPD Critical Issues Meeting on Magnets in Philadelphia

---

The Advanced Mirror Studies Group at Livermore thanks you for your participation in the workshop on superconducting coils for the Fusion Power Demonstrator. We believe the meeting was productive and very educational. The viewpoints of those less directly concerned with the FPD design were of special value. A more critical, less biased viewpoint is vital to prevent any tendency to "preach to the choir." We believe viewpoints differing from ours were well represented.

You recall that we attempted a final summary of all design criteria. The following is a reproduction of that list to assist us in beginning the design of the FPD magnet set.

1. Fraction of the critical current to be used in design:

    - for NbTi use $\approx 70\%$

    - for Nb_3Sn monolith use $\approx 50\%$

2. The minimum energy margin was set at 200 millijoules per cc.

3. The maximum allowable terminal voltage during a dump:

    - 1000 volts for a magnet cooled by pool boiling

    - 3000 volts for a magnet cooled by forced convection

4. Maximum internal temperaure during a quench should be 300 K for all coils, regardless of whether cooled by pool boiling or forced convection.

5. Stress limits

    a. Steel structure at 4.2 K or lower; use 100,000 psi design stress (assumes 150,000 psi minimum yield point) and fracture toughness of 200 ksi $\sqrt{in}$ minimum.

    b. Conduit for conductor; use 100,000 psi design stress and fracture toughness of 80 psi $\sqrt{in}$.

    c.   High purity copper; 28,000 psi design stress.

    d.   Insulator (polyimide); 30,000 psi compression.

6.   Allowable conductor surface heat flux for recovery:

    a.   Pool boiling - Helium I - 0.3 watts/cm^2

    b.   Pool boiling - Helium II -

        NbTi   1.0 watts/cm^2

        Nb_3Sn 2.0 watts/cm^2

    c.   Forced convection   0.2 watts/cm^2

7.   Conductor strain shall be 0.33% maximum for all designs.

8.   The question of instability resulting from coolant vapor lock was felt to be entirely design specific so no attempt was made to specify any parameters.

9.   Radiation limit to electrical insulation - 10^{11} rads maximum.

10. Radiation limit to superconductor

    - for NbTi - 10^{18} fast neutrons/cm^2 will result in a 20% decrease in critical current. Annealing at room temperature will regain 70% of that 20%.

    - for Nb_3Sn - 4×10^{18} fast neutrons/cm^2 will result in a 20% increase in critical current. A greater fluence then causes a fairly rapid decrease in critical current, so use 4×10^{18} neutrons/cm^2 as an upper limit.

The next three items on the list require immediate action by LLNL, assisted by the FEDC.

11. Establish a few (3 or 4) baseline magnet configurations that satisfy stability criteria and cover a range of radii (we suggest $r_{min} = 0.7$, 0.8, 0.9, 1.0).

12. For each configuration above calculate a profile of nuclear heating vs depth into magnet.

13. Establish an experiment schedule.

   - number of shots
   - number of thermal cycles
   - duration of and time between thermal cycles.

If you believe this summary requires correction, please contact me at 415-422-6747 or FTS 532-6747.

W. S. Neef, Jr.
Advanced Mirror Studies Group

WSN:lc
1914z

MEMORANDUM
LLNL-FPD-84-024

TO: FPD Distribution
FROM: L. John Perkins JP.
SUBJECT: FPD Plasma Engineering: Critical Issues

    A meeting was held at LLNL on December 21, 1983 to discuss critical
plasma engineering issues for FPD. This had the objective of defining
tasks to be undertaken in the next few months. These tasks are documented
below; suggested participants are listed at the end of each item. Those
items marked with an asterisk denote near-term tasks to be completed for
the February FPD meeting at the FEDC.

  1. FPD baseline parameters.[*] A (reasonably) consistent physics
      parameter set is required for general distribution especially to FPD
      engineering personnel. Further consideration of end cell trapping
      rates (both H_{DT} and H_α) are required before this set can be
      finalized (see also item 10 below). (RBC/MEF/RSD/LJP)

  2. Effect of coil geometry on c. cell ripple, field taper, beta and
      cost.[*] Trade study between sheet type magnets and discrete
      (MARS-like) magnets. Control of ripple from discrete magnets by
      means of Fe inserts. (RHB/LJP/GWH/BMJ)

3. Effect of end cell coil geometry on off-axis field distortion. (RHB/BMJ)

4. Benchmarking of TEBASCO with the new 3D MHD equilibrium code to examine spurious flux tube distortions. (RHB)

5. Continuing effort on the radial transport code TMT with applications to:
   (a) Halo physics (see also 7 below).
   (b) Wall potential control.
   (c) Pellet fueling.   (JMG/GWH)

6. Neutron source in end cell.[*] Generate neutron source distributions for various end cell magnet configurations for use in shielding studies. (RBC/JDL)

7. Halo and direct convertor analysis. Generation of particle and power flows to direct converter, halo scraper and halo dump including peaking factors where applicable. Evaluation of pumping geometry at end dumps. Initiation of halo fluid-flow model for accurate quantification of halo parameters including required power input. Couple with TMT results when available. (WLB/WNK/GWH/JMG)

8. Startup (time to get serious about this!). Employment of TREQ code to address startup issues for FPD. (MER)

9. Anchor ICRH analysis.[*] Evaluation of:
   (a) Sufficiency of passing ion fueling of anchor for MHD stability.
   (b) Inclusion of anchor ICRH power in power balance.
   (c) TEBASCO runs with off-midplane density distribution (sloshing-ion-type distribution) rather than present model of midplane-peaked distribution. (RBC/MEF/RHB)

A-40

10. Differential trapping rates of D and T in transition region. Formal consideration of D and T transition trapping rates, over and above a simple $\sqrt{m}$ dependence. This may, for example, lead to the requirement for other than a 50/50 D/T mix in the central cell with implications for c. cell power balance. (RSD/RBC/MEF)

11. Alpha (central cell) and sloshing ion (end-cell) adiabaticity. Effect of field profiles, etc. on adiabaticity limits and resulting consequences for beta. (LJP/RSD/RBC)

12. ECRH physics. Inclusion of new (strong ECRH) physics models. Evaluation of updated models for synchrotron radiation, reflection, and reabsorption. (GWH/RBC)

13. Replacement of existing DT cross sections with new LANL evaluations.[*] Examination of effects on system parameters. (LJP)

14. Work will also continue in the following ancillary areas:
    (a) TMRBAR upgrade -- modular version with flexible I/O. (MEF)
    (b) TMRBAR-TMG coupling requirements. (RHB/MEF/RBC/LJP)
    (c) Evaluation of smaller TMRs based on novel end-cell concepts. (RSD)

TO: Distribution   LLNL-FPD-84-42
                                                          March 5, 1984
FROM: W. S. Neef, Jr.

SUBJECT: Report on the Critical Issues Meeting on Pellet Injection into FPD,
          February 28, 1984

Gordon Hamilton presented a review of the MARS fueling requirements and capped it off with a summary of similar calculations for FPD using the parameter set considered valid on February 23, 1984. It is attached to this memo. About $1.5(10)^{21}$ atoms per second will be required. This could be provided by 2.8-mm outside diameter pellets introduced at a rate of 2.1 per second.

Calculations by Campbell and Gilmore on pellet penetration give disturbingly high velocity requirements for MARS. Their most optimistic calculations show the need for about 30 km/sec pellet velocity and some of their work shows that 100 km/sec may be marginally sufficient for MARS. This compares to current accomplishments for railguns at Livermore of 3 km/sec. (The maximum velocity ever achieved by any railrun is 12 km/sec!)

The biggest unknown in physics understanding appears to be the correct radial diffusion laws that would reveal how far we really must penetrate the plasma to uniformly fuel it across its diameter. The laws governing pellet evaporation in hot plasma seem to be well understood and have been confirmed by experimental results (with no α power present).

Stan Milora of ORNL surveyed their experimental efforts. Both centrifugal and pneumatic injectors can be used as pre-accelerators to a railgun. Their injector on Doublet III (GA Technologies) can fire 20-40 pellets per second at a velocity of 0.8 km per second. They are developing a pneumatic injector for use on TFTR in 1986 or 1987. It will shoot 3.5-mm-diameter pellets at 1.5 km per second.

The injector that ORNL used on the PDX experiment has a "magazine" of only four pellets, each 1.6 mm diameter, and has velocity capability of only 1 km per second. The four pellets can be adjusted as to time interval. The gun barrel length is one meter.

Current gas injectors use hydrogen at 1300 psi and 250 °C released through a modified solenoid valve. The pressure rise behind the pellet occurs in about 2 microseconds. The pellets remain cylindrical but appear to have "eroded" in diameter about 0.5 mm when they emerge from the barrel and also appear to be about 0.5 mm longer than when they were cut off the extrusion.

Any slight misalignment or tube curvature causes pellets to break in half and fly as two shorter cylinders. Milora estimates that to avoid this breakage tube curvatures must have at least a 30-40-meter radius. (This eliminates any possibility of avoiding coils or shielding by employing curved tubes.)

Experiments at the University of Illinois were reviewed by Prof. Kevin Kim. They have accelerated plastic pellets to date with a density 15 times that of a D-T pellet. A gas injector pre-accelerator followed by a 20-cm railgun achieves plastic pellet velocities of 0.15 km per second. Their initial tests have been with circular pellets in a square bore. They intend to convert to a circular bore to solve the blow-by problem which results in an undesired spark in front of the pellet as well as the desired one behind the pellet.

Ron Hawke of Livermore discussed his railgun results. He mentioned several key lessons learned experimentally:

o   .0005 inches run-out is necessary to avoid pellet breakage of 1.5- to 5-m-long railguns.

o   Sealing the gas at low velocity in the pre-accelerator is difficult. Once at speed the problem is not severe.

o   Any gun capable of 50 km per second is going to have to be 50 to 100-m long.

o   A sabot is probably going to be necessary to reach 50 km per second.

Ron believes any experimental program to achieve 50-km-per-second railguns will cost over $10 million (but not as much as $100 million.)

General conclusions that can be drawn from the meeting:

o   Radial transport scaling is certainly different than in tokamaks. Some experiments in TMX-U or MFTF-B would be most helpful in testing the validity of theory. Since MFTF-B will have 2-3(10)^{13} deuterium particles per cc and ion temperature of about 15 keV, the most reactor-relevant data would be obtained there. Of course no hot alphas would be present.

o   The use of sabots to help achieve high pellet velocities should be more thoroughly evaluated. We should try separation of sabot and pellet, probably magnetically if a metal sabot is employed.

o   Another interesting idea was use of a sabot of low z material
     which permits deeper penetration of the hot plasma. This sabot
     continues on through the plasma, dumping its D-T load as it
     traverses the plasma diameter. It then enters a "get lost"
     hole in the wall on the far side of the plasma. Some of the
     sabot will ablate from the plasma but if the atomic weight is
     very low that may be tolerable.

                                    Bill

                          W. S. Neef, Jr.
                          Advanced Mirror Studies

WSN:lc
2035z

TO: Distribution   LLNL-FPD-84-47
                                                   March 19, 1984
FROM: W. S. Neef, Jr.

SUBJECT: Correction to the Report on the Critical Issues Meeting on Pellet
         Injection into FPD

Professor Kevin Kim of the University of Illinois called my attention to
an error in the previously distributed meeting report (LLNL-FPD-84-42 dated
March 5, 1984). On page 2 the information in the second paragraph is
incorrect.

He has achieved plastic pellet velocities of <u>500 meters per second</u>
<u>without a gas pre-accelerator.</u> Considering the density ratio of <u>15:1</u> between
plastic and a frozen hydrogen pellet, this is equivalent to achieving a
hydrogen pellet velocity of 7.5 kilometers per second.

I apologize for the misinformation. Please attach this "erratum memo" to
your document dated March 5, 1984.

W. S. Neef, Jr.
Advanced Mirror Systems

WSN:lc

TO: Distribution   LLNL-FPD-84-50
                                                          April 10, 1984
FROM: W. S. Neef, Jr.

SUBJECT: Report on the RF Critical Issues Workshop at TRW, Inc. on March 21,
          1984

On Wednesday, March 21, we held an RF Workshop related to the Fusion
Power Demonstration. Attendees were:

LLNL	TRW
R. Bulmer	J. Boyer
W. Cummins	T. Christianson
J. Doggett	T. Romesser
J. Lee	
W. Neef	**INEL**
J. Yugo	
	P. Hsu
FEDC	
	TSSC
S. Freije (TRW)	
D. Nelson	J. Erickson

A competing meeting in Rome on RF issues related to tokamaks (especially
INTOR) restricted our attendance. Neither MIT nor the University of Wisconsin
were able to send a representative to this FPD discussion. Those able to
attend were treated to excellent reviews of plasma heating on TMX-U (now in
progress) and MFTF-B (in design).

We are sending along with this letter three sets of viewgraphs:

    Set #1 - from FEDC on $\alpha + T$, FPD, MARS (presented by Freije)

    Set #2 - ECRH on MFTF-B (presented by Yugo)

    Set #3 - ICRH on MFTF-B (presented by Romesser)

    Set #4 - ICRH on TMX-U (presented by Cummins)

In addition the following comments and/or suggestions were extracted from
notes taken by me during the meeting.

1. Relativistic electron ray tracing code development is being done at Livermore in their Electronics Engineering Department (contact J. Yugo for details). Don Batchelor at ORNL is also working on ray tracing at high voltage. Since the discriminatory powers of the plug plasma are being questioned relative to RF power aimed at points "a" and "b" (refer to MARS Interim Report), it would be appropriate to follow progress closely in this ray tracing area.

2. One-megawatt gyrotrons should be available by 1993 or 1994 on the way to 2.5 MW tubes targeted for early in the next century. For FPD one megawatt seems reasonable. Both larger and small converter-transformers have been built and successfully operated.

3. Bill Cummins gave his view that vacuum waveguides (no windows) are probably okay if pumped at both ends. High voltage gradients will give more problems than poor vacuum.

4. Any vacuum cavity for mirrors of a quasi-optical system needs isolation valves on both sides, i.e., to gyrotrons (allows gyr. removal and replacement) and to plasma (allows adjustments on mirror positions without losing main vacuum).

5. On MARS the angle at which ECRH entered the plasma proved to be "risky business." Plasma trapping and reflection were profoundly affected. The gyrotron produces a gaussian beam but what "mode" arrives at the turning/focusing mirror?

6. During plasma startup a wide range of frequencies are expected to be needed. The gyrotron cavity "changes shape" at different frequencies so electron beam energy recovery may be inefficient under some conditions. If we desire (need?) 80% recovery it may require a many-stage converter covering a wide voltage range.

7. In MFTF-B waveguides will be at vacuum (windows are regarded as risky hardware and are being eliminated). Reflectors are to be used to aim the beam as it emerges from the waveguide. Steering of these reflectors will be accomplished by air motors. Three or four degrees steering allows for support position change due to magnet cooling to 4 K. Aiming accuracy required is $\pm$ 1 degree or within a few inches (measured on the magnetic axis).

8. MFTF-B gyrotrons must have very good mode control to fit various plasma operating conditions.

    a) Ordinary wave is poorly absorbed at low electron temperature.

    b) Fortunately resonant plasma surface shifts help bridge the gaps between frequencies and modes.

    c) Absorption sometimes suffers due to angle of approach (a ray tracing calculation will show this).

9. OSHA is requiring many RF detectors at the TFTR facility. Analysis of stray microwave signals showed that painted liquid nitrogen panels reflect only 30% of incident power, hence they are a good "sink" for stray RF power.

10. Steve Freije reports that the LIS program is driving big gyrotron development now. Present accomplishments are 100 kW (CW) at 140 gHz for LIS.

The 60 gHz development program is nearly complete – but with poor mode output for our use – because no particular mode had been specificed.

The 120 gHz development program at Varian is seven years from completion. They may achieve their target of 2.5 MW by 1996. (This makes our prediction of 1.0 MW for FPD look sound.)

Varian's present research is on closed-cavity (one frequency) gyrotrons. We need more variable frequency research. DOD is funding the Free Electron Maser (FEM) development - not fusion!

Steve feels we have been optimistic in our efficiency estimates for all aspects of big gyrotron operation. One example is in electron direct conversion. Our 81% estimate (MARS) perhaps should be 60%.

11. Mode conversion was discussed. Very long waveguide mode convertors are one of the reasons we chose a quasi-optical system. Milled reflectors do mode conversion in "zero" length, replacing space-consuming waveguide convertors.

12. ICRH future requirements are not expected to be greatly different than current operating procedures. We now inject 1.5-2.0 MW for short pulses with system efficiency of 54%. Present use of Faraday shields is a debatable issue. Japanese and German researchers report better results with the shields. But the shield has to be so close to the plasma that it acts as a sort of limiter, so it may have very limited life.

13. Cummins reports that TMX-U will use two 170^0 loop antennas to surround a circular plasma cross section. The Faraday shield consumes about 70% of the power broadcast. A new "slot" antenna conforming to the plasma shape is being built also. The slot length is about one meter in the plasma axis direction. It has (1) high plasma coupling coefficient, (2) two frequency exitation ranges, (3) low impedence, (4) is a low loss coupler, has good vacuum characteristics.

Bill says to watch out for voltage holding problems - sharp corners - insulator flashover (the same old stuff, which seems to have been forgotten by present mechanical designers).

14. Tom Romesser, during his viewgraph presentation, mentioned overall
ICRH efficiency (wall plug to at:)rbed power) around 80%. The
Faraday shield is one of the prime consumers of "wasted" power. He
says wall plug to _ion_ efficiency is about 50%.

Shield heat load is a serious concern primarily because radiation
from halo plasma and convection from halo plasma are not well
understood. Tom thinks it may be possible to back off a few
centimeters from the plasma edge - with some sacrifice in efficiency.

New gyrotrons will have higher efficiency than conventional ICRH
driver amplifiers. We badly need tunable systems because we don't
have room for two or three separate systems at frequencies chosen tc
fit special plasma conditions (startup, etc.).

One message came through clearly. Use a "plywood dryer" instead of
communication system components which are too easily damaged. A
sudden load change was likened to being struck with a hammer - and
the antenna, shield, and amplifiers should be able to recover from
such rude treatment. Another clear message from Tom, "Try not to
have to be close to hot plasma!" Also, "Get rid of RF windows!"

15. Often a semiconductor is a better "insulator" than Al_2O_3. It
allows a little bleed-off current. No charge islands build up on
the surface resulting in high dE/dx and electrical breakdown. In
all cases avoid hydrogenous materials.

16. The weak link in the reliability chain is both ICRH and ECRH power
tubes.

17. Instrumentation and control on RF power seems reasonably reliable at
the present and little improvement should be required to meet
expected needs.

Thanks for your interest in furthering our FPD design. We believe this
workshop brought out many interesting lessons learned and will serve as an
effective guide to our applications of RF power to reactor designs.

W. S. Neef, Jr.
Advanced Mirror Systems Group

WSN:lc
2109z

TO: Distribution   LLNL-FPD-84-56
                                              April 23, 1984
FROM: W. S. Neef, Jr.

SUBJECT: Report on the Critical Issue Meeting on Negative Ion Neutral Beam
         Injection into the Fusion Power Demonstrator

On April 5, 1984, the Lawrence Berkeley Laboratory hosted a meeting on
negative ion neutral beams. This meeting was instigated by the LLNL Advanced
Mirror Reactor Group. We plan to use negative ions for the "sloshing" beams
in the FPD end plugs. So it is necessary to know the performance level to be
expected from high energy ion injection by the year 1995.

Grant Logan gave a brief review of sloshing ion production by RF vs
negative ion beams. About 300 keV ion energy will be required with
$n_{peak}/n_{midplane} = 1.4-2.0$. The density difference is difficult to achieve
with RF heating. He showed that it is also difficult to limit the density of
hot electrons and also have a high Q for reactor performance if RF heating is
used. It is essential that high efficiency 300 keV neutral beams be available
for optimum plug performance because they put the ions right where you want
them.

The Berkeley team of Cooper, Ehlers and Anderson gave excellent status
reports on the source, accelerator, and transverse field beam transport.
Attached to this memo are copies of all viewgraphs presented.

Joel Fink, Negion, Inc., is a consultant to both LLNL and LBL on neutral
beam studies. He reviewed the three promising methods of converting
accelerated ions to neutrals. They are 1) gas neutralizer, 2) plasma
neutralizer, and 3) photodetachment neutralizer. His viewgraphs are also
attached to this memo. One conclusion reached was that photodetachment can be
very efficient but also very costly. In addition it has an impressive list of
technical problems headed by the laser development. Its technical advantages
are important but the price appears today to be too high. Joel concludes that
all three approaches should be developed. There is clearly no best or
cheapest way at this time.

The design of beam dumps was discussed by Alan Paterson, LBL mechanical
engineer. I summarize his comments here.

1. Inclined copper plates can be used for about one second with a flux
    of 2000 w/cm^2 normal to the copper surface.

2. McDonnell-Douglas zirconium-copper panels have coolant pressure drop
    of 100 psi. A 120 keV at 60 ampere beam will be the maximum
    capability of that design.

3. In Europe two unusual designs are operating and bear watching:
a) rotating targets (Germany), and b) hyper-evapotron (JET at
Culham).

In reviewing my notes taken during our discussions, I find some
disconnected but pertinent comments made during the afternoon discussions. I
list them here in no particular order as food for thought.

1. It may be necessary for LBL to increase their present neutralizer
clearance around the beam. It was made quite tight to restrict
conductance, thus minimizing pumping requirements both upstream and
downstream. The beam "edge" is not sharp so we may be restricting
beam delivery to the target by the present close clearance.

2. Filaments have about a 40-minute life in positive ion source
chambers. This points to a reliability problem. Perhaps some sort
of RF plasma generator might be a more reliable method--but this
must be demonstrated by operational experience.

3. The amperes per meter already achieved by the negative ion sources
at LBL is only a factor of two below the FPD requirement. They feel
6 amperes per meter should be achieved without great difficulty.

4. Neutron effects on sumarium-cobalt permanent magnets should be
investigated.

5. It may be difficult to supply coolant to high voltage cryopumps.
Some pumps may be at 200 to 300 kilovolts from ground potential in
an FPD design.

6. Will laser windows tolerate neutrons? Even well shielded beam lines
will have many scattered neutrons in and near a photodetachment
neutralizer and its laser optics.

As a final note, it has come to our attention that during the week of
April 9-13 the positive ion source selection committee met at DOE and selected
the LBL design over the ORNL competition. The final deliberations and reasons
for selection have not yet been made public. The importance of this to the
FPD design team is in the planning of a 5 MW/m^2 test section in the central
cell. Such an engineering test regime would be positive-ion driven. To date
the blanket test section proposed employs ORNL beams. No major changes in
concept should result from that switch.

W. S. Ncef, Jr.
Advanced Mirror Systems Group

WSN:1c
2155z

SITING AND SAFETY CRITERIA

MEMORANDUM
LLNL-FPD-84-032

TO: FPD Team
FROM: Grant Logan and Dave Dorn
SUBJECT: FPD Siting and Safety Criteria

At this stage in the FPD design phase, it seems useful to document our criteria on siting and safety considerations. These considerations are distilled from our discussions at INEL on January 19, 1984. As such, they are subject to change as outside influences change and as our perceptions change. However, for now we are asking that they be adopted by the entire FPD community as working criteria. If any of you have problems with these criteria, please surface them early so that we can all work toward the same goals. Call or write either of us before the next FPD meeting (February 22-23, 1984 at FEDC) or present your suggestions at that meeting.

INTRODUCTION

The FPD/ETR Safety Critical Issues meeting was held at the Idaho National Engineering Laboratory (INEL) on January 19, 1984. Appendix A lists the attendees. Steve Piet reported on recent experimental data from the Hanford Engineering Development Laboratory (HEDL) on combustion tests of LiPb. There were no temperature increases, no visible flames, and no aerosols were detected. Questions as to the level of detection of aerosols were raised and further experiments were suggested. He further reported that potential first wall materials were investigated. Among these were vanadium, PCA, and HT-9. The HT-9 looked best from the viewpoint of safety considerations and is suggested as the material of choice.

Dave Dorn also presented a "straw man" set of siting and safety criteria for the FPD. There was general agreement with the proposed criteria and some suggestions for augmentation. Further consultation and thought have resulted in the following set.

GENERAL CRITERIA

Site Selection Criteria

1. Relationship to population centers and density. There should be no conflict between the operation of the fusion facility during its lifetime and the master plan for development in the vicinity.
2. It is desirable that adequate electrical power be available without requiring new substations and power lines.
3. Heat disposal (cooling towers, rivers, lakes, oceans) should be readily accomplished with little or no adverse environmental effects.
4. There should be an area of the site that can be dedicated to a hot cell facility for processing radioactive material and parts.
5. It is highly desirable that it be possible to dispose of radioactive waste onsite. To do this will require that the site meet the NRC requirements for near surface burial as outlined in 10 CFR 61.
   a) Operational wastes - machine parts that need regular replacement, expended material, protective clothing, rags, sludge, solvents, etc.
   b) Decommissioning wastes -
6. In the event that radioactive material cannot be disposed of onsite, it will be necessary to identify offsite disposal areas, readily available. Material to be handled will be the same as in 5 above.
   a) Transportation routes must be identified.
   b) If there are local ordinances restricting radioactivity transport, alternate routes must be found.
7. The seismic safety criteria followed in the design must be consistent with the local seismic requirements.
8. If there are tornado hazards, they must be considered in the design of the buildings and the facilities.

9. If there are flood hazards, they too must be taken into account.
10. Proximity to airports and airplane flight paths may require additional precautions against possible effects of airplane crashes.
11. The projected radioactive dose rates at the fence-line need to conform to existing and proposed DOE and EPA regulations. If buffer zones will be needed, it must be possible to acquire them.
12. Limits on inventories of radioactive materials for a site may be forced by special hydrology, unusual leach rates, and unusual nuclide migration rates.

Reactor Design Criteria

1. Since we cannot anticipate all failure modes and the necessary maintenance procedures, hands-on maintenance capability should be emphasized in those parts of the design where possible. We recognize that hands-on maintenance will be possible only in selected places outside of the outer machine shield.
2. In regions where hands-on maintenance is highly desirable, use materials which will "cool" quickly if activated. This will make general access easier and will simplify remote handling when needed.
3. Recognizing that most of the FPD will require remote maintenance, remote handling capability and design for remote maintenance should be major considerations of design studies right from the start.
4. Use materials which when activated can be handled and disposed of by near surface burial.
5. There should be no routine release of radioactivity to surface or near surface water.
6. In regions of high activation, avoid use of materials that can be volatilized easily in an accident situation.

SPECIFIC CRITERIA APPLICABLE IF FPD CONSTRUCTED AT LLNL

The seismic criteria we intend to follow in constructing the FPD are:
- o   No loss of life at 0.5g horizontal acceleration.
- o   No collapse of building or major internal structures at 0.5g.
- o   No major economic loss at 0.5g.
- o   No loss of function of safety systems (for instance - emergency tritium clean-up system, atmospheric confinement) at 0.5g.

The seismic response spectrum assumed for the LLNL site is shown in Fig. 1.

As far as regulations on radioactivity, the Lawrence Livermore National Laboratory, as a Department of Energy research facility does not come under the NRC. We operate under the DOE and the EPA regulations. The current DOE regulations are contained largely in "Requirements for Radiation Protection", DOE Order 5480.1, Chapter XI. There are no current EPA regulations governing radioactive dose rates; however, EPA has proposed regulations for the offsite dose rates ("Clean Air Act, Radiological Emissions Standards", Federal Register, April 6, 1983) which were to have been adopted September 1, 1983. These regulations are to apply to routine operations, not accident situations.

Accident scenarios are handled differently. The NRC regulation as published in 10 CFR 100 sets the offsite dose from a maximum credible accident in a power reactor at 25 rem. Such an accident should have a probability of no more than 10^{-4}/yr. DOE Order 5480 speaks about a type 3 accident, perhaps occurring three times in the plant lifetime. The offsite dose limit for the type 3 accident is 5 rem. Again, to put this into context, a release of 120 g of tritium from the LLNL tritium facility is calculated to give rise to about 3-4 rem to a person residing at the fence line during passage of the cloud.

LLNL exposure limits for onsite personnel and routine operations, as listed in the LLNL Health and Safety Manual Section 33, are based on the DOE Order 5480.1, Chapter XI. The exposure limits are the same as those stated in the NRC 10 CFR 20 and are the recommendations of the National Council on Radiation Protection (NCRP) and the International Council on Radiation Protection (ICRP). These are:

1. Whole body, head and trunk, bone marrow, gonads and lens of the eye - 3 rem/quarter or 5 rem/year.

2. Skin of whole body exposure to beta of E < 700 kev or x or gamma of E < 10 kev shall not exceed 5 rem/quarter or 15 rem/year.

3. Hands, feet or ankles shall not exceed 25 rem/quarter or 75 rem/year. These dose limits are the maximum permitted from routine operations; however, the exposure policy of DOE and LLNL is to keep radiation exposures as low as reasonably achievable (ALARA). ALARA is subject to many definitions, but a draft on ALARA submitted to DOE by Kathren and Selby of Pacific Northwest Laboratory in April, 1980 states:

"Both costs and dose reductions are difficult to evaluate and there may be significant variability in the peception and acceptance of risk by individuals and society. In general, dose reductions that cost less than $2000 per person-rem of dose spared are probably always cost-beneficial, while costs in excess of $60,000 per person-rem of dose spared are probably not cost-beneficial. In the absence of sound cost figures, an ALARA program cannot rely upon cost-benefit analysis. In such cases, the criterion must be whether or not dose reduction is reasonably achievable, given the limits of economics and practicality."

In the past, DOE has set the ALARA limit at 1/5 of the limits presented above; i.e., the design limit for DOE is: whole body 0.6 rem/quarter or 1 rem/year. The policy at LLNL has been to design to half of this - 300 mrem/quarter or 500 mrem/year. It is also LLNL policy that the casual passer-by (walking by the building) not be exposed to more than 0.25 mrem/hour.

Offsite limits are controlled by the EPA. In the "Clean Air Act, Radiological Emissions Standards", the EPA proposes radiation dose guidelines of 10 mrem/year whole body and 30 mrem/year to any organ for any member of the public assumed to reside at the site boundary. This dose limit for the general public includes radiation dose from all radioactivity which is air-born. For fusion experiments, it includes dose from any tritium released, dose from neutron activation products from the air in the experimental area, plus any other radiation dose sources that may be connected with the experiment. It also includes

any "sky shine" and radiation which escapes the shielding around the experimental facility. At the time of the publication of the proposed regulations, the effective date was set for September 1, 1983. It was not made effective at that date; however, it is clear that something like these standards will be adopted. This limit is consistent with that imposed on the fission industry. The current NRC site boundary limits for an operating reactor are 5 mrem/year - whole body and 15 mrem/year - organ.

LLNL presently has an operating tritium facility which releases about 2000 Ci/year (200 mg/year) during the course of normal operation. The effects of this at the site boundary have been measured at about 0.13 mrem/year. The present tritium facility is up-grading their equipment and procedures and expects to drop their releases to less than 500 Ci/year (50 mg/year). However, other programs at LLNL also have tritium operations and routine releases. Among those identified are the Linear Accelerator, the RTNS, the Laser target facility. Others may also exist.
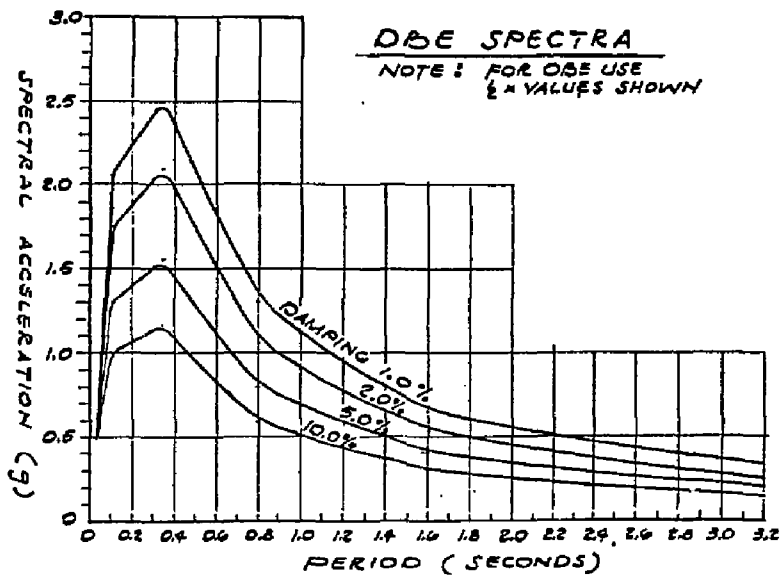
A-58

FIGURE 1.

The Seismic Response Spectrum Assumed for the LLNL Site.